IEEE STANDARDS ASSOCIATION

IEEE Standard Specification Format Guide and Test Procedure for Linear Single-Axis, Nongyroscopic Accelerometers

IEEE Aerospace and Electronic Systems Society

Sponsored by the
Gyro and Accelerometer Panel

IEEE
3 Park Avenue
New York, NY 10016-5997
USA

IEEE Std 1293™-2018
(Revision of
IEEE Std 1293-1998)

IEEE Std 1293™-2018
(Revision of
IEEE Std 1293-1998)

IEEE Standard Specification Format Guide and Test Procedure for Linear Single-Axis, Nongyroscopic Accelerometers

Sponsor

Gyro and Accelerometer Panel
of the
IEEE Aerospace and Electronic Systems Society

Approved 23 October 2018

IEEE-SA Standards Board

Abstract: The specification and test requirements for a linear, single-axis, nongyroscopic accelerometer for use in inertial navigation, guidance, and leveling systems are defined. A standard specification guide and a compilation of recommended test procedures for such accelerometers are provided. Informative annexes are given on the various types of such accelerometers (force or pendulous torque rebalance with analog or digital output, vibrating beam, and micromechanical) and error effects, on filtering, noise, and transient analysis techniques, and on calibration and modeling techniques (multipoint tumble analysis, vibration and shock test analyses, and geophysical effects in inertial instrument testing).

Keywords: accelerometer, geophysical effects, IEEE 1293™, inertial instrument, inertial sensor, micromechanical accelerometer, pendulous accelerometer, power spectral density, specification, testing, vibrating beam accelerometer, vibration and shock

---

The Institute of Electrical and Electronics Engineers, Inc.
3 Park Avenue, New York, NY 10016-5997, USA

PDF: ISBN 978-1-5044-5524-4 STD23537
Print: ISBN 978-1-5044-5525-1 STDPD23537

Important Notices and Disclaimers Concerning IEEE Standards Documents

IEEE documents are made available for use subject to important notices and legal disclaimers. These notices and disclaimers, or a reference to this page, appear in all standards and may be found under the heading "Important Notices and Disclaimers Concerning IEEE Standards Documents." They can also be obtained on request from IEEE or viewed at http://standards.ieee.org/ipr/disclaimers.html.

Notice and Disclaimer of Liability Concerning the Use of IEEE Standards Documents

IEEE Standards documents (standards, recommended practices, and guides), both full-use and trial-use, are developed within IEEE Societies and the Standards Coordinating Committees of the IEEE Standards Association ("IEEE-SA") Standards Board. IEEE ("the Institute") develops its standards through a consensus development process, approved by the American National Standards Institute ("ANSI"), which brings together volunteers representing varied viewpoints and interests to achieve the final product. IEEE Standards are documents developed through scientific, academic, and industry-based technical working groups. Volunteers in IEEE working groups are not necessarily members of the Institute and participate without compensation from IEEE. While IEEE administers the process and establishes rules to promote fairness in the consensus development process, IEEE does not independently evaluate, test, or verify the accuracy of any of the information or the soundness of any judgments contained in its standards.

IEEE Standards do not guarantee or ensure safety, security, health, or environmental protection, or ensure against interference with or from other devices or networks. Implementers and users of IEEE Standards documents are responsible for determining and complying with all appropriate safety, security, environmental, health, and interference protection practices and all applicable laws and regulations.

IEEE does not warrant or represent the accuracy or content of the material contained in its standards, and expressly disclaims all warranties (express, implied and statutory) not included in this or any other document relating to the standard, including, but not limited to, the warranties of: merchantability; fitness for a particular purpose; non-infringement; and quality, accuracy, effectiveness, currency, or completeness of material. In addition, IEEE disclaims any and all conditions relating to: results; and workmanlike effort. IEEE standards documents are supplied "AS IS" and "WITH ALL FAULTS."

Use of an IEEE standard is wholly voluntary. The existence of an IEEE standard does not imply that there are no other ways to produce, test, measure, purchase, market, or provide other goods and services related to the scope of the IEEE standard. Furthermore, the viewpoint expressed at the time a standard is approved and issued is subject to change brought about through developments in the state of the art and comments received from users of the standard.

In publishing and making its standards available, IEEE is not suggesting or rendering professional or other services for, or on behalf of, any person or entity nor is IEEE undertaking to perform any duty owed by any other person or entity to another. Any person utilizing any IEEE Standards document, should rely upon his or her own independent judgment in the exercise of reasonable care in any given circumstances or, as appropriate, seek the advice of a competent professional in determining the appropriateness of a given IEEE standard.

IN NO EVENT SHALL IEEE BE LIABLE FOR ANY DIRECT, INDIRECT, INCIDENTAL, SPECIAL, EXEMPLARY, OR CONSEQUENTIAL DAMAGES (INCLUDING, BUT NOT LIMITED TO: PROCUREMENT OF SUBSTITUTE GOODS OR SERVICES; LOSS OF USE, DATA, OR PROFITS; OR BUSINESS INTERRUPTION) HOWEVER CAUSED AND ON ANY THEORY OF LIABILITY, WHETHER IN CONTRACT, STRICT LIABILITY, OR TORT (INCLUDING NEGLIGENCE OR OTHERWISE) ARISING IN ANY WAY OUT OF THE PUBLICATION, USE OF, OR RELIANCE UPON ANY STANDARD, EVEN IF ADVISED OF THE POSSIBILITY OF SUCH DAMAGE AND REGARDLESS OF WHETHER SUCH DAMAGE WAS FORESEEABLE.

Translations

The IEEE consensus development process involves the review of documents in English only. In the event that an IEEE standard is translated, only the English version published by IEEE should be considered the approved IEEE standard.

Official statements

A statement, written or oral, that is not processed in accordance with the IEEE-SA Standards Board Operations Manual shall not be considered or inferred to be the official position of IEEE or any of its committees and shall not be considered to be, or be relied upon as, a formal position of IEEE. At lectures, symposia, seminars, or educational courses, an individual presenting information on IEEE standards shall make it clear that his or her views should be considered the personal views of that individual rather than the formal position of IEEE.

Comments on standards

Comments for revision of IEEE Standards documents are welcome from any interested party, regardless of membership affiliation with IEEE. However, IEEE does not provide consulting information or advice pertaining to IEEE Standards documents. Suggestions for changes in documents should be in the form of a proposed change of text, together with appropriate supporting comments. Since IEEE standards represent a consensus of concerned interests, it is important that any responses to comments and questions also receive the concurrence of a balance of interests. For this reason, IEEE and the members of its societies and Standards Coordinating Committees are not able to provide an instant response to comments or questions except in those cases where the matter has previously been addressed. For the same reason, IEEE does not respond to interpretation requests. Any person who would like to participate in revisions to an IEEE standard is welcome to join the relevant IEEE working group.

Comments on standards should be submitted to the following address:

Secretary, IEEE-SA Standards Board
445 Hoes Lane
Piscataway, NJ 08854 USA

Laws and regulations

Users of IEEE Standards documents should consult all applicable laws and regulations. Compliance with the provisions of any IEEE Standards document does not imply compliance to any applicable regulatory requirements. Implementers of the standard are responsible for observing or referring to the applicable regulatory requirements. IEEE does not, by the publication of its standards, intend to urge action that is not in compliance with applicable laws, and these documents may not be construed as doing so.

Copyrights

IEEE draft and approved standards are copyrighted by IEEE under U.S. and international copyright laws. They are made available by IEEE and are adopted for a wide variety of both public and private uses. These include both use, by reference, in laws and regulations, and use in private self-regulation, standardization, and the promotion of engineering practices and methods. By making these documents available for use and adoption by public authorities and private users, IEEE does not waive any rights in copyright to the documents.

Photocopies

Subject to payment of the appropriate fee, IEEE will grant users a limited, non-exclusive license to photocopy portions of any individual standard for company or organizational internal use or individual, non-commercial use only. To arrange for payment of licensing fees, please contact Copyright Clearance Center, Customer Service, 222 Rosewood Drive, Danvers, MA 01923 USA; +1 978 750 8400. Permission to photocopy portions of any individual standard for educational classroom use can also be obtained through the Copyright Clearance Center.

Updating of IEEE Standards documents

Users of IEEE Standards documents should be aware that these documents may be superseded at any time by the issuance of new editions or may be amended from time to time through the issuance of amendments, corrigenda, or errata. A current IEEE document at any point in time consists of the current edition of the document together with any amendments, corrigenda, or errata then in effect.

Every IEEE standard is subjected to review at least every ten years. When a document is more than ten years old and has not undergone a revision process, it is reasonable to conclude that its contents, although still of some value, do not wholly reflect the present state of the art. Users are cautioned to check to determine that they have the latest edition of any IEEE standard.

In order to determine whether a given document is the current edition and whether it has been amended through the issuance of amendments, corrigenda, or errata, visit IEEE Xplore at http://ieeexplore.ieee.org/ or contact IEEE at the address listed previously. For more information about the IEEE-SA or IEEE's standards development process, visit the IEEE-SA Website at http://standards.ieee.org.

Errata

Errata, if any, for all IEEE standards can be accessed on the IEEE-SA Website at the following URL: http://standards.ieee.org/findstds/errata/index.html. Users are encouraged to check this URL for errata periodically.

Patents

Attention is called to the possibility that implementation of this standard may require use of subject matter covered by patent rights. By publication of this standard, no position is taken by the IEEE with respect to the existence or validity of any patent rights in connection therewith. If a patent holder or patent applicant has filed a statement of assurance via an Accepted Letter of Assurance, then the statement is listed on the IEEE-SA Website at http://standards.ieee.org/about/sasb/patcom/patents.html. Letters of Assurance may indicate whether the Submitter is willing or unwilling to grant licenses under patent rights without compensation or under reasonable rates, with reasonable terms and conditions that are demonstrably free of any unfair discrimination to applicants desiring to obtain such licenses.

Essential Patent Claims may exist for which a Letter of Assurance has not been received. The IEEE is not responsible for identifying Essential Patent Claims for which a license may be required, for conducting inquiries into the legal validity or scope of Patents Claims, or determining whether any licensing terms or conditions provided in connection with submission of a Letter of Assurance, if any, or in any licensing agreements are reasonable or non-discriminatory. Users of this standard are expressly advised that determination of the validity of any patent rights, and the risk of infringement of such rights, is entirely their own responsibility. Further information may be obtained from the IEEE Standards Association.

Participants

This standard represents a large-scale group effort. A total of 111 individuals attended 50 bimonthly meetings of the Gyro and Accelerometer Panel during preparation of this standard. The following individuals were members of the Gyro and Accelerometer Panel when the standard was first developed:

Sid Bennett, *Chair*

David Anderson
Michael E. Ash
Cleon H. Barker
Steve F. Becka
Joseph S. Beri
Stephen Bongiovanni
Pierre Bouniol
James Brewer
Herbert T. Califano
A. T. (Ted) Campbell*
Joseph J. D'Angello Jr.
George W. Erickson
Joseph Ficalora
Scott A. Finken
Thomas A. Fuhrman
Frank Garcia
Michael D. Hooser
Bert Katz
Jean-François Kiefer
Lalit Kumar
Kurt Lantz
Thomas Lear*
David D. Lynch
R. D. (Sam) Marquess
Harold D. Morris
Gerald E. Morrison*
Bart Morrow Jr.
Jay Murphy
Rex B. Peters*
Loren Richardson
Gerald L. Shaw
Phillip B. Simpson
Clifford O. Swanson*
Mohammad Tehrani
Leroy O. Thielman
Christopher V. Trainor
Akira Umeda
Bud J. Wimber*
David J. Winkel
Bruce R. Youmans

*Past Chair

A total of 62 individuals attended 30 bimonthly meetings of the Gyro and Accelerometer Panel during preparation of this standard. At the time this standard was completed, the Sensors Working Group had the following membership:

Austin Prach, *Chair*

Cleon H. Barker
Steve F. Becka
Jason Bingham
Timothy Buck
Calvin Burrell
Randall Curey
Harry Davis
Rayna DeMaster-Smith
George W. Erickson
Marius Gheorghe
Kamal Joshi
Jean-Francois Kieffer
Ken Marino
Edward Schlatter
Reese Sturdevant
David Syse
David Tarrant
Daniel Tazartes
Leroy O. Thielman
Margaret Trevino
Randy Wells
David J. Winkel
Bruce R. Youmans

The following members of the individual balloting committee voted on this standard. Balloters may have voted for approval, disapproval, or abstention.

Cleon H. Barker
Jason Bingham
Demetrio Bucaneg Jr.
Keith Chow
Randall Curey
Randall C. Groves
Werner Hoelzl
Jean-Francois Kieffer
Robert Robinson
Christopher Searles
Walter Struppler
Ganesh Subramanian
Daniel Tazartes
Leroy O. Thielman

Introduction

This introduction is not part of IEEE Std 1293-2018, IEEE Standard Specification Format Guide and Test Procedure for Linear Single-Axis, Nongyroscopic Accelerometers.

This standard is provided as a guide for the preparation of an accelerometer specification (Part I) and an accelerometer test procedure (Part II). The accelerometer considered in this standard uses a linear, single-axis, nongyroscopic acceleration sensor. The capture-loop, pickoff, oscillator, and readout electronics, when used, can be considered either as a part of the accelerometer or as separately provided by the user. The format was prepared by the Gyro and Accelerometer Panel of the Aerospace and Electronic Systems Society of the Institute of Electrical and Electronics Engineers (IEEE). It is intended to provide a common meeting ground of terminology and practice for manufacturers and users.

The user is cautioned not to overspecify; only those parameters that are required to guarantee proper performance in the specific application should be controlled. In general, the specification should contain only those requirements that can be verified by test or inspection. Parameters in addition to those given in this format are not precluded.

Blank spaces permit the insertion of specific parameter values and their tolerances. Brackets are used to enclose alternate choices of dimensional units, sign, axes, and so on. Boxed statements are included for information only and are not part of the specification format nor test procedure. The figures presented are to be used as a guide for the preparation of specific figures or drawings.

The annexes are informative and cover

— Typical block diagrams for accelerometer response
— The various types of accelerometers considered (including pendulous torque rebalance, vibrating beam, and micromechanical)
— Error effects
— Filtering, noise, and transient analysis techniques
— Calibration and modeling techniques (multipoint tumble analysis, vibration and shock test analyses, and geophysical effects in inertial instrument testing)

The following documents were used in the development of this standard:

IEEE/ASTM SI 10™-1997, Standard for Use of the International System of Units (SI): The Modem Metric System.

IEEE Std 260.1™-1993, American National Standard Letter Symbols for Units of Measurement.

IEEE Std 280™, IEEE Standard Letter Symbols for Quantities Used in Electrical Science and Electrical Engineering.

IEEE Std 315™-1975, IEEE Standard, American National Standard, Canadian Standard Graphic Symbols for Electrical and Electronics Diagrams (Including Reference Designation Letters).

IEEE Std 315A™, Supplement to IEEE Std 315.

IEEE Std 528™-1994, IEEE Standard for Inertial Sensor Terminology.

IEEE 100™, *The Authoritative Dictionary of IEEE Standards Terms*.

In this standard, the symbol *g* (italic) is used to denote an acceleration equal in magnitude to the local value of gravity at the test site. This symbol is thus distinguished from g (nonitalic), which is the standard symbol for gram. The standard value of gravity g_o is 9.806 65 m/s^2.

The accelerometer is used to provide an analog, digital, or frequency output that is a measure of acceleration or velocity increment, or both. An acceleration applied along the input axis of the acceleration sensor causes its proof mass to deflect. For open-loop accelerometers, the pickoff error signal caused by this motion is the measure of acceleration.

For force-rebalance accelerometers, the pickoff error signal is used in the electronics to produce a restoring force or torque. When static equilibrium is reached, the reaction force or torque of the proof mass to the average acceleration is balanced by the mean value of the restoring force or torque. The average rebalance current or pulse rate required to maintain this equilibrium condition is proportional to the average acceleration and provides the analog or digital output signal.

For vibrating beam accelerometers (VBAs), acceleration causes one resonator to increase in frequency (f_1) and the other resonator to decrease in frequency (f_2). The difference ($f_1 - f_2$) is a measure of the applied acceleration. The VBA difference frequency scale factor is the sum of the individual resonator scale factors. Thus, using the difference frequency observable in a dual-resonator VBA doubles the scale factor as well as rejects many common mode error effects.

In this standard, no distinction is made between input axis (IA) and input reference axis (IRA) [similarly between output axis (OA) and output reference axis (ORA) and pendulous axis (PA) and pendulous reference axis (PRA)]. When dealing with the accelerometer, sensor physics IA, OA, and PA would typically be used. When orienting the accelerometer, package IRA, ORA, and PRA would typically be used. In some cases, it may be desirable to attempt to orient the IA, OA, and/or PA by observing a signal (such as the output or a reference voltage). Even in these cases, the IRA, ORA, and/or PRA can be used as a check if the approximate orientation between IA, OA, and PA and the IRA, ORA, and PRA is known. In all cases, users should determine which set of axes is appropriate for their application.

Contents

1. Overview 14
1.1 Scope 14
1.2 Purpose 14
1.3 Document structure 14

2. Normative references 15

Part I—Specification format 15

3. Overview 15
3.1 Scope 15
3.2 Purpose 16

4. Applicable documents 16
4.1 Specifications 17
4.2 Standards 17
4.3 Drawings 17
4.4 Bulletins 17
4.5 Other publications 17

5. Requirements 17
5.1 Description 17
5.2 General requirements 20
5.3 Performance 21
5.4 Mechanical requirements 38
5.5 Electrical and magnetic requirements 42
5.6 Environmental requirements 46
5.7 Reliability 49

6. Quality assurance 49
6.1 Classification of tests 50
6.2 Acceptance tests 52
6.3 Qualification tests 54
6.4 Reliability tests 54
6.5 Test conditions and equipment 55
6.6 Test methods 55
6.7 Data submittal 58

7. Preparation for delivery 58

8. Notes 58
8.1 Intended use 58
8.2 Ordering data 58
8.3 Model equation 58

Part II—Test procedure 63

9. Test procedure overview 63

10. Description 63

11. Test conditions and equipment ... 63
11.1 Standard test conditions ... 63
11.2 Test equipment ... 65

12. Test procedure ... 68
12.1 Test setup ... 68
12.2 Accelerometer nonoperating tests ... 69
12.3 Accelerometer operating tests ... 74
12.4 Electromagnetically torqued pendulous accelerometer tests ... 105
12.5 VBA tests ... 115
12.6 Micromechanical accelerometer tests ... 117
12.7 Life tests ... 121
12.8 Reliability tests ... 123
12.9 Environmental tests ... 124

Part III—Accelerometer descriptions ... 128

Annex A (informative) Accelerometer dynamic block diagrams ... 128
A.1 Introduction ... 128
A.2 Open-loop operation ... 128
A.3 Closed-loop operation ... 129
A.4 Open-loop operation of closed-loop accelerometer ... 130
A.5 Operation with voltage-to-frequency conversion ... 130
A.6 Operation with digital capture loop ... 131
A.7 Accuracy of capture-loop readout ... 131

Annex B (informative) Digital accelerometers and comments concerning their test methods ... 132
B.1 Introduction ... 132
B.2 Description of commonly encountered digital output formats ... 132
B.3 Comments concerning test methods associated with digital instruments ... 134

Annex C (informative) Characteristics of pendulous accelerometers ... 137
C.1 Design principles ... 137
C.2 Applications ... 137
C.3 Error sources ... 138
C.4 Trade-offs ... 143
C.5 Environmental effects ... 144
C.6 Testing ... 144
C.7 Special requirements in the specification ... 144
C.8 Advantages and disadvantages ... 145

Annex D (informative) Overview of the characterization and use of the VBA ... 146
D.1 Introduction ... 146
D.2 Historical background ... 146
D.3 VBA—Theory of operation ... 147
D.4 VBA signal processing ... 151
D.5 VBA error sources ... 155
D.6 Related developments ... 159

Annex E (informative) VBA resonator frequency as a function of applied acceleration ... 160
E.1 Geometry and elastic properties of vibrating beam ... 160
E.2 Square-root relationship derived from energy considerations ... 161
E.3 Direct frequency versus force relation ... 164
E.4 Frequency versus force numerical evaluation ... 169
E.5 Comparison of fit coefficients and square-root Taylor coefficients ... 171

Annex F (informative) Micromechanical accelerometers 173
F.1 Micromachining 173
F.2 Micromachined silicon accelerometer—flexured-mass configurations 173
F.3 Micromachined silicon VBAs 183

Annex G (informative) Outline of error sources in accelerometers...188
G.1 Introduction 188
G.2 Sensor characterization by mechanization 188
G.3 Typical sensor characterization by manufacturing process..189
G.4 Error categories..189
G.5 Sensor physics 190

Part IV—Filtering, noise, and transient analyses 192

Annex H (informative) Digital filtering 192
H.1 Types of filtering and decimation 192
H.2 Rectangular filtering 193
H.3 Triangular filtering...193
H.4 Higher order filtering 194

Annex I (informative) Noise characterization 195
I.1 Stochastic processes 195
I.2 Autocorrelation function of a stochastic process...195
I.3 Estimation of the autocorrelation function 196
I.4 Power spectral density (PSD) of a stationary stochastic process..197
I.5 Estimation of the PSD 198
I.6 Numerical evaluation and plotting of the PSD 202
I.7 Characteristic PSD noise slopes 203
I.8 Characteristic Allan variance noise slopes 207
I.9 Estimation of Markov noise parameters...208

Annex J (informative) Characterization of transient behavior 213
J.1 Types of transient behavior...213
J.2 Second-order ordinary differential equation transient..213
J.3 Exponential, square root, and logarithmic transients 214
J.4 Estimation of transient parameters...216

Part V—Calibration and modeling techniques 217

Annex K (informative) Calibrating accelerometer model coefficients from static multipoint tumble data.217
K.1 Multipoint tumble test and analysis procedures...217
K.2 Model equation for multipoint tumble analysis 221
K.3 Multipoint tumble analysis with a single accelerometer observable...227
K.4 Multipoint tumble analysis with dual orthogonal accelerometer observables 233
K.5 Multipoint tumble analysis with orthogonal accelerometer magnitude-squared-of-*g* observable ...235
K.6 Least-squares maximum likelihood estimation..236

Annex L (informative) Vibration test equipment, test procedures, and analysis techniques 242
L.1 Test equipment and test fixtures...242
L.2 Test scenarios 245
L.3 Error sources 246
L.4 Test instrumentation and procedures..247
L.5 General comments on analysis techniques 248
L.6 Calibration of nonlinear coefficients from vibration along different instrument axes 249
L.7 Summary 259

Annex M (informative) Geophysical effects in inertial instruments testing 260
M.1 Introduction 260
M.2 Seismic environment 260
M.3 Tilt and azimuth variations 261
M.4 Effect of lunar–solar earth tides 261
M.5 Effect of ocean tides 263
M.6 Variations in earth rotation 264

Annex N (informative) Bibliography 266

IEEE Standard Specification Format Guide and Test Procedure for Linear Single-Axis, Nongyroscopic Accelerometers

1. Overview

1.1 Scope

The specification and test requirements for a linear, single-axis, nongyroscopic accelerometer for use in inertial navigation, guidance, and leveling systems are defined. A standard specification format guide and a compilation of recommended test procedures for such accelerometers are provided. Informative annexes are given on the various types of such accelerometers (force or pendulous torque rebalance with analog or digital output, vibrating beam, and micromechanical) and error effects, on filtering, noise, and transient analysis techniques, and on calibration and modeling techniques (multipoint tumble analysis, vibration and shock test analyses, and geophysical effects in inertial instrument testing).

1.2 Purpose

A standard specification format guide is provided, along with a compilation of recommended test procedures for the preparation of a linear, single-axis, nongyroscopic accelerometer specification. These test procedures are derived from those currently in use in the industry.

1.3 Document structure

This standard consists of five parts: The first two parts are in the normative portion of the standard, and the other three are in the informative portion. Part I is a specification format guide for the preparation of a linear single-axis, nongyroscopic accelerometer specification. Part II is a compilation of recommended procedures for testing a linear single-axis, nongyroscopic accelerometer. Part III contains descriptions of various types of accelerometers. Part IV discusses filtering, noise, and transient analysis. Part V contains calibration and modeling techniques.

2. Normative references

The following referenced documents are indispensable for the application of this document (i.e., they must be understood and used, so each referenced document is cited in text and its relationship to this document is explained). For dated references, only the edition cited applies. For undated references, the latest edition of the referenced document (including any amendments or corrigenda) applies.

ANSI/ASQ Z1.4, Sampling Procedures and Tables for Inspection by Attributes.[1]

IEEE Std 836™, IEEE Recommended Practice for Precision Centrifuge Testing of Linear Accelerometers.[2, 3]

IEEE Std 1332™, IEEE Standard Reliability Program for the Development and Production of Electronic Products.

ISO 5347, Parts 1–21 and Part 23, Methods for the Calibration of Vibration and Shock Pick-Ups.[4]

MIL-STD-461, Requirements for the Control of Electromagnetic Interference Characteristics of Subsystems and Equipment.[5]

MIL-STD-810, Environmental Engineering Considerations and Laboratory Tests.

MIL-STD-1916, DoD Preferred Methods for Acceptance of Product.

MIL-STD-2073-1, DoD Standard Practice for Military Packaging.

Part I—Specification format

3. Overview

This specification defines the requirements for a linear, single-axis, nongyroscopic accelerometer. The accelerometer is used as a sensing element to provide an electrical signal proportional to acceleration or velocity change with a transfer function that is nominally low pass (rather than bandpass). The output is [an analog voltage, an analog current, a binary pulse train, a ternary pulse train, pulse width modulated, a frequency output, ______] representing [acceleration, velocity change].

This specification defines not only the performance requirements of an inertial accelerometer as a unique device but also its specific variational but repeatable and predictable performance parameters.

3.1 Scope

This specification defines requirements for [accelerometer type].

[1] ANSI publications are available from the American National Standards Institute (http://www.ansi.org/).
[2] IEEE publications are available from the Institute of Electrical and Electronics Engineers (http://standards.ieee.org/).
[3] The IEEE standards or products referred to in Clause 2 are trademarks owned by the Institute of Electrical and Electronics Engineers, Incorporated.
[4] ISO publications are available from the International Organization for Standardization (http://www.iso.org/) and the American National Standards Institute (http://www.ansi.org/).
[5] MIL publications are available from the U.S. Department of Defense (http://quicksearch.dla.mil/).

This specification format guide and test procedure standard applies to force-rebalance accelerometers (pendulous or translational proof mass), vibrating beam accelerometers (VBAs), and micromechanical accelerometers (see 5.1).

All accelerometers have biases, scale factors, misalignments, nonlinearities, noise characteristics, and other parameters. Many of the specification requirements and verification test methods for these parameters; their stabilities; their temperature, magnetic, and other sensitivities; the accelerometer behavior through and across vibration, shock, and other environments; and the accelerometer lifetime and reliability are independent of the accelerometer type. Requirements and tests that are specific to a particular accelerometer type are described separately.

Only the clauses applicable to the given accelerometer type should be used.

This specification is not intended to define requirements for the pendulous integrating gyroscopic accelerometer (PIGA) or for the specific force integrating receiver (SFIR). These high-precision single degree-of-freedom (DOF) accelerometers use gyroscopic precessional torque to rebalance the specific force effect of nongravitational acceleration acting on a pendulous proof mass on the gyro float.

This specification also does not apply to devices (such as seismometers or open-loop piezoelectric accelerometers) that measure ac rather than low-pass and dc accelerations. Gravimeters are also not considered.

3.2 Purpose

This specification describes the design and performance requirements for ______ [model number, part number, change letter (if any), other identification], manufactured by ______ [name, address].

4. Applicable documents

The following documents form a part of the specification to the extent specified herein. For dated documents, only the edition cited applies. For undated documents, the latest edition of the document (including any amendments, change notices, etc.) applies. In the event of a conflict between this document and the listed documents, this document shall govern.

Give the identification number, title, date of issue, and revision letter of each document referenced in the completed specification.

4.1 Specifications

4.1.1 Government

4.1.2 Industry/technical

4.1.3 Company

4.2 Standards

4.2.1 Government

4.2.2 Industry/technical

4.2.3 Company

4.3 Drawings

4.3.1 Government

4.3.2 Industry/technical

4.3.3 Company

Figure 1, Figure 3, and Figure 4 are conceptual examples of the types of drawings that might be delivered with an accelerometer.

4.4 Bulletins

4.4.1 Government

4.4.2 Industry/technical

4.4.3 Company

4.5 Other publications

Other applicable documents should be listed under appropriate subclauses.

5. Requirements

5.1 Description

The accelerometer shall comprise a single-axis, nongyroscopic acceleration sensor [operating, to be operated] with [its own, user-supplied] electronics.

Figure 1a, Figure 1b, and Figure 1c apply to pendulous proof-mass accelerometers. The forcer in Figure 1a is called a *torquer*. The figures must be appropriately modified for a translational proof-mass accelerometer.

Torque-rebalance, capture-loop electronics and/or pickoff electronics are shown in Figure 1a. VBA oscillator electronics are shown in Figure 1b and Figure 1c. The accelerometer may employ a temperature sensor for thermal modeling, control, or monitoring.

The dashed lines in Figure 1a, Figure 1b, and Figure 1c enclose the sensor part of the accelerometer, which responds to the acceleration input. The term "seismic system" is sometimes used in place of the term "acceleration sensor."

The electronics outside the dotted lines used to generate the accelerometer output and the temperature output, if needed, may be self-contained within or separate from the accelerometer package. The user-supplied electronics may include such items as power conditioner, capture electronics, output signal conditioner, temperature controller, reference clock, and test points.

The sensor may employ stops to limit proof-mass displacement.

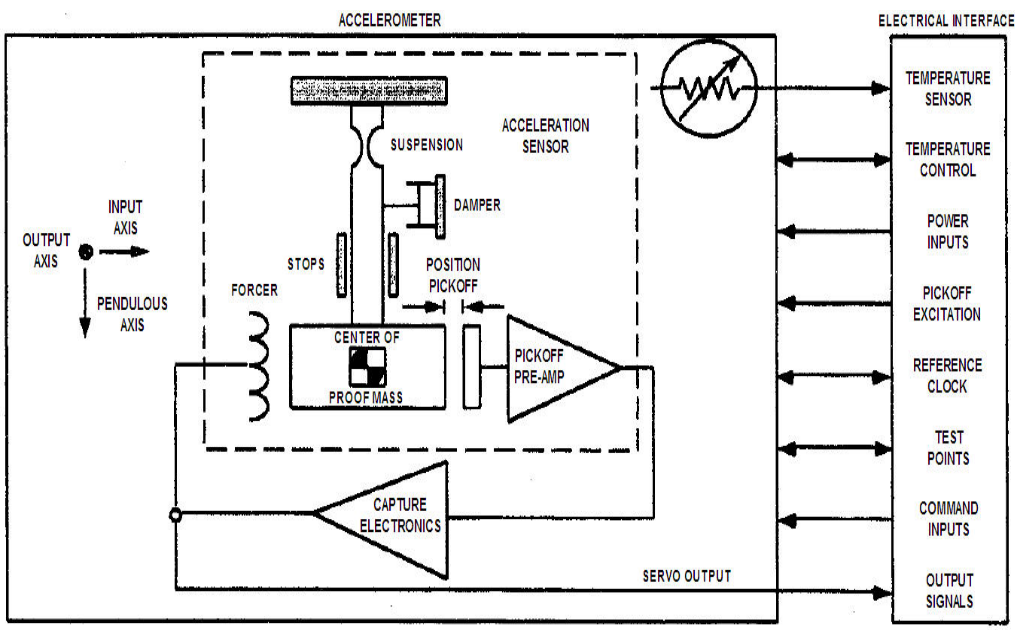

Figure 1a—Diagram of torque-rebalance accelerometer system

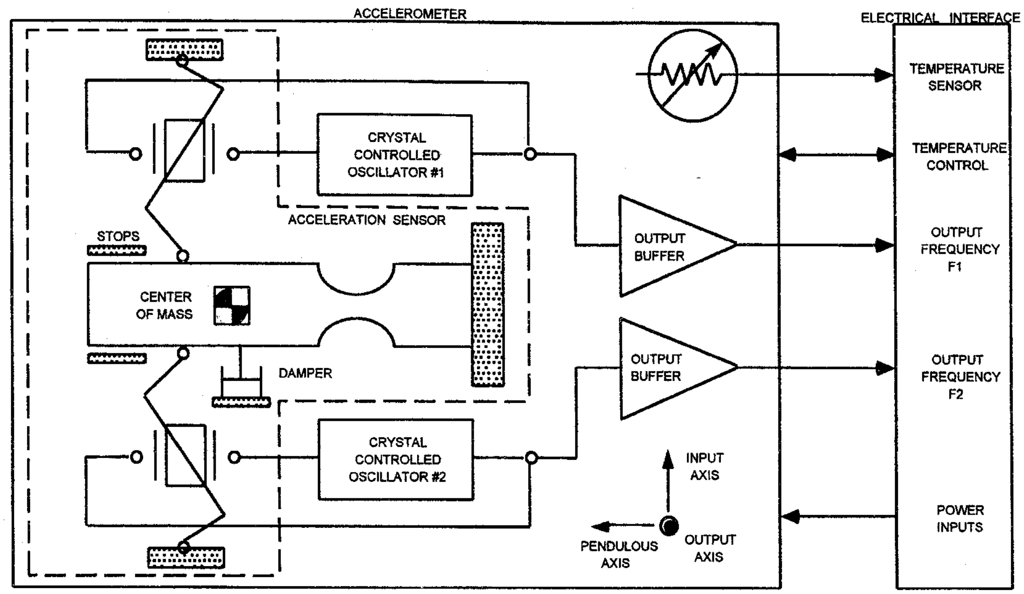

Figure 1b—Diagram of single proof-mass VBA system

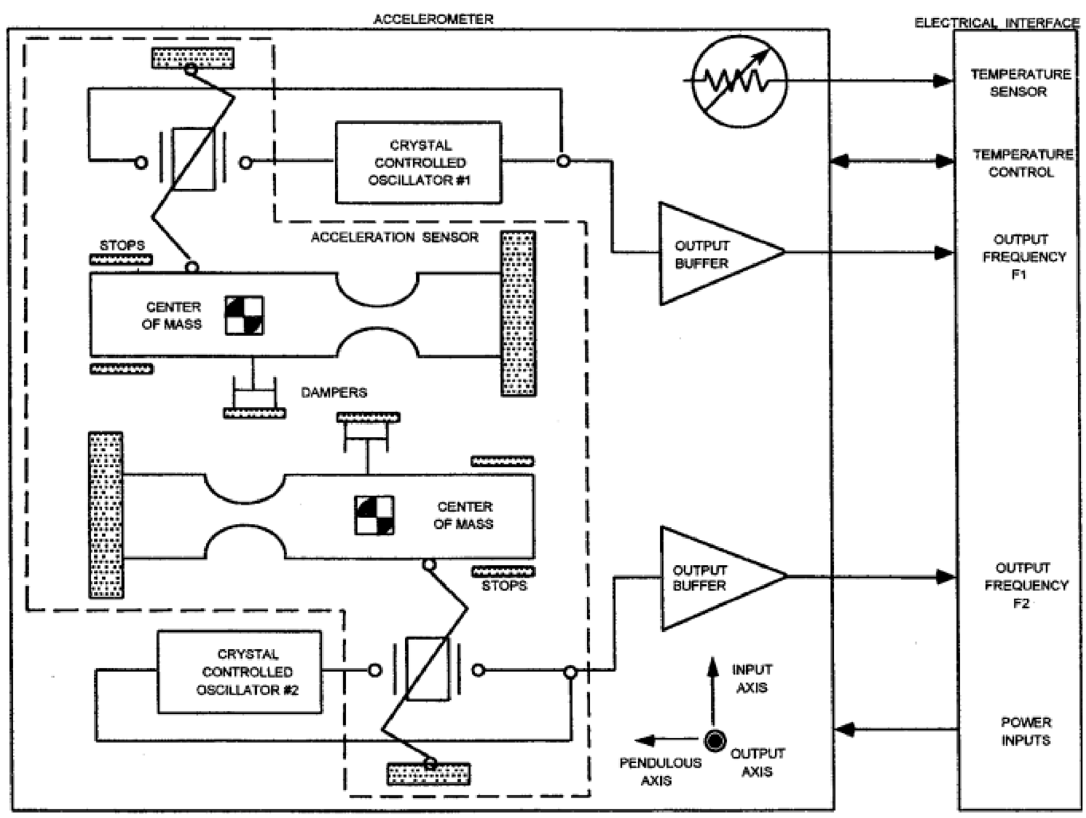

Figure 1c—Diagram of dual proof-mass VBA system

The torque-rebalance capture-loop electronics in Figure 1a may be analog-torque feedback or pulsed-torque feedback, providing as an output either an analog voltage signal proportional to acceleration or a pulse-train, each pulse representing an increment of velocity gained or lost. The method of pendulum torquing or proof-mass forcing may be specified (for example, binary pulse, ternary pulse, pulse-width modulation, analog, or analog converted into pulse-train output by use of a voltage- or current-to-frequency converter).

The pickoff could be electromagnetic, capacitive, optical, or piezoresistive.

Figure 1a applies to a closed-loop micromechanical accelerometer as well as to a macro-sized pendulous accelerometer, although electrostatic capacitive forcing might be used in the former rather than the electromagnetic torquing commonly used in the latter.

An open-loop micromechanical accelerometer dispenses with the servoed capture-loop electronics and measures acceleration by the movement of the proof mass as restrained by the suspension flexure(s). The position pickoff could be capacitive, or the movement of the proof mass could be measured piezoresistively from the strain in the flexure(s).

Open-loop piezoelectric accelerometers, which measure acceleration by the voltage generated by the strain in a piezoelectric proof-mass support, are not considered in this document because leakage of the piezoelectrically generated charge restricts these devices to measuring ac rather than dc accelerations.

VBAs are by their nature open-loop devices as far as proof-mass movement is concerned. That movement is mostly restrained by the stiffness of the crystal resonators (usually piezoelectric quartz or silicon). Usually two crystal resonators are kept vibrating at their resonant frequency by oscillator circuits with a piezoelectric drive for quartz and a capacitive drive for silicon.

The resonators are mounted in a push–pull mode with a single proof mass (Figure 1b) or separate proof masses (Figure 1c). Under acceleration, one resonator goes into tension and increases in frequency and the other goes into compression and decreases in frequency. The measure of acceleration is the difference frequency, in order to obtain improved linearity and lower sensitivities to clock errors, physical environment, and aging effects (see Annex D for more details). The oscillator electronics are usually self-contained within the accelerometer package.

The VBA acronym (see D.3) is commonly applied to all vibrating resonator accelerometers, even if the resonator has other-than-beam geometry (e.g., a double-ended tuning fork).

5.2 General requirements

5.2.1 Precedence

In the event of conflict among the purchase agreement, this specification, and other documents referred to herein, the order of precedence shall be as follows:

a) Purchase agreement
b) This specification and its applicable drawings
c) Other applicable documents

List other applicable documents in order of precedence; see Clause 2 and Clause 4.

5.2.2 Deliverables

The deliverable item includes the serialized inertial accelerometer plus any accompanying serialized numerical data representing the predictable parameters, such as bias, scale factor, scale factor nonlinearity, and misalignment as defined in this specification.

5.2.3 Other

The application of this accelerometer may require performance parameters defining bias, scale factor, scale factor nonlinearity, and input axis (IA) misalignment with a degree of accuracy not achievable without analytical modeling based on *a priori* knowledge of repeatable variation of these parameters. Bias, scale factor, and IA misalignment may be modeled as polynomial functions of the internal temperature indication of the sensor, whereas scale factor nonlinearity may be modeled as a function of indicated acceleration independent of temperature.

List other applicable general requirements.

5.3 Performance

The following clauses are used to specify the performance of a complete accelerometer or an acceleration sensor only, with 5.3.24 through 5.3.29.2 being applicable to an acceleration sensor only. Table 3 lists the test procedure clauses for verifying the 5.3 through 5.7 requirements clauses.

If modeling is necessary to meet performance requirements, then during the acceptance testing of each accelerometer for this application, the bias, scale factor, two components of the IA misalignment, nonlinearities, and other parameters if necessary shall be determined over the operating temperature range. The output of the temperature sensor as well as the ambient temperature shall be determined at each temperature data point. The form of the model and the number and precision of the coefficients shall be mutually agreed to by the producer and the user. The minimum model requirements will be shown in 8.3. Each serialized accelerometer shall be accompanied by serialized coefficients as defined in this specification. These serialized items shall be a matched set reflecting proven test data derived from acceptance testing and calibration of the matched set of coefficients. In the performance paragraphs affected by the need for modeling, each paragraph shall include both the uncompensated error allowable and the magnitude of the allowable error after compensation.

5.3.1 General

When tested with its capture or other electronics, the acceleration sensor shall comply with the performance requirements of this specification before, during (if applicable), and after exposure to the defined combinations of environments specified in 5.6.

Turn-on transients may affect accelerometer performance, and this issue shall be addressed as required for the specific application. For these cases, power-on time and other test conditions prior to taking data should be specified. Define critical combinations of environments in 5.6.

5.3.2 Input range

The minimum input range shall be ± ___________ [m/s^2, ft/s^2, _____].

The specified input range shall be large enough to include the maximum (peak) translational acceleration combined with the maximum response to vibration falling within the bandwidth of the sensor. The input range need not be symmetrical about the null.

5.3.3 Overload capacity

The accelerometer shall perform to all specification requirements after an acceleration of __________ [m/s^2, ft/s^2, _____] has been applied along the __________ [axis, axes] for __________ s a total of __________ times.

5.3.4 Accelerometer temperature

The accelerometer may be specified for thermally controlled applications at a specified temperature or for operation over a wide range of temperatures.

5.3.4.1 Operating temperature

The operating temperature shall be [__________ ± ___________ °C, __________ °C minimum to __________ °C maximum] at point ____________ in the accelerometer.

The point within the accelerometer at which the operating temperature range is specified could be at the mounting flange or at the location of the accelerometer’s temperature sensor (if any).

For temperature-controlled operation, the mounting flange temperature and surrounding ambient temperature (unless the accelerometer were surrounded with insulation with the heat flow path out through the mounting flange) could be specified, with the interior control set point temperature also specified (which is particularly important for fluid-filled or floated accelerometers).

5.3.4.2 Temperature sensor

A temperature sensor shall be provided [on, within] the accelerometer to indicate the accelerometer temperature over the operating range. The temperature sensor output shall be definable by a model equation that permits recovery of accelerometer temperature to an accuracy of ± ___________ °C. The form of the temperature model and the number and precision of the coefficients shall be mutually agreed to.

For thermally controlled applications, it may be appropriate to specify the absolute value and tolerance of the sensor output and its temperature coefficient at the nominal operating temperature.

For temperature-compensated applications, instead of converting the temperature sensor output in, for example, volts to °C for compensating the accelerometer output as a function of °C, the calibration of the compensation model could be in terms of temperature sensor output directly (i.e., volts in this example). In this case, a precise calibration of the relationship between temperature sensor output and °C would be unnecessary.

5.3.5 Scale factor

5.3.5.1 Absolute value

The scale factor K_1 shall be _____± _____ [V, mA, p/s, Hz]/[m/s^2, ft/s^2, _____], measured to an uncertainty of _____ [%, ppm], under the standard test conditions of 11.1.

When verifying accelerometer scale factor via a tumble test and tracking its variation over time or over changes in temperature and other environments, it is natural to express the scale factor in terms of the local acceleration due to gravity. Alternatively, the scale factor could be expressed in terms of absolute units, such as m/s^2.

When expressing the scale factor in terms of the local acceleration due to gravity, if the accelerometer is used in a location that is different than the calibration site or scale factors are measured on the same accelerometer at different test sites, then the scale factor has to be expressed in terms of g_o (standard gravity) or m/s^2.

The scale factor K_1 when expressed in terms of p/s may be used to obtain velocity quantization.

When K_1 is expressed in (p/s)/g

$$\text{velocity quantization in (m/s)/p} = \frac{\text{local value of gravity in (m/s}^2)/g}{K_1 \text{ in (p/s)}/g}$$

or when expressed in (p/s)/(m/s^2)

$$\text{velocity quantization in (m/s)/p} = \frac{1}{K_1 \text{ in (p/s)}/(m/s^2)}$$

The VBA difference frequency scale factor is the sum of the individual resonator scale factors. Thus, using the difference frequency observable in a dual-resonator VBA doubles the scale factor as well as rejects many common mode error effects. Typical VBA scale factor units are Hz/g or Hz/(m/s^2).

5.3.5.2 Asymmetry

The difference between the scale factor measured with positive applied acceleration and with negative applied acceleration shall not exceed ± ___________ [%, ppm] of the average scale factor for both positive and negative accelerations.

Separate scale factors may be supplied for positive and negative applied accelerations to better define scale factor asymmetry (see 8.3).

5.3.5.3 Short-term stability

The standard deviation of the scale factor from its mean value over a period of __________ [s, min, h, d] of continuous operation under constant conditions shall be less than ___________ [%, ppm].

Alternative means of specifying stability may be used, such as curve fitting for trend determination, or frequency domain analysis.

5.3.5.4 Long-term stability

The least-squares straight line slope of the scale factor over a period of ___________ [h, d, yr] of continuous operation measured under constant conditions shall be less than ___________ [%, ppm]/[h, d, yr]. The standard deviation of the scale factor data points from the best fit line shall be less than __________ [%, ppm].

Other criteria for establishing stability may be used, such as the root mean square (rms) about the mean, or frequency domain analyses. Stability tests have constant conditions between calibrations, whereas repeatability tests have temperature cycles or other variations between calibrations.

5.3.5.5 Repeatability

The standard deviation of the scale factor from the mean of measurements taken under constant conditions shall be less than ___________ [%, ppm]. Between successive measurements, the accelerometer shall be [heated, cooled] to __________ °C for at least ___________h.

> Other environmental exposures may be substituted or added to the temperature environment specified. In addition, combinations of various successive environments (e.g., vibration, shock, temperature, remount, and power interrupt of specified duration) may be specified. Sufficient time should be allotted to attain thermal equilibrium before making a measurement. Other conditions for repeatability may be specified, such as power-off time with the accelerometer maintained at some fixed temperature.
>
> Alternative means of specifying repeatability may be used, for example, rms deviation about the first day mean, or peak-to-peak deviation.

5.3.5.6 Sensitivity

The absolute value of the sensitivity coefficients of scale factor to variations from the standard test conditions of 11.1 shall not exceed the limits listed as follows:

a) Input excitation voltage(s): ___________ [%, ppm]/V

b) Input excitation frequency(ies): __________ [%, ppm]/Hz

c) Operating temperature: ___________ [%, ppm]/°C

d) Temperature gradient: ___________ [%, ppm]/Δ°C

e) Temperature rate of change: ___________ [%, ppm]/(°C/min)

f) External magnetic induction [ac, dc, or both]: ___________ [%, ppm]/[mT, G] per axis

g) Pressure: ___________ [%, ppm]/Pa

> One of several methods of curve fitting (such as least-squares straight line or polynomial fit) should be specified to determine the value of each sensitivity coefficient since the scale factor may not be a linear function of the input variable (see 12.3.11).

> An accelerometer could have one or several input dc or ac voltage excitations, with or without internal regulation. The sensitivity of the accelerometer output to independent variations in each of these voltages and in the frequency of each ac input voltage (such as for a pickoff excitation) must meet these requirements.
>
> Tesla (Wb/m^2 = V·s/m^2 in SI units) and gauss (10^{-4} tesla in cgs electromagnetic units) are units of magnetic induction B. The relation between B in tesla and the magnetic field H in A/m in an isotropic homogeneous medium is $B = \mu H$, where μ is the permeability of the medium. The permeability of empty space is $\mu_0 = 4\pi \times 10^{-7}$ H/m in SI units. In the cgs electromagnetic system of units in which B is measured in gauss, the permeability of empty space is $\mu_0 = 1$, so that $B = H$, where H has units of oersteds. Hence, magnetic induction sensitivity per gauss has often been referred to as magnetic field sensitivity.

5.3.6 Nonlinearity

The absolute values of the second-order nonlinearity coefficient K_2 and the third-order nonlinearity coefficient K_3 shall be less than __________ [(m/s^2)/(m/s^2)^2, _____] and ___________ [(m/s^2)/(m/s^2)^3, _____], respectively. The absolute value of the odd quadratic coefficient K_{oq} shall be less than ___________ [(m/s^2)/(m/s^2)^2, _____].

The standard deviation of the residuals shall be less than ______ [m/s^2, ft/s^2, ______].

The K_2, K_{oq}, and K_3 coefficients are also commonly expressed in g/g^2, g/g^2 and g/g^3, respectively.

A simpler means of specifying nonlinearity for lesser accuracy accelerometers is to place limits on composite error as a function of input acceleration, that is, what is commonly known as an envelope specification.

The simplest envelope is to specify that the maximum error over the operating range is a specified percentage of the accelerometer full-span output, especially for lesser accuracy accelerometer applications where it is not intended to compensate for accelerometer nonlinearities that meet the specifications.

Acceleration nonlinearities typically arise from structural compliance. Changes in accelerometer temperature that occur under acceleration (such as due to varying current through an electromagnetic torquer) could manifest themselves as an apparent acceleration nonlinearity. The maximum such effect could be required to be less than the nonlinearity requirement, or the heating could be regarded as a separate temperature sensitivity problem with compensation using temperature sensor measurements if possible.

5.3.7 Bias

5.3.7.1 Absolute value

The absolute value of bias K_0 shall not exceed ___________ [m/s^2, ft/s^2, _____], measured to an uncertainty of ___________ [m/s^2, ft/s^2, _____], under the standard test conditions of 11.1.

5.3.7.2 Asymmetry

The difference between the bias measured with positive applied acceleration and with negative applied acceleration shall not exceed ___________ [m/s^2, ft/s^2, _____].

Separate biases may be supplied for positive and negative applied accelerations to define bias asymmetry better (see 8.3).

5.3.7.3 Short-term stability

The standard deviation of the bias from its mean value over a period of [s, min, h, d] of continuous operation shall be less than ____________ [m/s^2, ft/s^2, _____].

Alternative means of specifying stability may be used, such as curve fitting for trend determination or frequency domain analysis.

5.3.7.4 Long-term stability

The least-squares straight line slope of the bias over a period of ___________ [h, d, yr] of continuous operation, measured under constant conditions, shall be less than ___________ [m/s^2, ft/s^2, _____]/[h, d, yr]. The standard deviation of the bias data points from the best fit line shall be less than ___________ [m/s^2, ft/s^2, _____].

Other criteria for establishing stability may be used, such as the rms about the mean or frequency domain analyses. Stability tests have constant conditions between calibrations, whereas repeatability tests have temperature cycles or other variations between calibrations.

5.3.7.5 Repeatability

The standard deviation of the bias from the mean of __________ measurements taken under constant conditions shall be less than __________ [m/s^2, ft/s^2, _____]. Between successive measurements, the accelerometer shall be [heated, cooled] to __________ °C for at least ___________ h.

Other environmental exposures may be substituted or added to the temperature environment specified. In addition, combinations of various successive environments (e.g., vibration, shock, temperature, remount, power interrupt of specified duration) may be specified. Sufficient time should be allotted to attain thermal equilibrium before making a measurement. Other conditions for repeatability may be specified, such as power-off time with the accelerometer maintained at some fixed temperature. Alternative means of specifying repeatability may be used, for example, rms deviation about the first day mean or peak-to-peak deviation.

5.3.7.6 Sensitivity

The absolute value of the sensitivity coefficients of the bias to variations from the standard test conditions of 11.1 shall not exceed the limits listed as follows:

a) Input excitation voltage(s): ___________ [m/s^2, ft/s^2, _____]/V
b) Input excitation frequency(ies): __________ [m/s^2, ft/s^2, _____]/Hz
c) Operating temperature: ___________ [m/s^2, ft/s^2, _____]/°C
d) Temperature gradient: ___________ [m/s^2, ft/s^2, _____]/Δ°C
e) Temperature rate of change: ___________ [m/s^2, ft/s^2, _____]/°C/min)
f) External magnetic induction [ac, dc, or both]: ___________ [m/s^2, ft/s^2, _____]/[mT, G, _____] per axis
g) Pressure: ___________ [m/s^2, ft/s^2, _____]/Pa

One of several methods of curve fitting (such as least-squares straight line or polynomial fit) should be specified to determine the value of each sensitivity coefficient since the bias may not be a linear function of the input variable (see 12.3.11).

5.3.8 IA misalignment

Only IA misalignment components about pendulous axis (PA) and output axis (OA) are considered because misalignments of the other axes about IA do not have a material effect on the performance of a single-axis accelerometer.

5.3.8.1 About pendulous axis (PA)

The absolute value of the IA misalignment about the PA, δ_p, shall be less than __________ [μrad, mrad, ″, °], measured to an uncertainty of __________ [μrad, mrad, ″, °], under the standard test conditions of 11.1.

5.3.8.2 About output axis (OA)

The absolute value of the IA misalignment about the OA, δ_o, shall be less than ___________ [μrad, mrad, ″, °], measured to an uncertainty of ___________ [μrad, mrad, ″, °], under the standard test conditions
of 11.1.

Since misalignment angles (δ_o, δ_p) are typically small, an alternative method is to specify the total misalignment angle using small angle approximation as follows:

$$\delta_t = \sqrt{\delta_o^2 + \delta_p^2}$$

5.3.8.3 Short-term stability

The standard deviation of the two IA misalignment angles from their mean values over a period of ___________ [s, min, h, d] of continuous operation and measured under constant conditions shall be less than ___________ [µrad, mrad, ″, °].

Alternative means of specifying stability may be used, such as curve fitting for trend determination or frequency domain analysis.

5.3.8.4 Long-term stability

The least-squares best fit slope of the IA misalignment angle data points over a period of __________ [h, d, yr] shall be less than ___________ [µrad, mrad, ″, °]/[h, d, yr]. The standard deviation of the misalignment angle data points from the best fit line shall be less than __________ [µrad, mrad, ″, °].

Other criteria for establishing stability may be used, such as the rms about the mean or frequency domain analyses. Stability tests have constant conditions between calibrations, whereas repeatability tests have temperature cycles or other variations between calibrations.

5.3.8.5 Repeatability

The standard deviation of the IA misalignment angles from the mean of ___________ measurements taken under constant conditions shall be less than ___________ [µrad, mrad, ″, °]. Between successive measurements, the accelerometer shall be [heated, cooled] to ___________ °C for at least __________ h.

Other environmental exposures may be substituted or added to the temperature environment specified. In addition, combinations of various successive environments (e.g., vibration, shock, temperature, remount, and power interrupt of specified duration) may be specified. Sufficient time should be allotted to attain thermal equilibrium before making a measurement. Other conditions for repeatability may be specified, such as power-off time with the accelerometer maintained at some fixed temperature.

Alternative means of specifying repeatability may be used, for example, rms deviation about the first day mean or peak-to-peak deviation.

5.3.8.6 Sensitivity

The absolute value of the sensitivity coefficients of the IA misalignments to variations from the standard test conditions of 11.1 shall not exceed the limits listed as follows:

a) Input excitation voltage(s): ___________ [µrad, ″]/V

b) Input excitation frequency(ies): __________ [µrad, ″]/Hz

c) Operating temperature: ___________ [µrad, ″]/°C

d) Temperature gradient: ___________ [µrad, ″]/Δ°C

e) Temperature rate of change: ___________ [µrad, ″]/(°C/min)

f) External magnetic induction [ac, dc, or both]: ___________ [µrad, ″]/[mT, G] per axis

g) Pressure: ___________ [µrad, ″]/Pa

One of several methods of curve fitting (such as least-squares straight line or polynomial fit) should be specified to determine the value of each sensitivity coefficient since the misalignment may not be a linear function of the input variable (see 12.3.11).

5.3.9 Temperature model and temperature hysteresis

5.3.9.1 Temperature-controlled operation

For temperature-controlled operation in the range *T* ± ___________ °C, the temperature sensitivities of the scale factor, bias, and IA misalignments for variations about *T* °C, as determined by least-squares straight line fits to calibrated values at temperature set points in the operating temperature range *T* ± __________ °C, shall be less than the values specified in 5.3.5.6, 5.3.7.6, and 5.3.8.6. These sensitivities can be used for linear temperature model compensation for temperature variations measured by the temperature sensor around the control set point *T* °C.

The temperature hysteresis of the scale factor, bias, and misalignments over the operating temperature range shall be less than __________ [%, ppm], __________ [m/s^2, ft/s^2, _____], and _____ [μrad, ″], respectively.

The temperature hysteresis in a parameter is the width of the plot of the calibrated value of the parameter versus temperature sensor output for increasing and then decreasing values of temperature over the operating temperature range. A measure of the lumped bias and misalignment temperature hysteresis is provided by the width of the plot of the accelerometer output in the IA horizontal orientation versus the temperature sensor output for increasing and then decreasing values of temperature. This same test in the IA vertical orientation gives the lumped scale factor and bias temperature hysteresis.

The temperature hysteresis value indicates how closely the output of the accelerometer at a temperature arrived at in the increasing temperature direction is equal to its output arrived at in the decreasing temperature direction. The error caused by hysteresis after appropriate modeling is half the hysteresis width.

5.3.9.2 Non–temperature-controlled operation

For non–temperature-controlled, temperature-compensated operation in the temperature range __________ °C to ___________ °C, the scale factor, bias, and IA misalignments shall be modeled as polynomials of order __________ in the temperature sensor output relative to the reference temperature __________ °C.

The reference temperature is typically midway in the temperature range. The temperature model could be expanded to include the effects of temperature gradients and/or temperature rates of change.

For approximately ___________ equally spaced temperature set points in an increasing and then decreasing temperature variation over the temperature range, the results of polynomial fits to the calibrated scale factor, bias, and IA misalignments from four-point or other tumble tests at each temperature set point shall satisfy the values in Table 1.

Table 1—Temperature model calibration requirements

Quantity	Scale factor [%, ppm]	Bias [m/s^2, ft/s^2, _____]	Misalignments [μrad, ″]
[First-order coefficient]	< ____________ per °C	< ____________ per °C	< ____________ per °C
[Second-order coefficient]	< ____________ per °C^2	< ____________ per °C^2	< ____________ per °C^2
etc.			
Rms residual	< ____________	< ____________	< ____________
Hysteresis	< ____________	< ____________	< ____________

5.3.10 Cross-axis nonlinearity

The absolute value of the cross-axis nonlinearity coefficients K_{oo}, K_{pp} shall be less than __________ [(m/s^2)/(m/s^2)^2, _____].

The K_{oo} and K_{pp} coefficients are commonly expressed in g/g^2.

A common cause of cross-axis nonlinearity is case compliance, which allows the IA to move relative to the case reference axes. As such, cross-axis nonlinearity can be specified as a structural compliance in ___________ μrad/*g*.

5.3.11 Cross coupling

The absolute values of the cross-coupling coefficients K_{ip}, K_{io}, and K_{po} shall be less than ___________ [(m/s^2)/(m/s^2)^2, _____].

5.3.12 Warm-up time

The output of the accelerometer shall be within ___________ [m/s^2, ft/s^2, _____] of its steady-state value in no more than __________ [s, min] after power application [from ____________°C, over the temperature range ____________°C to ____________°C].

To define the turn-on characteristics fully, several individual items could be specified, such as the peak deviation from the steady-state or final value of the output along with the time constant of the transient, beginning at a specific point in time after turn-on.

Alternatively, one could specify the maximum output drift rate averaged over a specified period of time, beginning at a specific point in time after power application, in output units per time increment. The allowable drift could also be specified in terms of the maximum integral of the deviation of the output from its steady-state or final value, in velocity units, beginning at a specific point in time after power application.

One could also define limits for the output transient and/or lost information resulting from a specified power interruption.

5.3.13 Acceleration threshold

The threshold shall be less than ___________ [m/s^2, ft/s^2, _____].

5.3.14 Acceleration resolution

The resolution shall be less than ___________ [m/s^2, ft/s^2, _____].

5.3.15 Acceleration dead band

5.3.15.1 Force-rebalance dead band

The dead band shall be less than __________ [m/s^2, ft/s^2, _____].

5.3.15.2 Vibrating beam accelerometer (VBA) frequency lock

The effect of VBA frequency lock shall be less than ____________ [m/s^2, ft/s^2, _____] peak to peak.

5.3.15.3 VBA activity dips

Activity dips shall be less than ___________ [m/s^2, ft/s^2, _____] peak to peak within the plus or minus local gravity range.

Activity dips shall be less than ___________ [m/s^2, ft/s^2, _____] peak to peak within the range of ___________ [m/s^2, ft/s^2, _____] to ___________ [m/s^2, ft/s^2, _____].

> Activity dips need to be smaller in the plus or minus local gravity range as they can affect the calibration of the instrument error terms.

5.3.16 Repeatability across shut-down or nonoperational environment

After the output has stabilized, the standard deviation of a series of ____________turn-on measurements shall be less than ___________ [m/s^2, ft/s^2, _____] under the standard test conditions of 11.1.

> Application of environments between measurements may be specified, such as vibration, shock, and temperature cycling, either singly or in combination. In addition, turn-on repeatability may be specified in various orientations with respect to the gravity vector. Alternative means of specifying turn-on repeatability may be used, such as peak-to-peak deviation from the mean of the ensemble of data.

5.3.17 Turn-on hysteresis

The absolute value of the turn-on hysteresis shall be less than ___________ [m/s^2, ft/s^2, _____].

5.3.18 Inversion transient

The output of the accelerometer shall be within ____________ [m/s^2, ft/s^2, _____] of its steady-state value in no more than ___________ [s, min] after inversion. The magnitude of the inversion transient shall be less than ____________ [m/s^2, ft/s^2, _____].

> When an accelerometer is rotated from +1 *g* to –1 *g*, or vice versa, transient settling behavior may be significant in high-precision applications. The shift and/or transient across an inversion could vary at different temperature set points within the operating temperature range. To define the inversion transient characteristics fully, several individual items could be specified, such as the peak deviation from the steady-state or final value of the output along with the time constant of the transient beginning at a specific point in time after the inversion is completed. See Annex J.

5.3.19 Velocity storage

The time integral of acceleration (velocity) stored in an accelerometer as a result of its dynamics is a function of accelerometer design. It is sometimes verified by analysis rather than by actual test.

The velocity storage of a fluid damped accelerometer is linearly proportional to the viscosity of the damping fluid, which can vary greatly with non–temperature-controlled operation.

5.3.19.1 Normal operation

The maximum velocity stored in the accelerometer during normal operation shall not exceed ___________ [m/s, ft/s, _____].

For a force-rebalance accelerometer, the amount of velocity stored in normal operation is a function of the tightness of the torque loop. For a pulse-torqued accelerometer, it is a function of the pulse quantization as well as of the dynamics of the torque loop (including moding effects).

5.3.19.2 Over-range operation

The minimum velocity storage for an over-range acceleration pulse shall exceed ___________ [m/s, ft/s, _____].

The amount of velocity that can be stored in over-range operation or across a power interrupt before the pendulum hits the stops is larger with fluid damping than it is with gas damping.

5.3.19.3 Across power interrupt

The velocity storage for normal operation across a power interrupt up to ___________ [µs, ms] in duration shall exceed ___________ [m/s, ft/s, _____].

The velocity stored across a power interrupt or over-range input is recovered in the accelerometer output when, for instance, a torque-rebalance loop is reclosed, except for any error effects that have accumulated while the loop was open.

For a VBA, the resonator(s) keep vibrating because of their high quality factor *Q* when power is interrupted. Velocity storage in a VBA is accomplished by reconstructing the unobserved cycles that have occurred during the power interrupt using analytic algorithms in a microprocessor attached to the VBA.

5.3.20 Noise

The power spectral density (PSD) of the self-generated output noise when measured at ___________ [m/s^2, ft/s^2, _____] with the power supply noise less than __________ mV rms from ___________ Hz to __________ Hz shall have an average not exceeding __________ [$(m/s^2)^2$, $(ft/s^2)^2$, _____]/Hz from __________ Hz to __________ Hz and not exceeding ___________ [$(m/s^2)^2$, $(ft/s^2)^2$, _____]/Hz from __________ Hz to __________ Hz.

The velocity random walk due to the white noise portion of the acceleration PSD shall be less than _______ [m/s, ft/s, _____]/√h.

PSD limits of the output noise are sometimes defined in graphical form and in the velocity domain rather than in the acceleration domain. Allan variance can also be used to define noise requirements. See Annex I.

With the IA vertical, the standard deviation of the accelerometer output, with a filter output interval of __________ s, shall be less than __________ [m/s^2, ft/s^2, _____] for __________ [h, d].

5.3.21 Frequency response

The frequency response of the accelerometer shall meet the requirements given in [Table, Equation, Figure] ___________.

System frequency response for linear analog capture loops may be specified by defining the required amplitude and phase behavior versus frequency using equations or tables, which may include allowable limits. For nonlinear capture loops, such as the pulse-rebalance type, the describing function interpretation may be invoked, whereby the response is derived as the ratio of the output at the fundamental frequency to the input, neglecting the output harmonics generated by the nonlinear system. Caution must be exercised to assure that the describing function exists for a given system. Frequency response may be determined by either analysis or test, which should include the effects of temperature, pressure, and so on. Note that generally the undamped natural frequency is

$$f_n = \sqrt{f_{45} f_{135}}$$

where

f_n is the natural frequency
f_{45} is the frequency at which the phase shift is 45°
f_{135} is the frequency at which the phase shift is 135°

5.3.22 Vibration-induced errors

The rectification error shall not exceed ___________ [m/s^2, ft/s^2, _____] while the accelerometer is subjected to the vibration environment of Figure ___________ along any combination of axes.

Vibropendulous and anisoelastic effects are two causes of rectification errors, as is asymmetry. Vibropendulous error shall be specified for vibration acceleration applied in a plane normal to the OA and at 45° to the IA. Most vibration-induced errors are approximately proportional to the square of the vibration input, although scale-factor asymmetry is an example of one that is not.

Rectification errors maybe specified for specific environments that best represent the actual application environment, such as sine vibration with specific amplitude and frequency or random vibration with PSD as a function of frequency.

5.3.23 Self-test scale factor

The accelerometer self-test scale factor shall be ___________ ± ____________ [m/s^2, ft/s^2, _____]/mA.

In some cases, the self-test scale factor may be specified in units of (p/s)/V or as a response to a logic or fixed input.

Subclauses 5.3.24 through 5.3.29.2 are necessary to specify the interface between the acceleration sensor and its analog or digital capture loop, which is required when ***only*** the ***acceleration sensor*** is being specified. (These clauses are ***not*** required when the ***complete*** accelerometer is being specified.)

5.3.24 Pickoff characteristics

5.3.24.1 Pickoff excitation

Pickoff excitation parameters shall not exceed the following limits:

a) Voltage: ___________ ± ___________V [ac, dc]

b) Frequency: ___________ ± __________ Hz

c) Nominal current: ___________ A

d) Harmonic content: __________ %, maximum

This specification may be necessary for both sensor only and complete accelerometer.

5.3.24.2 Scale factor

The pickoff scale factor shall be ___________ ± __________ V [ac,dc]/[rad,cm] at nominal pickoff excitation.

In some cases, it may be desirable to specify the pickoff linearity.

5.3.24.3 Phase/polarity

For a square-wave excitation, it may be necessary to specify the duty cycle and logic state voltages in addition to the following characteristics:

a) *Sensor with ac output.* When the displacement of the proof mass is positive, the output voltage measured from terminal ___________ (high) to terminal ___________ (low) shall [lead, lag] the pickoff excitation by ___________ ± ___________°.

   For opposite displacement, the output voltage (high to low) shall [lead, lag] the pickoff excitation by ___________ ± ____________°. These requirements shall be met for all output voltages greater than ___________ V rms.

b) *Sensor with dc output*. For positive displacement of the proof mass, the pickoff output (high-to-low) shall be ____________ [positive, negative], and for opposite displacement, ____________ [negative, positive].

5.3.24.4 Electrical null

The minimum electrical output shall not exceed ____________ V rms when normally loaded.

In ac output cases, it may be desirable to specify the fundamental, its harmonics, and the quadrature components of the residual null. The rms output includes random noise.

5.3.24.5 Output limits

The magnitude of the output voltage for maximum proof-mass deflection in each direction shall be ___________ ± ___________ V [rms, dc].

The output limits need not be symmetrical about the null.

5.3.24.6 Output impedance

The pickoff output impedance at nominal excitation frequency shall be ___________ ± ___________ [+,–] j ___________ ±__________ Ω.

5.3.24.7 Frequency response

The transfer function of the pickoff shall meet the requirements given in [Table, Equation, Figure] ___________.

5.3.25 Reference constants

Some users may request the manufacturer to supply nominal values of the following reference constants for use in users' servo analyses or evaluation of proposed acceleration sensors. Nominal values can be obtained from mathematical analysis or from physical measurements. Although analyses may be carried out without knowledge of these constants by use of data required in other portions of the document, they provide insight into the design of the sensor.

The VBA dual-resonator crossover frequency should be outside the ±l-*g* range, where the input is likely to dwell (see D.5.9). The resonator zero temperature coefficient (ZTC) temperatures should be matched as closely as possible to obtain the greatest common mode rejection of temperature effects (see D.5.2). Operation near the ZTC temperature yields the lowest noise performance.

Table 2—Reference constants for acceleration sensors

Reference constant	Nominal value
Pendulum parameters (rotational proof mass)	
Effective moment of inertia	________ ± ________ g·cm^2
Pendulosity	________ ± ________ g·cm
Damping coefficient	________ ± ________ dyn·cm·s
Anisoinertia	________ ± ________ cm
or Translational proof mass	________ ± ________ g
Force-rebalance parameters	
Forcer or torquer scale factor	
Electromagnetic	________± ________ [dyn, dyn·cm]/[mA, mA^2]
Electrostatic or capacitive	________± ________ [dyn, dyn·cm]/[V, V^2, V^2·s]
Pickoff sensitivity	
Rotational proof mass	________ ± ________ V/rad
Translational proof mass	________ ± ________ V/cm
VBA resonator parameters	
Quality factor *Q*	> ________
Unstressed frequency	
Individual resonator	________ ± ________ Hz
Dual-resonator match	________ $<\lvert f_1 - f_2 \rvert <$ ________ Hz
Zero temperature coefficient (ZTC) temperature	
Nominal	________ ± ________°C
Dual-resonator match	________°C

5.3.26 Torquer polarity

With a positive voltage applied to terminal __________ (high) referenced to terminal ___________ (low), the pickoff output voltage shall be [in phase, out of phase, positive, negative] with respect to [pickoff excitation voltage, ground reference].

5.3.27 Sensor transfer function

The open-loop transfer function of the acceleration sensor as measured from forcer current input to pickoff output shall fall within the limits given in [Table, Equation, Figure] ___________ for magnitude and phase over the specified frequency range.

The open-loop transfer function of the acceleration sensor must be specified in absolute terms, defined, and toleranced so that when it is combined with the transfer function of the associated capture-loop specified in 5.3.29.2, the required servo stability of the accelerometer is attained. The limits specified in 5.3.27 must be defined in cooperation with the acceleration sensor manufacturer.

5.3.28 Proof-mass elastic restraint

The elastic restraint K_r for a rotational proof-mass pendulum shall be ___________ ± ___________ [m/s^2, ft/s^2, _____]/rad for displacements within the range of 0 ± __________ radians. The elastic restraint K_r for a translational proof mass shall be ___________ ± __________ [(m/s^2) /cm, (ft/s^2)/in, _____].

Proof-mass elastic restraint includes all restraints such as flex lead spring restraint, pivot spring restraint, and pickoff reaction torque, but it does not include the principal restraint (rebalance torque provided by the capture loop). K_r is related to K_e of Annex A by the following relationship: $K_r = K_e$ / (980 × pendulosity), where 980 cm/s^2 is the approximate value of the local acceleration due to gravity.

5.3.29 [Analog, Pulse-rebalance] capture-loop electronics

The capture-loop electronics shall have the following characteristics to achieve the specified acceleration sensor performance.

The following parameters are for a capture loop that uses an input from a typical ac pickoff and must be modified for other pickoff types.

5.3.29.1 Capture-loop input characteristics

Capture-loop input characteristics shall not exceed the following limits:

a) Input impedance: __________ ± _________ [+, –] j ___________ ± ___________Ω
b) Input voltage, maximum: __________ V [ac, dc]
c) Input voltage, quadrature: __________ V [rms, peak to peak]
d) Input voltage, harmonics: __________ V [rms, peak to peak]
e) Input phase angle (relative to reference voltage): ___________ ± ___________°
f) Pickoff excitation frequency: __________ ± __________ Hz

5.3.29.2 Capture-loop frequency response

The transfer function of the [analog, digital] capture loop shall meet the requirements given in [Table, Equation, Figure] __________.

The specification must define the transfer function of the capture loop required to produce the desired closed-loop response characteristics. See box note under 5.3.21.

Subclauses 5.3.29.3 through 5.5.5 are general and are ***required*** regardless of whether the sensor only or the complete accelerometer is being specified.

5.3.29.3 Capture-loop output characteristics

Capture-loop output characteristics shall not exceed the following limits:

a) Analog output characteristics

1) Load impedance: __________ ± __________ [+,–] j __________ ± __________ Ω
2) Output impedance: __________ ± __________ [+,–] j __________ ± __________ Ω
3) Polarity positive with [in-phase, out-of-phase] input
4) Voltage range: + __________ ± __________ V to – __________ ± __________V
5) Current range: + __________ ± __________ mA to – __________ ± __________ mA
6) With grounded input, output: < __________ Vdc
7) Quadrature rejection: > __________ dB (applicable only to ac-pickoff servo)
8) Noise: < __________ mV rms, 0 to __________ Hz for all input conditions of 5.3.29.1
9) Gain K_A: __________ ± __________ Vdc/V [rms, dc] with the above specified output load impedance

b) Digital output characteristics

Digital output pulses indicating positive velocity increments on one signal line and pulses indicating negative velocity increments on a second line are assumed. Other types of outputs are possible, depending on the user's interface. See Annex B.

1) Source impedance: __________± __________ [+,–] j __________±__________Ω
2) Load impedance: __________± __________ [+,–] j __________±__________Ω
3) Phasing with respect to clock reference: [+,–] __________ ± __________ s
4) Polarity of output signal with +*g* along the input reference axis
5) Wave shape: (see Figure 2)
6) Repetition rate: __________ pulses/s (p/s)

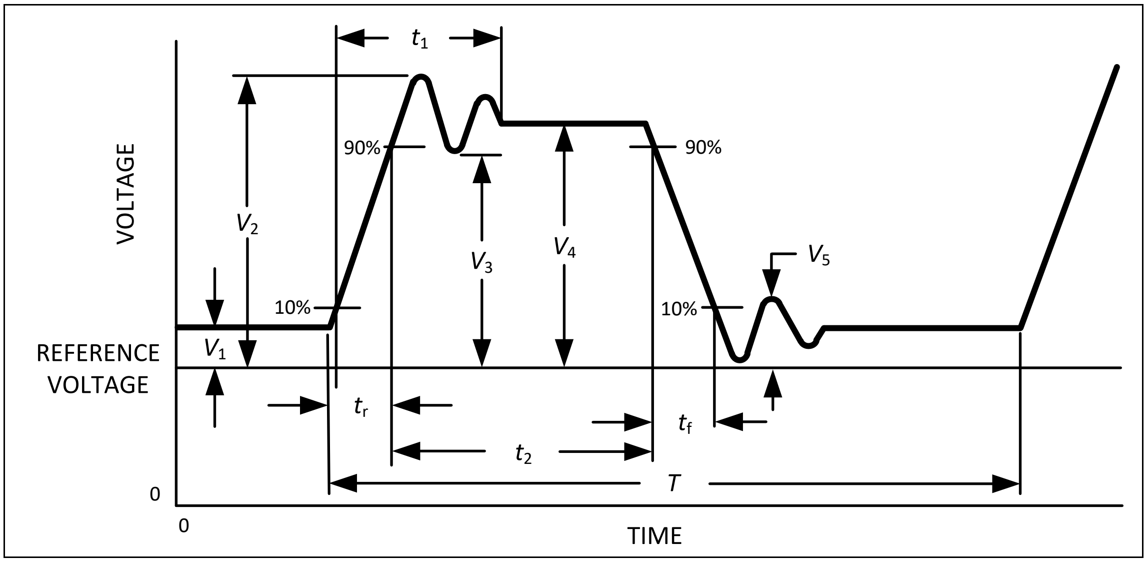

Units	Maximum	Minimum	Results
V_1 volts	________	________	Steady-state low voltage
V_2 volts	________	N/A	Overshoot voltage
V_3 volts	N/A	________	Undershoot voltage
V_4 volts	________	________	Steady-state high voltage
V_5 volts	________	N/A	Maximum low-voltage transient
t_r seconds	________	________	Rise time
t_f seconds	________	________	Fall time
t_1 seconds	________	________	Duration of turn-on transient time
t_2 seconds	________	________	Duration of high voltage on time
t_1/t_2	________	N/A	Ratio of the turn-on transient time to required on time
T seconds	________	________	Waveform period
t_2/T	________	________	duty cycle

Figure 2—Wave shape requirements for pulse-type signals

5.3.29.4 Command input(s)

Specify the type and characteristics of command input(s). For example,

a) Type
   1) On/Off
   2) Self Test
b) Characteristics
   1) Source input impedance: __________ ± __________ [+,–] j __________ ± __________ Ω
   2) Load impedance: __________ ± __________ [+,–] j __________ ± __________ Ω
   3) Input voltage: __________ ± __________ [V dc, V ac]

5.3.29.5 Clock reference

Specify the characteristics of the clock reference, which are necessary only for digital output sensors. For example,

a) Source input impedance: __________ ± __________ [+,–] j __________ ± __________ Ω
b) Load impedance: __________ ± __________ [+,–] j __________ ± __________ Ω
c) Repetition rate: __________ ± __________ p/s
d) Wave shape: (see Figure 2)
e) Stability: __________ ppm per __________ [h, d, yr]

5.4 Mechanical requirements

The following mechanical requirements apply to the external case to the extent specified.

5.4.1 Exterior surfaces

All exterior surfaces must withstand the environment specified herein and the handling expected in the normal course of operation, testing, transportation, and maintenance without deterioration that would cause nonconformance to this specification.

Additional requirements controlling surface finish, protective treatment, metals, dissimilar metals, workmanship, and so on, may be designated. Mounting surfaces that define the location of the IA usually require special consideration.

5.4.2 Dimensions

The outline, mounting dimensions, and center of gravity shall conform to Figure __________.

Figure 3 is a sample outline drawing. Controlled dimensions should be required only for critical parameters, as dictated by the application.

5.4.3 Identification of product

The accelerometer sensor case shall be marked __________.

The following information is typically required by the purchase agreement, although additional information may be specified:

a) Name of component
b) Model number
c) Vendor code
d) Part number
e) Contract number
f) Unit serial number
g) Manufacturer's name or symbol

5.4.4 Sensor axes

The input reference axis (IRA), pendulous reference axis (PRA), and output reference axis (ORA) are nominally along the sensor IA, PA, and OA, respectively, and are defined with respect to the accelerometer mounting surfaces. The axes are designated so that the cross product of the IRA and PRA is along the ORA.

The positive directions of the reference axes shall be identified by external markings, and by reference mounting surface(s) on the case, or by other means to allow for correct installation (see Figure 3).

A micromechanical accelerometer for which IA misalignment and cross-axis error compensation is not employed may have only the IA direction marked on the external package.

For a pendulous accelerometer, the PA points toward the pendulosity from the center of rotation of the pendulum, when the pendulum is at the neutral position. Nongravitational acceleration along the IA causes the pendulum to rotate about the OA. The amount of this sensed rotation against elastic restraint is the measure of acceleration for an open-loop accelerometer or is used to determine the commanded torque to return the pendulum to the neutral position for a closed-loop accelerometer. The amount of commanded torque is then the measure of acceleration.

Hence the designations *IA*, *PA*, and *OA* are natural terminologies for open-loop or torque-rebalance pendulous accelerometers. One example of a pendulous accelerometer has a cylinder with a pendulosity along a radial axis that is neutrally buoyant in a fluid with any off-buoyancy compensated by magnetic suspensions. The OA is along the cylindrical axis. There is essentially no physical contact between the pendulous cylinder and the accelerometer case. The more common pendulous accelerometer design has the pendulum constrained to rotate about the OA by a hinge or flexure (see Annex C). The OA is then sometimes called the *hinge axis* (HA) or the *flexure axis* (FA), with various conventions for the axis orientation (see F.2.4).

A VBA commonly has its resonators attached to pendulous proof mass(es) with nongravitational acceleration along the IA putting one resonator in tension and the other in compression. The measure of acceleration is the difference frequency of the two resonators. The PA is naturally chosen to be the PA of one of the pendulums. The cross product of the IA and PA is still designated the OA, even though sensed rotation about the OA is not the measure of acceleration nor is it used in a torque-rebalance loop.

For a translational proof-mass accelerometer, the motion in response to nongravitational acceleration along the IA is also along the IA. The natural designation of the axes other than the IA would depend on the particular design.

In the design in which the translational motion is restrained and guided by flexures [e.g., see c) of F.2.2], there might be a natural designation for a FA. The third axis (the cross product of the IA and FA) would then have no relationship to the terminology "OA."

A translational proof-mass design used to measure low-level nongravitational accelerations in space has capacitive sensing of the position of a proof mass in a cavity with the electrostatic force required to keep the proof mass centered being the measure of acceleration. One device can potentially measure all three acceleration DOFs; therefore, the natural designation of the accelerometer axes is IA_1, IA_2, and IA_3.

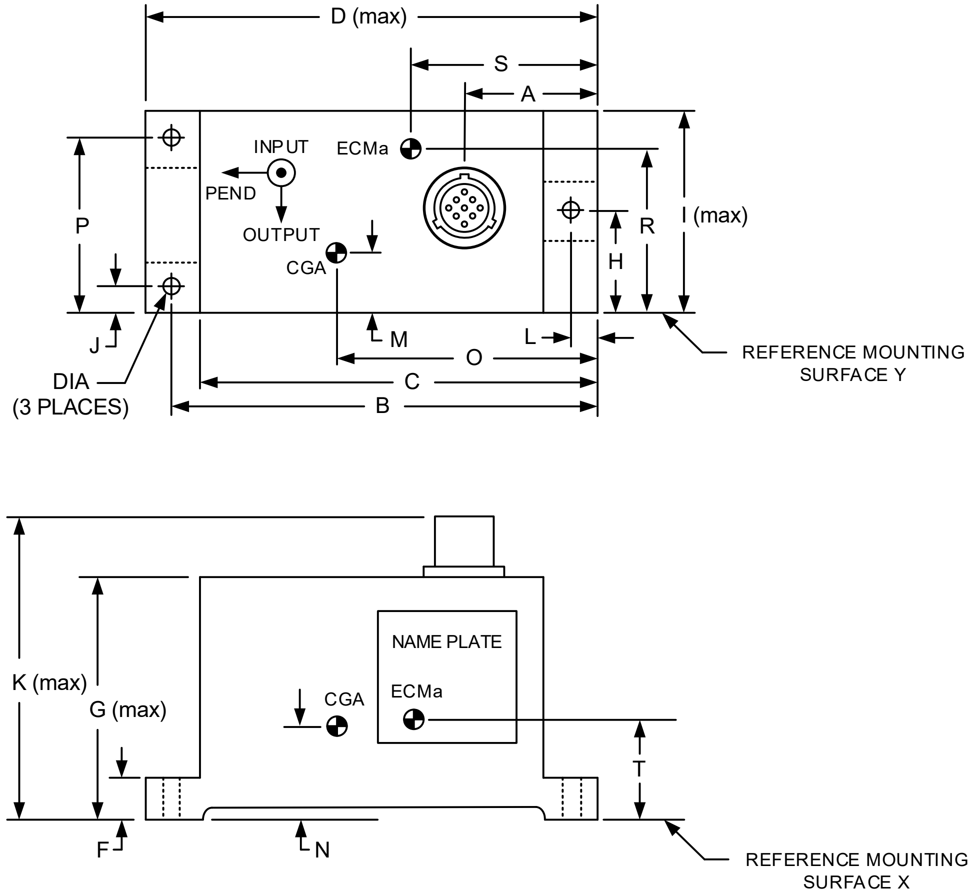

PIN	DESCRIPTION
A	
B	
C	
etc	

CGA = CENTER OF GRAVITY OF THE ACCELEROMETER

ECMa = EFFECTIVE CENTER OF MASS (PERCUSSION)

THE REFERENCE MOUNTING SURFACES X AND Y ARE USED FOR LOCATING THE INPUT REFERENCE AXIS

It is not intended that this sample drawing offer specific information, but it is intended to be used as a guide. The accelerometer may be cylindrical, square, and so on. Give nominal dimensions and tolerances.

Figure 3—Outline drawing

5.4.5 Weight or mass

The mass of the [acceleration sensor, accelerometer] shall be __________ ± __________ [g, kg, ______].

If appropriate, only the maximum mass need be specified. When accessories such as cable and connector are to be included in the mass requirement, the specification shall so state.

5.4.6 Seal

The following requirements shall be met:

Specify either item a), item b), or item c) as appropriate.

a) *Fluid filled.* No fluid leakage shall be detected under __________ power magnification after being subjected to an external vacuum at __________ ± __________ Pa and a temperature of __________ ± __________ °C for a minimum period of __________ [s, min].

b) *Gas-filled or evacuated.* Maximum gas leakage rate shall not exceed __________ cm^3/s of __________ gas measured at standard conditions for a minimum period of__________ [s, min] while being subjected to a vacuum of __________ ± __________ Pa at a temperature of __________ ± __________ °C.

c) There shall be no flow of bubbles after __________ [s, min].

Tracer gases may be added to the fill gas to facilitate leak detection.

5.5 Electrical and magnetic requirements

The accelerometer's electrical and magnetic design requirements shall be as specified as follows and shall meet the performance criteria of 5.3 during all reasonable variations of the inputs of 5.5.1.

5.5.1 Electrical interface

The electrical interface may consist of the connections illustrated in Figure 4a and Figure 4b, as modified for the particular accelerometer under test.

Other connections may also be included for which electrical characteristics must be specified. The following characteristics are measured in nonoperating tests, whereas the electrical characteristics in 5.3.24 and 5.3.29, for example, are measured in operating tests.

5.5.1.1 Torquer or forcer characteristics

Torquer or forcer characteristics shall not exceed the following limits:

a) Resistance: __________ ± ______ Ω
b) Inductance: __________ ± ______ H
c) Capacitance: __________ ± ______ F

These data are needed for acceleration sensor-only specification.

5.5.1.2 Pickoff characteristics

Pickoff characteristics shall not exceed the following limits:

a) Resistance: __________ ± ______ Ω
b) Inductance: __________ ± ______ H
c) Capacitance: __________ ± ______ F

5.5.1.3 Heater characteristics

Heater characteristics shall not exceed the following limits:

a) Resistance: __________ ± ______ Ω
b) Inductance: __________ ± ______ H

The nonoperating measurement of the heater characteristics is done with a small current level at room temperature unless otherwise specified. The resistance will change at operating current levels and temperature.

5.5.1.4 Temperature sensor characteristics

Temperature sensor characteristics shall not exceed the following limits:

a) Resistance: __________ ± ______ Ω
b) Inductance: ± __________ ± ______ H

The nonoperating measurement of the temperature sensor characteristics is done at room temperature. The resistance will vary as the temperature varies during operation. Other types of temperature sensors may have different characteristics and outputs (e.g., frequency and current).

5.5.1.5 Self-test torquer or forcer characteristics

Self-test torque or forcer characteristics shall not exceed the following limits:

a) Resistance: __________ ± ______ Ω
b) Inductance: __________ ± ______ H
c) Capacitance: _________ ± ______ F

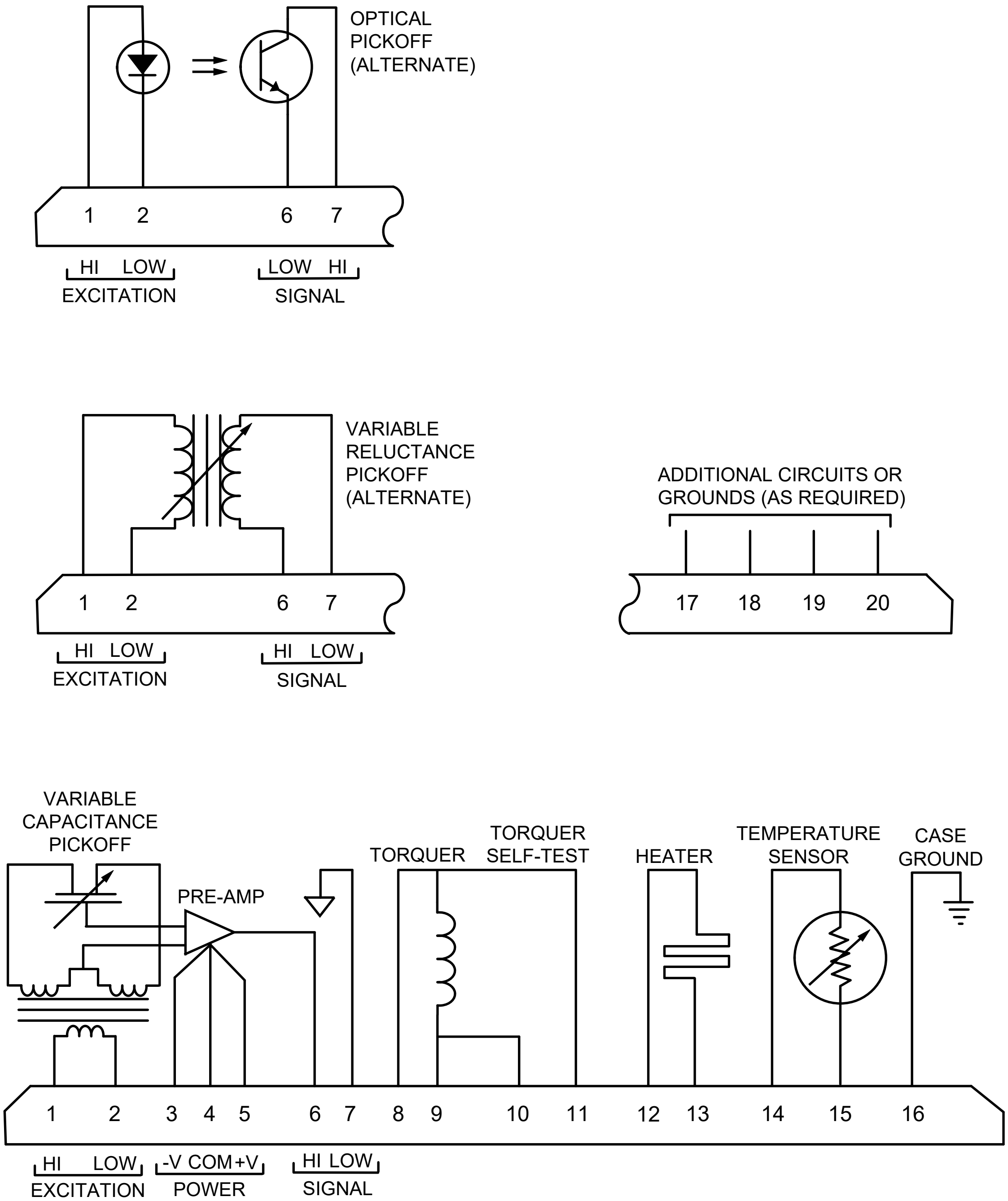

Figure 4a—Example of torque-rebalance electrical interface

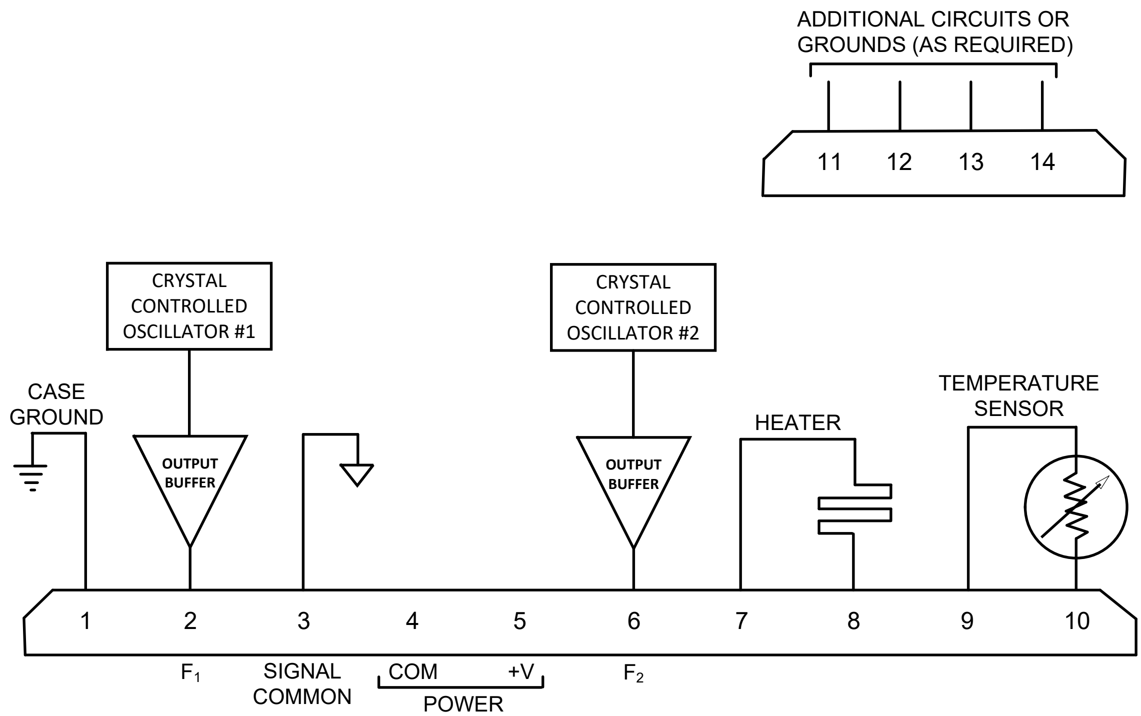

Figure 4b—Example of VBA electrical interface

5.5.2 Electromagnetic interference/compatibility

Describe the requirements for electromagnetic radiated and conducted emissions and susceptibility. In the United States, the requirements and test methods may be selected from MIL-STD-461.[6]

5.5.3 Insulation resistance

The insulation resistance between the isolated interface circuits and the case shall not be less than __________ MΩ measured at __________ ± __________ V dc applied for _________ ± __________ s.

Different voltages may be specified for different circuits. A time duration is specified for the measurement to detect any breakdown phenomenon in the resistance between the isolated circuits at the applied voltage.

5.5.4 Dielectric strength

The leakage current shall not exceed __________ mA when __________ ± __________V rms at __________ Hz are applied between isolated circuits and between the accelerometer case and circuits isolated from the case, for __________ ± __________ s.

Different voltages may be specified for different circuits. In some instances, lower voltages may be specified for subsequent tests.

5.5.5 Magnetic leakage

The magnetic leakage shall not exceed __________ [mT, G] at a distance of __________ m from the accelerometer sensor in any direction.

[6] Information on references can be found in Clause 2.

5.6 Environmental requirements

The accelerometer may be subjected to the environmental conditions in this clause during storage, transportation, handling, or operation. The accelerometer shall be designed to satisfy the performance requirements in 5.3 during (if appropriate) and after exposure to these environments.

5.6.1 Nonoperating environment

The following conditions, occurring separately or in combination, may be encountered during transportation, handling, or storage. The accelerometer shall conform to all the performance requirements of 5.3 after exposure to any reasonable combination of the specified conditions.

Where appropriate, the environment specified must be adjusted for the protection afforded by packaging.

5.6.1.1 Temperature

Ambient temperature may vary from a minimum of __________ °C to a maximum of __________ °C.

5.6.1.2 Thermal shock

From __________ °C to __________ °C, the heating and cooling rates of the ambient environment shall not exceed __________ °C/s.

For cyclic conditions, temperature limits must be specified for each level, with dwell times and sequence.

5.6.1.3 Vibration

Describe the vibration environment. For sinusoidal vibration, specify the vibration amplitude versus frequency, duration or sweep rate, and axes of application. For random vibration, specify power spectral density (provide figure if applicable), tolerance, bandwidth, peak acceleration level, total rms acceleration, duration, and axes of application.

5.6.1.4 Mechanical shock

Specify the shock duration and wave shape or the shock spectrum, tolerances, number of shocks, and axes of application.

5.6.1.5 Pressure

The ambient pressure shall be in the range __________ [Pa, psia] to __________ [Pa, psia]. The rate of change of pressure shall be nominally __________ [Pa/s, psia/s].

If desired, pressure may be expressed in terms of maximum altitude during transportation and rate of climb.

5.6.1.6 Humidity

The relative humidity shall not exceed __________ % RH.

5.6.1.7 Magnetic induction

Define magnitude, direction with respect to each axis, and duration. If there is exposure to magnetic induction resulting from ac, specify the intensity versus frequency.

5.6.1.8 Nuclear radiation

Describe the nuclear environment(s). For each environment, include the type of radiation (e.g., X-ray, gamma, and neutron), intensity, spectrum, exposure duration, and axes of application.

5.6.1.9 Other nonoperating environments

Include any other appropriate nonoperating environmental conditions, such as acceleration, acoustic noise, rain, fungus, salt spray, sand, and dust.

5.6.1.10 Storage life

Under the storage conditions of 5.6.1, the accelerometer shall meet the requirements of this specification after a storage interval of __________ yr. The maximum allowed parameter changes across the storage environment are as follows:

a) Bias: ______ [m/s^2, ft/s^2, _____]

b) Scale factor: ______ ppm

c) IA misalignment: ______ [µrad, ″]

Maximum allowed changes in nonlinearity and other parameters may also be specified. Any allowed repairs during the storage life may also be specified.

5.6.2 Operating environment

The following conditions, occurring separately or in combination, may be encountered during operation. The accelerometer shall conform to all the performance requirements of 5.3 during, unless otherwise specified, and after exposure to any reasonable combination of the specified service conditions.

5.6.2.1 Temperature (high and low)

Ambient air temperature may vary from __________ °C to __________ °C.

5.6.2.2 Thermal shock

From __________ °C to __________ °C, the heating and cooling rates of the ambient environment shall not exceed __________ °C/s.

For cyclic conditions, specify temperature limits for each level, dwell times, and sequence.

5.6.2.3 Other thermal conditions

Other thermal conditions that may affect performance shall be specified, for example, equivalent heat sink, radiant energy from surrounding surfaces, and power dissipation. Restrictions on allowable heat transfer may also be specified as, for example, conduction only, radiation only, or convection only. If cooling air is available, its characteristics must be specified, providing volume, rate, and air temperature.

5.6.2.4 Vibration

Describe the vibration environment. For sinusoidal vibration, include the specific vibration amplitude versus frequency, duration or sweep rate, and axes of application. For random vibration, specify power spectral density (provide figure if applicable), tolerance, bandwidth, peak acceleration level, total rms acceleration, duration, and axes of application.

5.6.2.5 Mechanical shock

Specify the shock duration and wave shape or the shock spectrum, tolerances, number of shocks, and axes of application.

5.6.2.6 Acceleration

Specify the maximum acceleration along each of the three axes and the duration.

5.6.2.7 Pressure

The ambient pressure shall be in the range __________ [Pa, psia] to __________ [Pa, psia]. The rate of change of pressure shall be nominally __________ [Pa/s, psia/s].

If desired, pressure may be expressed in terms of maximum altitude and rate of climb.

5.6.2.8 Humidity

The operating relative humidity shall not exceed __________ % RH.

5.6.2.9 Acoustic noise

Describe the acoustic noise environment. Supply the specific noise spectrum in decibels versus frequency, tolerance, bandwidth, peak level, and duration. Use a 0-dB reference of 20 µPa.

5.6.2.10 Magnetic induction

Define magnitude, direction with respect to each axis, and duration. If there is exposure to magnetic induction resulting from ac, specify the intensity versus frequency.

5.6.2.11 Nuclear radiation

Describe the nuclear environments(s). For each environment, include the type of radiation (e.g., X-ray, gamma, and neutron), intensity, spectrum, exposure duration, and axes of application.

5.6.2.12 Other operating environments

Include any other appropriate operating environmental conditions, such as rain, fungus, salt spray, sand, and dust.

5.6.2.13 Operating life

Under the specified operating conditions of 5.6.2, the accelerometer shall be capable of operating and performing within the requirements of this specification for a minimum accumulated operating period of __________ [h, d, yr] for a minimum of __________ and a maximum of __________ on–off cycles. The maximum allowed lifetime parameter changes are as follows:

a) Bias: _________ [m/s^2, ft/s^2, _____]
b) Scale factor: __________ ppm
c) IA misalignment: __________ [μrad, ″]

Maximum allowed changes in nonlinearity and other parameters may also be specified. Any allowed repairs during the operating life may also be specified.

5.6.3 Dormancy environment

The following conditions, occurring separately, in combination, or in a defined sequence, may be expected during dormant storage.

The temperature, pressure, vibration, shock, radiation, and other environments shall be specified.

The accelerometer shall perform to the requirements of 5.3 after __________ [d, yr] of dormancy. The maximum allowed parameter changes across dormancy are as follows:

a) Bias: __________ [m/s^2, ft/s^2, _____]
b) Scale factor: __________ ppm
c) IA misalignment: __________ [μrad, ″]

Periodic monitoring may be a condition of dormancy. The parameters to be monitored and the period of monitoring shall be specified. Maximum allowed changes in nonlinearity and other parameters may also be specified.

5.7 Reliability

5.7.1 Reliability program

The reliability program shall be in accordance with __________.

In the United States, a commonly used standard is IEEE Std 1332™.

5.7.2 Mean time between failure (MTBF)

The MTBF shall be a minimum of __________ h with a lower confidence limit of __________%.

6. Quality assurance

All tests required by this specification shall be conducted in accordance with detailed test procedures prepared by the contractor and approved by the buyer.

6.1 Classification of tests

The inspection and testing of the accelerometer shall be classified as follows:

a) *Acceptance tests*. Acceptance tests are those performed on accelerometers submitted for acceptance under contract.

b) *Qualification tests*. Qualification tests are those performed on samples submitted for qualification as a satisfactory product.

c) *Reliability tests*. Reliability tests are those performed to demonstrate the level of reliability and to assure the ability to maintain, with a certain confidence level, the required reliability.

d) *Analysis*. A process used in lieu of or in addition to testing to verify compliance with specifications. The technique typically includes interpretation or interpolation/extrapolation of analytical or empirical data under defined conditions or reasoning to show theoretical compliance with stated requirements.

Acceptance test environments are those expected to be encountered in the application for which the accelerometer is intended. Qualification test environments are usually more severe than those used in acceptance testing, since the purpose of qualification testing is to demonstrate design margin. Accelerometers that have undergone qualification testing are usually not considered mission-worthy. Accelerated reliability and life testing may involve more severe than operational environments.

The cross reference Table 3 provides a summary of the verification methods and test procedures typically used to satisfy the requirements. The table should serve as a guideline. For each requirement, a verification method (acceptance test, qualification test, reliability test, or analysis) is agreed upon by the manufacturer and the procuring organization. Requirements can also be verified by similarity of a given accelerometer with previously tested accelerometers, or by demonstration based on data from subcomponent tests or tests of technologically related accelerometers. Requirements can be added to or deleted from this list.

Table 3—Test requirement matrix

Requirement		Verification method				Test procedure(s)
		Acceptance test	Qualification test	Reliability test	Analysis	
5.3	Performance					
5.3.2	Input range					12.3.14
5.3.3	Overload capacity					12.3.14
5.3.4	Accelerometer temperature					12.2.7
5.3.5	Scale factor					12.3.4, 12.3.5, 12.3.8 to 12.3.12, 12.3.18
5.3.6	Nonlinearity					12.3.5, 12.3.15, 12.3.17
5.3.7	Bias					12.3.4, 12.3.5, 12.3.8 to 12.3.12, 12.3.18
5.3.8	IA misalignment					12.3.4, 12.3.5, 12.3.8 to 12.3.12
5.3.9	Temperature model & temp. hysteresis					12.3.12
5.3.10	Cross-axis nonlinearity					12.3.5, 12.3.15, 12.3.17
5.3.11	Cross coupling					12.3.5, 12.3.15, 12.3.17
5.3.12	Warm-up time					12.3.7
5.3.13	Acceleration threshold					12.3.6
5.3.14	Acceleration resolution					12.3.6
5.3.15	Acceleration dead band					
5.3.15.1	Force-rebalance dead band					12.3.6
5.3.15.2	VBA frequency lock					12.5.1
5.3.15.3	VBA activity dips					12.5.2
5.3.16	Repeatability across shut-down, nonoperational environment					12.3.10
5.3.17	Turn-on hysteresis					12.4.5
5.3.18	Inversion transient					12.3.3
5.3.19	Velocity storage					
5.3.19.1	Normal operation					12.3.20, 12.4.8
5.3.19.2	Over-range operation					12.3.20, 12.4.7
5.3.19.3	Across power interrupt					12.3.13
5.3.20	Noise					12.3.2
5.3.21	Frequency response					12.3.16

Table 3—Text requirement matrix (*continued*)

Requirement		Verification method: Acceptance test	Qualification test	Reliability test	Analysis	Test procedure(s)
5.3.22	Vibration-induced errors					12.3.20
5.3.23	Self-test scale factor					12.4.6
5.3.24	Pickoff characteristics					12.4.1
5.3.25	Reference constants					12.3.21, 12.4.4, 12.6.2
5.3.26	Torquer polarity					12.4.2
5.3.27	Sensor transfer function					12.4.3
5.3.28	Proof-mass elastic restraint					12.4.4, 12.6.2, 12.6.6
5.3.29	[Analog, Pulse-rebalance] capture-loop electronics					12.2.3, 12.3.1, 12.3.16
5.4	Mechanical requirements					
5.4.1	Exterior surfaces					12.2.1
5.4.2	Dimensions					12.2.1
5.4.3	Identification of product					12.2.1
5.4.4	Sensor axes					12.2.1
5.4.5	Weight or mass					12.2.2
5.4.6	Seal					12.2.6
5.5	Electrical and magnetic requirements					
5.5.1	Electrical interface					12.1.2.1, 12.2.3
5.5.2	Electromagnetic interference/compatibility					NA
5.5.3	Insulation resistance					12.2.5
5.5.4	Dielectric strength					12.2.4
5.5.5	Magnetic leakage					12.3.22
5.6	Environmental requirements					
5.6.1	Nonoperating environment					12.7.1, 12.9
5.6.2	Operating environment					12.7.2, 12.9
5.6.3	Dormancy environment					12.7.1, 12.9
5.7	Reliability					
5.7.1	Reliability program					NA
5.7.2	Mean time between failure (MTBF)					12.8

6.2 Acceptance tests

Acceptance tests shall consist of individual and/or sample tests.

6.2.1 Individual tests

Each accelerometer shall be subjected to the following tests described under 6.6.

The list of individual tests should be specified by the procuring organization based on the requirements. The number or type of individual tests specified is at the discretion of the procuring organization. Tests frequently specified as individual tests are listed as follows:

- Examination of product: 6.6.2.1
- Seal: 6.6.2.6
- Impedance: 6.6.2.3
- Dielectric strength: 6.6.2.4
- Insulation resistance: 6.6.2.5
- Pickoff characteristics: 6.6.4.1
- Torquer and self-test torquer polarity: 6.6.4.2
- Frequency response: 6.6.3.16
- Velocity storage across power interrupt: 6.6.3.13
- Scale factor and bias: 6.6.3.4.1
- IA misalignment: 6.6.3.4.2
- Turn-on hysteresis: 6.6.4.5
- Repeatability: 6.6.3.10
- Short-term stability: 6.6.3.8
- Centrifuge input range: 6.6.3.14

Other individual tests are not generally specified but may be included, and some listed earlier may be deleted, depending on the requirements of the specific application.

6.2.2 Sampling plan and tests

6.2.2.1 Sampling plan

Accelerometers selected per [describe sampling method] shall be subjected to the tests specified in 6.2.2.2.

This paragraph is intended to designate a sampling plan whereby samples are periodically selected for more complete tests, if required. Sampling plans are at the discretion of the procuring organization based on usage, size of contract, individual requirements, and so on.

In the United States, selection according to MIL-STD-1916 or ANSI/ASQ Z1.4 is common.

6.2.2.2 Sampling tests

Accelerometers selected in accordance with 6.2.2.1 shall be subjected to the following tests described in 6.6.

The procuring organization should specify the tests that shall be performed on accelerometers selected in accordance with the sampling plan, 6.2.2.1. Tests frequently specified for sample tests are listed as follows. Sampling plan units may be used for delivery unless the procuring organization specifies life tests or other destructive tests under the sampling plan.

- Individual tests: 6.2.1
- Weight or mass: 6.6.2.2
- Warm-up time: 6.6.3.7
- Static multipoint: 6.6.3.5
- Precision centrifuge: 6.6.3.15
- Threshold, resolution, and dead band: 6.6.3.6
- Magnetic leakage: 6.6.3.22
- Temperature (high, low): 6.6.9.5

6.2.3 Rejection and retest

When a unit fails to meet the specification requirements, the action taken shall be in accordance with contractual agreements between the user and the producer.

The contract may call for notification of any acceptance test failures and possibly for a failure analysis to an appropriate level. The contract may also specify requirements for repair and retest.

6.2.4 Defects in accepted items

The investigation of a test failure could indicate that defects may exist in items already accepted. If so, the manufacturer shall fully advise the procuring organization of defects likely to be found and of methods for detecting and correcting them.

6.3 Qualification tests

6.3.1 Qualification test samples

A preproduction sample of __________ accelerometers manufactured in accordance with the requirements of this specification shall be subjected to qualification tests specified herein. The procuring organization may designate an independent facility at which one or more of these tests may be performed.

If the product is later modified in any way, the modified form shall be subjected to and pass those qualification tests designated by the procuring organization.

The qualification test samples shall be identified with the manufacturer's own part number and any other information required by the procuring organization.

6.3.2 List of qualification tests

The procuring organization should specify from 6.6 the tests that should be performed on the qualification test samples.

6.4 Reliability tests

The MTBF requirements of 5.7.2 shall be demonstrated by testing __________ production units for __________ h minimum each and a minimum time of __________ h combined.

Other methods of demonstration testing may be selected at the discretion of the procuring organization. A demonstration test plan should be prepared to define test conditions, types of tests, failures, and so on. In some cases, it may be desirable to combine reliability and life tests.

6.5 Test conditions and equipment

The procuring organization should specify from Clause 11 of this standard the nominal test conditions and the requirements for the test equipment. The test equipment may be listed by name and model, part number, or performance requirements. The conditions should apply to all tests unless otherwise specified. When a test condition is specified, the complete test conditions should be detailed in this specification.

6.6 Test methods

Instructions for performing specified tests are detailed in Clause 12 of this standard. When a test is specified, the complete test method shall be detailed in this specification, including requirements to be met after test to determine satisfactory performance. A test method should not be listed in 6.6 unless a requirement exists in Clause 5 of this specification.

6.6.1 Test setup

6.6.1.1 Nonoperating test setup

6.6.1.2 Operating test setup

6.6.2 Accelerometer nonoperating tests

6.6.2.1 Examination of product

6.6.2.2 Weight or mass

6.6.2.3 Impedance

6.6.2.4 Dielectric strength

6.6.2.5 Insulation resistance

6.6.2.6 Seal

6.6.2.7 Temperature sensor characteristics

6.6.3 Accelerometer operating tests

6.6.3.1 Functional checkout

6.6.3.2 Noise

6.6.3.3 Inversion transient

6.6.3.4 Four-point tumble

6.6.3.4.1.1 Scale factor and bias

6.6.3.4.1.2 IA misalignment

6.6.3.5 Static multipoint

6.6.3.6 Threshold, resolution, and dead band

6.6.3.7 Warm-up time

6.6.3.8 Short-term stability

6.6.3.9 Long-term stability

6.6.3.10 Repeatability

6.6.3.11 Sensitivity

6.6.3.12 Temperature model calibration and temperature hysteresis

6.6.3.13 Velocity storage across power interrupt

6.6.3.14 Centrifuge input range and overload capacity

6.6.3.15 Precision centrifuge

6.6.3.16 Frequency response

6.6.3.17 Vibration calibration (nonlinear terms)

6.6.3.18 Vibration and shock calibration (scale factor and bias)

6.6.3.19 Performance through and across environment

6.6.3.20 Velocity storage in normal and over-range shock

6.6.3.21 Slew calibration

6.6.3.22 Magnetic leakage

6.6.4 Electromagnetically torqued pendulous accelerometer tests

6.6.4.1 Pickoff characteristics

6.6.4.2 Torquer and self-test torquer polarity

6.6.4.3 Open-loop frequency response

6.6.4.4 Pickoff scale factor and pendulum elastic restraint

6.6.4.5 Turn-on hysteresis

6.6.4.6 Self-test torquer scale factor

6.6.4.7 Velocity storage—Open-loop test

6.6.4.8 Velocity storage—Pulse-torque steady-state operation

6.6.5 VBA tests

6.6.5.1 VBA frequency lock

6.6.5.2 VBA activity dips

6.6.6 Micromechanical accelerometer tests

6.6.6.1 Wafer level tests

6.6.6.2 Proof-mass suspension resonant frequency

6.6.6.3 Proof-mass freedom

6.6.6.4 Pickoff and torquer electrode capacitor values

6.6.6.5 Pickoff scale factor

6.6.6.6 Flexure elastic restraint

6.6.7 Life tests

6.6.7.1 Life—Storage or dormant

6.6.7.2 Life—Operating

6.6.8 Reliability tests

6.6.8.1 Laboratory reliability test

6.6.8.2 Field reliability experience

6.6.9 Environmental tests

6.6.9.1 Vibration

6.6.9.2 Mechanical shock

6.6.9.3 Acceleration

6.6.9.4 Angular acceleration and spin

6.6.9.5 Temperature (high, low)

6.6.9.6 Thermal shock

6.6.9.7 Thermal radiation

6.6.9.8 Pressure (high, low)

6.6.9.9 Acoustic noise

6.6.9.10 Electromagnetic interference

6.6.9.11 Electromagnetic susceptibility

6.6.9.12 Magnetic induction

6.6.9.13 Fungus

6.6.9.14 Humidity

6.6.9.15 Salt spray

6.6.9.16 Sand and dust

6.6.9.17 Nuclear radiation

6.7 Data submittal

The format for all data organization and the method of submittal shall be specified.

7. Preparation for delivery

Give detailed procedures for 1) preservation and packaging, 2) packing, and 3) marking of shipping containers. A common U.S. specification covering preservation and packaging is MIL-STD-2073-1. Other organizations may use different supporting documents.

8. Notes

8.1 Intended use

Describe application if it is considered necessary or helpful.

8.2 Ordering data

Procuring documents should specify the title, number, and date of this specification. In addition, the following, or other items, should be specified as applicable:

a) Level of packaging and packing desired

b) Mode of shipment required

c) Sampling-plan tests, if any

d) Number of preproduction samples to be submitted for qualification testing

e) Data package

8.3 Model equation

The model equation of the accelerometer is defined as a series that mathematically relates the accelerometer output E to the components of applied acceleration, angular velocity, and angular acceleration along the accelerometer reference axes.

The following model equation contains more terms than might usually be employed and can be shortened or have other terms added as necessary depending on the application.

$$E = K_1 \left\{ K_0 + \frac{K_0'}{2}\operatorname{sign}(a_i) + \left(1 + \frac{K_1'}{2}\operatorname{sign}(a_i)\right) a_i + K_{oq} a_i |a_i| + K_2 a_i^2 + K_3 a_i^3 + \sum_{n \ge 4} K_n a_i^n + \delta_o a_p \right.$$
$$\left. - \delta_p a_o + K_{ip} a_i a_p + K_{io} a_i a_o + K_{po} a_p a_o + K_{pp} a_p^2 + K_{oo} a_o^2 + K_{spin} \omega_i \omega_p + K_{ang.accel} \dot{\omega}_o + \varepsilon \right\}$$

where

E	is the accelerometer output in accelerometer output units (such as volts)
ε	is the measurement and process noise and unmodeled error (m/s^2)
K_1	is the scale factor (output units per (m/s^2))
a_i, a_p, a_o	are the applied acceleration components along the IA, PA, and OA (m/s^2)
sign(a_i)	is $\begin{cases} +1 \text{ if } a_i > 0 \\ -1 \text{ if } a_i < 0 \\ \ \ 0 \text{ if } a_i = 0 \quad \text{(ambiguous in bias asymmetry model)} \end{cases}$
ω_i, ω_p	are the angular velocity components along the IA, and PA(rad/s)
$\dot{\omega}_o$	is the angular acceleration component along the OA (rad/s^2)
K_0	is the bias (m/s^2)
K_0'	is the bias asymmetry (m/s^2)
K_1'	is the scale-factor asymmetry (dimensionless)
K_{oq}	is the odd quadratic coefficient ($(m/s^2)/(m/s^2)^2$)
K_2	is the second-order coefficient ($(m/s^2)/(m/s^2)^2$)
K_3	is the third-order coefficient ($(m/s^2)/(m/s^2)^3$)
K_n	is the other higher order along IA terms, n = 4, 5, 6, …, to order appropriate for given accelerometer ($(m/s^2)/(m/s^2)^n$)
δ_o, δ_p	are the misalignment of the IA with respect to the input reference axis about the OA and PA, respectively (rad)
K_{ip}, K_{io}, K_{po}	are the cross-coupling coefficients ($(m/s^2)/(m/s^2)^2$)
K_{pp}, K_{oo}	are the cross-axis nonlinearity coefficients ($(m/s^2)/(m/s^2)^2$)
K_{spin}	is the spin correction coefficient, equal to $-[(J_i - J_p) - Pr_c]/P$ [converted to $(m/s^2)/(rad/s)^2$]
$K_{ang.accel}$	is the angular acceleration coefficient, equal to $[J_o - Pr_c]/P$ [converted to $(m/s^2)/(rad/s)^2$]

where (see Annex C)

J_i, J_p, J_o	are the pendulum principal moments of inertia relative to the center of hinge ($g{\cdot}cm^2$)
P	is the pendulum pendulosity = pendulum mass times distance of mass from the center of hinge (g·cm)
r_c	is the distance from the center of hinge to a point at the null position of the pendulum at which acceleration are assumed to act on the pendulum (cm)

Acceleration may be expressed in alternative units, such as ft/s^2, as long as the units are consistent throughout the model equation.

When calibrating the scale factor and other parameters in an up–down, four-point, or multipoint tumble test at a specific site, it is natural to use the local acceleration due to gravity as the reference unit of acceleration g. The magnitude of gravity varies with location, including effects of latitude and altitude, so that the local gravity differs somewhat from the international standard value $g_o = 9.80665$ m/s^2. The absolute calibration of the local value of gravity is best accomplished with a falling laser corner cube gravimeter.

The acceleration along the arm in a centrifuge test is $r\omega^2$, where r is the distance from the rotation axis of the centrifuge and ω is the centrifuge rate. The latter accurately measures the relative variation in acceleration at different centrifuge rates, with compensation, if necessary, for measured variations in arm length and droop by laser interferometer or other techniques. The constant part of the arm length r is absorbed in the scale factor for the test (which is not used in applications) when the scale factor is estimated simultaneously with the acceleration nonlinearity model coefficients. Hence, for the purpose of estimating the nonlinearity coefficients for applications, the units of $r\omega^2$ can be g (regardless of whether local g or the standard gravity g_o is used unless the acceleration nonlinearities need to be calibrated to better than 0.1%).

Calibration of acceleration nonlinearity model terms in a vibration test uses the rms acceleration measured with monitor piezoelectric accelerometers, which are accurate to at best 1% and usually expressed in g. Absolute calibration of a piezoelectric accelerometer could be accomplished by laser interferometer observations of a vibrating element on which it rests.

Thus, for carrying out tests at a specific test site, the unit of acceleration used in the model equation is most conveniently taken to be the local value of the acceleration due to gravity g. When using the scale factor and other parameters calibrated at a local test site in an application or when comparing scale factors and other parameters measured on the same accelerometer at different test sites, the units should be changed to the standard gravity g_o or to m/s^2.

The coefficients in the model equation may be functions of other variables (e.g., time, input voltage(s), input frequency(ies), operating temperature, external magnetic induction, and pressure) and may represent either error terms or modeled coefficients that define the nominal behavior of the accelerometer. Some terms might not be excited in a given test or might not be separable from other terms.

For example, the model in a four-point tumble test is restricted to scale factor, bias, and one of the misalignment angles. The resulting estimate of bias has lumped into it some of the effect due to K_2, and that of scale factor has lumped into it some of the effect of K_3 (see Annex K).

In a multipoint tumble test about OA, the parameters δ_p, K_{oo}, and so on. are not excited, and K_2 and K_{pp} cannot be simultaneously estimated when bias K_0 is also estimated. Similarly, K_2 and K_{oo} cannot be simultaneously estimated in a tumble about PA (see K.2.4). Also, K_{ip} or K_{io} cannot be simultaneously estimated with K_2 and K_0, and K_3 cannot be simultaneously estimated with K_1, in dual orthogonal accelerometer tests using the magnitude-squared-of-g observable that is insensitive to angle-setting errors, or if angle-setting errors are estimated with individual accelerometer observables (see K.5.2).

The indicated acceleration is $A_{\text{ind}} = E/K_1$. The scale factor can be written as $K_1 = K_1^{\text{o}}(1 + k_1)$, where K_1^{o} is a nominal scale factor, such as determined in an IA up–down test, and k_1 is a scale factor correction whose product with other model coefficients is insignificant. Then the model equation for $A_{\text{ind}} = E/K_1^{\text{o}}$ is the expression in brackets in the model equation for E, and the 1 term multiplying a_i is replaced by $1 + k_1$.

Applied acceleration refers only to nongravitational acceleration (e.g., from rocket thrust or air drag) since an accelerometer cannot sense the acceleration of free fall. The downward attractive force of gravity acts equally on the accelerometer proof mass and case; therefore, the output of an earthbound accelerometer is due to the upward reaction force to gravity of the support acting on the accelerometer case and thence to the pendulum hinge and gives the same indication as an applied acceleration of 1 *g* upward.

Angular motion environments produce several specific forms of nongravitational acceleration

a) Centripetal acceleration, which is associated with steady-state spin $(\vec{\omega} \times \vec{\omega} \times \vec{r})$

b) Tangential acceleration, which is associated with time-varying spin $\left(\dot{\vec{\omega}} \times \vec{r}\right)$

c) Coriolis acceleration, which arises when a point of interest moves with velocity $\vec{v}$ relative to a rotating frame of reference $\left(2(\vec{\omega} \times \vec{v})\right)$

Centripetal and tangential accelerations both depend on $\vec{r}$, which is the vector distance from the instantaneous center of the angular motion to the point at which the acceleration forces are assumed to act. Coriolis acceleration depends on velocity, that is, the rate of change of position, and therefore, it is not dependent on position per se.

The measurement and process noise in ε could have quantization, white, random walk, flicker, or other components. The process noise distinct from the noise due to the analog-to-digital converter, voltage-to-frequency converter, or other digitization readout system can be regarded as due to accelerometer random bias instability, separate from any systematic models of bias variation such as trend or temperature and other sensitivities.

Characterization of the measurement and process noise in the output observable can be done with PSD and Allan variance techniques. The process noise can be modeled in a guidance system Kalman filter model using augmented Markov process states.

The unmodeled error in ε should be made as small as required by the application by means of design improvements and/or addition of calibratable model terms that best represent the underlying physics of the device.

An accelerometer attached to a moving frame may be assumed to measure a single component of the acceleration that exists at a point in the frame that is coincident with its effective center of mass. Since acceleration fields typically have spatial gradients associated with them, this coincidence must be carefully defined. In a pendulous accelerometer, the effective mass center is on the PA, located at a distance r_c outward from the HA or OA. The optimal value, of all possible values to be chosen for r_c, depends in a somewhat complicated way on the mass properties of the pendulum.

Ideally, the true effective center of mass would correspond to a choice of r_c so that the error terms K_{spin} and $K_{ang.accel}$ are both made equal to zero. Theoretically, both error terms could be made zero in a dry accelerometer with an infinitesimally thin pendulum. In real accelerometers, whose pendulums have finite thickness and that may be further affected by fluid effects in liquid filled accelerometers, error torques are generated that make impossible cancellation of both error terms by proper choice of r_c.

It is possible to choose a value of r_c so that K_{spin} is equal to zero or to choose another value so that $K_{ang.accel}$ is equal to zero but not to have both error terms equal zero at the same time. In general, if the value of r_c that is chosen is between these two values, the error will be bounded by the fact that the sum of the two angular motion coefficients is equal to a constant: $K_{spin} + K_{ang.accel} = K_{ai}$, the anisoinertia coefficient.

A common solution to this idiosyncrasy of pendulous accelerometers in strapdown inertial navigation systems is to define r_c so that $K_{ang.accel}$ is zero (literally: no sensitivity to angular acceleration about any axis through the chosen point) and then correct the residual spin error by using the measured values of ω_i and ω_p, which are available as part of the system state vector.

The angular motion sensitivity terms that are included in the example model equation of this clause neglect the normally small terms that arise from pendulum products of inertia and from products of spin coefficients with the pendulum misalignment coefficients. See Annex C for further details. Angular velocity and angular acceleration error terms are not excited in any nonrotating environment or in a discrete position tumble test, where the local gravity vector includes the effect of the centripetal acceleration due to earth rotation.

Alternative expressions for the bias and scale factor asymmetry model terms are

$$K_{0+} = K_0 + \frac{K_0'}{2},\ K_{0-} = K_0 - \frac{K_0'}{2}$$

$$K_{1+} = K_1\left(1 + \frac{K_1'}{2}\right),\ K_{1-} = K_1\left(1 - \frac{K_1'}{2}\right)$$

where K_{0+} and K_{1+} are the bias and scale factor, respectively, for positive a_i, and K_{0-} and K_{1-} are the bias and scale factor, respectively, for negative a_i. The bias in either formulation of the asymmetry model is ambiguous when $a_i = 0$, or from a practical standpoint when a_i is near zero.

The average bias and the difference in positive and negative acceleration biases (bias asymmetry) are

$$K_0 = \frac{1}{2}(K_{0+} + K_{0-}),\ K_0' = K_{0+} - K_{0-}$$

The average scale factor and the fractional difference in positive and negative acceleration scale factors (scale factor asymmetry) are

$$K_1 = \frac{1}{2}(K_{1+} + K_{1-}),\ K_1' = (K_{1+} - K_{1-})/K_1$$

Part II—Test procedure

9. Test procedure overview

This test procedure describes the test requirements for __________ [model number, part number, change letter (if any), other identification], manufactured by ______ [name, address].

10. Description

See 5.1 for the description to be applied for the test procedure.

11. Test conditions and equipment

11.1 Standard test conditions

11.1.1 Ambient environment

The following conditions define the requirements for the environment in the immediate vicinity of the accelerometer. They are not intended as environmental tests, which are described in 12.9.

11.1.1.1 Atmospheric conditions

Atmospheric conditions shall be as follows:

a) Pressure: __________ ± __________ [Pa, lbf/in^2]
b) Ambient temperature: __________ ± __________ °C
c) Relative humidity: __________ to __________ %

11.1.1.2 Magnetic induction

Magnetic induction shall be as follows:

a) Horizontal component: __________ T, maximum
b) Vertical component: __________ T, maximum

In some applications, careful consideration should be given to the magnitude of ac magnetic inductions.

11.1.1.3 Vibration

The total seismic background vibration measured at the mounting location shall be less than __________ [m/s^2, ft/s^2, _____] rms over the frequency range of __________ to __________ Hz.

These limits normally apply to each of the three axes of the accelerometer coordinate system.

11.1.1.4 Other conditions

Specify other environmental conditions for the test area as required.

11.1.2 Installation requirements

The design requirements for the mounting fixture(s) shall be specified in 11.1.2.1 and 11.1.2.2. Other requirements may be necessary to simulate the application conditions and, if so, must also be specified.

11.1.2.1 Mechanical conditions

The test unit should be mounted in such a way that the misalignment of its three reference axes with respect to the axes of the test fixture is maintained within __________ [μrad, mrad, ″, °] under all specified test conditions. The three reference axes of the test unit are those defined by external case markings and mounting [surface, surfaces] as indicated in Figure 3.

The surface roughness of the mounting fixture shall be less than __________ [μm, ________], and the perpendicularity and parallelism between the mounting surfaces and other equipment surfaces (such as dividing head, centrifuge, or vibrator face plate) shall be within __________ [rad, ′].

Attachment conditions shall be specified. For example, if a mounting bolt is used, then the mounting torque shall be specified, if a clamp is used, then the clamping force shall be specified, and so on.

A macro-sized accelerometer usually has a mounting flange with mounting bolt holes. A packaged microsized accelerometer or inertial system might have mounting bolt holes, or it could be soldered or otherwise attached to a circuit board inserted in a card cage. In the latter case, the outer enclosure should have an indication of at least the IA direction(s) and a method of attachment to a surrounding structure, usually with mounting bolts.

If a micro-sized accelerometer is tested before being placed in its final packaging, other attachment methods to the test fixture might be required, such as soldering to a circuit board that is then clamped or bolted to the mounting fixture. Care should be taken in using soldering and other such attachment techniques since they can affect performance. Proper support and strain relief of wires and cables should be provided.

11.1.2.2 Operating temperature

If a specified operating temperature is required

a) The unit shall be at thermal equilibrium as evidenced by__________.
b) The unit operating temperature shall be stabilized at a point in the range __________ °C to __________ °C with a peak-to-peak variation of __________ °C.
c) Determination of the temperature shall be as specified in __________.
d) Thermal gradients across the accelerometer shall be less than __________ °C.

A typical approach to determine thermal equilibrium is to measure the rate of change of temperature.

In designing the mounting fixture, consideration shall be given to the installation conditions of the application. Reference to the thermal and mechanical design, and so on, of a specific mounting block may be necessary if deemed important to meet performance requirements. Precise temperature control of the mounting fixture may or may not be necessary.

A temperature-controlled mounting fixture provides a method of varying the temperature of the accelerometer during temperature sensitivity tests, in lieu of enclosing the accelerometer, mounting fixture, and perhaps other equipment (such as a dividing head) in a thermally controlled (heated and/or refrigerated) chamber, for example.

A temperature-controlled mounting fixture could surround the accelerometer, or the accelerometer could be covered with insulation with heat flowing through the mounting flange to the temperature-controlled fixture. A thermal shim or spacer might be required between a temperature-controlled mounting fixture and a dividing head, centrifuge, or vibrator face plate.

Fixture control with electric heaters requires that the operating temperature be above room temperature. Thermoelectric heater-coolers under the mounting flange allow below-room-temperature testing. Water condensation should be avoided.

If the accelerometer has its own temperature control, with or without a thermally controlled mounting fixture, evidence of thermal equilibrium shall be in compliance with 5.3.4.1.

11.1.2.3 Electrical interconnections

The electrical interconnections may be specified in a schematic (included as a figure) or as a separate engineering drawing. Several schematics may be required for the various test arrangements required. Each schematic shall indicate such things as grounding, test points, circuit protection, precautionary notes, allowable lead length, and shielding. The detailed test procedures shall ensure that all electrical parameters are set within the allowable tolerances specified for the electrical interface.

11.2 Test equipment

11.2.1 General requirements

The selection of test equipment and facilities shall be based on accuracy requirements compatible with the performance specifications and the required verification procedures. Test equipment should have a nominal accuracy better than one tenth of the tolerance of the attribute being tested, or in the case of a single limit tolerance, the test equipment error shall be applied to the specified parameter in a direction that assures the specified parameter is being met.

The bandpass of the measuring devices shall be chosen to provide information within the frequency spectrum of interest for the tests. Calibration of test equipment shall be traceable to a standard or reference agreed upon by the customer and the producer. All test software developed for, or in support of, the testing of the accelerometer shall be documented in an acceptable manner.

Because of the trend toward commercial off-the-shelf hardware, requirements such as traceability of test equipment calibration might not be desirable in a purchase requisition to control costs, especially for parameters that will be recalibrated by the user before a mission in any case. However, the desirability of a producer is enhanced if it has procedures in place for calibrating test equipment relative to primary standards as part of its total quality management effort.

In the United States, the National Institute of Standards and Technology (NIST) is the primary standard for calibrating test equipment (e.g., voltmeters) and provides absolute standards of atomic time.

The falling laser corner cube gravimeter provides the most accurate absolute method of calibrating the local acceleration due to gravity, which is used as a reference in calibrating accelerometer scale factor and other parameters. Measurement of centrifuge arm stretch and droop for calibrating accelerometer nonlinearities can be accomplished by laser interferometer or other techniques. Calibration of the piezoelectric accelerometer used as a reference in calibrating accelerometer nonlinearities in vibration tests can be done with laser interferometer observations of a vibrating element on which it rests.

11.2.2 Description of test equipment

All special-purpose and commercial test equipment shall be listed by name, model, part number, and performance capability as agreed upon by the customer and the producer. The test equipment should have the required performance in the acceleration and frequency range employed in the testing and be calibrated prior to being used in the test program.

11.2.2.1 General equipment

Commercial power supplies, voltmeters, ammeters, wattmeters, resistance- or impedance-measuring bridges, oscilloscopes, counters, frequency measurement or other readout devices, atomic or other time and frequency references, tilt meters, thermistor monitors, and the data acquisition and other equipment used in the test program should be listed.

A tilt meter might be an electronically read bubble level or pendulum. The tilt variation of the test platform relative to the local vertical can also be monitored by a horizontally oriented accelerometer.

Many test voltages are read by an analog-to-digital converter board in the data acquisition computer. However, a voltage output proportional to rebalance force is more accurately acquired by an integrating voltmeter with digital output read by the data acquisition computer.

Alternatively, this voltage could be read by a voltage-to-frequency converter, with a frequency-driven continuous counter latched and read by the data acquisition computer. A voltage-to-frequency converter is likely to be a specially built piece of test equipment.

Besides listing the data acquisition hardware, the digital signal processing, automatic test control, and analysis software can also be specified.

11.2.2.2 Accelerometer-specific equipment

Besides the electronics that are an integral part of an accelerometer, support electronics could also be required in instrument-level tests beyond simple power supplies, without which the accelerometer could not operate.

The grounding and electrical isolation scheme for the accelerometer readout and data acquisition equipment electronics and test station should be specified, with the aim of avoiding ground loops, sensitivity to power line variations, noise and cross talk from the power line, other accelerometers in multi-accelerometer testing, and other equipment. Optical isolation is recommended for digital signals going into the data acquisition computer and other equipment.

11.2.2.3 Dividing head and mounting fixture

If great accuracy is not required for positioning the accelerometer axes in the gravity field, it might be sufficient to attach the accelerometer to a block that is oriented by hand on a table surface to place the accelerometer IA in the up and down orientations.

For greater accuracy and other orientations, a dividing-head or indexing table is required for placing the accelerometer IA at various discrete positions relative to the gravity vector. The dividing-head table could be placed on a concrete seismic pier or slab isolated from the building floor to minimize tilt and azimuth movements, such as caused by diurnal and seasonal heating and ground water effects. The seismic and tilt environment of the pier and test table should be evaluated.

The accelerometer is mounted on a fixture and aligned on the dividing head as described in K.1.3. Remaining misalignments are estimated along with accelerometer bias, scale factor, and other parameters when analyzing tumble test data (see 12.3.4, 12.3.5, and Annex K). With the accelerometer IA perpendicular to the dividing-head rotation axis, it is assumed that the IA is nominally along the gravity vector at the 90° up and 270° down dividing-head positions and nominally horizontal at the 0° and 180° positions.

11.2.2.4 Vibration and shock equipment

The characteristics of commercially available electrodynamic and hydraulic vibrators for imparting vibration and shock profiles to an accelerometer are described in Annex L. The control and monitoring of the vibration and shock acceleration during a test are accomplished using a piezoelectric accelerometer that has a calibrated accuracy of approximately 1%. The acceleration imparted to the test article by such a machine averages zero.

Therefore, a drop-test machine for imparting precise nonzero average shocks is sometimes employed. For imparting imprecise shocks, an accelerometer may simply be dropped from a specified height onto a specified surface.

Higher level shock and acceleration profiles can also be provided by an air gun or other specially built device.

Functional check of a high-*g* micromechanical accelerometer can be done by striking or tapping the accelerometer enclosure or support with a hammer (perhaps with a plastic or rubber-cushioned head) and observing the voltage output of the accelerometer on an oscilloscope. This technique is, of course, not used in performance testing.

11.2.2.5 Centrifuge

Precision centrifuge instrumentation for calibrating model coefficients is described in IEEE Std 836™.

A lesser accuracy centrifuge can be used for determining such quantities as overload capacity.

11.2.2.6 Environmental chambers

Thermal, barometric, and other environmental chambers should be described along with the methods of measuring and controlling the environment and calibrating the instrumentation.

A test fixture on a dividing head could be inserted into a thermal chamber (refrigerated and/or heated over a wide temperature range) for doing tumble tests at each temperature setting in order to calibrate accelerometer model coefficients as functions of temperature.

A temperature-controlled barometric chamber with a rapid drop in temperature and pressure to near vacuum conditions could be used to observe the effects of launching an accelerometer or a whole guidance system into space.

12. Test procedure

12.1 Test setup

12.1.1 Nonoperating test setup

Nonoperating test setup shall be as follows:

a) Unless otherwise specified, all nonoperational tests shall be performed in a normal laboratory environment as described in 11.1.1.

b) After examination, the accelerometer shall be mounted on a simple mounting fixture that will minimize the chances for accidental mechanical damage.

c) The electrical leads, if required, shall be brought out to a junction box or equivalent device that will minimize the chance of accidental damage due to shorting across leads, and so on. Terminal designations shall be as shown on the electrical schematic.

12.1.2 Operating test setup

12.1.2.1 Interconnections

Interconnections, test points, and grounding shall be as specified on the schematic diagram in Figure __________ (see 5.5.1).

12.1.2.2 OA rotation mounting position

OA rotation mounting position test setup shall be as follows:

a) Unless otherwise specified, the [acceleration sensor, accelerometer] shall be operated under the standard test conditions of 11.1.

b) With the rotation axis of the dividing head horizontal within __________ [µrad, mrad], attach the mounting fixture to the face plate of the dividing head so that the accelerometer can be mounted on the reference mounting [surface, surfaces] with the following requirements:

   1) The IA is horizontal within __________ [µrad, mrad].

   2) The positive PA points downward.

   3) The OA is parallel to the rotation axis of the head within __________ [µrad, mrad].

This position of the dividing head shall be considered the zero acceleration reference position. When the dividing head is rotated by 90°, the positive input reference axis shall be aligned parallel to the local gravity vector in the up direction.

c) The accelerometer and immediate environment (including the dividing head) shall be allowed to reach thermal equilibrium before proceeding with the test, IA pointing upward.

12.1.2.3 PA rotation mounting position

PA rotation mounting position test setup shall be as follows:

a) Unless otherwise specified, the [acceleration sensor, accelerometer] shall be operated under the standard test conditions of 11.1.
b) With the rotation axis of the dividing head horizontal within __________ [μrad, mrad], attach the mounting fixture to the face plate of the dividing head so that the accelerometer can be mounted on the reference mounting [surface, surfaces] with the following requirements:
    1) The IA is horizontal within __________ [μrad, mrad].
    2) The positive OA points downward.
    3) The PA is parallel to the rotation axis of the head within __________ [μrad, mrad].

    This position of the dividing head shall be considered the zero acceleration reference position. When the dividing head is rotated by 90°, the positive input reference axis shall be aligned parallel to the local gravity vector in the up direction.

c) The accelerometer and immediate environment (including the dividing head) shall be allowed to reach thermal equilibrium before proceeding with the test, IA pointing upward.

12.2 Accelerometer nonoperating tests

These methods are intended to assure the conformance of the accelerometer to the nonoperating mechanical and electrical requirements.

12.2.1 Examination of product

The accelerometer shall be examined visually for proper identification markings, surface finish, workmanship, and dimensional conformance to the outline drawing in Figure __________.

Figure 3 is a sample outline drawing.

12.2.2 Weight or mass

Measure the mass of the [acceleration sensor, accelerometer]. The mass shall conform to the requirements of 5.4.5.

12.2.3 Impedance

Care must be taken in the choice of the junction box and the size and length of leads to avoid affecting the characteristics of the accelerometer circuits and resulting performance.

12.2.3.1 Purpose

The purpose of this test is to measure the impedance of the accelerometer's electrical circuits.

12.2.3.2 Test equipment

The following test equipment specified in 11.2 is required for this test:

a) Impedance measuring equipment

b) Resistance measuring equipment

12.2.3.3 Test setup

The test setup shall be in accordance with 12.1.1.

12.2.3.4 Test procedure

Measure the impedances of each circuit listed as follows.

The following measurements of resistance and impedance usually apply to specifications for acceleration sensors only. For accelerometers that contain integral capture electronics, the list of measurements required will be different and should be selected as applicable. In some cases, it may be desirable to conduct the impedance test at operating temperature.

a) Pickoff

  1) Input impedance of the pickoff between terminals __________ and __________at __________ ± __________ Hz.

  2) Output impedance of the pickoff between terminals __________ and __________ at __________ ± __________ Hz.

b) Heaters

  1) Impedance of the warm-up heater between terminals __________ and __________ at __________ ± __________ Hz.

  2) Impedance of the control heater between terminals __________ and __________ at __________ ± __________ Hz.

c) Temperature sensor. Resistance of the temperature sensor between terminals __________ and __________.

d) Torquer. Impedance of the torquer between terminals __________ and __________ at __________ ± __________ Hz.

e) Self-test torquer. Resistance of the self-test torquer between terminals __________ and __________.

12.2.3.5 Test results

The resistance and impedance measurements shall conform to the requirements of 5.5.1.

12.2.4 Dielectric strength

12.2.4.1 Purpose

The purpose of this test is to ascertain that the accelerometer circuits can operate safely at their rated voltage and withstand overvoltage due to switching, surges, and so on, by monitoring the leakage current between isolated circuits and between the accelerometer case and circuits isolated from the accelerometer case.

Extreme caution must be observed in selecting the proper pins at which to apply voltage to avoid damaging internal components. Consult the manufacturer for proper pin selection.

12.2.4.2 Test equipment

The following test equipment specified in 11.2 is required for this test: adjustable ac high-voltage source equipped with voltage- and current-measuring capabilities.

12.2.4.3 Test setup

The test setup shall be in accordance with 12.1.1.

12.2.4.4 Test procedure

Apply __________ ± __________ V rms at __________ Hz between isolated circuits and between each circuit and the accelerometer case. The test voltage shall be raised from zero to the specified value as uniformly as possible at a rate of __________ V rms/s. The test voltage shall be maintained for __________ s and then reduced to zero at a rate of __________ V rms/s. During each test, the current meter shall be monitored for leakage current and the result recorded.

12.2.4.5 Test results

The leakage current shall conform to the requirements of 5.5.4.

12.2.5 Insulation resistance

12.2.5.1 Purpose

The purpose of this test is to measure the insulation resistance between isolated circuits and between the accelerometer case and circuits isolated from the case.

Extreme caution must be observed in selecting the proper pins to avoid damaging internal components. Consult the manufacturer for proper pin selection.

12.2.5.2 Test equipment

The following test equipment specified in 11.2 is required for this test: megohmmeter.

12.2.5.3 Test setup

The test setup shall be in accordance with 12.1.1.

12.2.5.4 Test procedure

Apply __________ ± __________ V dc for a period of __________ ± __________ s between isolated circuits and between each circuit and the accelerometer case. Record the minimum resistance readings.

Different voltages may be specified for different circuits.

12.2.5.5 Test results

The minimum insulation resistance shall conform to the requirements of 5.5.3.

12.2.6 Seal

12.2.6.1 Purpose

The purpose of this test is to determine that the accelerometer is properly sealed.

This procedure is written to accommodate either fluid-filled, gas-filled, or evacuated accelerometers. It may be desirable to cycle the accelerometer several times over the full environmental temperature range before starting this procedure. The appropriate subparagraphs that follow should be chosen.

In some cases, other procedures may be more appropriate, such as the use of fluorescent tracers in fluids, the measurement of weight loss, or the use of helium tracer gas mixed with the normal fill gas.

12.2.6.2 Test equipment

The following test equipment specified in 11.2 is required for this test:

a) Fluid-filled accelerometer
   1) Binocular microscope
   2) Vacuum enclosure
b) Gas-filled accelerometer
   1) Leak detector or immersion fluid (specify)
   2) Vacuum enclosure
c) Evacuated accelerometer: some method of measuring performance change with leakage

12.2.6.3 Test setup

The test setup shall be in accordance with 12.1.1.

12.2.6.4 Test procedure

The test procedure shall be based on the type of accelerometer as follows:

a) *Fluid-filled accelerometer*. After thorough cleaning of all surfaces, the accelerometer shall be placed in a vacuum enclosure at less than __________ [Pa, torr] and at an accelerometer temperature of __________ ± __________ °C for a minimum period of __________ [s, min]. The accelerometer shall then be removed and visually examined for evidence of leakage at a magnification of __________ power.
b) *Gas-filled accelerometer*. The accelerometer shall be placed in a vacuum enclosure at less than __________ [Pa, torr] and at an accelerometer temperature of __________ ± __________ °C for a

minimum period of __________ [s, min]. External gas leakage shall be then measured using a leak detector.

or

The accelerometer shall be submerged in a fluid and placed in a vacuum enclosure at less than __________ [Pa, torr] and at an accelerometer temperature of __________ ± __________ °C for a minimum period of __________ [s, min]. The presence or absence of a flow of bubbles after __________ [s, min] shall be noted. Care must be taken to distinguish bubbles due to leakage from those due to absorbed gases on the outer surface or those due to absorbed gases released from the fluid.

c) *Evacuated accelerometer*. Determine the gas leakage into the evacuated accelerometer case by the performance change with time.

For a VBA, the change in resonator *Q* is a measure of vacuum decay.

12.2.6.5 Test results

The results shall conform to the requirements of 5.4.6.

12.2.7 Temperature sensor characteristics

12.2.7.1 Purpose

The purpose of this test is to determine the output characteristics of the accelerometer's temperature sensor(s) over the accelerometer's operating temperature range.

12.2.7.2 Test equipment

The following test equipment specified in 11.2 is required for this test:

a) Temperature-controlled environmental enclosure

b) [Resistance, Voltage, Other output] measuring equipment

In some cases, care must be taken not to induce self-heating of the temperature sensor due to the excitation current.

12.2.7.3 Test setup

The accelerometer shall be placed in a temperature-controlled environmental enclosure. All accelerometer circuits shall be de-energized.

In some cases, the accelerometer circuits may be energized to simulate the actual application more closely.

12.2.7.4 Test procedure

Stabilize the sensor temperature at __________ ± __________ °C. Measure the output of the temperature sensor. Repeat the test for the following sensor temperatures: __________, __________, __________, …, __________ ± __________ °C.

Select a sequence of temperatures that adequately covers the operating range and defines the nonlinearity and repeatability of the temperature sensor output in, for example, volts, as a function of temperature in °C.

Bridge and operational amplifier electronics for measuring the resistance of a thermistor can be designed to have a voltage output. For a vibrating crystal thermal sensor that changes its frequency with temperature variation, a frequency counter may be used.

12.2.7.5 Test results

Perform a least-squares fit to the data of a polynomial model of the temperature sensor output versus temperature to determine compliance with 5.3.4.2.

If the accelerometer uses a thermostatic temperature control instead of a resistive sensor, the temperature at which the device opens on a rising temperature and closes on a falling temperature should be measured.

12.3 Accelerometer operating tests

These tests are intended to determine the [acceleration sensor, accelerometer] performance characteristics.

Many accelerometer operating tests use the gravity at the test site to provide acceleration input, especially for measuring scale factor, bias, and misalignments. Even accelerometers operating at moderately high acceleration levels use the l-*g* calibration results for these first-order parameters. Hence, where high accuracy is required, the local acceleration due to gravity should be calibrated by a gravimeter to compare results between different test sites or to use locally calibrated parameters in a mission.

The gravity calibration can be accomplished with a gravimeter that measures variations in gravity brought from a location whose absolute value of gravity acceleration is known. A more precise calibration can be done with the falling laser corner cube gravimeter that measures the fall in a vacuum of a corner cube reflector with a laser interferometer, thereby calibrating gravity against atomic time and distance standards.

Other accelerometer operating tests are done on a centrifuge or on vibration and shock machines to measure higher order model coefficients for the more accurate accelerometers, or scale factor and bias for very high-*g* lesser accurate accelerometers. For these purposes, the measure of the input acceleration has to be known with lesser accuracy than the local value of gravity.

For the $r\omega^2$ acceleration input on a centrifuge, the rotation rate ω can be accurately measured, but the arm length r is only approximately measured (but accurately enough for calibrating scale factor for lesser accurate accelerometers). The important thing for calibrating higher order accelerometer model coefficients is that the arm stretch and droop variations with centrifuge rate be accurately measured with laser or other techniques.

Vibration and shock calibrations of higher order accelerometer model coefficients use monitor or control piezoelectric accelerometers as references. These devices can be calibrated to ~1% accuracy by monitoring vibration test motions with, for example, a laser interferometer. The manufacturer’s calibration is often employed.

In the tests that follow, the accelerometer output measurement test equipment and technique may significantly influence the test results. Specify the sequence of operations required to bring the accelerometer and test equipment to operating condition for each test setup.

The specific tests and test sequence required will depend on the intended application.

Voltage gradients between the accelerometer case and internal circuitry may produce extraneous forces on the proof mass and should be given careful consideration.

12.3.1 Functional checkout

12.3.1.1 Purpose

The purpose of this test is to determine that all of the operational electrical interface functions are within their allowable tolerances.

12.3.1.2 Test equipment

The following test equipment specified in 11.2 is required for this test:

a) Dividing head and mounting fixture

b) Electronic equipment required to operate the accelerometer and measure its output

c) Other special equipment, dependent on the accelerometer being tested

Specify additional test equipment required to make measurements at the electrical interface, such as variable power supplies, variable frequency supplies, oscilloscopes, electronic counters, ammeters, precision voltmeters, and wattmeters.

12.3.1.3 Test setup

The test setup shall be in accordance with 12.1.2.1 and 12.1.2.2 in the IA vertical orientation.

Other dividing-head positions may be specified during the test to evaluate interface functions with various values of *g* as an input. For example, measurements on a pendulous accelerometer's pickoff can be made in the IA horizontal orientation with the capture loop open.

12.3.1.4 Test procedure

Specify the test methods that are required to determine that the functions at the electrical interface are within their allowable tolerances, for example,

a) Measure input current(s).

b) Measure test point wave shapes.

c) Measure output signal wave shapes.

d) Measure test point wave shapes with input line voltages at the allowable extremes.

e) Measure output signal wave-shape characteristics with input line voltages at the allowable extremes.

f) Measure phase relations between critical signals.

g) Measure distortion of critical signals, and so on

12.3.1.5 Test results

The measured test results shall conform to the requirements of 5.3.29.

12.3.2 Noise

12.3.2.1 Purpose

The purpose of this test is to characterize the noise in the accelerometer output over a wide frequency band. Noise characterization is done by calculating the PSD, Allan variance, and/or standard deviation of the output in an IA vertical drift test with or without a trend removed.

The test is specified for the IA vertical (IA up or down) orientation. It can also be done at other orientations, such as IA horizontal. Since the accelerometer is maximally sensitive to tilt in the IA horizontal orientation, mounting in the IA vertical orientation will likely result in quieter data.

The accelerometer noise measurement could be corrupted by the seismic noise environment of the test station, generally above 1 Hz (see M.2). Hence, the seismic environment of the test station should be evaluated. If necessary, noise testing should be done in a remote location to lessen the effect of cultural electromagnetic and seismic noise.

Dual rather than single accelerometer testing might be required to separate the inherent noise in the accelerometer from environmental noise effects. Performing noise computations on the difference of IA-parallel or the sum of IA-antiparallel accelerometer outputs (scaled by each accelerometer's scale factor if necessary) would obtain a measurement of noise that has the environmental noise common mode rejected and the indicated noise level raised over that of an individual accelerometer by a factor of $\sqrt{2}$. Common mode rejection of environmental noise occurs only if the accelerometers have comparable performance and transfer functions and are co-aligned. Cross-PSD analysis can also be used in dual accelerometer testing to separate the effect of common environmental input noise from the inherent noise of the accelerometers (see I.7.4).

12.3.2.2 Test equipment

The following test equipment specified in 11.2 is required for this test:

a) Dividing head and mounting fixture for IA parallel or antiparallel accelerometer testing, resting on a test pier

b) Electronic equipment required to operate the accelerometer and measure its output

The test pier should be at or below ground level isolated from the building floor and foundation to minimize seismic environmental effects. Whether the pier is imbedded in soil or goes down to bed rock depends on local geologic conditions. Testing at a remote site and/or dual accelerometer test techniques might be required to minimize the corrupting effects of environmental noise.

12.3.2.3 Test setup

The test setup shall be in accordance with 12.1.2.1 and 12.1.2.2 with IA vertical for accelerometer testing.

12.3.2.4 Test procedure

Orient the accelerometer(s) with IA vertical (dividing-head angle 90° or 270°).

Collect data at a high output rate, at least twice the frequency used in the application for which the accelerometer is intended, for at least a power of 2 number of points [16 384, 32 768, etc., for PSD analysis using the fast Fourier transform (FFT)].

If memory is of concern, the test may be repeated with a slower data acquisition rate over a longer data span such as hours or days. The data should be acquired at the high rate with a higher order filter applied to the raw data before it is decimated (say, 100-point decimation) to the lower output rate for storage by the data acquisition computer to reduce aliasing of high-frequency noise into the low-frequency output (see Annex H). If continuous counter data are being collected, for example, then high-frequency counter readings should be triangularly or better filtered, rather than sampling the counter at a lower rate, which is applying only a rectangular filter to the data.

The purpose of splitting the test into two or more segments is that the data storage requirements could be too large to record all the data at the highest rate of interest over the complete time span of interest. Data recorded at the high rate are used to characterize the high-frequency accelerometer noise, whereas the data recorded at a lower rate with real-time digital filtering to prevent aliasing of the high-frequency noise into the low-frequency output are used to characterize the longer term behavior of the accelerometer.

Multiple accelerometer testing with IAs parallel or antiparallel is advantageous in detecting anomalies in the data that are due to external causes and in distinguishing accelerometer noise from environmental (such as seismic) input noise.

12.3.2.5 Test results

The collected data shall be analyzed as follows:

a) Plot the individual accelerometer data and the difference or sum data for IA parallel or antiparallel accelerometers for the high-rate and the low-rate segments of the data. Bad data points (more than, say, 5 standard deviations from the mean) can be replaced by the average of surrounding points if there is a reason for them not to be due to imperfections in the accelerometer (for instance, if they appear simultaneously in all accelerometers being tested).

   The data can also be plotted with various levels of triangular or better filtering with and without trend removed and with thermal and other compensation applied. Compute the rms statistics of the data, and verify that the requirements of 5.3.20 are satisfied.

b) If the drift test data residuals are on the order of, or less than, 0.1 μg and the period of interest is on the order of hours, then compensation for the effects of the lunar-solar earth tide signature may be required. The lunar-solar earth tide magnitude is on the order of 0.1 μg with a period of approximately 12.4 h [see Annex M].

c) Compute the PSD and/or square root of Allan variance of the accelerometer data and of the difference or sum data for IA parallel or antiparallel accelerometers [see Annex I]. If both PSD and Allan variances are computed, the PSD frequency band of the high-frequency data shall overlap that of the Allan variance low-frequency data. The results shall satisfy the requirements of 5.3.20.

   Cross-PSD analysis can also be done on IA parallel or antiparallel dual accelerometer test data to separate accelerometer from environmental noise [see I.7.4].

12.3.3 Inversion transient

12.3.3.1 Purpose

The purpose of this test is to determine, after a long stabilization in the direction opposite of local vertical, the transient in the output of the accelerometer that occurs when it is positioned in the direction of local vertical and vice versa.

12.3.3.2 Test equipment

The following equipment specified in 11.2 is required for this test:

a) Dividing head and mounting fixture

b) Temperature controller (if required)

c) Electronic equipment required to operate the accelerometer and measure its output

12.3.3.3 Test setup

The test setup shall be in accordance with 12.1.2.1 and 12.1.2.2.

12.3.3.4 Test procedure

The test procedure shall be as follows:

a) Rotate the dividing head to the 90° IA up position and wait __________ h to reach stabilization of the accelerometer's output.

b) Rotate the dividing head to the 270° IA down position and continuously measure the accelerometer output as soon as the position is reached. Record the measurements for __________ h.

c) Rotate the dividing head to the 90° IA up position and continuously measure the accelerometer output as soon as the position is reached. Record the measurements for __________ h.

d) Repeat Step b) and Step c) __________ times.

12.3.3.5 Test results

Plot the data in the IA vertical up and down positions as functions of time. Determine the magnitude and duration of the transient in each data span and whether there is any shift or change in trend in the data in a given orientation across a dwell in the opposite orientation. See Annex J.

The inversion transient magnitude and duration shall conform to the requirements of 5.3.18.

It may be useful to thermally compensate the accelerometer output to separate the portion of the inversion transient due to the 2-*g* change in acceleration level and any shock caused by dividing-head movement from the portion due to the thermal transients resulting from the change in orientation.

Another test is to rotate the dividing head 360° to see whether there is any shift or transient when returning to the same IA vertical position. At the IA vertical up or down positions, the ±1-*g* input to the accelerometer is insensitive to small errors in dividing-head repeatability.

12.3.4 Four-point tumble

This test describes one method of determining scale factor, bias, and IA misalignment. A two-position up–down test is sufficient to measure scale factor and bias. Another test for measuring accelerometer model coefficients is described in 12.3.5.

The rotational sequence of the dividing head selected is arbitrary.

The duration of settling and data collection time at each position should be chosen to obtain the desired accuracy.

12.3.4.1 Purpose

The purpose of this test is to determine the bias K_0, the scale factor K_1, and IA misalignment δ_o or δ_p. Note that this test needs to be executed twice: once to measure δ_o and again to measure δ_p.

12.3.4.2 Test equipment

The following equipment specified in 11.2 is required for this test:

a) Dividing head and mounting fixture

b) Electronic equipment required to operate the accelerometer and measure its output

12.3.4.3 Test setup

To measure δ_o, the test setup shall be in accordance with 12.1.2.1 and 12.1.2.2. To measure δ_p, the test setup shall be in accordance with 12.1.2.1 and 12.1.2.3.

12.3.4.4 Test procedure

The test procedure shall be as follows:

a) Rotate the dividing head to the 90° position (input reference axis up) within ________ [µrad, ″]. Record the accelerometer output as E_{90}.

b) Rotate the dividing head to the 270° position (input reference axis down) within ________ [µrad, ″]. Record the accelerometer output as E_{270}.

c) Rotate the dividing head to the 0° position (input reference axis horizontal) within ______ [µrad, ″]. Record the accelerometer output as E_0.

d) Rotate the dividing head to the 180° position (input reference axis horizontal) within _____ [µrad,″]. Record the accelerometer output as E_{180}.

e) Calculate K_1, K_0, and misalignment using the following algebraic equations:

$$K_1 = \frac{E_{90} - E_{270}}{2} \quad \text{output units / [m/s}^2\text{, ft/s}^2\text{, \_\_\_\_\_]} \tag{1}$$

$$K_0 = \frac{E_{90} + E_{270}}{2K_1} \quad \text{[m/s}^2\text{, ft/s}^2\text{, \_\_\_\_\_]} \tag{2}$$

$$\delta_o = \frac{E_0 - E_{180}}{2K_1} \quad \text{rad} \qquad \text{(3, for 12.1.2.2 orientation)}$$

$$\delta_p = \frac{E_{180} - E_0}{2K_1} \quad \text{rad} \qquad \text{(4, for 12.1.2.3 orientation)}$$

The bias and scale factor obtained from the IA up–down data by this method include the effects of the second-order term K_2 and the third-order term K_3, respectively. See Annex K.

An alternative method of measuring bias is to obtain the accelerometer outputs at the cardinal positions. This value represents the bias with (nominally) no acceleration applied along the IA and is

$$K_0 = \frac{E_0 + E_{180}}{2K_1} \ g$$

where E_0 and E_{180} are the accelerometer outputs measured in the two horizontal positions. The two positions must be 180° apart within 1" for each 2.5-μ*g* allowable uncertainty in the bias measurement.

The misalignment angles as obtained earlier include angular errors of the mounting fixture, dividing-head errors, and mounting errors as well as the misalignment between the input reference axis and the IA. There is no way of distinguishing between a misalignment and a cross-axis sensitivity. An alternative method is to align the input reference axis parallel to the horizontal dividing-head rotation axis and to obtain measures of indicated acceleration at each of the four cardinal case positions.

For high-acceleration applications, when ±l-*g* testing might not adequately determine bias, scale factor, and misalignment, a four-point tumble test on a centrifuge relative to the centrifuge arm direction could be used. Care must be taken to have the accelerometer effective center of mass (for spin) directly over the tumble rotation axis.

For applications where an accelerometer maximum range is less than ±1 *g*, the ±1-*g* points cannot be used for calibration. In this case, calibration can be attempted using small angles about the horizontal zero *g* position. For example, placing the IA at ±30 degrees about the local horizontal might be used to represent ±0.5-*g* input along the IA. In this case, the level of calibration accuracy achievable will depend on the absolute knowledge of the angles used. Because testing at small angles about the horizontal zero *g* position introduces accelerations perpendicular to the input axis, the knowledge of the value of any possible cross-axis or cross-coupling coefficients is necessary for compensation.

This technique may not be adequate for calibrating a triaxial low *g* accelerometer, as one of the three axes may be mechanically saturated in any practical test position. In this situation, calibration in space is an option.

12.3.4.5 Test results

The results shall conform to the requirements of 5.3.5.1, 5.3.7.1, 5.3.8.1, and 5.3.8.2.

12.3.5 Static multipoint

12.3.5.1 Purpose

The purpose of the static multipoint test is to determine the coefficients of the assumed model equation by a series of measurements in the gravitational field.

See Annex K for a discussion on the static multipoint test and the data reduction procedure.

12.3.5.2 Test equipment

The following test equipment specified in 11.2 is required for this test:

a) Dividing head and mounting fixture

b) Electronic equipment required to operate the accelerometer and measure its output

12.3.5.3 Test setup mounting position 1

The test setup shall be in accordance with 12.1.2.1 and 12.1.2.2.

12.3.5.4 Test procedure mounting position 1

At each head angle $\theta = 0°$, $\Delta\theta$, $2\Delta\theta$, …, $k\Delta\theta$, …, $(n - 1)\,\Delta\theta$, take and record __________ measurements of the accelerometer output E_{kp}, where $\Delta\theta = 360/n$, n and k are integers, n = __________, and $0 \leq k \leq n - 1$. The dividing-head angles shall be set within __________ [μrad, ″].

> The choice of the number of test positions n is usually based on statistical considerations.
>
> Instead of equal increments of angle, there could be equal increments of acceleration or some other pattern of dividing-head angles. Caution should be used in including data near the 0° and 180° IA horizontal positions since some accelerometers might display asymmetries in bias, scale factor, or misalignment.
>
> Depending on the desired test accuracy and the output characteristics of the particular accelerometer, the following items should be specified:
>
> a) Sequence of dividing-head positions
>
> b) Settling time allowed at each position
>
> c) Number of individual measurements at each position
>
> d) Averaging interval associated with each measurement
>
> e) Dividing-head accuracy
>
> f) Pier stability

12.3.5.5 Test setup mounting position 2

The test setup shall be in accordance with 12.1.2.1 and 12.1.2.3.

12.3.5.6 Test procedure mounting position 2

At each head angle $\theta = 0°$, $\Delta\theta$, $2\Delta\theta$, ..., $k\Delta\theta$, ..., $(n - 1)\Delta\theta$, take and record __________ measurements of the accelerometer output E_{ko}, where $\Delta\theta = 360/n$, n and k are integers, n = __________, and $0 \leq k \leq n - 1$. The dividing-head angles shall be set within __________ [μrad, ″].

12.3.5.7 Test results

The collected data shall be analyzed as follows:

a) From the test data taken in the two mounting positions, compute the best estimate of each of the model equation coefficients, the uncertainties of the coefficients, and the standard deviation or rms of the postfit residuals.

> Specify the data reduction procedure or the data reduction program to be used. See Annex K for suggested data reduction procedures.

b) The best estimate of the model equation coefficients and their uncertainties shall conform to the requirements from 5.3.5.1, 5.3.5.2, 5.3.6, 5.3.7.1, 5.3.7.2, 5.3.8.1, 5.3.8.2, and 5.3.11, which are also listed in Table 4.

Table 4—Multipoint tumble model coefficient estimates and uncertainties

Coefficient	Estimated		Requirement	Units
	Value	Uncertainty		
K_0	______	________	$\|K_0\| <$ __________	[m/s^2, ft/s^2, _____]
$K_0' = K_{0+} - K_{0-}$	______	________	$\|K_0'\| <$ _________	[m/s^2, ft/s^2, _____]
K_1	______	________	$\|K_1\| =$ ____ ± ____	output units/[m/s^2, ft/s^2, _____]
$K_1' = (K_{0+} - K_{0-})/K_1$	______	________	$\|K_1'\| <$ _________	[dimensionless, ppm]
K_{oq}	______	________	$\|K_{oq}\| <$ _________	[m/s^2, ft/s^2, _____]/[m/s^2, ft/s^2, _____]^2
K_2	______	________	$\|K_2\| <$ __________	[m/s^2, ft/s^2, _____]/[m/s^2, ft/s^2, _____]^2
K_3	______	________	$\|K_3\| <$ __________	[m/s^2, ft/s^2, _____]/[m/s^2, ft/s^2, _____]^3
δ_o	______	________	$\|\delta_o\| <$ __________	[rad, μrad]
δ_p	______	________	$\|\delta_p\| <$ __________	[rad, μrad]
K_{ip}	______	________	$\|K_{ip}\| <$ __________	[m/s^2, ft/s^2, _____]/[m/s^2, ft/s^2, _____]^2
K_{io}	______	________	$\|K_{io}\| <$ __________	[m/s^2, ft/s^2, _____]/[m/s^2, ft/s^2, _____]^2

For lesser accuracy accelerometers, nonlinearity may be specified as the maximum deviation from a least-squares, best-fit straight line over full span, in percent of the full span of the accelerometer.

K_{po} is not listed because it cannot be estimated from tumbles about OA or PA. Also, K_{pp} or K_{oo} cannot be estimated simultaneously with K_2 in a multipoint tumble test when bias K_0 is also estimated (see K.2.4). For accurate accelerometers, either K_{pp} and K_{oo} have to be calibrated from centrifuge or vibration tests and K_2 estimated in a dual orthogonal accelerometer tumble test using these calibrated values, or vice versa, using the magnitude-squared-of-*g* observable or estimating angle-setting errors, as described in Annex K.

However, the dual orthogonal accelerometer approach to eliminate the effect of angle-setting errors does not allow for the estimation of K_{ip} or K_{io} simultaneously with bias K_0 and K_2, nor of K_3 simultaneously with scale factor K_1 (see K.5.2). Quadratic, cubic, and other acceleration nonlinearities are best determined from centrifuge or vibration tests at acceleration levels comparable to those encountered in the mission in which the accelerometer is used (see 12.3.15 and 12.3.17).

Equivalent results are obtained whether K_0, K_0' are estimated or the biases for positive and negative accelerations K_{0+}, K_{0-} are estimated. Similarly, it is equivalent whether K_1, K_1' are estimated or the scale factors for positive and negative accelerations K_{1+}, K_{1-} are estimated.

If the bias and scale factor asymmetry terms K_0' and K_1' and the odd quadratic term K_{oq} are found to be statistically insignificant, they should be left out of the multipoint tumble fit because they degrade the precision of the estimation of the other parameters, such as bias K_0, scale factor K_1, and misalignment δ_o or δ_p.

Equivalent results are obtained whether scale factor K_1 is estimated or a scale factor error k_1 is estimated with the scale factor calculated from $K_1 = K_1^0\,(1 + k_1)$, where K_1^0 is a nominal value of the scale factor chosen so that the squares and products of k_1 and the other estimated parameters can be ignored. Such disregard is desirable in some theoretical manipulations.

The uncertainty of a parameter estimate is the standard deviation of the parameter estimate in the multipoint tumble fit (see K.6). Because of small sample sizes and unmodeled effects, a more realistic indication of the parameter estimate uncertainties is the variation in the parameter estimates in repetitions of the multipoint tumble test, if the time between tests is not so long as to have the resulting comparisons corrupted by trends or other parameter instabilities.

c) The standard deviation or rms of the residuals shall not exceed __________ [m/s^2, ft/s^2, _____].

12.3.6 Threshold, resolution, and dead band

12.3.6.1 Purpose

The purpose of this test is to determine the magnitude of acceleration or change in acceleration that causes the accelerometer output or change in output to be at least 50% of that expected using the calibrated scale factor.

12.3.6.2 Test equipment

The following test equipment specified in 11.2 is required for this test:

a) Dividing head and mounting fixture

b) Electronic equipment required to operate the accelerometer and measure its output

12.3.6.3 Test setup

The test setup shall be in accordance with 12.1.2.1 and 12.1.2.2. Care should be taken to rotate the dividing head slowly and smoothly between positions.

12.3.6.4 Test procedures

The threshold, resolution, and dead band test procedures shall be as follows:

a) Threshold

1) Rotate the dividing head to the $\theta_{+0} = 0°$ position (zero gravity) within __________ [μrad, ″] and record the accelerometer output E_{+0}.

2) Rotate the dividing head + __________ [μrad, ″] to the θ_{+1} position and record the accelerometer output E_{+1}.

3) Repeat Step 2) for __________ increasing increments of angle, recording the accelerometer outputs E_{+j} at each θ_{+j} position.

4) Rotate the dividing head to the $\theta_{-0} = 0°$ position (zero gravity) within __________ [μrad, ″] and record the accelerometer output E_{-0}.

5) Rotate the dividing head __________ [μrad, ″] to the θ_{-1} position, and record the accelerometer output E_{-1}

6) Repeat Step 5) for __________ decreasing increments of angle, recording the accelerometer outputs E_{-j} at each θ_{-j} position.

7) Using the scale factor K_1 determined in 12.3.4.4, calculate the difference between the indicated acceleration at each table angle position $\theta_{\pm j}$ and at the θ_0 position

$$\Delta A_{\text{ind},\pm j} = \frac{E_{\pm j} - E_{\pm 0}}{K_1} \text{ [m/s}^2\text{, ft/s}^2\text{, \_\_\_\_\_]}$$

8) Threshold in [m/s², ft/s², _____] is the smallest input acceleration $\Delta A_{\text{input},\pm j} = \sin\theta_{\pm j}$ at which $\Delta A_{\text{ind},\pm j}$ is at least 50% of the input. Record thresholds for both positive and negative inputs.

b) Resolution. Repeat Step 1) through Step 7) of a) in 12.3.6.4, except that the dividing head starts at initial angles θ_0 to induce input acceleration levels of $\pm g/2$ and $\pm g$, respectively, instead of 0. The angular increments at $\pm g/2$ are to be ± __________ [μrad, ″] and at $\pm g$ the angular increments are to be ± __________ [μrad, ″]. Resolution is the smallest $\Delta A_{\text{input},\pm j} = (\sin\theta_{\pm j} - \sin\theta_{\pm 0})$ for which $\Delta A_{\text{ind},\pm j}$ is at least 50% of $\Delta A_{\text{input},\pm j}$. Record resolution for both directions of input rotation.

Other or additional input acceleration levels may be used if desired. In particular, the acceleration input steps starting from ±1 *g* may be chosen to be equal increments of ΔA_{input} rather than equal increments of $\Delta\theta$.

c) Dead band

The procedure in 12.5.2 for searching for the location of VBA activity dips can be used to find the location of accelerometer dead bands besides at the naturally suspicious location of 0 *g* input. The following test then characterizes the dead band found in the ±1-*g* range.

1) Rotate the dividing head about the OA or PA of the accelerometer to the angle that produces an indicated change in output in [m/s^2, ft/s^2, _____] that is a small fraction [1%, 10%, 30%] of the expected maximum dead band. Record this as the reference angle and reference output for the following measurements.

Measurement of accelerometer output must be made to an accuracy much better than the desired measurement of dead band, averaging any measurement noise so that it will have minimal effect on the measurement.

2) Slowly rotate the dividing head clockwise from the reference angle in small increments, applying small increments of acceleration. Continue to measure the accelerometer output, stopping when the accelerometer total change of output from the reference output is greater than 50% of that expected from total change of input acceleration. Record the value of delta-input acceleration.

3) Slowly rotate the dividing head counter-clockwise from the reference angle in small increments of angle from the starting angle of Step 1), applying increments of acceleration of the opposite polarity. Continue to measure the accelerometer output, stopping when the accelerometer's total change of output from the reference output is greater than 50% of that expected from the total change of input acceleration. Record the value of delta-input acceleration.

4) Compute the dead band of the accelerometer at the given reference acceleration as the sum of the absolute values of the delta-inputs in Step 2) and Step 3) in [m/s^2, ft/s^2, _____].

For digital accelerometers, these measurements must be based on the change in pulse-rate where acceleration readings are made as pulses-per-unit-time divided by the unit scale factor. Accordingly, the time duration over which the pulse rate is determined must be chosen to provide a resolution of input acceleration that is no larger than [1%, 10%, 30%] of the expected maximum dead band to allow determination of the reference angle and the dead band using the procedure given here.

12.3.6.5 Test results

Threshold, resolution, and dead band shall conform to the requirements of 5.3.13, 5.3.14, and 5.3.15.1, respectively.

12.3.7 Warm-up time

12.3.7.1 Purpose

The purpose of this test is to determine the time required for the accelerometer output to come within a specified value of the steady-state or final indicated output after power turn-on in a specified ambient environment.

12.3.7.2 Test equipment

The following test equipment specified in 11.2 is required for this test:

a) Dividing head and mounting fixture

b) Electronic equipment required to operate the accelerometer and measure its output

c) Equipment required to establish the specified ambient environment

12.3.7.3 Test setup

The test setup shall be in accordance with 12.1.2.1 and 12.1.2.2, and with 11.1.2.2 a), b), and c), except that the initial ambient temperature shall be room temperature.

12.3.7.4 Test procedure

The test procedure shall be as follows:

a) Set the dividing head at 0°.

b) Establish the ambient thermal environment at __________ ± __________ °C. Allow __________ [s, min] for the accelerometer to reach thermal equilibrium.

c) Energize the accelerometer and test equipment as quickly as possible in accordance with 11.1.1 and 11.1.2.2.

d) Record the accelerometer output as a function of time until a steady state is reached.

12.3.7.5 Test results

The collected data shall be analyzed as follows:

a) Plot the value of the accelerometer output as a function of time.

b) The output obtained from the test shall conform with 5.3.12.

In all cases, the initial thermal ambient environment and thermal mounting conditions must be carefully specified. Care must be taken to ensure that the specified thermal environment does not affect the dividing-head positioning accuracy. For some applications, other orientations may be specified.

12.3.8 Short-term stability

12.3.8.1 Purpose

The purpose of this test is to determine the short-term stability of the accelerometer bias K_0 and scale factor K_1.

12.3.8.2 Test equipment

The following test equipment specified in 11.2 is required for this test:

a) Dividing head and mounting fixture

b) Electronic equipment required to operate the accelerometer and measure its output

12.3.8.3 Test setup

The test setup shall be in accordance with 12.1.2.1 and 12.1.2.2.

12.3.8.4 Test procedure

The test procedure shall be as follows:

a) Stabilize the accelerometer at the standard test conditions specified in 11.1.

b) Determine and record the bias and scale factor using the procedure of 12.3.4.4.

c) Repeat Step b) __________ times per [s, min, h, d] for __________ [s, min, h, d] of continuous operation. Measurements shall be made at least __________ [s, min, h] apart.

> For an application that requires stability over seconds, scale-factor and bias short-term stability could not be verified from the repeated discrete position tumble tests in 12.3.4 or 12.3.5. Rather, they would have to be verified, for instance, by oscillating the accelerometer back and forth or continuously rotating the IA between ±1 *g* at a period that is a fraction of the short-term stability period and estimating scale factor and bias for each cycle.

12.3.8.5 Test results

Determine the standard deviation of the bias and scale factor from their mean values obtained in 12.3.8.4. The results shall conform to the requirements of 5.3.5.3 and 5.3.7.3.

> In some applications, it may be desirable to modify the test to determine the stability of additional parameters such as IA misalignment. Horizontal rotation about IA can be used to determine IA misalignment short-term stability.
>
> Other criteria for establishing stability may be used such as the unbiased estimate of the standard deviation, curve fitting for trend determination, or computer analyses to determine the autocorrelation times.

12.3.9 Long-term stability

12.3.9.1 Purpose

The purpose of this test is to determine the long-term stability of the accelerometer bias K_0 and scale factor K_1.

12.3.9.2 Test equipment

The following test equipment specified in 11.2 is required for this test:

a) Dividing head and mounting fixture

b) Electronic equipment required to operate the accelerometer and measure its output

12.3.9.3 Test setup

The test setup shall be in accordance with 12.1.2.1 and 12.1.2.2.

12.3.9.4 Test procedure

The test procedure shall be as follows:

a) Stabilize the accelerometer at the standard test conditions specified in 11.1.

b) Determine and record the bias and scale factor using the procedure of 12.3.4.4.

c) Repeat Step b) __________ times per day for __________ days of continuous operation. Measurements shall be made at least __________ [min, h] apart.

12.3.9.5 Test results

Obtain the best-fit linear curves to the bias and scale-factor data points of 12.3.9.4 by the method of least squares. Determine the standard deviation of the data points from the best-fit lines. The results shall conform to the requirements of 5.3.5.4 and 5.3.7.4.

In some applications, it may be desirable to modify the test to determine the stability of additional parameters such as IA misalignment.

12.3.10 Repeatability

12.3.10.1 Purpose

The purpose of this test is to determine the repeatability of the bias K_0 and the scale factor K_1 across cooldown and/or shutdown.

12.3.10.2 Test equipment

The following test equipment specified in 11.2 is required for this test:

a) Dividing head and mounting fixture

b) Electronic equipment required to operate the accelerometer and measure its output

12.3.10.3 Test setup

The test setup shall be in accordance with 12.1.2.1 and 12.1.2.2.

12.3.10.4 Test procedure

The test procedure shall be as follows:

a) Stabilize the accelerometer at the standard test conditions specified in 11.1.

b) Determine and record the bias and scale factor using the procedure of 12.3.4.4.

c) De-energize and cool the accelerometer to __________ ± __________ °C. Soak at least __________ h.

d) Repeat Step a), Step b), and Step c) __________ times.

Instead of doing an up–down, four-point, or multipoint tumble test in Step b), the accelerometer could be kept in a fixed orientation across cooldowns and/or shutdowns. Then the rms variation in the mean settled output of the accelerometer across the sequence of cooldowns and/or shutdowns is a measure of the combined repeatability of the scale factor and bias in the IA vertical orientation and of the bias and misalignment in the IA horizontal orientation.

12.3.10.5 Test results

The results shall conform to the requirements of 5.3.5.5, 5.3.7.5, and 5.3.16.

In some applications, it may be desirable to modify the test to determine the stability of additional parameters such as IA misalignment. Repeatability across other environmental conditions besides cooldown and/or shutdown may be specified, such as vibration, shock, variations in operating temperature, and remount.

12.3.11 Sensitivity

12.3.11.1 Purpose

The purpose of the sensitivity test is to determine the changes in accelerometer scale factor K_1 and bias K_0 caused by variations in the following:

a) Input excitation voltage(s)

b) Input excitation frequency(ies)

c) Operating temperature

d) Temperature gradient

e) Temperature rate of change

f) External magnetic induction

g) Pressure

For some applications, it may be desirable to increase or reduce the number of test conditions to be varied and to test for the sensitivity of other accelerometer parameters such as IA misalignment.

12.3.11.2 Test equipment

The following test equipment specified in 11.2 is required for this test:

a) Dividing head and mounting fixture

b) Electronic equipment required to operate the accelerometer and measure its output

c) Equipment required to produce the excitation variations and environmental changes

12.3.11.3 Test setup

The test setup shall be in accordance with 12.1.2.1 and 12.1.2.2.

12.3.11.4 Test procedure

This test is performed by varying each parameter individually while maintaining all other test conditions constant per the requirements of 11.1. An example is presented for input voltage.

a) Determine the accelerometer scale factor and bias per 12.3.4.4 with the input voltage increased to __________ ± __________ V.

b) Decrease the input voltage to __________ ± __________ V, and repeat the test.

For other parameter variations, repeat the test described in 12.3.11.4 for each parameter listed in 12.3.11.1, making sure the accelerometer has reached steady state before calibrating scale factor and bias.

Select the appropriate parameter changes for each test.

Generally the conditions of environmental exposure should be specified, such as rate of temperature and pressure changes and the direction of the magnetic induction. Care must be taken to separate or eliminate the effect of changes in test equipment characteristics caused by variations in environment.

12.3.11.5 Test results

The test data shall be reduced to determine the sensitivity coefficients.

An example of an accelerometer sensitivity coefficient calculation is as follows:

a) The scale factor sensitivity with variations of input voltage is

$$\frac{(K_{1a} - K_{1b})}{K_1(V_a - V_b)}$$

where

K_1 is the nominal scale factor
V_a is the maximum pickoff excitation
V_b is the minimum pickoff excitation
K_{1a} is the scale factor measured with V_a applied
K_{1b} is the scale factor measured with V_b applied

b) The bias sensitivity with variations of pickoff excitation is

$$\frac{K_{0a} - K_{0b}}{V_a - V_b}$$

where

K_{0a} is the bias measured with V_a applied
K_{0b} is the bias measured with V_b applied

Determine the other sensitivity coefficients in a similar manner.

The sensitivity coefficients shall be equal to or less than the limits in 5.3.5.6 and 5.3.7.6, which are also listed in Table 5.

Table 5—Sensitivity coefficient limits

Parameter	Sensitivity	
	Scale factor	**Bias**
Input excitation voltage(s)	______ [%, ppm]/V	______ [m/s^2, ft/s^2, _____]/V
Input excitation frequency(ies)	______ [%, ppm]/Hz	______ [m/s^2, ft/s^2, _____]/Hz
Operating temperature	______ [%, ppm]/°C	______ [m/s^2, ft/s^2, _____]/°C
Temperature gradient	______ [%, ppm]/Δ°C	______ [m/s^2, ft/s^2, _____]/Δ°C
Temperature rate of change	______ [%, ppm]/[°C /min]	______ [m/s^2, ft/s^2, _____]/(°C/min)
External magnetic induction	______ [%, ppm]/[mT, G]	______ [m/s^2, ft/s^2, _____]/[mT, G]
Pressure	______ [%, ppm]/Pa	______ [m/s^2, ft/s^2, _____]/Pa

In some applications, it may be desirable to modify the test to determine the stability of additional parameters such as IA misalignment.

If a particular sensitivity is nonlinear, the result obtained from this procedure can be misleading. It may be desirable to obtain more data points to see whether there is any hysteresis and to determine such characteristics as linearity and maximum slope from a higher order polynomial fit.

12.3.12 Temperature model calibration and temperature hysteresis

12.3.12.1 Purpose

The purpose of this test is to estimate the accelerometer temperature model coefficients and the postfit residuals and hysteresis over a temperature cycle.

12.3.12.2 Test equipment

The following test equipment specified in 11.2 is required for this test:

a) Dividing head and mounting fixture, possibly for multiple accelerometers

b) Electronic equipment required to operate the accelerometer(s) and measure its (their) output

c) Temperature-controlled chamber and/or temperature-controlled mounting fixture for the accelerometer(s)

12.3.12.3 Test setup

The test setup shall be in accordance with 12.1.2.1 and 12.1.2.2, with the accelerometer(s) in the temperature-controlled chamber.

12.3.12.4 Test procedure

Control successively at temperatures $T+j\Delta T$ °C in a schedule

$$T, T+\Delta T, \ldots, T+(n-1)\Delta T, T+n\Delta T, T+(n-1)\Delta T, \ldots, T+\Delta T,$$

$$T, T-\Delta T, \ldots, T-(n-1)\Delta T, T-n\Delta T, T+(n-1)\Delta T, \ldots, T-\Delta T, T$$

in the temperature range $T \pm n\Delta T$ °C. After the accelerometer(s) reach steady thermal state at a temperature setting, perform the four-point tumble test of 12.3.4 to estimate scale factor, bias, and misalignment at that temperature before the temperature is changed to the next setting.

Steady thermal state is indicated by scale factor and bias estimates differing by less than __________ ppm and __________ μ*g*, respectively, in successive tumble tests at a given temperature. The static multipoint test of 12.3.5 can be done at each temperature setting to also estimate nonlinearity and other parameters, if they can be adequately estimated in a static multipoint test. Alternatively, vibration or centrifuge tests can be used to estimate nonlinearity coefficients at each temperature.

12.3.12.5 Test results

Make polynomial of order __________ least-squares fits to the scale factor, bias, and misalignment estimates as functions of temperature sensor output. The polynomial temperature sensitivity coefficients to be used for temperature compensation during operational use, the postfit rms residuals, and temperature hysteresis shall satisfy the requirements of 5.3.9.1 for a temperature-controlled accelerometer or of 5.3.9.2 for a nontemperature-controlled accelerometer.

The coefficients in a temperature gradient and/or a derivative of temperature model can be similarly estimated. The test can be modified to use continuously varying rather than discrete temperature changes. When continuously varying the temperature, care must be taken to interpolate the accelerometer output recorded at the four positions to the same temperature before calculating the scale factor, bias, and misalignment.

12.3.13 Velocity storage across power interrupt

12.3.13.1 Purpose

The purpose of this test is to determine the maximum power interrupt duration for which there is velocity storage in the accelerometer across the normal operating range and the value of this maximum velocity storage. This is accomplished by measuring the maximum power interrupt duration when the IA is parallel with the local gravity field.

The duration for this amount of velocity storage in the operating acceleration range is then the duration measured in the local gravity field divided by the maximum operating acceleration.

12.3.13.2 Test equipment

The following test equipment specified in 11.2 is required for this test:

a) Dividing head and mounting fixture

b) Electronic equipment required to operate the accelerometer and measure its output

c) Electronic circuit to interrupt power to the accelerometer for precisely specified periods of time

12.3.13.3 Test setup

The test setup shall be in accordance with 12.1.2.1 and 12.1.2.2, with the power interrupt circuit added to the electronics to interrupt power to the accelerometer but not to the data acquisition equipment. For a torque-rebalance accelerometer, the power interrupt circuit should only interrupt power to the torquer; power to the pickoff should be maintained throughout the test if possible (see Figure 5).

If acceleration is being measured, such as from an analog-torque loop analog-to-digital converter, the recording interval should be much smaller than the power interrupt interval. If velocity increment is being recorded, such as from a voltage-to-frequency converter, the recording interval could be of the order of the power interrupt interval.

For a pendulous torque-rebalance accelerometer, the pickoff signal output should be recorded if possible (except during power interrupt unless the pickoff signal was still activated even though the torquer was disconnected) at an interval much smaller than the power interrupt interval. In this way, the motion of the pendulum away from null across a power interrupt can be monitored, and it can be detected if the pendulum hits a stop.

For a VBA, the resonator(s) keep vibrating because of their high Q when power is interrupted. Velocity storage in a VBA is accomplished by reconstructing the unobserved cycles that have occurred during the power interrupt using analytic algorithms in a microprocessor attached to the VBA. The maximum allowed duration of a power interrupt and the amount of velocity that can be stored in a VBA are given by the maximum time that unobserved cycles can be reconstructed using information from two resonators in a dual-resonator VBA in the face of the maximum acceleration variation that can occur across a power interrupt interval (see Annex D).

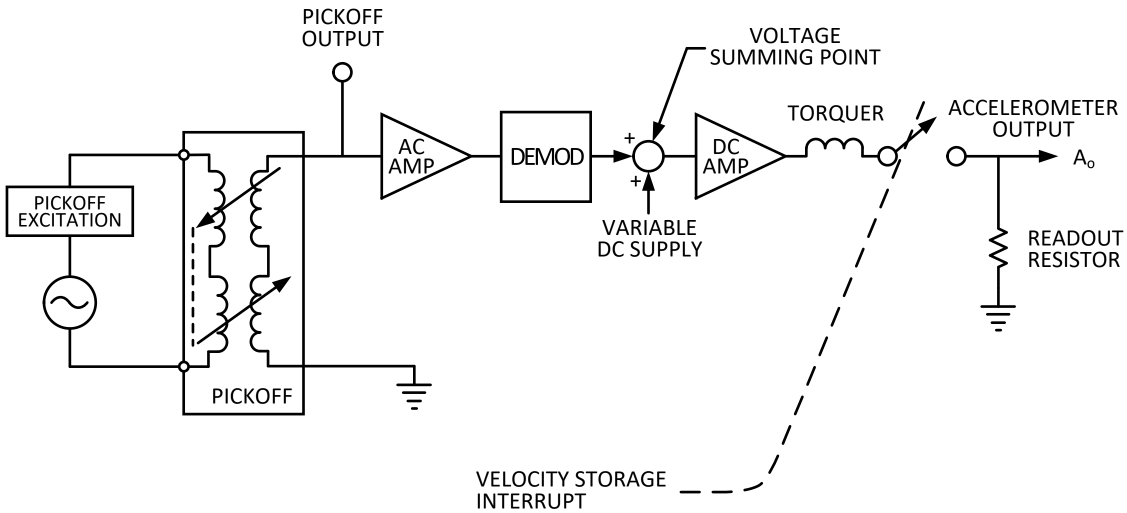

Figure 5—Test circuit for measurement of pickoff scale factor, pendulum elastic restraint, and velocity storage with control-loop interruption

12.3.13.4 Test procedure

In the IA vertical orientation (dividing-head angle 90°), perform the following steps:

a) Collect data for ______ min.

b) Interrupt power to the accelerometer for __________ µs, where the initial power interrupt interval is well below the velocity storage duration capability of the accelerometer when the IA is parallel with the local gravity field.

c) Continue to collect data for __________ min.

d) Increment the power interrupt time by __________ µs, repeat Steps b) through d) until the power interrupt interval exceeds __________ [µs, ms], a duration greater than the velocity storage duration capability of the accelerometer when the IA is parallel with the local gravity field.

12.3.13.5 Test results

Plot the acceleration measurements. At a power interrupt time, the output acceleration will go below the pre-interrupt level in magnitude, and then above it, to return to the pre-interrupt level. If the acceleration level does not return to the pre-interrupt level, the repeatability specification across power interrupt is violated (5.3.5.5 and 5.3.7.5).

Plot the accumulated velocity output of the accelerometer. At a power interrupt time, the accumulated velocity will go below in magnitude the extrapolated accumulated velocity line from before the interrupt time and then return to the extrapolated accumulated velocity line (if there is no shift across power interrupt), until the maximum power interrupt duration capability of the accelerometer is exceeded. Record this maximum power interrupt duration capability and the amount of velocity stored in the accelerometer. Divide this power interrupt duration capability by the maximum acceleration range in 5.6.2.6, and determine whether the resulting power interrupt duration and the velocity storage conform to the requirements of 5.3.19.3.

12.3.14 Centrifuge input range and overload capacity

12.3.14.1 Purpose

The purpose of this test is to establish that the accelerometer input acceleration range or overload capacity is equal to or greater than the specified value.

12.3.14.2 Test equipment

The following equipment specified in 11.2 is required for this test:

a) Mounting fixture

b) Electronic equipment required to operate the accelerometer and measure its output

c) Centrifuge (lesser precision than centrifuge required for calibrating model coefficients)

12.3.14.3 Test setup mounting position A

Mounting position A test setup shall be as follows:

a) Unless otherwise specified, the accelerometer shall be operated under the standard test conditions of 11.1 for operative closed-loop tests.

b) The axis of rotation of the centrifuge shall be vertical within ______ [μrad, ″].

c) The accelerometer shall be attached to the mounting fixture on the centrifuge arm with the input reference axis normal to the centrifuge axis within __________ [μrad, ″] and pointing toward the rotation axis (positive input acceleration). The nominal radius from the centrifuge axis to the proof-mass center of gravity within __________ cm shall be determined and recorded.

d) The starting procedure shall be executed.

State sequence of operations required to bring accelerometer and test equipment to operating conditions.

e) The accelerometer and the immediate environment shall be allowed to reach thermal equilibrium as evidenced by the stability of the accelerometer output within __________ output units for __________ measurements spaced __________ min apart before proceeding with the test.

12.3.14.4 Test procedure mounting position A

Mounting position A test procedure shall be as follows:

a) Successively apply centripetal accelerations of __________, …, __________ [m/s^2, ft/s^2, _____] ± __________ [m/s^2, ft/s^2, _____], where

   1) For the input range, the upper acceleration limit is slightly beyond (110%) the upper limit to be encountered in an application but below the value that would disqualify the accelerometer from being used in the application.

   2) For the overload capacity, the upper acceleration limit is at the overload capacity requirement. Axes other than IA could be along the centrifuge arm, if required by 5.3.3.

b) Record the accelerometer output while dwelling for __________ min at each acceleration level.

12.3.14.5 Test setup mounting position B

Perform the same steps as in 12.3.14.3 except that the direction of the input reference axis shall be reversed (negative input acceleration).

12.3.14.6 Test procedure mounting position B

Perform the same steps as in 12.3.14.4.

12.3.14.7 Test results

Plot the average accelerometer output at each acceleration level versus the acceleration level for the positive and negative input accelerations. A break in the curve indicates that the accelerometer is not responding to acceleration above that level. The acceleration input range for which there is no break in the curve shall equal or exceed the requirements of 5.3.2.

For the accelerometer overload capacity, there may be a break in the curve with the accelerometer proof mass hitting the stops. However, after __________ repetitions of the overload capacity test, the accelerometer shall perform to all specification requirements, per 5.3.3.

12.3.15 Precision centrifuge

12.3.15.1 Purpose

The purpose of this test is to determine the magnitude of the nonlinear acceleration-sensitive model equation coefficients K_2, K_3, K_{oq}, and so on.

Precision centrifuge tests are usually not required for accelerometers with low input ranges (for example, less than ±2 *g*).

12.3.15.2 Test equipment

The following equipment specified in 11.2 is required for this test:

a) Mounting fixture

b) Electronic equipment required to operate the accelerometer and measure its output

c) A precision centrifuge and timing equipment to measure the centrifuge period

12.3.15.3 Test setup mounting position A

Mounting position A test setup shall be as follows:

a) Unless otherwise specified, the accelerometer shall be operated under the standard test conditions of 11.1 for operative closed-loop tests.

b) The axis of rotation of the centrifuge shall be vertical within ______ [μrad, ″].

c) The accelerometer shall be attached to the mounting fixture on the centrifuge arm with the input reference axis normal to the centrifuge axis within ______ [μrad, ″] and pointing toward the rotation axis (positive input acceleration). The nominal radius from the centrifuge axis to the proof mass center of gravity shall be determined and recorded.

d) The starting procedure shall be executed.

State sequence of operations required to bring accelerometer and test equipment to operating conditions.

12.3.15.4 Test procedure mounting position A

Mounting position A test procedure shall be as follows:

a) Set the centrifuge angular rate to a value equivalent to a centripetal acceleration at the accelerometer proof mass of __________ [m/s^2, ft/s^2, _____], nominally.

b) Measure the accelerometer output and the centrifuge period simultaneously, and record for __________ readings.

c) Repeat Step a) and Step b) at nominal centripetal acceleration levels of __________, __________, __________, …, and __________ [m/s^2, ft/s^2, _____].

12.3.15.5 Test setup mounting position B

Perform the same steps as in 12.3.15.3, except that the direction of the input reference axis shall be reversed (negative input acceleration).

12.3.15.6 Test procedure mounting position B

Perform the same steps as in 12.3.15.4.

> By having other axes and cross axes along the centrifuge arm (i.e., by essentially doing a tumble test at the end of the centrifuge arm), cross-axis nonlinearities and cross-coupling terms may be estimated from the centrifuge data to verify requirements 5.3.10 and 5.3.11. For pendulous accelerometers, a measure of the anisoinertia term may also be obtained to verify the anisoinertia requirement in 5.3.25. See IEEE Std 836.

12.3.15.7 Test results

Perform a regression analysis of the input versus indicated acceleration data to obtain values of the nonlinear acceleration-sensitive model equation coefficients and the test residuals. The resulting coefficients shall conform to the requirements of 5.3.6.

> For lesser accuracy accelerometers, nonlinearity may be specified as the maximum deviation from a least-squares, best-fit straight line over full span, in percent of the full span of the accelerometer.

> If the arm stretch of the centrifuge cannot be compensated, the estimated K_{oq} will represent a combination of both arm stretch and accelerometer effects.

> The measurement precision is directly related to the test accuracy desired, and careful attention must be given to these considerations when designing a centrifuge test. In some cases, it may be necessary to measure the arm compliance (arm bending and change in arm length) that occurs between test acceleration levels. Equipment to perform these measurements is usually provided as part of the centrifuge apparatus.
>
> The test procedure or the regression analysis, or both, must be designed to minimize the impact of these effects as well as uncompensated changes in centrifuge radius and acceleration attitude relative to gravity that might occur between the positive (IA in) and negative (IA out) halves of the test. If these effects are not removed or compensated for, large errors in the derived values of the model equation coefficients can occur.
>
> Examine the residuals (differences between the actual data points and the fitted curves) to verify that the model equation used reasonably reflects the accelerometer response.

12.3.16 Frequency response

12.3.16.1 Purpose

The purpose of this test is to determine the accelerometer closed-loop frequency response.

The test described uses physical vibration to excite the test accelerometer. In some cases for a force rebalance accelerometer, it may be acceptable or even desirable to simulate vibration by means of current torquing. Current torquing of a servo accelerometer is accomplished by connecting an adjustable or programmable current source across the torque coil. The test is simple and flexible and can greatly simplify combined environment tests, but it has at least two significant limitations.

a) It requires that both ends of the torque coil be available as test points.

b) It may be inaccurate in the presence of sensor mechanical resonances, and it frequently is inaccurate at frequencies greater than ~1.5 times the loop closure frequency (depending on feedback method and the relative sizes of the load and torque coil resistances).

When subjected to vibration, the output frequency of a VBA is modulated by the input acceleration frequency. To measure the frequency response of a VBA, one could use the voltage command of a voltage-controlled oscillator (VCO) included in a phase-locked loop (PLL) on the VBA output. This voltage will be an image of the VBA output frequency change and can, therefore, be compared in phase and amplitude to the input acceleration signal.

12.3.16.2 Test equipment

The following test equipment specified in 11.2 is required for this test:

a) Vibration exciter and vibration control electronics

b) Mounting fixture with accelerometer IA along the vibration axis (temperature controlled if necessary below the temperature set point of the accelerometer)

c) Piezoelectric accelerometer(s) attached to the mounting fixture to monitor the vibration acceleration and allow for control of the vibration input to the test accelerometer by the control electronics

d) Pickoff excitation supply (if required)

e) Rms voltmeter

f) Phase angle voltmeter

g) Oscilloscope

h) Signal generator

i) Spectrum analyzer

j) Electronic equipment required to operate the accelerometer and measure its output

12.3.16.3 Test setup

The accelerometer shall be operated under the standard test conditions of 11.1. Mount the accelerometer on the vibration exciter with its IA aligned within __________ [mrad, ′] with the vibration exciter motion axis. Allow the accelerometer and its immediate environment, including the mounting fixture, to reach thermal equilibrium before proceeding with the test.

The vibration axis should be vertical to minimize the effects of misalignments with the accelerometer IA along the vibration axis.

The test description applies to completed sensors for which mounting is usually provided by bolts through, for example, a flange. For subcomponent testing of a silicon chip sensor, soldering or epoxy attachment might be required for mounting the device on an adapter plate to the vibrator.

12.3.16.4 Test procedure

Use the pickoff signal and/or the vibrator's reference accelerometer to control the vibration level and frequency.

a) With a true rms voltmeter and a phase angle voltmeter,

   1) Choose a certain number of discrete frequencies within the bandwidth where the closed-loop frequency response is to be determined.

   2) For each frequency, measure both reference and tested accelerometer outputs with the rms voltmeter.

   3) For each frequency, measure the phase between the reference and tested accelerometer outputs.

b) Alternatively, with a spectrum analyzer,

   1) Use constant amplitude discrete frequencies, a constant amplitude sine sweep, or a random vibration with given rms amplitude over a given bandwidth.

   2) During vibration, measure the reference and tested accelerometer outputs with the spectrum analyzer.

When subjected to vibrations, the output frequency(ies) of a VBA are modulated by the input acceleration amplitude.

To measure the frequency response of a VBA, one could use the voltage command of a VCO included in a PLL readout of the VBA frequency(ies). This voltage will be an image of the VBA output frequency(ies) change and can, therefore, be compared in phase and amplitude to the input acceleration signal measured by the reference accelerometer. The VBA frequency response calculated with this procedure will, however, include the PLL frequency response.

Alternatively, the VBA output frequency(ies) may be digitally sampled at a sufficiently high rate, and the computed variance may be used as a measure of amplitude response.

12.3.16.5 Test results

Plot the following:

a) The ratio in decibels of the tested accelerometer output to the reference accelerometer output versus vibration frequency.

b) The phase angle of the tested accelerometer output relative to the reference accelerometer output versus vibration frequency.

The results shall conform to the requirements of 5.3.21.

12.3.17 Vibration calibration (nonlinear terms)

12.3.17.1 Purpose

The purpose of this test is to calibrate nonlinear coefficients in the accelerometer performance model using the observed vibration rectification.

12.3.17.2 Test equipment

The following test equipment specified in 11.2 is required for this test:

a) Electrodynamic or hydraulic vibrator oriented vertically, or horizontally with a slip table, and vibration control electronics [see Annex L]

b) Mounting fixture to orient the accelerometer properly relative to the vibrator axis

c) Piezoelectric accelerometer(s) attached to the mounting fixture to monitor the vibration acceleration and allow for control of the vibration input to the test accelerometer by the control electronics

d) Electronic equipment required to operate the accelerometer and measure its output

If the mounting fixture is thermally controlled, it might require a thermal shim or insulated spacer between the fixture and the vibrator. A vibration fixture should not have structural resonances in the frequency band excited in the test. This requirement generally means that such fixtures are fairly massive, especially if the fixture is used in environmental tests (see 12.9) with random, frequency sweep, or shock vibrations extending above 1,000 Hz.

12.3.17.3 Test setup

The accelerometer shall be operated under the standard test conditions of 11.1. Orient the accelerometer so that the vibrator axis is along IA, PA, or OA if K_2, K_{pp}, or K_{oo} is being estimated, respectively, or along a bisector of the appropriate pair of principal axes if K_{ip}, K_{io}, or K_{po} is being estimated (see L.6.2.3 and L.6.3.3).

Because of the vibration environment, a dividing head should not be used to vary the accelerometer orientation relative to the vibration input. Rather, the mounting fixture could be attached to the vibrator on different faces with appropriate bolt-hole patterns with the accelerometer in a fixed orientation within the fixture, or the fixture could have a fixed orientation on the vibrator with different accelerometer mounting surfaces on the fixture.

12.3.17.4 Test procedure

At a given frequency, dwell for __________ [min, _____] each at ________, _______, …, and ________ [m/s^2, ft/s^2, _____] [rms, _____] vibration levels.

Record the rms output of the piezoelectric vibration monitor accelerometer, the average output of the accelerometer under test, and appropriate auxiliary signals, such as temperatures, at an appropriate data acquisition rate. For an electrodynamic vibrator, the zero acceleration data are collected with the field on with a zero input waveform, to avoid the shifts that occur when the field is turned off.

Repeat the test at several vibration frequencies, such as 20 Hz, 50 Hz, and 100 Hz, for an electrodynamic vibrator. The dynamics of the accelerometer might be such that lower vibration frequencies should be used, such as 3 Hz or 5 Hz with a hydraulic long-stroke vibrator. The dwell time at each vibration amplitude level should be long enough that a fractional cycle missed in calculating the average of the accelerometer output at a given level causes small errors relative to the accuracy sought in the test.

In those cases where the error of a partial cycle cannot be tolerated, the data acquisition could be timed to read data at integral cycle times of the vibration. Alternatively, data could be acquired continuously, while at zero acceleration, then brought up to a given acceleration level for a period of time, and then returned to zero acceleration, before repeating the sequence at the next acceleration level. This latter approach mitigates the problem of missing a fractional vibration cycle in calculating the average of the accelerometer output. The average of the accelerometer output containing the effect of vibration rectification is compared to the time average of the square of the piezoelectric accelerometer output from zero acceleration to the given acceleration level back to zero acceleration in the least-squares estimation of nonlinear coefficients from the data at all acceleration levels.

Determine whether there is any change in the zero acceleration accelerometer outputs from before to after the test. If this change is due to a trend in the output (such as due to uncompensated parts of any thermal variations), then this trend can be taken into account in estimating the accelerometer's nonlinear coefficients. More serious is a change in accelerometer output due to a shift across vibration caused by the vibration itself.

12.3.17.5 Test results

Calculate the average output of the accelerometer under test at each vibration level, corrected for temperature and other effects using the auxiliary signals if appropriate. Also calculate the average rms output of the piezoelectric vibration monitor accelerometer at each vibration level.

Estimate the coefficients K_2, K_3, K_{pp}, K_{oo}, K_{ip}, K_{io}, K_{po}, and even asymmetry and odd quadratic terms using the technique described in L.6.2 and L.6.3. The nonlinear coefficient estimate results shall conform to the requirements of 5.3.6, 5.3.10, and 5.3.11.

Odd power sinusoids do not average zero if not symmetrical about zero, which is why K_3 can be estimated in a vibration test using IA up and down on a vertically oriented vibrator (see L.6.2 and L.6.3).

Least-squares fits of the models in L.6.2 and L.6.3 to the data at the various vibration levels yield estimates of the nonlinear model coefficients with estimation uncertainties that are functions of the data residuals from the fits. The variation in the estimations from repetitions of the test at various vibration frequencies gives a truer measure of the uncertainty.

The limited precision of the piezoelectric monitor accelerometer, the misalignments of the accelerometer axes relative to the vibrator axis, cross-axis motions, and the ability to control the vibration amplitude at each level limit the relative accuracy of the results (see L.6.4). If the coefficients being estimated are not too large relative to the accuracy being sought, then calibration of nonlinear model coefficients with a vibration test is a useful technique.

12.3.18 Vibration and shock calibration (scale factor and bias)

12.3.18.1 Purpose

The purpose of this test is to calibrate the scale factor and bias of an accelerometer used in applications with high levels of acceleration, especially in vibration and shock environments for which a local gravity tumble test calibration is inadequate.

12.3.18.2 Test equipment

The following test equipment specified in 11.2 is required for this test:

a) Electrodynamic vibrator or drop test shock machine and mounting fixture [see Annex L]

b) Laser interferometer or other device to measure the motion in the vibration or shock

c) Electronic equipment required to operate the accelerometer and measure its output

Laser interferometry giving high-rate measurements of displacement and displacement velocity is described in ISO 5347. Commercially available piezoelectric accelerometers have inadequate resolution for this test, although they still could be used for rough control of the vibration with precise measurement of the actual motion being done with the laser interferometer. For low-frequency vibrations, a macro-sized pendulous torque-rebalance accelerometer could be used as a monitor if a 1-*g* tumble test calibration of its scale factor and bias were adequate in the high-*g* vibration environment as verified by comparison with a laser interferometer monitor.

The test description herein uses a single laser interferometer along the IA vertical axis. The effect of cross-axis inputs and misalignments might require laser interferometer observations along the other two axes as well, depending on requirements.

12.3.18.3 Test setup

Mount the accelerometer on the vibration or shock machine with IA along the vibration or shock axis oriented in the vertical direction. Allow the accelerometer to stabilize at its operating temperature.

In this orientation, misalignments with the gravity vector have minimal effect.

12.3.18.4 Test procedure

Apply the vibration or shock motion with high-rate data being acquired from the accelerometer under test and from the laser interferometer.

12.3.18.5 Test results

Numerically integrate the accelerometer output to yield displacement and its velocity using first guesses for the accelerometer parameters (scale factor, bias, and possibly K_2 nonlinearity) and the displacement initial conditions. Compute the differences of the integrated accelerometer output with the laser interferometer outputs, and compute the partial derivatives of these differences with respect to the accelerometer parameters and the displacement initial conditions. Make a least-squares adjustment to the accelerometer parameters and displacement initial conditions, and continue the least-squares iteration until convergence is obtained [see K.6].

Instead of least-squares maximum likelihood estimation, Kalman filter or system identification estimation could be used [see I.9.3].

The estimated scale factor and bias shall conform to the requirements of 5.3.5.1 and 5.3.7.1. Repeated calibrations over time and temperature and other environmental variations can be used to determine scale-factor and bias short- and long-term stability, repeatability, and sensitivities.

The differential equations for the accelerometer dynamic behavior and the partial derivatives of these differential equations with respect to initial conditions and accelerometer parameters would likely have to be numerically integrated to process the data from this experiment. As a simplified example without pendulum and other dynamics, suppose that an input–output model of the accelerometer is valid even at the high data rates of this experiment

$$E = K_0 + K_1 a_i$$

where a_i is the nongravitational acceleration along the IA-up direction (m/s^2) and where the units of bias and scale factor are appropriate for the units of the accelerometer output E. Let x_0 and v_0 (m and m/s) be the initial position and velocity along the vibration or shock direction. After k time increments Δt, the velocity v_k and displacement x_k (positive in the up direction) are

$$v_k = v_0 + \sum_{j=1}^{k} \left[\frac{E - K_0}{K_1} - g \right] \Delta t$$

$$x_k = x_0 + v_0 k \Delta t + \sum_{j=1}^{k} \left[\frac{E - K_0}{K_1} - g \right] \left(k + \frac{1}{2} - j \right) \Delta t^2$$

The partial derivatives of these theoretical values of the interferometer measurements with respect to x_0, v_0, K_0, and K_1 are straightforward to calculate. Using the observed minus theoretical values and the partial derivatives, the normal equations (see K.6.2) are formed using the data from $k = 1, ..., N$ time points for a total of $m = 2N$ measurements. The solution of the normal equations gives adjustments to x_0, v_0, K_0, and K_1. Using the new values of these quantities, the process is repeated until convergence is obtained.

12.3.19 Performance through and across environment

12.3.19.1 Purpose

The purpose of this test is to determine the performance of the accelerometer during the application of random vibration and shock and to determine whether there are any shifts in the accelerometer output across this environment.

12.3.19.2 Test equipment

The following test equipment specified in 11.2 is required for this test:

a) Electrodynamic vibrator and mounting fixture [see Annex L]

b) Electronic equipment required to operate the accelerometer and measure its output

12.3.19.3 Test setup

The test setup shall be as follows:

a) Program the vibrator for the normal operation random vibration profile from 5.6.2.4 and the shock profile from 5.6.2.5. Test these profiles on a dummy test article.

b) Mount the accelerometer on the vibration fixture so that the IA is vertical along the vibrator axis. Operate the accelerometer under the standard test conditions of 11.1.

Vibration or shock along other accelerometer axes can also be done, as called for in 5.3.22.

12.3.19.4 Test procedure

The test procedure shall be as follows:

a) Record the accelerometer output for __________ s prior to the application of the random vibration or shock.

b) Apply the random vibration profile for __________ s, or apply the shock profile, and record the accelerometer output during the given environment.

c) Record the accelerometer output for __________ s after the application of the random vibration or shock.

12.3.19.5 Test results

Determine whether there is any shift in the accelerometer output from before to after the application of the random vibration or shock. This procedure repeats the environmental tests in 12.9 with normal environments.

Compute the accumulated velocity during the test, and compare with the extrapolation of the accumulated velocity line from before the application of the environment. Any permanent deviation of the accumulated velocity from the extrapolated accumulated velocity line during the application of the random vibration or shock with average zero acceleration variation is due to vibration rectification (or insufficient velocity storage in over-range shock) and shall be less than called for in 5.3.22.

If VBA vibration rectification is not adequately canceled by taking the difference of antiparallel resonator outputs, additional high-rate signal processing in a microprocessor attached to the VBA might be required (see Annex D).

12.3.20 Velocity storage in normal and over-range shock

12.3.20.1 Purpose

The purpose of this test is to determine the maximum velocity storage capability of the accelerometer during normal and over-range shock.

12.3.20.2 Test equipment

The following test equipment specified in 11.2 is required for this test:

a) Shock machine with shock recording instrumentation (see Annex L for shock generated by a stationary vibrator with net average zero acceleration)

b) Electronic equipment required to operate the accelerometer and measure its output

c) Digital recorder for recording each output pulse from a pulsed-torqued accelerometer or recording analog-torque loop, analog-to-digital converter readings or voltage-to-frequency converter readings at a high rate, plus recording the pickoff signal output at a high rate if possible

12.3.20.3 Test setup

The test setup shall be as follows:

a) Program the shock machine for the maximum normal operation shock profile from 5.6.2.5 and for the maximum over-range shock profile from 5.3.19.2. Test these profiles on a dummy test article.

b) Mount the accelerometer on the shock machine such that its IA is parallel to the direction of applied shock within __________ [mrad, ′].

The test is preferably run on a vertical axis shock machine. If the motion and sensing axes are horizontal, large errors may occur as a result of alignment instability in the shock machine.

12.3.20.4 Test procedure

The test procedure shall be as follows:

a) Energize the accelerometer.

b) Allow the accelerometer and the immediate environment to reach thermal equilibrium as evidenced by the stability of the accelerometer output being within __________ [m/s^2, ft/s^2, _____] for __________ measurements spaced __________ min apart before proceeding with the test.

c) Compute the average acceleration during the __________ s measurement period prior to the application of the shock.

d) Impart the maximum normal operation shock to the accelerometer with net average zero acceleration. The peak value of the integral of the shock acceleration time history (before it returns to zero because the shock machine is stationary) is the amount of velocity storage required of the accelerometer through the shock.

e) Using the average acceleration computed in Step c), extrapolate the accumulated velocity during and after application of the shock as if the shock were not present. Subtract this extrapolated accumulated velocity from the accumulated velocity from the output of the accelerometer. If the absolute value of the difference is less than __________ [m/s, ft/s, _____] __________ s after application of the shock, then velocity storage was successfully accomplished through the shock, and the velocity storage is the maximum of the absolute value of the difference during the shock. The velocity storage should be consistent with the amount of proof-mass movement observed in the pickoff signal output during the shock. If the proof mass hits the stops during the shock, then complete velocity storage is not obtained.

f) Using increasing levels of shock up to the maximum specified over-range shock, repeat Step b) through Step e).

12.3.20.5 Test results

The velocity storage in the normal shock test shall be less than the value in 5.3.19.1. The maximum velocity storage in the over-range shock test shall exceed the value in 5.3.19.2.

12.3.21 Slew calibration

12.3.21.1 Purpose

The purpose of this test is to calibrate angular-velocity-sensitive and acceleration-sensitive coefficients in the accelerometer performance model using high-rate slews.

12.3.21.2 Test equipment

The following test equipment specified in 11.2 is required for this test:

a) Single-axis or multiaxis rotary test table (single axis would require accelerometer remount between slews)

b) Mounting fixture to orient the accelerometer properly relative to the rotation axis(es)

c) Electronic equipment required to operate the accelerometer and measure its output

12.3.21.3 Test setup

Orient the accelerometer so that angular slews are about IA, PA, or OA or about bisectors of these axes.

12.3.21.4 Test procedure

Perform the following slew profile about IA, PA, OA, and the bisector axes:

a) Keep stationary for __________ s.

b) Apply angular acceleration of $+x$ rad/s² for T_1 s.

c) Apply constant angular velocity $y = xT_1$ rad/s for T_2 s.

d) Apply angular acceleration of $-x$ rad/s² for $2T_1$ s.

e) Apply constant angular velocity $-y = -xT_1$ rad/s for T_2 s.

f) Apply angular acceleration of $+x$ rad/s² for T_1 s.

g) Keep stationary for __________s.

Perform these slew profiles for various values of angular acceleration x up to the maximum angular acceleration of the strapdown navigation system in which the accelerometer will be used and for various values of angular velocity y up to the maximum angular velocity of the strapdown navigation system in which the accelerometer will be used.

Record the rotary table angles, their rates, the output of the accelerometer under test, and the appropriate auxiliary signals, such as temperatures, at an appropriate data acquisition rate.

12.3.21.5 Test results

Using the table rotation time history and the values of the scale factor and nonlinear acceleration-sensitive terms from the results of other calibration tests, estimate from the accelerometer output the K_{spin} coefficient and the bias, misalignments, and lever arm coordinates from the test table rotation center to the center of percussion in the accelerometer pendulum. Least-squares or Kalman filter estimation can be used.

The angular velocity coefficient K_{spin} estimate shall be consistent with the pendulum anisoinertia in 5.3.25.

The center of percussion of the accelerometer pendulum is the point where the angular acceleration sensitivity $K_{ang.accel}$ is 0 (see 8.3 and Annex C).

In this test, the acceleration components a_i, a_p, a_o in the model equation in 8.3 include the reaction acceleration to gravity, centripetal acceleration due to the spinning test table and rotating earth, tangential acceleration due to table angular acceleration, and Coriolis acceleration. The angular velocity components ω_i, ω_p include the angular velocities of the table and earth rotation. The misalignments and lever arm coordinates enter into the model equation through these terms.

This test would be done only at the accelerometer level to verify the design. The equivalent test would have to be done on a strapdown guidance system to estimate the lever arms from the guidance system center of navigation to the center of percussion reference points within the accelerometers at which accelerations are considered to be acting (see "size effect" in C.3.3), along with the K_{spin}, misalignment, and other model terms.

12.3.22 Magnetic leakage

12.3.22.1 Purpose

The purpose of this test is to determine the magnitude of the magnetic induction emanating from the accelerometer.

12.3.22.2 Test equipment

The following test equipment specified in 11.2 is required for this test:

a) Electronic equipment required to operate the accelerometer and measure its output

b) Magnetic induction measuring equipment

c) Nonmagnetic mounting fixture

The earth's magnetic induction will influence the measurements. If this effect is significant, shielding or compensation should be specified.

12.3.22.3 Test setup

Secure the nonmagnetic mounting fixture to a suitable base. Measure and record the magnitude and direction of the ambient magnetic induction at the following positions surrounding the mounting fixture without the accelerometer present.

Install the accelerometer in the fixture.

12.3.22.4 Test procedure

Measure and record the magnitude and direction of the ambient magnetic induction at positions ___________, ___________, ..., and ___________ surrounding the nonoperating accelerometer.

Stabilize and operate the accelerometer at the standard test conditions of 11.1. Repeat the measurement of the magnetic induction at the given positions.

12.3.22.5 Test results

The magnetic leakage for the nonoperating accelerometer is the maximum of the magnetic induction of the nonoperating accelerometer minus the magnetic induction without the accelerometer present.

The magnetic leakage for the operating accelerometer is the maximum of the magnetic induction of the operating accelerometer minus the magnetic induction without the accelerometer present.

The magnetic leakage shall conform to the requirements of 5.5.5.

12.4 Electromagnetically torqued pendulous accelerometer tests

12.4.1 Pickoff characteristics

12.4.1.1 Purpose

The purpose of this test is to determine the pickoff voltages at the positive and negative stops. For an ac pickoff, this test is also used to determine the phase relationship between the pickoff excitation and the output voltage and the minimum voltage at electrical null.

This test is usually of interest only for those accelerometers in which the electronics and the sensor/detector are separate. Useful measurements of the output voltages are possible only when external connections or test points allow direct access to the pickoff output circuitry (which may include a buffer amplifier). Phase measurements are possible when the pickoff excitation is accessible as well. For accelerometers with integral electronics, this test would be of interest as at most a preclosure production test and should not appear in a top assembly specification. The pickoff null is best measured when a 90° phase shift is seen in the pickoff output.

12.4.1.2 Test equipment

The following test equipment specified in 11.2 is required for this test:

a) Dividing head and mounting fixture
b) Pickoff power supply (if required)
c) Temperature controller
d) AC/DC voltmeter
e) Phase angle voltmeter
f) Oscilloscope

12.4.1.3 Test setup

The test setup shall be in accordance with 12.1.2.1 and 12.1.2.2.

12.4.1.4 Test procedure

The test procedure shall be as follows:

a) Rotate the dividing head in the positive direction from the zero acceleration reference position until the maximum output voltage V_{0+} [rms, dc] is reached at the positive stop. Measure and record V_{0+}. For an ac pickoff, also measure and record the phase angle of the output voltage with respect to the pickoff excitation.
b) Return the dividing head to the zero acceleration reference position and repeat this procedure for the negative direction to obtain the maximum absolute value output voltage V_{0-} [rms, dc] at the negative stop. Measure and record V_{0-}. For an ac pickoff, also measure and record the phase angle of the output voltage with respect to the pickoff excitation.
c) For an ac output pickoff, rotate the dividing head until the minimum rms output voltage V_0 is obtained at the electrical null. Measure and record V_0.

12.4.1.5 Test results

The test results shall conform to the requirements as follows:

a) For an ac pickoff, the phase relationship between the pickoff excitation and output voltage shall conform to the requirements of a) in 5.3.24.3.

b) The dc pickoff output voltage polarity shall conform to the requirements of b) in 5.3.24.3.

c) The maximum absolute value output voltages V_{0+}, V_{0-} at each stop shall conform to the requirements of 5.3.24.5.

d) For an ac output pickoff, the minimum output voltage V_0 at electrical null shall conform to the requirements of 5.3.24.4.

This test also checks the motional freedom of the proof-mass pendulum between the stops. The pickoff could saturate before the pendulum hits the stops.

12.4.2 Torquer and self-test torquer polarity

12.4.2.1 Purpose

The purpose of these tests is to determine the relationship between specified currents applied to the torquer and self-test torquer coils and the resulting pendulum motion as evidenced by the pickoff output.

The torquer polarity test is of interest only for those accelerometers in which the electronics and the sensor/detector are separate. With integral electronics, stable-loop closure with the correct sign on the scale factor is sufficient evidence of correct polarity. Similarly, self-test polarity may be judged by the correct sign of the self-test scale factor, as measured at the accelerometer output.

12.4.2.2 Test equipment

The following test equipment specified in 11.2 is required for these tests:

a) Dividing head and mounting fixture

b) Pickoff power supply (if required)

c) Temperature controller

d) DC voltmeter

e) Phase angle voltmeter

f) Oscilloscope

g) DC current supply

12.4.2.3 Test setup

The test setup shall be in accordance with 12.1.2.1 and 12.1.2.2.

12.4.2.4 Test procedure

The test procedure shall be as follows:

a) Connect the dc current supply to the torquer so that terminal __________ is positive with respect to terminal __________ for positive torquing. Increase the current to __________ ± __________ A.

Specify a test current that will not damage the accelerometer but is sufficient to drive the pendulum against the stop.

b) Measure and record the phase of the pickoff output voltage relative to the pickoff excitation.

c) Repeat Step b) with the torquer current reversed.

d) Connect the dc supply to the self-test torquer so that terminal __________ is positive with respect to terminal __________. Increase the current to __________ ± __________ A.

e) Measure and record the phase of the pickoff output voltage relative to the pickoff excitation.

f) Repeat Step e) with the self-test torquer current reversed.

For dc pickoffs, polarity rather than phase should be measured.

12.4.2.5 Test results

The results shall conform to requirements of 5.3.26.

12.4.3 Open-loop frequency response

This test is usually of interest only for those accelerometers in which the electronics and the sensor/detector are separate, but it may sometimes be conducted on complete accelerometers to gain added insight into loop stability margins. In either case, the important distinction from 12.3.16 is that the servo loop is either fully open or effectively open at frequencies of interest (typically, above a few hertz). With separate electronics, that effect can be accomplished by leaving the loop closure connections open, as in Figure 5, and monitoring pickoff output. With integral electronics, a similar effect may be created in many accelerometers by substituting a sufficiently large value for the load resistor. In general, the appropriate connections will vary with the design and must be defined in cooperation with the manufacturer.

12.4.3.1 Purpose

The purpose of this test is to determine the accelerometer open-loop frequency response.

12.4.3.2 Test equipment

The following test equipment specified in 11.2 is required for this test:

a) Dividing head and mounting fixture

b) Pickoff power supply (if required)

c) Temperature controller

d) Rms voltmeter

e) Phase angle voltmeter

f) Oscilloscope

g) Signal generator

h) Amplifier/demodulator

i) Precision current-sensing resistor

j) Spectrum analyzer

In some cases, a combination of pickoff signal, phase angle voltmeter, and rms voltmeter may be substituted in place of a spectrum analyzer.

12.4.3.3 Test setup

The test setup shall be in accordance with 12.1.2.1 and 12.1.2.2, except that the capture electronics shall be connected to the pickoff output.

12.4.3.4 Test procedure

Rotate the dividing head until the [accelerometer, pickoff] is nulled within __________ V. Apply a sinusoidal signal from __________ Hz to __________ Hz at a rate of __________ decades/min across a series combination of the precision current-sensing resistor and the torquer. Measure and record the voltage across the resistor, the [accelerometer, pickoff] output signal, and the phase angle between these two voltages.

12.4.3.5 Test results

Plot the ratio in decibels of the [accelerometer, pickoff] output voltage to the input voltage measured across the resistor. Plot the phase and gain versus frequency. The results shall conform to the requirements of 5.3.27.

12.4.4 Pickoff scale factor and pendulum elastic restraint

12.4.4.1 Purpose

The purpose of these tests is to determine the pickoff voltage change and the pendulum elastic restraint change as functions of pendulum angular displacement.

The pickoff scale factor is the output voltage change as a function of pendulum displacement.

Pendulum elastic restraint includes all restraints such as flex lead spring restraints, pivot spring restraints, and pickoff reaction torque restraints, but it does not include the principal restraint (rebalance torque supplied by the servo loop).

12.4.4.2 Test equipment

The following test equipment specified in 11.2 is required for these tests:

a) Dividing head and mounting fixture
b) Electronic equipment required to operate the accelerometer and measure its output
c) Phase angle voltmeter
d) DC voltmeter
e) Variable dc power supply

12.4.4.3 Test setup

The test setup shall be in accordance with 12.1.2.1 and 12.1.2.2, except that the electrical connections of 12.1.2.1 shall be modified to conform to Figure 5.

12.4.4.4 Test procedure

The test procedure shall be as follows:

a) Reduce the capture electronics gain to __________ ± __________ Vdc/Vrms. Position the dividing head at 0° (IA nominally horizontal). Turn on the dc voltage supply and increase its output to

__________ ± __________ V, which will displace the pendulum a suitable amount about the positive OA direction +θ.

b) Measure and record the accelerometer output as E_a and the pickoff in-phase output voltage as V_a.

The amplifier must be operating in its nonsaturated region. Sets of points may be taken at varying displacements to determine pickoff and elastic restraint linearity.

c) Decrease the output of the dc supply to zero. Reverse its polarity and its output to the same voltage to offset the pendulum in the negative direction –θ. Measure and record the accelerometer output as E_b, and measure the pickoff in-phase output voltage as V_b.

d) Rotate the dividing head 180^0 ±__________ [μrad, ″]. Turn on the dc voltage supply and increase its output to the same voltage as in Step a). Measure and record the accelerometer output reading as E_c, and measure the pickoff in-phase output voltage as V_c.

e) Using the procedure described in Step c), reverse the output of the dc supply, measure and record the accelerometer output as E_d, and measure the pickoff in-phase output voltage as V_d.

12.4.4.5 Test results

The collected data shall be analyzed as follows:

a) Calculate the IA deviation G about the OA for each of the two modes of operation using the following equations:

$$G_{+\theta} = \frac{E_a + E_d}{2K_1} \text{ rad}$$

$$G_{-\theta} = \frac{E_b + E_c}{2K_1} \text{ rad}$$

where K_1 is the nominal accelerometer scale factor in output units/[m/s^2, ft/s^2, _____].

b) Compute the pickoff scale factor K_{po} and the pendulum elastic restraint K_r using the following equations:

$$K_{po} = \frac{1}{2}\left[\frac{(V_a - V_b) - (V_c - V_d)}{G_{+\theta} - G_{-\theta}}\right] \text{ V/rad}$$

$$K_r = \frac{1}{2K_1}\left[\frac{(E_a - E_d) - (E_b - E_c)}{G_{+\theta} - G_{-\theta}}\right] [\text{m/s}^2, \text{ft/s}^2, \_\_\_\_]/\text{rad}$$

c) The values calculated in Step b) shall satisfy the requirements of 5.3.24.2 and 5.3.28.

An alternative method of conducting this test is to sum an ac voltage with the pickoff output voltage to effectively shift the pickoff null position.

12.4.5 Turn-on hysteresis

12.4.5.1 Purpose

The purpose of this test is to determine the displacement hysteresis associated with moving the pendulum from either stop to the operating null position as a result of power turn-on.

The test will be conducted using reductions in loop gain in lieu of power turn-on to preclude any dithering effects from a sudden loop closure. The measured values yield a maximum window of displacement hysteresis torque that the pendulum will fall into after power turn-ons.

12.4.5.2 Test equipment

The following test equipment specified in 11.2 is required for this test:

a) Dividing head and mounting fixture

b) Electronic equipment required to operate the accelerometer and measure its output

12.4.5.3 Test setup

The test setup shall be in accordance with 12.1.2.1 and 12.1.2.2.

12.4.5.4 Test procedure

The test procedure shall be as follows:

a) Rotate the dividing head to the 270° IA-down position.

b) Reduce the servo loop gain smoothly, allowing the pendulum to move to the stop.

c) Reestablish the normal servo gain smoothly.

d) Rotate the dividing head smoothly to the 90° IA-up position.

e) Reduce the servo loop gain smoothly, allowing the pendulum to move to the stop.

f) Reestablish normal servo gain smoothly.

g) Rotate the dividing head smoothly to the 270° IA-down position, and measure the accelerometer output E_g.

h) Reduce the servo loop gain smoothly, allowing the pendulum to move to the stop.

i) Reestablish normal servo gain smoothly, and measure the accelerometer output E_i.

j) Rotate the dividing head smoothly to the 90° IA-up position, and measure the accelerometer output E_j.

k) Reduce the servo loop gain smoothly, allowing the pendulum to move to the stop.

l) Reestablish normal servo gain smoothly, and measure the accelerometer output E_ℓ.

m) Repeat Step g) through Step l)__________times.

The angle of the accelerometer with respect to the gravity vector may be varied to provide less than 1 *g* along the IA if desired. If the accelerometer under test has no provision for loop gain adjustment, other means for moving the pendulum smoothly into each stop may be used, for example, by current torquing. Power supply adjustment works in some cases but needs to be evaluated.

12.4.5.5 Test results

The collected data shall be analyzed as follows:

a) Calculate the turn-on hysteresis for each set of data. Use the accelerometer's nominal scale factor for K_1

$$H_{\text{turn-on}} = \frac{\lfloor E_g - E_i \rfloor + \lfloor E_j - E_\ell \rfloor}{K_1} \text{ [m/s}^2\text{, ft/s}^2\text{, \_\_\_\_\_]}$$

This test provides a measure of the variation in output associated with power turn-on or loop capture. Another type of hysteresis is the variation in output at a given input resulting from exercising the pendulous mass within its operating range (similar to magnetic hysteresis). To determine this characteristic, a current injection or similar technique may be employed to swing the pendulum back and forth through its operating range without moving the accelerometer case. A plot of the restoring current versus the current on an *X–Y* recorder will produce a hysteresis loop, the maximum opening of which is the operating hysteresis.

This test should be conducted with the accelerometer in the 0-*g* (0°) position so that torque values are not affected by gravity. Both tests are primarily of interest to pivot and jewel mechanisms, but they will give meaningful results with flexured constraints as well.

b) For each test, the absolute value of the [mean, median] determination shall conform to the requirements of 5.3.17.

12.4.6 Self-test torquer scale factor

12.4.6.1 Purpose

The purpose of this test is to determine the scale factor of the self-test torquer.

12.4.6.2 Test equipment

The following test equipment specified in 11.2 is required for this test:

a) Dividing head and mounting fixture
b) Electronic equipment required to operate the accelerometer and measure its output
c) DC current supply

12.4.6.3 Test setup

The test setup shall be in accordance with 12.1.2.1 and 12.1.2.2, except that the dividing head shall be set at 0°.

12.4.6.4 Test procedure

The test procedure shall be as follows:

a) Apply __________ ± _________ mA dc to the self-test torquer winding. Record the accelerometer output as E_h.

Specify a current that will not damage the accelerometer nor cause the pendulum to hit a stop.

b) Reverse the polarity of the applied self-test torquer current. Record the accelerometer output as E_j.

12.4.6.5 Test results

Calculate the self-test torquer scale factor K_s by

$$K_s = \frac{2 I_s K_1}{E_h - E_j} \text{ mA/[m/s}^2\text{, ft/s}^2\text{, \_\_\_\_]}$$

where

K_s is the self-test scale factor, in mA/[m/s^2, ft/s^2, _____]

I_s is the self-test current, in mA

E_h, E_j are the accelerometer outputs, in output units

K_1 is the accelerometer scale factor obtained from 12.3.4.4 in output units/[m/s^2, ft/s^2, _____]

The result shall conform to the requirements of 5.3.23.

12.4.7 Velocity storage—Open-loop test

This test is usually of interest for fluid- (rather than gas-) damped accelerometers in which the electronics and the sensor/detector are separate and which have sufficient pickoff travel range. Useful measurements of the output voltages are possible only when external connections or test points allow direct access to the pickoff output circuitry (which may include a buffer amplifier). Phase measurements are possible when the pickoff excitation is accessible as well. For accelerometers with integral electronics, it would be of interest as at most a preclosure production test, and should not appear in a top assembly specification. In any case, it requires that the servo loop be open (see box note in 12.4.3).

12.4.7.1 Purpose

The purpose of this test is to infer the maximum velocity storage capability of the accelerometer from data recorded in open-loop operation.

12.4.7.2 Test equipment

The following test equipment specified in 11.2 is required for this test:

a) Dividing head and mounting fixture

b) Electronic equipment required to operate the accelerometer and measure its output

c) Digital recorder for recording the pickoff signal output

12.4.7.3 Test setup

The test setup shall be in accordance with 12.1.2.1 and 12.1.2.2 with the accelerometer in an open-loop configuration (see Figure 5).

12.4.7.4 Test procedure

The test procedure shall be as follows:

a) Set the output value of the pickoff to a reference voltage V_{ref} near null by positioning the dividing head with IA close to horizontal and PA down. Record the dividing-head position and V_{ref}.

It is difficult to make V_{ref} exactly null with an ac pickoff.

The test method is to measure the damping time constant τ in the model

$$V - V_{ref} = Ae^{-(t-t_0)/\tau}$$

for displacements of the pendulum from the reference position. From the damping time constant τ in the local gravity field and the distance to the stops, the amount of velocity storage in the damped pendulum movement is calculated.

b) Rotate the dividing head towards accelerometer IA up until the pickoff output exceeds __________ mV, and allow the pickoff output to stabilize at this value.

The offset pickoff value is chosen to be about two thirds of the distance to the stop.

Return the table to the reference position. Record and plot the pickoff voltage versus time until the pickoff voltage reaches V_{ref}. Pick times t_1 and t_2 for which the corresponding reference voltages satisfy

$$\frac{V_1 - V_{\text{ref}}}{V_2 - V_{\text{ref}}} = \frac{1}{\text{e}} = 0.368$$

so that τ_+, $= t_1$ - t_2. Alternatively, the damping time constant τ_+ for positive displacement of the pendulum can be determined from a least-squares fit of the exponential decay model to the pickoff voltage versus time data.

This test procedure is not feasible for a gas-damped accelerometer, as the time for the pendulum to move to the new position is much shorter than it is for a fluid-damped accelerometer.

c) Rotate the dividing head towards accelerometer IA down until the pickoff output is less than –__________mV, and allow the pickoff output to stabilize at this value.

Again, the offset pickoff value is chosen to be about two-thirds of the distance to the stop.

Return the table to the reference position. Record and plot the pickoff voltage versus time until the pickoff voltage reaches V_{ref}. Pick times t_3 and t_4 for which the corresponding reference voltages satisfy

$$\frac{V_3 - V_{\text{ref}}}{V_4 - V_{\text{ref}}} = \frac{1}{\text{e}} = 0.368$$

so that $\tau_- = t_3 - t_4$. Alternatively, the damping time constant τ_- for negative displacement of the pendulum can be determined from a least-squares fit of the exponential decay model to the pickoff voltage versus time data.

d) Average the settling time data collected in Step b) and Step c) to calculate the characteristic time τ in seconds

$$\tau = \frac{\tau_+ + \tau_-}{2}$$

e) Calculate the positive and negative pendulum stop angles θ_+ and θ_-, respectively, using the data generated in 12.4.1 and 12.4.4

$$\theta_+ = \frac{V_{0+}}{K_{\text{po}}} \text{ mrad}$$

$$\theta_- = \frac{-V_{0-}}{K_{\text{po}}} \text{ mrad}$$

where

V_{0+} is the maximum positive pickoff output as measured in 12.4.1 (mV)

V_{0-} is the maximum negative pickoff output as measured in 12.4.1 (mV)

K_{po} is the pickoff sensitivity as measured in 12.4.4 (mV/mrad)

f) Calculate the velocity storage v_{s+} and v_{s-} in the IA-up and IA-down orientations, respectively

$v_{s+} = g\tau\, \theta_+$ [m/s, ft/s, _____]

$v_{s-} = g\tau\, \theta_-$ [m/s, ft/s, _____]

12.4.7.5 Test results

The velocity storage inferred from the open-loop test shall exceed the values given in 5.3.19.2 for over-range operation and in 5.3.19.3 across power interrupt.

Contamination in the damping fluid is indicated if the pickoff versus time is not monotonically smooth and/or is not asymptotic to the original reference voltage in all repetitions of the test.

12.4.8 Velocity storage-pulse-torqued steady-state operation

12.4.8.1 Purpose

The purpose of this test is to determine the maximum velocity stored in the accelerometer for steady-state low acceleration pulse-torque operation.

12.4.8.2 Test equipment

The following test equipment specified in 11.2 is required for this test:

a) Dividing head and mounting fixture

b) Electronic equipment required to operate the accelerometer and measure its output

c) Digital recorder for recording each output pulse from a pulsed-torqued accelerometer plus recording the pickoff signal output if possible

12.4.8.3 Test setup

The test setup shall be in accordance with 12.1.2.1 and 12.1.2.2.

12.4.8.4 Test procedure

The test procedure shall be as follows:

a) For a pulse-torqued accelerometer, rotate the dividing head to the 0° position (zero acceleration input) within __________ [µrad, ″].

b) Record individual accelerometer output pulses for a period of__________ s.

c) Compute the average acceleration output of the accelerometer over the specified measurement period.

d) Compute the velocity versus time using the average acceleration computed in Step c).

e) Compare the indicated velocity (summation of output pulses) with the computed velocity from Step d). The low-acceleration normal operation velocity storage is the peak difference, which can be compared for consistency with the maximum pendulum excursion indicated by the pickoff signal output during the test.

Other or additional input acceleration levels may be used if desired.

12.4.8.5 Test results

The velocity storage in the low-acceleration pulse-torque operation test shall not exceed the value given in 5.3.19.1.

The maximum velocity storage for analog-torque loop normal steady-state operation can be determined by analysis, or perhaps by measuring the maximum pickoff angle over time, and shall not exceed the value given in 5.3.19.1. A properly designed torque loop will force the average pickoff angle to zero, with the instantaneous deviation from zero being due to torque loop limit cycling and noise.

12.5 VBA tests

The tests defined in this clause are unique to VBAs and should be considered to be required in addition to the other tests specified herein.

12.5.1 VBA frequency lock

12.5.1.1 Purpose

The purpose of this test is to determine the amplitude of the disturbance that can occur in the dual-resonator VBA at the frequency crossover.

12.5.1.2 Test equipment

The following test equipment specified in 11.2 is required for this test:

a) Dividing head or precision centrifuge and mounting fixture

b) Electronic equipment required to operate the accelerometer and measure its output

c) Temperature controller

A dividing head is used if the frequency crossover takes place between –1 *g* and +1 *g*. If a centrifuge is required to reach the frequency crossover, the performance of the centrifuge must be carefully compared with the resolution and stability needed to perform such a test.

12.5.1.3 Test setup

The test setup shall be in accordance with 12.1.2.1 and either 12.1.2.2 (dividing head) or 12.3.15.3 and 12.3.15.5 (centrifuge).

12.5.1.4 Test procedure

The test procedure shall be as follows:

a) Calculate the acceleration A_{co} where the frequency crossover is expected to occur.

b) Rotate the dividing head or servo the centrifuge to provide the acceleration $A = A_{co} -$ __________ mm/s^2 and measure the accelerometer output.

c) Add __________ µm/s^2 to A. Rotate the dividing head or servo the centrifuge to provide this acceleration, and measure the accelerometer output.

d) Repeat Step c) until the new acceleration to be applied is more than $A_{co} +$ _________mm/s^2.

12.5.1.5 Test results

Perform a least-squares straight line fit of the accelerometer output versus the applied acceleration, and compute the residual between the data and the straight line. The crossover frequency-lock disturbance is the peak-to-peak value of the residual from the best-fit line.

Care must be taken not to consider the usual output noise of the accelerometer as being the amplitude of the frequency-lock disturbance. It may be necessary to repeat the test with a smaller acceleration step to have a better measurement of the frequency-lock disturbance.

The amplitude of the frequency-lock disturbance shall conform to the requirements of 5.3.15.2.

12.5.2 VBA activity dips

12.5.2.1 Purpose

The purpose of this test is to determine the location and amplitude of the activity dips that can occur within the acceleration operating range of a VBA.

12.5.2.2 Test equipment

The following test equipment specified in 11.2 is required for this test:

a) Dividing head and mounting fixture

b) Precision centrifuge and mounting fixture

c) Electronic equipment required to operate the accelerometer and measure its output

d) Temperature controller

12.5.2.3 Test setup

The test setup shall be in accordance with 12.1.2.1 and either 12.1.2.2 (dividing head) or 12.3.15.3 and 12.3.15.5 (centrifuge).

12.5.2.4 Test procedure

To find the location of the activity dips, the whole operating range of the accelerometer must be swept (see D.5.9.2.2).

a) In the ±*g* range, rotate the dividing head from +*g* to –*g* in __________ $\mu m/s^2$ steps, dwelling at each position sufficiently long to get useful resolution. Plot the accelerometer output versus acceleration. Activity dips will show as transient disturbances.

b) For the high acceleration range, servo the centrifuge to the maximum positive acceleration specified for the accelerometer. Let the centrifuge coast down to a stop, while measuring the accelerometer output and the acceleration. Plot the accelerometer output versus acceleration. Activity dips will show as transient disturbances.

c) Repeat Step b) for negative accelerations.

d) At each acceleration where an activity dip is observed to occur, perform the frequency-lock test procedure in 12.5.1 to determine the amplitude of the disturbance.

12.5.2.5 Test results

Perform a least-squares straight line fit of the accelerometer output versus the applied acceleration, and compute the residual between the data and the straight line. The activity-dip disturbance is measured by the peak-to-peak value of the residual of the best-fit line.

The existence and amplitude of activity dips shall conform to the requirements of 5.3.15.3.

12.6 Micromechanical accelerometer tests

The tests defined in this clause are unique to micromechanical accelerometers and should be considered to be required in addition to the other tests specified herein.

12.6.1 Wafer-level tests

The piece parts for a silicon micromechanical accelerometer can have several tests performed on them while at the silicon wafer level. These tests can in fact be crucial to controlling the cost of these devices, both for preventing defective parts from being built up into an accelerometer and for eliminating the need for certain tests at the completed accelerometer level.

Similarly, the quartz resonators for a macro- or micro-sized VBA can receive their electrode plating while at the wafer level and can be connected to oscillator circuits to measure bias frequency and bias temperature sensitivity while in the wafer. Such wafer-level tests allow the matching of pairs of resonators that are used in a VBA assembly.

This performance specification and test description document does not deal with wafer level or other subassembly tests used in the manufacture of an accelerometer.

12.6.2 Proof-mass suspension resonant frequency

12.6.2.1 Purpose

The purpose of this test is to determine the resonant frequency and quality factor Q of a capacitively torqued micromechanical accelerometer's proof mass and suspension.

This test is done in a vacuum since gas damping in the operational configuration of the micromechanical accelerometer makes the resonant frequency less discernible. Hence, the test is normally performed only on a sample of micromechanical accelerometers before they are encapsulated as an engineering evaluation test and not an acceptance test.

12.6.2.2 Test equipment

The following test equipment specified in 11.2 is required for this test:

a) Dividing head and mounting fixture

b) Electronic equipment required to operate the accelerometer and measure its output

c) Dynamic signal analyzer providing ac input excitation and output analysis

d) Vacuum bell jar

12.6.2.3 Test setup

The test setup shall be in accordance with 12.1.2.1 and either 12.1.2.2 or 12.1.2.3, with IA horizontal and the torque servo loop disconnected and with the variable frequency ac voltage from the dynamic signal analyzer driving the capacitive torquer.

12.6.2.4 Test procedure

Place the micromechanical accelerometer in the vacuum bell jar on the mounting block with IA horizontal. Draw a vacuum on the bell jar. Place a +__________ V bias voltage on a torquer plate. With the dynamic signal analyzer input ac peak voltage set at __________ V (less than or equal to the bias voltage), vary the frequency of the ac input voltage to the torquer plate from __________ Hz to __________ kHz at a sweep rate of __________ Hz/s. Record the pickoff signal as a function of input frequency, and use the signal analyzer to measure the transfer function. The resonant frequency is where the pickoff signal is a maximum. The height of the maximum and width of the curve around the maximum is a measure of the *Q* of the proof mass and flexure structure.

Repeat the test with the other torquer plate, or excite both torquer plates simultaneously 180° out of phase relative to the bias voltage.

Because torque is proportional to voltage squared, exciting a single torquer plate with a negative voltage has the same effect as using positive voltage in moving the proof mass on one side of the flexure. The positive and negative ac voltage from the signal analyzer can be used in this test because the sum of the bias and ac voltages is always nonnegative. Exciting the opposite plate is required to move the proof mass on the opposite side of the flexure.

The test could be done with different magnitude torquer voltages to evaluate the effect of torquer voltage on the resonant frequency measurement.

12.6.2.5 Test results

The proof-mass suspension resonant frequency shall be in agreement with the reference constants in 5.3.25 and 5.3.28.

12.6.3 Proof-mass freedom

12.6.3.1 Purpose

The purpose of this test is to demonstrate the motional freedom and freedom from sticking of a capacitively torqued micromechanical accelerometer's proof mass.

The direct output of the pickoff buffer amplifier is required to perform this test.

12.6.3.2 Test equipment

The following test equipment specified in 11.2 is required for this test:

a) Dividing head and mounting fixture

b) Electronic equipment required to operate the accelerometer and measure its output

c) Variable dc voltage source

12.6.3.3 Test setup

The test setup shall be in accordance with 12.1.2.1 and either 12.1.2.2 or 12.1.2.3. Then position the IA horizontal. With the torque servo loop disconnected, attach the variable dc voltage source to the capacitive torquer.

12.6.3.4 Test procedure

For a pendulous accelerometer, having PA and IA horizontal and OA vertical minimizes gravity error effects in this test.

In increments of__________ V, apply successively larger positive voltages to one of the torquer capacitor plates. Monitor the pickoff signal as a function of applied voltage. The proof mass has hit a stop when the pickoff signal no longer changes with increases in voltage. Remove the voltage and watch the pickoff signal return to null on an oscilloscope or with a high-speed data acquisition system. Repeat the procedure with the opposite torquer capacitor plate to move the proof mass in the opposite direction.

12.6.3.5 Test results

The accelerometer proof mass shall have complete motional freedom between the stops without sticking at a stop as indicated by the pickoff signal returning to null due to flexure elastic restraint when the torque voltage is removed. If the (parabolic) plot of the motion between the stops as a function of applied voltage is not smooth or if the pickoff does not return to null when the voltage is removed, it is indicative of a problem in the micromechanical accelerometer, such as particle contamination, sticking, or a crack in a flexure. Contamination could also cause the voltages required to reach the stops to be different on the two sides.

The magnitudes of the pickoff output voltage at the stops shall conform to the requirements of 5.3.24.5.

12.6.4 Torquer and pickoff electrode capacitor values

12.6.4.1 Purpose

The purpose of this test is to determine the torquer and pickoff electrode capacitor values from the transfer function characteristics of each internal micromechanical accelerometer capacitor and the accelerometer buffer amplifier.

12.6.4.2 Test equipment

The following test equipment specified in 11.2 is required for this test:

a) Dividing head and mounting fixture

b) Electronic equipment required to operate the accelerometer and measure its output

c) Dynamic signal analyzer providing ac input excitation and output analysis

12.6.4.3 Test setup

The test setup shall be in accordance with 12.1.2.1 and 12.1.2.3. Then position the IA horizontal. Attach the variable frequency ac signal from the signal analyzer to each of the internal accelerometer capacitors one at a time while keeping the other internal capacitors shorted to ground to reduce the effects of stray capacitance.

12.6.4.4 Test procedure

For a pendulous accelerometer, having PA and IA horizontal and OA vertical minimizes gravity error effects in this test.

With the dynamic signal analyzer input ac peak voltage set at __________ V, vary the frequency of the input ac signal from __________ Hz to __________ kHz at a sweep rate of __________ Hz/s. With the signal analyzer, measure the transfer function from the accelerometer capacitor input to the output of the buffer amplifier. Calculate the value of the buffer amplifier feedback capacitor using the known feedback resistance value and measured break frequency from the transfer function. Calculate each internal capacitor value of the accelerometer using the maximum gain obtained from the transfer function and the buffer amplifier feedback capacitor value.

12.6.4.5 Test results

The measured internal capacitances shall be in agreement with the requirements of 5.5.1.1 and 5.5.1.2.

12.6.5 Pickoff scale factor

12.6.5.1 Purpose

The purpose of this test is to measure the pickoff scale factor in V/rad for a rotational proof mass or in V/cm for a translational proof mass.

The direct output of the pickoff buffer amplifier is required to perform this test.

12.6.5.2 Test equipment

The following test equipment specified in 11.2 is required for this test:

a) Dividing head and mounting fixture

b) Electronic equipment required to operate the accelerometer and measure its output

c) Dynamic signal analyzer providing output analysis

d) Variable dc voltage source

12.6.5.3 Test setup

The test setup shall be in accordance with 12.1.2.1 and 12.1.2.3. Then position the IA horizontal. With the torque loop disconnected, attach the variable dc voltage source to the capacitive torquer.

12.6.5.4 Test procedure

For a pendulous accelerometer, having PA and IA horizontal and OA vertical minimizes gravity error effects in this test.

Measure the amplitude of the pickoff output voltage V_0 at the excitation frequency using the signal analyzer. Apply successively positive dc voltages to one of the torquer capacitor electrodes while monitoring the pickoff signal as a function of the applied voltage. The proof mass has hit a stop when the pickoff signal no longer increases with small increments of increasing applied torquer voltage. Record the value V_1 of the pickoff output voltage when the proof mass just touches the stop. Repeat the procedure except apply the dc voltage to the other torquer capacitor electrode to move the proof mass in the opposite direction, and record the value V_2 of the pickoff output voltage when the proof mass just touches the stop.

An alternative approach to measuring the pickoff scale factor is to let gravity move the proof mass for dividing-head angles θ above and below the horizontal. However, micromechanical accelerometers often have flexure stiffnesses that prevent the proof mass from hitting the stops in the ±1-*g* range ($\lvert\theta\rvert < 90°$).

12.6.5.5 Test results

For a rotational proof mass accelerometer, calculate the angles θ_1 and θ_2 of proof-mass deflection using the build air gap dimensions and the length of the proof mass from the center of rotation. For the teeter-totter configuration (see Annex F), the length of the proof mass from the center of rotation is different on opposite sides of the flexure. For a translational proof mass, use the nominal gap dimension h between the proof mass and the two stops.

The pickoff scale factor

$$K_{\text{pick}} = \frac{1}{2}\left[\frac{V_1}{\theta_1} + \frac{V_2}{\theta_2}\right] \text{ V/rad rotational proof mass}$$

$$K_{\text{pick}} = \frac{1}{2}\left[\frac{V_1}{h} + \frac{V_2}{h}\right] \text{ V/cm translational proof mass}$$

shall satisfy the requirements of 5.3.25.

12.6.6 Flexure elastic restraint

12.6.6.1 Purpose

The purpose of this test is to determine the flexure elastic restraint by measuring the change in restraining torque voltage resulting from “dummy-directing” (i.e., moving) the proof mass.

12.6.6.2 Test equipment

The following test equipment specified in 11.2 is required for this test:

a) Dividing head and mounting fixture

b) Electronic equipment required to operate the accelerometer and measure its output

c) Variable dc voltage source

d) Dynamic signal analyzer providing output analysis

12.6.6.3 Test setup

The test setup shall be in accordance with 12.1.2.1 and 12.1.2.3. Then position the IA horizontal.

12.6.6.4 Test procedure

For a pendulous accelerometer, having PA and IA horizontal and OA vertical minimizes gravity error effects in this test.

Measure the output of the accelerometer rebalance loop with a dc voltmeter (torquer voltage required to keep the pickoff signal at null). Inject +__________ Vdc into the summing junction of the integrator of the torque to balance loop to dummy-direct (i.e., move) the proof mass off of null. Measure the output of the accelerometer rebalance loop with a dc voltmeter and the pickoff peak output voltage with signal analyzer (measure of the amount of dummy-direct angle). Repeat the test with –__________ Vdc injected into the summing junction of the integrator of the torque to balance loop to move the proof mass off of null in the opposite direction.

12.6.6.5 Test results

The flexure elastic restraint in (m/s^2)/rad for a rotational proof-mass accelerometer or (m/s^2)/cm for a translational proof-mass accelerometer is

$$K_r = \frac{(\text{change in torque voltage}) \;/\; K_1}{(\text{change in pickoff voltage from dummy direct}) \;/\; K_{\text{pick}}}$$

where K_{pick} in V/rad or V/cm is from 12.6.5.5 and the capacitive torquer scale factor K_1 in V/[m/s^2, ft/s^2, _____] for normal closed-loop operation is measured by the four-point tumble or IA up–down test of 12.3.4. The value of K_r shall conform to the requirement of 5.3.28.

12.7 Life tests

12.7.1 Life—Storage or dormant

12.7.1.1 Purpose

The purpose of this test is to demonstrate that the accelerometer parameters vary by less than the requirements for the specified storage or dormancy period and that the accelerometer performs as required after the storage or dormancy period.

12.7.1.2 Test equipment

The following test equipment specified in 11.2 is required for this test:

a) Dividing head and mounting fixture

b) Electronic equipment required to operate the accelerometer and measure its output

12.7.1.3 Test setup

The setup for checking the accelerometer at the beginning and end of the test period shall be in accordance with 12.1.2.1 and 12.1.2.2.

12.7.1.4 Test procedure

The test procedure shall be as follows:

a) Determine the bias and scale factor using the procedure of 12.3.4.4.

b) Place the accelerometer in one of the following:

   1) Within any specified protective packaging in the storage environment, which may include periodic subjection to vibration, shock, temperature cycling, and/or other nonoperating environmental conditions

   2) In a dormant, nonoperating condition, which could be with its temperature at the operating point or some other point and with periodic structural, mechanical, electrical, or other environmental stresses

c) At the end of the storage or dormancy period of duration ________ [d, mo, yr], again determine the bias and scale factor.

If desired, periodic measurements of performance parameters during storage or dormant life may be specified and additional parameters such as misalignments and nonlinearities may be measured. However, removing the accelerometer from its test fixture affects misalignment estimates.

12.7.1.5 Test results

The bias and scale-factor values for all measurements shall meet the requirements of 5.6.1.10 or 5.6.3.

12.7.2 Life—Operating

12.7.2.1 Purpose

The purpose of this test is to demonstrate that the accelerometer parameters vary by less than the requirements for the specified operating life period and that the accelerometer performs as required during the operating life period.

12.7.2.2 Test equipment

The following test equipment specified in 11.2 is required for this test:

a) Dividing head and mounting fixture

b) Electronic equipment required to operate the accelerometer and measure its output

12.7.2.3 Test setup

The test setup shall be in accordance with 12.1.2.1 and 12.1.2.2. The accelerometer shall be operated continuously, except for periodic on–off cycles per the requirements of 5.6.2.13.

12.7.2.4 Test procedure

Every __________ [h, d] for __________ [mo, yr] measure the bias, scale factor, and misalignment angle using the procedure of 12.3.4.4. Accumulate the operating time and the number of on–off cycles per the requirements of 5.6.2.13.

12.7.2.5 Test results

The maximum parameter variations during the operating life shall be in accordance with the requirements of 5.6.2.13.

Nonlinearity and other parameters may also be tested for maximum allowed changes.

12.8 Reliability tests

12.8.1 Laboratory reliability test

12.8.1.1 Purpose

The purpose of this test is to demonstrate the MTBF statistics for a representative sample of accelerometers.

12.8.1.2 Test equipment

The following test equipment specified in 11.2 is required for this test:

a) Holding fixture, perhaps for multiple accelerometers

b) Electronic equipment required to operate the accelerometer and measure its output

12.8.1.3 Test setup

The setup shall be in accordance with 12.1.2.1 in the reliability test fixture.

If the reliability test is done simultaneously with the operating life test, the fixture should be mounted on a dividing head per 12.1.2.2 to allow periodic parameter calibrations.

12.8.1.4 Test procedure

Accumulate accelerometer operating hours with periodic on–off cycles per the requirements of 5.6.2.13.

Accelerated reliability testing would subject the accelerometer to periodic hot soaks, temperature cycles, increased on–off cycles, vibration, shock, and so on, in order to obtain a measure of the MTBF over the projected lifetime of the device in a shorter time than this lifetime. Accelerated reliability tests of key subassemblies may also be performed to estimate accelerometer MTBF. Typically the trade-off between forced environments and the amount of accelerated aging they cause is presented in the form of a matrix or table. The use of this matrix or table for qualification testing of the accelerometer must be agreed to by both the manufacturer and the customer.

12.8.1.5 Test results

The MTBF statistics from multiple accelerometer reliability tests shall conform to the requirements of 5.7.2.

12.8.2 Field reliability experience

The MTBF statistics for accelerometers in the field shall conform to the requirements of 5.7.2.

12.9 Environmental tests

12.9.1 Purpose

The purpose of these tests is to verify that the accelerometer performs as specified when subjected to environments outside of the standard operating conditions but within the specified environmental limits.

12.9.2 Test equipment

The following test equipment from 11.2 may be required depending on the chosen environmental test:

a) Equipment for providing the specified environment

> Examples of environmental equipment are as follows:
>
> — Thermal and/or barometric chamber
> — Electromagnetic or hydraulic vibrator that can be programmed for various types, frequencies, and amplitudes of vibration (sinusoidal, random, frequency sweep) and for various shock spectrums (half sine, full sine, sinusoidal with decaying exponential amplitude)
> — Drop-to-specified-surface or other shock machine that can impose a shock with nonzero average acceleration
> — Air gun
> — Centrifuge (lesser precision required for, e.g., determining overload capacity than for calibrating model coefficients)
> — Rotary table
> — Generators of electric and magnetic fields and pulses and of acoustic noise
> — X-ray, gamma ray, and neutron radiation sources

b) Means of measurement of environment and time

c) Adaptation of accelerometer to environmental equipment such as special holding fixtures, cables, and so on

d) Equipment for each accelerometer test to be performed before, during, and/or after application of the environment (such as a dividing head for before and after tumble calibrations)

12.9.3 Test setup

> List the test setups for before, during, and/or after the application of the environment.

12.9.4 Test procedure

Table 6 lists possible environmental tests (12.9.4.1 to 12.9.4.17) and life tests (12.7.1 and 12.7.2) versus examples of which accelerometer tests (12.2 through 12.6 and 12.8) could be conducted before, during, and after exposure to the environment. The environmental tests correlate with the tests identified in 6.6.9. The life tests correlate with the tests identified in 6.6.7. In some cases, it may be desirable to combine environments to simulate the expected operating conditions.

The application of the accelerometer, the expected environmental sensitivities of the accelerometer, and the cost effectiveness of the testing will determine which tests or combinations of tests are performed and their sequence.

Detail the procedure for the control of the environment, including tolerances and rates of change, integrated with the procedure for the accelerometer test. Procedures for most environmental tests are well covered by existing industry, government, and military documents such as MIL-STD-810. Rather than duplicate samples of existing procedures, Table 6 provides assistance in selecting the accelerometer parameters that will be most important to measure during or across each environment.

Caution notes on overload limits on the environmental intensity applied to the accelerometer can be specified if required.

12.9.5 Test results

The accelerometer performance shall meet the requirements of 5.3 after exposure to the nonoperating environments specified in 5.6.1, during and after exposure to the operating environments specified in 5.6.2, and after exposure to the conditions of 5.3.3.

Table 6—Environmental test matrix

Accelerometer tests	12.9 Environmental Tests	12.9.4.1 Vibration	12.9.4.2 Mechanical Shock	12.9.4.3 Acceleration	12.9.4.4 Angular acceleration & spin	12.9.4.5 Temperature (high, low)	12.9.4.6 Thermal shock	12.9.4.7 Thermal radiation	12.9.4.8 Pressure (high, low)	12.9.4.9 Acoustic noise	12.9.4.10 Electromagnetic interference	12.9.4.11 Electromagnetic susceptibility	12.9.4.12 Magnetic induction	12.9.4.13 Fungus	12.9.4.14 Humidity	12.9.4.15 Salt spray	12.9.4.16 Sand and dust	12.9.4.17 Nuclear radiation	12.7 Life tests	12.7.1 Life: storage or dormant (5)	12.7.2 Life: operating
12.2 Accelerometer nonoperating tests																					
12.2.1 Examination of product		NO	NO	NO		NO	NO		NO					N	N	N	N	NO		ND	O
12.2.2 Weight or mass																		NO			
12.2.3 Impedance		ND	NO	N		D				D										ND	O
12.2.4 Dielectric strength		NO	NO	N		N														ND	O
12.2.5 Insulation resistance		NOD	NO	N		N	N													ND	O
12.2.6 Seal		N	N			ND	ND		N									NO		ND	O
12.2.7 Temperature sensor characteristics						O	O	O			D	D						NO		ND	O
12.3 Accelerometer operating tests																					
12.3.1 Functional checkout		NO	NO	NO		NO	NO	NO	NO	D	D	D	D					NO		ND	O
12.3.2 Noise																		NO			
12.3.3 Inversion transient						D												NO		ND	O
12.3.4 Four point tumble																					
Scale factor and bias		ND	N	O		D	D	D			DO	DO	D					NO		ND	O
Input axis misalignment																		NO		ND	O
12.3.5 Static multipoint						D												O		ND	O
12.3.6 Threshold, resolution, & dead band		N	N			D												O		ND	O
12.3.7 Warm-up time						D												NO		ND	O
12.3.8 Short-term stability						D												NO		ND	O
12.3.9 Long-term stability						D												NO		ND	O
12.3.10 Repeatability		O	O	O		D												NO		ND	O
12.3.11 Sensitivity						D							D					O		ND	O
12.3.12 Temp. model calib. & temp. hysteresis																					
12.3.13 Velocity storage across power interrupt						D												O		ND	O
12.3.14 Centrifuge input range				D		D												O		ND	O
12.3.15 Precision centrifuge				D		D												O		ND	O
12.3.16 Frequency response		D				D												NO		ND	O
12.3.17 Vibration calibration (nonlinear terms)		D																			
12.3.18 Vib. & shock calib. (scale factor & bias)		D	D																		
12.3.19 Performance through & across env.		DO	DO																		
12.3.20 Vel. storage in normal & over range shock			DO																		
12.3.21 Slew calibration					D																
12.3.22 Magnetic leakage													D								
12.4 Electromag. torqued pendulous accel.																					
12.4.1 Pickoff characteristics		N	N	N		O												NO		ND	O
12.4.2 Torquer & self-test torquer polarity																					
12.4.3 Open-loop frequency response						D												NO		ND	O
12.4.4 Pickoff scale factor & pendulum elastic restr.		N	N			D												O		ND	O
12.4.5 Turn-on hysteresis						D												O			
12.4.6 Self-test torque scale factor						D												NO		ND	O
12.4.7 Velocity storage – open loop test						D												NO		ND	O
12.4.8 Velocity storage – pulse-torque steady-state op						D												NO		ND	O

Table 6—Environmental test matrix (*continued*)

Accelerometer tests	12.9 Environmental Tests	12.9.4.1 Vibration	12.9.4.2 Mechanical Shock	12.9.4.3 Acceleration	12.9.4.4 Angular acceleration & spin	12.9.4.5 Temperature (high, low)	12.9.4.6 Thermal shock	12.9.4.7 Thermal radiation	12.9.4.8 Pressure (high, low)	12.9.4.9 Acoustic noise	12.9.4.10 Electromagnetic interference	12.9.4.11 Electromagnetic susceptibility	12.9.4.12 Magnetic induction	12.9.4.13 Fungus	12.9.4.14 Humidity	12.9.4.15 Salt spray	12.9.4.16 Sand and dust	12.9.4.17 Nuclear radiation	12.7 Life tests	12.7.1 Life: storage or dormant (5)	12.7.2 Life: operating
12.5 VBA tests																					
12.5.1 VBA frequency lock		D																			
12.5.2 VBA activity dips		D																			
12.6 Micromechanical accelerometer tests																					
12.6.1 Wafer level tests																					
12.6.2 Proof-mass suspension resonant freq.		N	N			D												O		ND	O
12.6.3 Proof-mass freedom		N	N			D												O		ND	O
12.6.4 Torquer and pickoff electrode capacitor values		N	N			D												O		ND	O
12.6.5 Pickoff scale factor		N	N			D												O		ND	O
12.6.6 Flexure elastic restraint		N	N			D												O		ND	O
12.8 Reliability tests																					
12.8.1 Laboratory reliability tests (6)		NO	NO			NO															
Monitor indicated acceleration		D			D					D								D			
COMMENTS				1	2						3	4								5	

CODES
O Accelerometer tests conducted before and after specified environment and accelerometer operated during environment
N Accelerometer tests conducted before and after specified environment and accelerometer not operated during environment
D Accelerometer tests conducted during specified environment and accelerometer is operating or nonoperating as applicable

COMMENTS
(1) Demonstrate overload capability
(2) Spin offset and anisoinertia
(3) Generated by
(4) Subjected to
(5) Storage life is N, dormant life is D
(6) For accelerated reliability tests

Part III—Accelerometer descriptions

Annex A

(informative)

Accelerometer dynamic block diagrams

A.1 Introduction

This annex presents the equations and block diagrams of the dynamic response of a pendulous (or by analogy a translational proof-mass) accelerometer for which the measure of input acceleration is either the displacement of the pendulum (or proof mass) when operated in open-loop mode or the restoring torque (or force) when operated in closed-loop mode. For the latter case, operations with additional voltage-to-frequency conversion circuits or a digital capture loop are also discussed.

An idealized, linear, second-order model is assumed for the accelerometer pendulum (or translational proof mass). Blocks are used to represent added circuitry since it can have many forms, each with a different internal mechanization.

A.2 Open-loop operation

For an open-loop accelerometer typical of many silicon micromachined designs, the sensor responds to input acceleration by deflection of the pendulum (or translational proof mass) through an angle (or translational displacement) proportional to the input acceleration $a(t)$. The pickoff and electronics module sense the deflection and convert it into a proportional electrical output signal $V_\mathrm{o}(\mathrm{s})$. The output voltage is approximated by Equation (A.1) in the pendulous case (see Figure A.1)

$$V_\mathrm{o}(\mathrm{s}) = A(\mathrm{s})P\left[\frac{1}{J\mathrm{s}^2 + C\mathrm{s} + K_\mathrm{e}}\right][K_\mathrm{PO}(\mathrm{s})][K_\mathrm{OA}(\mathrm{s})] \tag{A.1}$$

where in Equation (A.1) and Figure A.1

$A(\mathrm{s})$	is the Laplace transform of the applied acceleration $a(t)$ along IA in cm/s^2
s	is the Laplace operator
P	is the pendulosity (g·cm)
J	is the moment of inertia of pendulum about OA (g·cm^2)
C	is the damping torque coefficient (dyn·cm/(rad/s))
K_e	is the pendulum elastic restraint (dyn·cm/rad)
$K_\mathrm{PO}(\mathrm{s})$	is the pickoff transfer function (V/rad)
$K_\mathrm{OA}(\mathrm{s})$	is the output amplifier transfer function (Vdc/Vac)
$T_\mathrm{i}(\mathrm{s})$	is the Laplace transform of driving torque (dyn·cm)
$\theta_\mathrm{PO}(\mathrm{s})$	is the Laplace transform of angular displacement of pendulum with respect to the case (rad)
$V_\mathrm{PO}(\mathrm{s})$	is the Laplace transform of pickoff voltage (Vrms)
$V_\mathrm{o}(\mathrm{s})$	is the Laplace transform of output voltage (V)

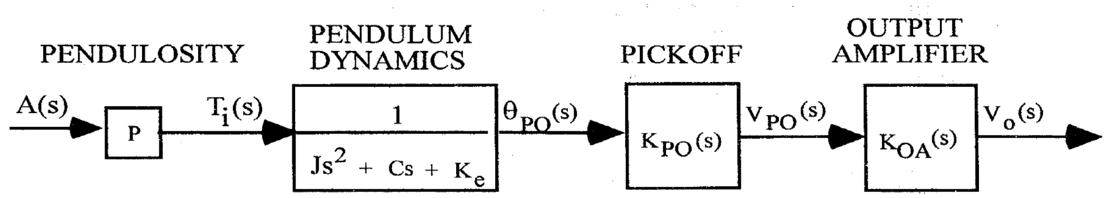

Figure A.1—Block diagram for open-loop operation

A.3 Closed-loop operation

Accelerometers can provide a higher performance for critical applications by use of classic negative feedback, using a torquer (or forcer) acting on the pendulum (or translational proof mass) to minimize the deflection of the pendulum (or proof mass) when it is subjected to torque (or force) T_i(s) produced by acceleration of the sensor case.

As shown in Figure A.2 for a pendulous accelerometer, the output voltage V_o(s) forces a current I_o(s) to flow through both the torquer and the sampling resistor R_L, causing a restoring torque T_r to be applied to the pendulum. By use of high loop gain, the negative feedback produces a nearly ideal equality of the feedback torque to the input torque T_i(s), causing the output current I_o to be a direct measure of the input acceleration. Again, assuming that the acceleration of the case along the IA is $a(t)$, the output voltage V_L can be approximated by Equation (A.2) for an electromagnetic torquer (see Figure A.2)

$$V_{\mathrm{L}}(\mathrm{s}) = A(\mathrm{s}) \frac{P\, K_{\mathrm{PO}}(\mathrm{s}) K_{\mathrm{A}}(\mathrm{s}) R_{\mathrm{L}}}{(J\mathrm{s}^2 + C\mathrm{s} + K_{\mathrm{e}})(R_{\mathrm{t}} + R_{\mathrm{L}} + L_{\mathrm{t}}\mathrm{s}) + K_{\mathrm{PO}}(\mathrm{s}) K_{\mathrm{A}}(\mathrm{s}) K_{\mathrm{t}}} \tag{A.2}$$

where in Equation (A.2) and Figure A.2

K_A(s)	is the servo amplifier transfer function (Vdc/Vrms)
T_r(s)	is the Laplace transform of capture torque (dyn·cm)
T_e(s)	is the Laplace transform of error torque (dyn·cm)
R_L	is the sampling resistor (Ω)
V_L(s)	is the Laplace transform of voltage across R_L (V)
I_o(s)	is the Laplace transform of servo output current (A)
K_t	is the torquer scale factor (dyn·cm/A)
R_t	is the torquer resistance (Ω)
L_t	is the torquer inductance (H)

All other symbols have the same definition as in Equation (A.1). All effects of the model equation error coefficients have been neglected.

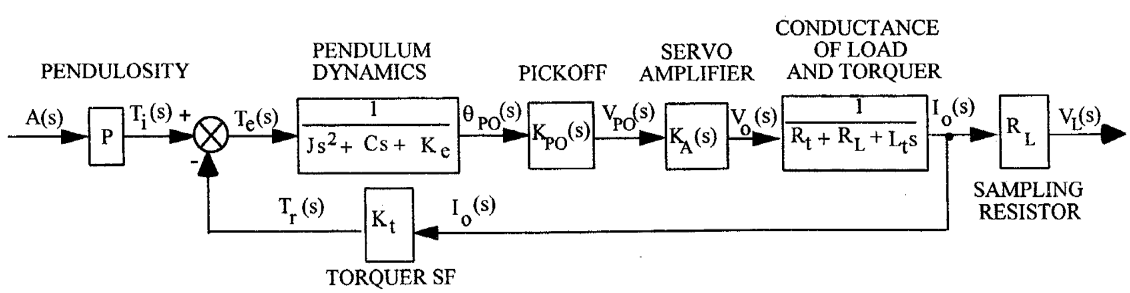

Figure A.2—Block diagram for closed-loop operation

A.4 Open-loop operation of closed-loop accelerometer

For several critical tests to investigate the internal parameters of a closed-loop accelerometer, the loop may be opened by disconnecting the torquer and using it to drive the mechanism of the accelerometer as shown in the block diagram of Figure A.3.

Let the hinge or OA of the sensor be vertical with the IA horizontal in order to minimize any effects of gravity on the measurement. If a voltage $v_{\mathrm{i}}(t)$ is applied to the torquer with input acceleration $a(t) = 0$, the output voltage is approximated by Equation (A.3) (see Figure A.3)

$$V_{\mathrm{o}}(\mathrm{s}) = V_{\mathrm{i}}(\mathrm{s})\left[\frac{K_{\mathrm{t}}}{R_{\mathrm{t}} + R_{\mathrm{L}} + L_{\mathrm{t}}\mathrm{s}}\right]\left[\frac{1}{J\mathrm{s}^2 + C\mathrm{s} + K_{\mathrm{e}}}\right][K_{\mathrm{PO}}(\mathrm{s})][K_{\mathrm{A}}(\mathrm{s})] \qquad \text{(A.3)}$$

where the notation is as above with

$V_{\mathrm{i}}(\mathrm{s})$ is the Laplace transform of applied voltage $v_{\mathrm{i}}(t)$ (V)

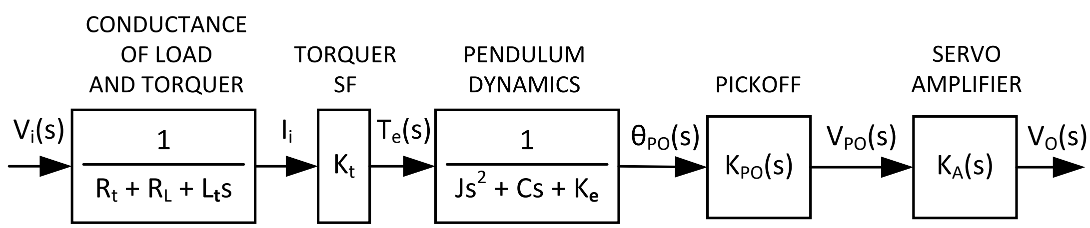

Figure A.3—Block diagram for open-loop test of closed-loop accelerometer

A.5 Operation with voltage-to-frequency conversion

Use of voltage-to-frequency (V-to-F) conversion permits the transmission of acceleration data and/or the accumulation of velocity data in digital form so that subsequent computations may be made with minimal error, taking advantage of the digital character of the data. The voltage-to-frequency converter is connected in cascade with the analog accelerometer, accepting its analog signal either as a voltage signal or as a current proportional to acceleration.

Consequently, the dynamic response of the data produced is identical to that produced by the accelerometer as described in A.3, modified only by the discrete nature of the individual output pulses, where each pulse represents a given increment of acceleration times time or represents a specific increment of velocity. In cases where the converter operates to a very high frequency, the resulting dynamic response from A(s) input to the frequency output $F_{\mathrm{o}}(\mathrm{s})$ may be indistinguishable from that of the analog accelerometer itself. Where low frequencies are used, the Z-transform of the voltage-to-frequency converter transfer function must be defined and used in dynamic analyses (see Figure A.4).

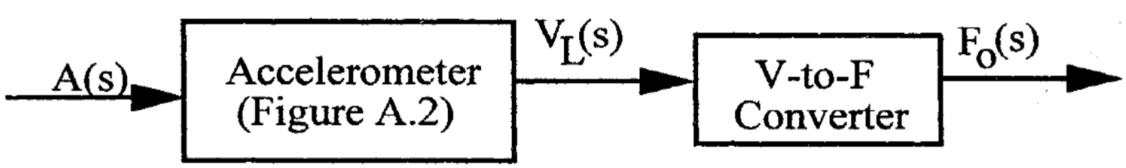

Figure A.4—Block diagram of accelerometer plus voltage-to-frequency converter

A.6 Operation with digital capture loop

Figure A.5 is a typical block diagram for the dynamic response of the accelerometer when operating in the closed-loop mode using a digital capture loop. An idealized, linear, second-order model is assumed for the acceleration sensor's pendulum. The symbols used in Figure A.5 are as defined earlier. (The digital electronics are shown as a single block since there are many configurations, each with its own internal mechanization and transfer functions, as discussed in Annex B.)

A.7 Accuracy of capture-loop readout

The accuracy of a capture-loop readout is directly dependent on the accuracy of a precision voltage source, typically no better than a part per million for nonsuperconducting technology. The precision voltage source is used to control the height of a digital torque pulse in a digital torque loop or is used as a reference in a voltage-to-frequency or analog-to-digital readout for an analog torque loop.

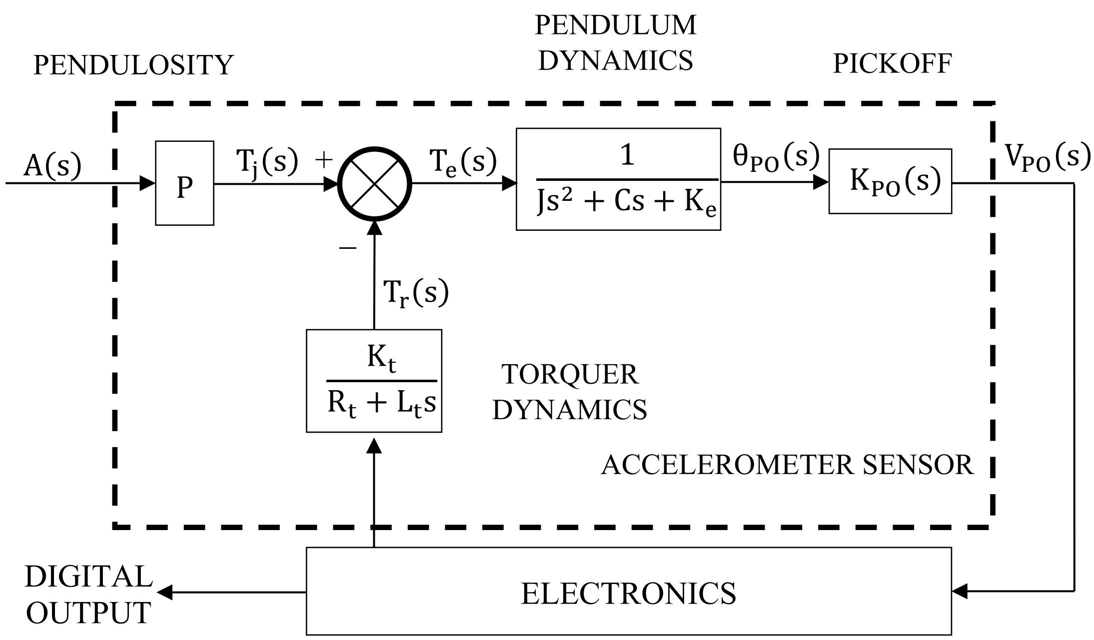

Figure A.5—Block diagram of accelerometer with digital capture loop

Annex B

(informative)

Digital accelerometers and comments concerning their test methods

B.1 Introduction

This annex presents a brief review of the more commonly used types of digital instrument outputs, followed by several comments concerning the testing of instruments having digital outputs. Annex H contains descriptions of some of the special techniques of digital filtering that have been found to be useful in inertial systems.

A principal advantage of digital interfaces is the ability to improve performance by modeling reproducible accelerometer and gyroscope errors. These errors may include, for example, linearity errors or temperature-induced variations in bias, scale-factor, and IA misalignment. See the second boxed note in 5.3. In the performance clauses affected by the need for modeling, each clause shall include both the uncompensated error allowable and the magnitude of the allowable error after compensation.

B.2 Description of commonly encountered digital output formats

B.2.1 Sample and hold with an analog-to-digital converter

One of the simplest schemes for digitizing the output of an analog instrument is to use a sample-and-hold circuit with its output fed into an analog-to-digital converter. Typically, the sample-and-hold circuit is commanded to sample the analog output signal in synchronism with an external clock signal of the desired sampling frequency. The hold portion of the circuit is designed to retain the level of the analog signal as it was at the instant of sampling. The signal serves as the input to an analog-to-digital converter, which typically generates the closest binary number, that is, the digital representation of the analog input at the time of sampling. A sign bit may or may not be provided, depending on the application, and other digital formats such as binary-coded decimal are sometimes used. Depending on the application, the number generated can be read out in series or in parallel.

B.2.2 Digitally captured accelerometers

In these applications, the accelerometer proof mass is rebalanced to null by a control loop generating pulses of torque or force. The rebalance can be accomplished by means of a train of fixed area pulses that are selected by logic circuitry to return the internal sensing element toward its null position. This type of rebalance loop is generally defined by the pulse sizes and types available to the logic circuit. Those pulses typically consist of a fixed electric current applied for a fixed time interval.

The output is obtained by observing logic signals that indicate the time of pulse application and which of the allowable types of pulses were applied.

These approaches typically use an analog pickoff signal from the sensor to detect deviations from null.

B.2.2.1 Binary

Binary pulse capture electronics generally imply that the logic selects from either of two kinds of pulses, positive or negative, to rebalance the proof mass. The two kinds of pulses are of fixed and nominally equal area. The pulses are usually applied in synchronism with an external clock. For example, with this type of loop, zero input usually implies that the output will oscillate alternately between single positive and negative pulses at the clock frequency. Accelerometer saturation in one direction implies that all available pulse slots will be filled with the sign of the pulse appropriate to the input direction. Between saturation and zero input, one observes a mixture of pulses. The average frequency obtained by counting the number of pulses (positive minus negative) over the output sampling interval is proportional to the input and is often taken as the accelerometer output.

It is frequently appropriate to accumulate the positive and negative pulses in an up/down counter, which continuously generates the net count as a function of time. The net count represents the integral of the frequency output and, therefore, the net velocity change. It can be sampled as required by the application.

This approach results in a constant power pulse train rebalancing the proof mass.

B.2.2.2 Ternary

A ternary pulse capture electronics is similar to a binary loop except that the following three states are available to the logic:

— Positive
— Negative
— No pulse

This loop is sometimes referred to as “pulse on demand” since positive and negative pulses are applied to the sensing element only when they are needed. Thus, zero input is nominally indicated by no pulse indicators on the output. Positive and negative saturation are indicated by the filling of all available pulse slots with the appropriate pulse signs. The output can be taken as the average net pulse frequency or the accumulation of net pulses as described in B.2.2.1.

In some applications, additional pulse scalings are used. Multiple pulse scalings are used in applications where improved resolution is desired when the input is low but high-level spurts of input are expected. Rescaling mitigates the occasional problem with pulse-on-demand systems that they exhibit very low data rates near zero input.

A characteristic of this ternary approach is that it results in a minimum power pulse train.

B.2.2.3 Time modulated

One form of time-modulated capturing uses a current waveform consisting of alternating positive and negative portions that are synchronized by one frequency (forced-limit-cycle) but time modulated in pulse duration by a closed loop control; The time modulation is synchronized by a higher frequency. This frequency is typically a synchronous multiple of the forced-limit-cycle frequency (see Ash and DeBitetto [B4][7]).

The result is that under steady-state conditions, the sensing element oscillates or limit-cycles around its null position as forced by the current pulse. The output is proportional to the net number of minor clock periods (that is, the number of minor clock periods that the limit cycle was positive minus the number that it was negative). For example, with zero input, the transition from positive to negative would nominally occur at the midpoint. Accelerometer saturation in one direction implies that the transition point occurs at the beginning or the end of the limit cycle, depending on the sign of the input. The sensor output can be taken as the average frequency of net minor clock periods over a fixed number of limit-cycle periods, or the output can be integrated by accumulating net minor clock periods.

This forced limit cycle approach to time-modulated rebalance current results in a constant power waveform as does the binary discrete pulse method. A time-modulated ternary system is also possible where pulses of variable width can be quantized on demand by the control loop, while otherwise zero current will result.

[7] The numbers in brackets correspond to those of the bibliography in Annex N.

B.2.3 Analog accelerometer with a voltage-to-frequency converter

Another technique for digitizing the output of an analog accelerometer is to convert the output by means of a voltage-to-frequency converter. This unit produces an output pulse frequency that is proportional to the analog output. Most voltage-to-frequency converters consist of an operational amplifier integrator equipped with a ternary pulse capture electronics, although it is possible to use other pulse-rebalance formats. With careful circuit design, the conversion can be accurate. As before, the voltage-to-frequency converter output can be sensed as average frequency, or the net counts can be accumulated and read out at the sampling frequency.

B.2.4 Biased outputs

In some instruments, the output frequency is biased so that, for example, zero-frequency output represents negative full-scale input, maximum frequency represents positive full-scale input, and one-half maximum frequency represents zero input. This format allows for use of cheaper and more widely available technology, such as single-quadrant voltage-to-frequency converters, and it solves the problem of having a very low data rate near zero input. However, it can cause confusion between changes in scale factor and changes in bias in temperature modeled systems (see B.3.6).

B.2.5 VBA

The VBA is a form of biased output accelerometer, in which the output frequencies (typically two of them) are generated by force-sensitive, crystal-controlled oscillators. Frequency variation is limited to ±3% to ±30% of the zero-load frequencies. Coupling between scale factor and bias is mitigated by the stability of the crystal resonators and by common mode rejection between the two output frequencies. See Annex C for details.

B.3 Comments concerning test methods associated with digital instruments

B.3.1 Aliasing

Reading out a digital instrument inherently involves digital sampling, which can lead to a phenomenon known as “aliasing” or “frequency folding.” If significant signal components exist at frequencies higher than one half of the sampling frequency (Nyquist frequency), they may be folded back around the half-sampling frequency and be mixed with the true signal components that fall below the half-sampling frequency. These components will then be indistinguishable from those signal components that are in the frequency range up to the Nyquist frequency and may result in misinterpretation of the output sensor data. Because of this situation, it is necessary to select a sample frequency that is more than twice as high as the highest significant signal component. In some cases, it is possible to insert a low-pass analog filter in the system ahead of the digitizer to attenuate unwanted high frequencies and thus prevent aliasing.

For the many applications in which accelerometer outputs are integrated to derive a measure of velocity, output formats in which voltage or current pulses represent increments of velocity have a great advantage. As long as all pulses are equally weighted and no counts are missed, aliasing error is greatly attenuated at low apparent frequencies and falls to zero at dc.

B.3.2 One-count uncertainty and moding

In some applications, the measurement of digital outputs involves measurement uncertainty associated with counting. For example, the possibility of counting one pulse more or one pulse less than ideal in the test interval can occur because of the location of the beginning and ending of the interval relative to the pulse train being measured. The statistics associated with this granularity shall be taken into consideration when designing tests for digital instruments.

Some digital instruments exhibit moding; that is, the digital output tends to overshoot in a recognizable pattern. An example of 3:3 moding in a sensor with binary output is that it will provide a pattern of three positive pulses followed by three negative pulses when the input is zero. Moding should be checked because it may indicate a system malfunction and will increase granularity and, therefore, test uncertainty.

B.3.3 Period measurement versus measurement of the number of pulses over a fixed time interval

In some cases, the resolution associated with the one-count uncertainty can be dramatically reduced by measuring the time period of *n* pulses rather than counting the number of pulses in a fixed time interval (which is assumed to be approximately equivalent to the period of *n* pulses). This improvement is obtained by using a high-frequency clock signal for making the period measurement. The one-count uncertainty is now made on the clock counter, and because of its high frequency, it can usually be acceptably small relative to the count associated with the total period determination. If the pulse train being measured contains jitter, then the trial-to-trial uncertainty may be greater than that predicted by the one-count-clock uncertainty, and this possibility should be checked.

B.3.4 Measurement of positive and negative pulses provided on separate data lines

It is sometimes beneficial to count the positive and negative output pulses with separate counters and obtain the net output by subsequent subtraction. A more conventional approach might be to use an up/down counter, which automatically increments for positive pulses and decrements for negative ones. The advantage of using two counters is that this configuration readily detects the mixing of pulses. Such occurrences, when not expected, may indicate a system malfunction that would go undetected with an up/down counter.

B.3.5 Asymmetry

Many digital accelerometers exhibit scale-factor or bias asymmetries, or both. In other words, the input/output function is separately linear in the positive and negative regions; however, the two halves are best represented by straight lines having different slopes or intercepts, or both. For example, ternary capture electronics often exhibit scale-factor asymmetry. This asymmetry results because separate circuits are used to generate the positive and negative pulses. Because of circuit tolerances or imperfections, or both, the areas of the positive and negative pulses are typically different, a situation that leads directly to scale-factor asymmetry. Digital accelerometer testing should consider this possibility as erroneous results can be obtained if the instrument has one or both of these problems and simple linearity is assumed.

B.3.6 Biased outputs

In B.2.3, it was noted that biased outputs can produce an anomalous apparent coupling between scale factor and bias. An example of this phenomenon is the presence of a scale factor temperature sensitivity, which is corrected by modeling.

If the data are normalized at each test temperature with the apparent scale factor, then an apparent bias temperature sensitivity (and the scale-factor temperature sensitivity) will be indicated, even if the bias frequency is not sensitive to temperature at all. Care should be taken in processing data in these situations.

B.3.7 Threshold and resolution (see 12.3.6)

The existing test paragraphs may be used as written but with two cautionary notes. For threshold, it shall be noted that a digital accelerometer instrumented with a pulse rate output can resolve no less than one pulse, each pulse representing a defined increment of velocity. It would theoretically be necessary to wait for an infinite time period to define zero-indicated acceleration. For this test, a measurement period corresponding to a detectable acceleration of 50% of the specified threshold is recommended.

$$\text{Measurement period} = \frac{\begin{array}{c}\text{minimum unit of}\\ \text{velocity increments (m/s)}\end{array}}{\begin{array}{c}\text{desired acceleration}\\ \text{threshold (m/s}^2\text{)}\end{array}}$$

For resolution, or in the case of biased output, there is no exactly analogous limitation, but the comments on period measurement versus frequency measurement should be noted.

Annex C

(informative)

Characteristics of pendulous accelerometers

C.1 Design principles

Accelerometer designs that have been marketed to date are based on Newton's equation $F = Ma$, and most commonly on single degree-of-freedom (DOF) embodiments of that equation, that is, forms in which the inertial mass M is constrained to motion in a single axis, so that the reaction force F may be treated as a scalar quantity. In the pendulous accelerometer, the constraint is a mechanical hinge or pivot that constrains the mass to a single rotational DOF. The operative equation is then transformed into

$$\mathrm{T} = M\ell a \tag{C.1}$$

where

T	is the reaction torque about the constraint axis
$M\ell$	is the mass imbalance (pendulosity P) with respect to the constraint axis

Typically, axes of pendulous accelerometers are named the input axis (IA), pendulous axis (PA), and output axis (OA), respectively, as illustrated in Figure C.1. IA and PA are intuitively clear, while the OA is named by analogy to gyro practice and has a positive direction defined by the vector operation

$$\overrightarrow{IA} \times \overrightarrow{PA} = \overrightarrow{OA} \tag{C.2}$$

The term "pendulous accelerometer" is usually reserved for accelerometers in which the OA as defined in Figure C.1, is fixed relative to the case, thus, making them distinct from gyroscopic pendulous accelerometers, such as pendulous integrating gyroscopic accelerometers (PIGAs) and specific force integrating receivers (SFIRs). The effective IA goes through the effective pendulum center of mass, often chosen to be the center of percussion (see C.3.2).

The constraints most commonly used are flexure hinges, pivot and jewel, and ball bearing and endstone. These variations differ somewhat in their performance characteristics, but all share the essential virtues and peculiarities of the pendulous design. Many of these accelerometers trace their origins to pivoted mechanisms that came from other uses, such as meter movements or rate gyros. They have remained popular because they have been generally more stable and predictable than nonpendulous competitors, whereas their peculiarities have proven to be acceptable once understood.

Pendulous accelerometers differ from nonpendulous designs in two major respects. The first is that finite stiffness causes an inherent rotation of the IA as a function of input acceleration, giving rise to cross-coupling and vibropendulous rectification (see C.3). The second is that angular motion (as, for example, in strapdown systems) gives rise to torques about the OA that are modelable but rarely negligible. Fortunately, cross-coupling may be made very small by proper design, and modeling of rotational effect often requires little more than an astute choice of coordinate axes.

C.2 Applications

In principle, any accelerometer application could be satisfied by a pendulous design. In practice, pendulous accelerometers have tended to be used mostly for medium- to high-accuracy (10 mg to 10 μg), medium bandwidth [dc to 1 kHz] applications, most often in the form of torque-balance servo accelerometers. In strapdown applications, with computer modeling, they are beginning to encroach on the very high accuracy domain of much more complex and expensive accelerometers, such as PIGAs and SFIRs. For bandwidths much greater than 1 kHz, the mechanism becomes so stiff that distinctions between pendulous and nonpendulous designs become blurred, but nonpendulous designs may have a slight edge because of somewhat simpler dynamics.

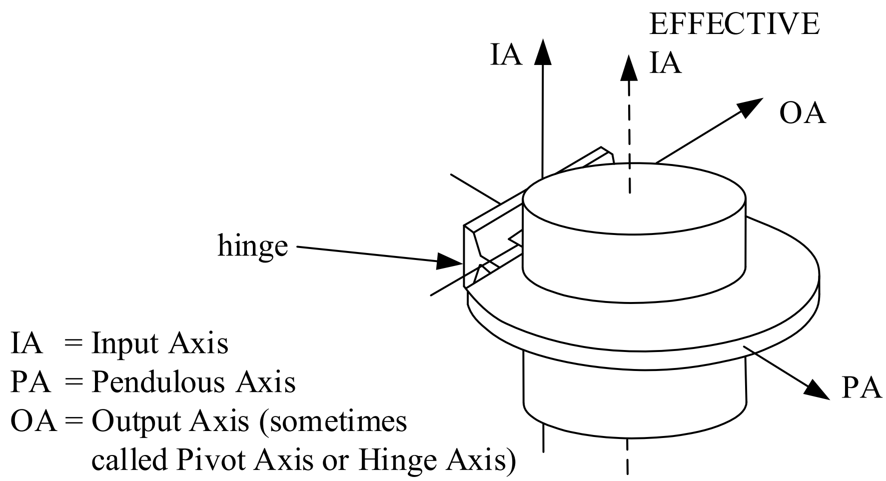

Figure C.1—Axes of an accelerometer pendulum

C.3 Error sources

Error sources that are specific to pendulous accelerometers may be divided into the categories of translational acceleration effects and rotational acceleration effects. Both require a more detailed understanding of the coordinate system shown in Figure C.1. The positive sense of the IA is the direction of applied specific force, which produces a positive output (gravity is positive upward). The positive sense of the PA is defined by that normal to the OA that passes through the center of mass of the pendulum. By definition, PA is also normal to IA. The positive sense of the OA is then defined by the vector cross product already defined.

C.3.1 Cross-coupling

When the sensor is subjected to a specific force along the positive IA, the most common reaction is for the pendulum to lag slightly so that it rotates through a small angle θ as shown in Figure C.2, a right-hand rule positive rotation. If a_i, a_p, and a_o are acceleration components along the unrotated axes of the accelerometer, the indicated accelerometer response may be written as

$$\begin{aligned} A_{\mathrm{ind}} &= a_\mathrm{i} \cos\theta + a_\mathrm{P} \sin\theta \\ &\approx a_\mathrm{i} + a_\mathrm{P}\theta \end{aligned} \tag{C.3}$$

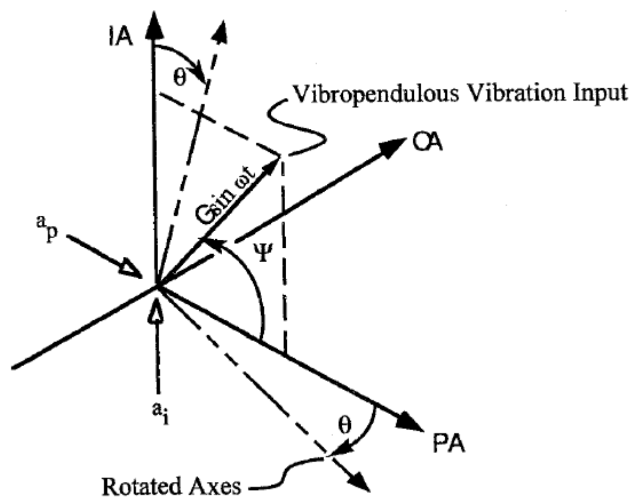

Figure C.2—Cross-coupling effects

The approximation is valid for the usual case where θ is a small angle. If θ is proportional to a_i, then this relationship may be written as

$$\begin{aligned} A_{ind} &= a_i + a_p\theta \\ &= a_i + a_p(K_{ip}a_i) \\ &= a_i + K_{ip}a_i a_p \end{aligned} \tag{C.4}$$

The coefficient K_{ip} is called the cross-coupling coefficient, and it is normally reported in units of μrad/g or μg/g^2.

Some data sheets report a quantity described as “cross-axis sensitivity, referred to the true sensitive axis.” The units are given as μg/g or mg/g. This quantity refers to the value of θ in microradians or milliradians when a_i has its maximum (full scale) value. It is related to K_{ip} by the equation

$$K_{ip} = \frac{\text{"Cross-axis sensitivity"}}{\text{full scale } g} \tag{C.5}$$

An important consequence of the cross-coupling effect arises when the input accelerations a_i and a_p are vibratory as, for example, in the case of sinusoidal vibration of amplitude G along an inclined axis

$$\begin{aligned} a_i &= G\sin\omega t\ \sin\psi, \qquad a_p = G\sin\omega t\ \cos\psi, \\ A_{ind} &= a_i + K_{ip}a_i a_p \\ &= G\ \sin\omega t\ \sin\psi + K_{ip}\ G^2\ \sin^2\omega t\ \sin\psi\ \cos\psi \end{aligned} \tag{C.6}$$

Since the long-term average of sin ωt is 0, but that of $\sin^2$ ωt is 1/2,

$$E[A_{ind}] = \frac{1}{2}G^2\ \sin\psi\ \cos\psi\ \cdot\ K_{ip} \tag{C.7}$$

The accelerometer appears to have a bias proportional to G^2, with a maximum value at $\psi = 45°$, 135°, and so on. This effect is known as "vibropendulous rectification." In this sinusoidal test, it may not be sufficient to consider K_{ip} as a constant scalar. If K_{ip} varies in amplitude and phase, then

$$E[A_{\text{ind}}] = \frac{1}{2} G^2 \ \sin\psi \ \cos\psi \ \cdot \ |K_{\text{ip}}| \cos\phi_{\text{ip}} \tag{C.8}$$

Vibropendulous rectification, therefore, may vary dramatically with frequency, particularly if the range of interest includes the sensor natural frequency, defined by $\phi_{ip} = 90°$ or $\cos\phi_{ip} = 0$. One consequence of this variation is that the magnitude of vibropendulous rectification is always less for band-limited random vibration than its maximum magnitude for sinusoidal vibration having the same root-mean-square (rms) amplitude over the same frequency range.

The coefficient for vibropendulous rectification is given by

$$K_v = |K_{\text{ip}}| \ \cos\phi_{\text{ip}}$$

or

$$E[A_{\text{ind}}] = K_v (G_{\text{rms}})^2 \sin\psi \cos\psi \tag{C.9}$$

where G_{rms} is the rms vibration level ($G/\sqrt{2}$ for sine vibration). This coefficient usually must be established by test, but the determination may be difficult (see C.6).

For broadband random inputs over a range of frequencies from f_L to f_H with frequency-dependent spectral density $S^2(f)$ in g^2/Hz,

$$E[A_{\text{ind}}] = \int_{f_L}^{f_H} S^2(f)\, K_v(f) df \tag{C.10}$$

C.3.2 Effective centers of mass

Pendulous accelerometers also have slightly anomalous responses to angular motions, such as those commonly encountered in strapdown systems. The effects can be analytically derived from the classic physics of rotating systems in the case of dry sensors. In fluid-filled sensors, the same approach can be used for steady-state rotations, but coefficients related to accelerated motion (e.g., angular acceleration, precession, or nutation) must be determined by test.

The coordinate system used to describe these effects is shown in Figure C.3. As before, the coordinate axes are IA, PA, and OA, but now coordinate magnitudes are indicated by the quantities *x, y,* and *z*

- $\vec{\omega}$ is a vector with components ω_I, ω_P, and ω_O, which passes through the point *a*, *b*, *c*
- $\vec{r}$ is a vector from 0, 0, 0 to the mass element *dm* at *x*, *y*, *z*
- $\vec{q}$ is a vector from *a*, *b*, *c* to the mass element *dm* at *x*, *y*, *z*
- $\vec{q}$ has components *x-a*, *y-b*, and *z-c*

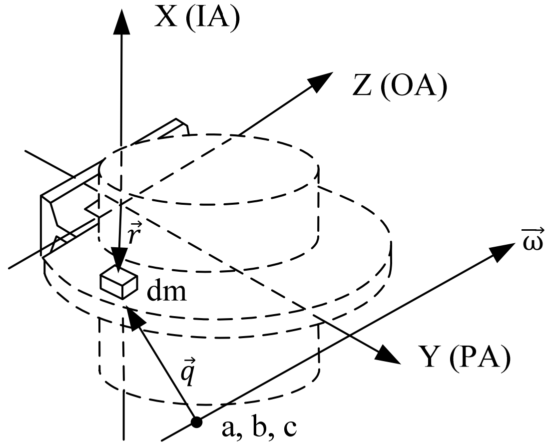

Figure C.3—Geometry for angular motion response

Forces and torques are summed by taking integrals over the volume of the moving system. In particular, since PA is an axis of no response to translational acceleration, by definition

$$\int \times \; dm = 0 \tag{C.11}$$

The element of force exerted on each mass element *dm* as a result of rotation is given by the vector equation

$$d\vec{F} = \left[\vec{\omega} \times (\vec{\omega} \times \vec{q}) + \left(\dot{\vec{\omega}} \times \vec{q}\right)\right] dm \tag{C.12}$$

The element of moment about the point 0, 0, 0 is given by

$$d\vec{L} = \vec{r} \times d\vec{F} \tag{C.13}$$

The restoring torque supplied by the accelerometer's servo system or spring restraint is the OA component of *L*. Equivalent acceleration is then given by

$$A_{\text{ind}} = \frac{L_{\text{OA}}}{M\ell} = \frac{\left[\int d\vec{L}\right]_{\text{OA}}}{\int y dm} \tag{C.14}$$

Carrying out the indicated operations results in

$$\begin{aligned} A_{\text{ind}} = & -\left(b - \frac{J_{\text{i}} - J_{\text{p}}}{M\ell}\right)\omega_{\text{i}}\omega_{\text{p}} - \left(c - \frac{J_{\text{po}}}{M\ell}\right)\omega_{\text{i}}\omega_{\text{o}} \\ & + a\left(\omega_{\text{p}}^2 + \omega_{\text{o}}^2\right) - \frac{J_{\text{io}}}{M\ell}\omega_{\text{p}}\omega_{\text{o}} + \frac{J_{\text{pi}}}{M\ell}\left(\omega_{\text{i}}^2 - \omega_{\text{p}}^2\right) \\ & + \left(b - \frac{J_{\text{o}}}{M\ell}\right)\dot{\omega}_{\text{o}} - \left(c - \frac{J_{\text{po}}}{M\ell}\right)\dot{\omega}_{\text{p}} + \frac{J_{\text{io}}}{M\ell}\dot{\omega}_{\text{i}} \end{aligned} \tag{C.15}$$

where

$M\ell$	is the mass imbalance $= \int y dm,$
J_i	is the mass moment of inertia about the IA $= \int (y^2 + z^2) dm$
J_p	is the mass moment of inertia about the PA $= \int (x^2 + z^2) dm$
J_o	is the mass moment of inertia about the OA $= \int (x^2 + y^2) dm$
$J_{io}, J_{po},$ and J_{pi}	are the cross products of inertia; for example, $J_{io} = \int \times\ z\, dm$; they are measures of symmetry

The significance of this equation is best appreciated by considering an idealized pendulous sensor having symmetry so that cross products of inertia are negligibly small, and pendulum thickness small enough that $\int x^2 dm$ may be neglected compared with $\int y^2 dm.$ Then $J_i - J_p \cong J_o$, and the equation reduces to

$$A_{\text{ind}} = -\left(b - \frac{J_i - J_p}{M\ell}\right)\omega_i\omega_p - c\omega_i\omega_o + a\left(\omega_p^2 + \omega_o^2\right) + \left(b - \frac{J_o}{M\ell}\right)\dot{\omega}_o - c\dot{\omega}_p \tag{C.16}$$

It can easily be shown that the real acceleration A_{real} at the origin, when $\overrightarrow{\omega}$ passes through a point u, v, w, has as its u component

$$A_{\text{real}} = -v\omega_i\omega_p - w\omega_i\omega_o + u\left(\omega_p^2 + \omega_o^2\right) + v\dot{\omega}_o - w\dot{\omega}_p \tag{C.17}$$

Comparing the last two equations, it can be seen that they are identical if $u = a$, $w = c$, and $v = b - \frac{J_i - J_p}{M\ell}$. Physically, that corresponds to measuring the true acceleration at a point in space that is on the PA ($u = a$, $w = c$) but translated along the positive PA the distance $\frac{J_i - J_p}{M\ell}$. With respect to this effective center, a thin symmetrical accelerometer behaves as an ideal point accelerometer. Angular testing will not reveal that it is pendulous.

Going back to real accelerometers again, but assuming the center of coordinates to be at $x = 0$, $y = \frac{J_i - J_p}{M\ell}$, $z = \frac{J_{po}}{M\ell}$, the error terms resulting from the pendulous character of the accelerometer will be

$$A_{\text{ind}} - A_{\text{real}} = \frac{-J_{io}}{M\ell}\omega_p\omega_0 + \frac{J_{pi}}{M\ell}\left(\omega_i^2 - \omega_p^2\right) + \frac{\left(J_i - J_p\right) - J_o}{M\ell}\dot{\omega}_o + \frac{J_{io}}{M\ell}\dot{\omega}_i \tag{C.18}$$

The point chosen, $x = 0$, $y = \frac{J_i - J_p}{M\ell}$, $z = \frac{J_{po}}{M\ell}$ is known as the "effective center of mass for spin," ECM_ω, or sometimes just ECM. The error terms relative to this point are all due to typically small cross products of inertia, except for the third one. The third one arises from the separation of ECM_ω from the effective center of mass for angular acceleration, or center of percussion, ECM_α. These ECMs differ only in the y coordinate (PA), and the difference typically is small, vanishing in the case of a thin pendulum, as already noted.

In low- to medium-accuracy applications, the effect of ECM separation may be neglected. The separation typically is of the order of 0.3 cm (although it can be 2 cm to 3 cm) and, thus, contributes less than 3 mg when $\dot{\omega}_o = 10$ rad/s^2. In addition, it is a transient error whose time integral is limited by the maximum spin rate of the vehicle.

The same transient behavior is also attributable to the last term, and in addition, it is typically even smaller than the ECM offset. The only cross product of inertia that is easily and routinely measured in pendulous accelerometers is J_{pi}. A typical magnitude for $\frac{J_{pi}}{M\ell}$ is 0.5 to 1 μg/(rad/s)^2, which is equivalent to a radius of 0.001 cm. If $\frac{J_{io}}{M\ell}$ were no greater than 0.003 cm, 10 rad/s^2 would contribute less than 30 μg.

The cross product J_{io} also controls the magnitude of the first term, which corresponds approximately to an ECM position error for spin orthogonal to the IA. Since 0.003 cm is normally much smaller than the uncertainty in as-installed ECM location, this term also is rarely, if ever, modeled.

The remaining term, driven by J_{pi} responds to spin axes parallel to the IA. Spin axes parallel to the IA ideally produces no response. It is, therefore, easily measured as well as being an occasionally significant error source. As noted, typical errors from this source are in the range of 0.5 to 1 μ*g*/(rad/s)^2, and specification limits of 20 μ*g*/(rev/s)^2 (0.51 μ*g*/(rad/s)^2) have been met successfully by either mechanical trim or sensor screening.

C.3.3 Anisoinertia

In high-accuracy applications, and especially strapdown navigation, it has become standard practice to model the difference between ECM_α and ECM_ω. This modeling is done as part of the "size effect" subroutine that corrects all accelerometers in the system to a common reference point. There is a choice in such modeling: One may either take ECM_ω as the accelerometer location and use $\dot{\omega}_o$ to correct or one may take ECM_α as the location and use $\omega_I\omega_P$ for correction. Since ω's are available among normally processed signals of a strapdown navigator, whereas $\dot{\omega}$'s are not, the latter choice is generally made.

In Equation (C.15), if cross-product terms are neglected, $= \frac{J_o}{M\ell}$, $a = c = 0$

$$A_{\text{ind}} - A_{\text{real}} = -\left(\frac{J_o}{M\ell} - \frac{J_i - J_p}{M\ell}\right)\omega_i\omega_p$$
$$= -K_{ai}\,\omega_i\omega_p \qquad \text{(C.19)}$$

The coefficient K_{ai}, which represents the separation between the two ECMs, is called the "anisoinertia coefficient." Its units may be either length or μ*g*/(rad/s)^2. The magnitude of this correction is maximum for a given total spin magnitude ω when $\omega_i = \omega_p = 0.707\omega$.

A typical value for K_{ai} is 70 to 100 μ*g*/(rad/s)^2 in dry sensors. In a nonspun environment, such as an aircraft navigator, ω_i and ω_p are typically 0.1 rad/s, so that $\omega_i\omega_p = 0.01$ (rad/s)^2 and the resulting correction will be of the order of 1 μ*g*. In spin-stabilized missiles, the correction may be larger, and the system designer may wish to consider putting the axis of maximum sensitivity some place other than directly along the spin axis.

C.4 Trade-offs

The most significant trade-off specifically related to pendulous sensors is the trade-off between bandwidth and cross-coupling effects. Accelerometers are frequently called on to measure small values of acceleration at low frequencies in the presence of much larger high-frequency inputs. The simplest way to improve a signal-to-noise ratio in such cases is to limit the sensor's bandwidth so that the sensor itself functions as a mechanical filter. In servo torque-balance sensors, this approach has the added advantage of reducing the required full-scale servo capability. Unfortunately, limited bandwidths equate to large inertial element deflections, at least in the midband of frequencies between f_n and ~0.1 f_n, and in pendulous sensors that, in turn, equates to large cross-coupling errors. This trade-off often limits the applicability of such simplistic filtering.

A variety of trade-offs exist between accuracy and environmental tolerance, especially shock and vibration, which take on added significance with pendulous sensors. Commonly, a choice must be made between suspension ruggedness and suspension bias errors. In pendulous designs, fluid filling provides an added variable to optimize the ratio of suspension reaction forces to operating torques by distributed flotation effects. These same effects may also be used to compensate in part for the temperature coefficient of scale factor (by making use of the fluid density change). These advantages may be offset in some applications, however, by an increased sensitivity of scale factor to temperature gradients along the pendulum as, for example, during thermal transients. Fluid-filled sensors also tend to have larger separations between ECM_ω and ECM_α than do dry sensors.

C.5 Environmental effects

Pendulous accelerometers respond to environments in a similar fashion to nonpendulous sensors, except in the following few areas:

a) Vibropendulous rectification must be considered in vibration environments.
b) There is some scale-factor sensitivity to thermal gradients or transients in fluid-filled sensors.
c) Modelable error terms related to spin or angular acceleration may be significant in some strapdown applications.

C.6 Testing

Static cross-coupling is most easily determined by a precision 1-*g* tumble test or at high acceleration by a centrifuge test. Current torque tests, in which servo sensors are subjected to simulated values of a_i with ±1 *g* along the cross axis, are simple and extremely sensitive, but they may not give accurate results in sensors that have significant suspension compliances.

Dynamic cross-coupling is best evaluated by observing vibropendulous rectification when the sensor is vibrated along an axis at 45° to both the IA and the PA. This test is difficult to perform and interpret correctly, however. The electromechanical shakers commonly employed nearly always have a significant amount of rotational motion coupled to their basic translational motion, and this coupling may be quite strong at certain characteristic frequencies.

This rotation produces an apparent cross-coupling effect, which is indistinguishable from true sensor error in any single test. A common ploy is to repeat the test along the other vibropendulous axis by rotating the sensor 180° about IA. The rotation ideally has no effect on the shaker contribution or on any contribution due to a_i^2 or a_p^2, but it reverses the sign of the vibropendulous error so that it may be separated by taking the difference between the two responses. The test requires careful fixture design to ensure that the rotation does not alter the mechanical impedance of the fixture, plus sensor, sufficiently to alter the shaker motions.

Measurement of the location of ECM_ω requires a spin table with an *x*–*y* micrometer stage mounted for adjustment orthogonal to the spin axis and provision for shimming the sensor to change its IA a few milliradians either way from alignment nominally parallel to the spin axis. The component of spin offset, which is due to eccentricity of ECM_ω, will be proportional to the shimmed angle and to the eccentricity, thus, allowing it to be separated from the J_{pi} response, which does not vary significantly with either position or small changes in alignment. The point at which spin offset becomes independent of alignment is the location of ECM_ω, and the residual spin offset at that location determines the magnitude of $\frac{J_{pi}}{M\ell}$.

Measurement of the location of ECM_ω requires a similar table that can be oscillated. In this test, the sensor is mounted with IA normal to the table axis and then translated along the micrometer stage axis that is orthogonal to the IA until the $\dot{\omega}$ signal from the test sensor disappears. In this test, responses due to $\dot{\omega}$ may be separated from those due to ω^2 by noting that the $\dot{\omega}$ signals are at table frequency, while those due to $\dot{\omega}^2$ are at twice table frequency.

C.7 Special requirements in the specification

The following quantities may be controlled in a specification for a pendulous accelerometer (beyond those pertinent to accelerometers in general):

— Maximum magnitude of cross-coupling coefficient, K_{ip}
— Maximum magnitude of vibropendulous rectification under some specified vibration condition
— Location of ECM or ECM_ω
— Location of ECM_α or center of percussion
— Separation of ECM_α and ECM_ω (anisoinertia coefficient)
— Maximum value of spin offset [$\frac{J_{pi}}{M\ell}$ in Equation (C.18)]

— Other terms in Equation (C.18) (rare)
— Orientation of PA and OA

C.8 Advantages and disadvantages

Pendulous accelerometers enjoy a leverage advantage on suspension-induced errors by comparison with nonpendulous designs. Operating torques can be increased arbitrarily with little or no change in error torques by simply placing the proof mass at a larger radius. This leverage allows them to offer generally superior mechanical stability, for example, better long-term alignment stability, more stable bias, and lower bias temperature coefficients. Because they are less critical to build, they usually offer a better performance-to-cost ratio than do nonpendulous designs.

Their disadvantages may be more properly termed "idiosyncrasies" since their error contributions can be made to be a minor part of most error budgets through careful design and simple modeling. These idiosyncrasies include spin effects and cross-coupling and its dynamic symptom vibropendulous rectification. Spin effects are significant in strapdown applications, but they are modelable, and the modeling frequently requires no more than proper specification of an ECM location (either spin or angular acceleration). In especially critical applications involving rotating or precessing spun vehicles, it may be necessary to define two ECMs and specify an upper limit for one cross product of inertia. The second ECM, or its equivalent in terms of anisoinertia, permits a small correction for angular rate product $\omega_i\omega_p$; and the symmetry requirement limits a spin offset, which may be significant in sensors mounted with IA parallel to the spin axis.

Annex D

(informative)

Overview of the characterization and use of the VBA

D.1 Introduction

Most accelerometers in use today are fundamentally analog devices. They feature an electrical output signal, which is a voltage or current proportional to the input acceleration. For many applications, however, and especially for most inertial navigation applications, it is desirable to be able to express the output in terms of digital words, preferably without the complexity and added error sources of a separate analog-to-digital converter. An increasingly popular way to do that is through the development of accelerometers whose direct output is a frequency related to acceleration. The vibrating beam accelerometer (VBA) is such an approach.

D.2 Historical background

D.2.1 Early frequency output devices

The pendulum was invented as a means of measuring time in the 16th century. It came to be recognized also as a means to measure gravity since its frequency of oscillation is proportional to the square root of gravitational acceleration. By the early 1800s, frequency stability on the order of 10 parts per million had been achieved, corresponding to an uncertainty of 20 μ*g*.

D.2.2 Vibrating string accelerometer

As a frequency output device, the pendulum measures only the magnitude of acceleration. It is easily upset by dynamic inputs because of its geometry and nonlinear response. In 1928, H. C. Hays invented a device that had the potential to correct both of those problems: the vibrating string accelerometer. The vibrating string accelerometer was based on the principle of the guitar string: Its frequency of vibration is proportional to the square root of the applied tension (see Slater [B51]).

A schematic representation can be seen in Figure D.1. A proof mass is supported by a metallic ribbon that is kept continuously in vibration by immersing it in a transverse magnetic field and passing an alternating current through it. In the simplest form, a biasing spring determines the ribbon's natural frequency in the absence of acceleration. The biasing spring and mechanical cross supports that restrict the proof mass to a single DOF allow this device to sense a single component of acceleration in the presence of complex base motion. When acceleration causes the tension to increase, the frequency goes up, and similarly with a decrease in tension, the frequency goes down. In this form, the principal error sources of the vibrating string accelerometer are variations in the force provided by the tension spring, as a function of time and temperature, and rectification errors due to the nonlinear output. The indicated acceleration is proportional to the square of the vibration frequency.

Both of these problems were addressed by an elegant design variant developed at Bosch-Arma. Instead of being connected to the frame at one end, the pretension spring was connected between two nearly mirror-image, proof-mass/ribbon assemblies. Frequency lock-in of the two ribbons was avoided by vibrating the ribbons in orthogonal planes and by designing the attachment points on each proof mass to be centers of percussion for each other (see Slater [B51]).

With two ribbons, one increasing in frequency when the other decreases, the indicated acceleration is proportional to the difference in the squares of the two frequencies: $A_{\text{ind}} = K(f_1^2 - f_2^2) = K(f_1 + f_2)$ $(f_1 - f_2)$. When the spring is made very soft and the frequency variation is small, the sum of the frequencies remains nearly constant. The Bosch-Arma accelerometer made the bias substantially constant and simultaneously made the indicated acceleration proportional to the difference of the two frequencies.

Since the time integral of frequency is phase and the time integral of acceleration is change of velocity, it was only necessary to read the difference of the outputs of two counters, or the output of a single up/down counter, to obtain a good estimate of delta velocity. The integration is essentially free.

In a laboratory environment, this form of the vibrating string accelerometer was able to track the tidal variations in earth's gravity to within 10 n*g*. In a missile environment, residual nonlinear effects were larger than that, but they were small enough for it to serve as the velocity control of the Atlas missile.

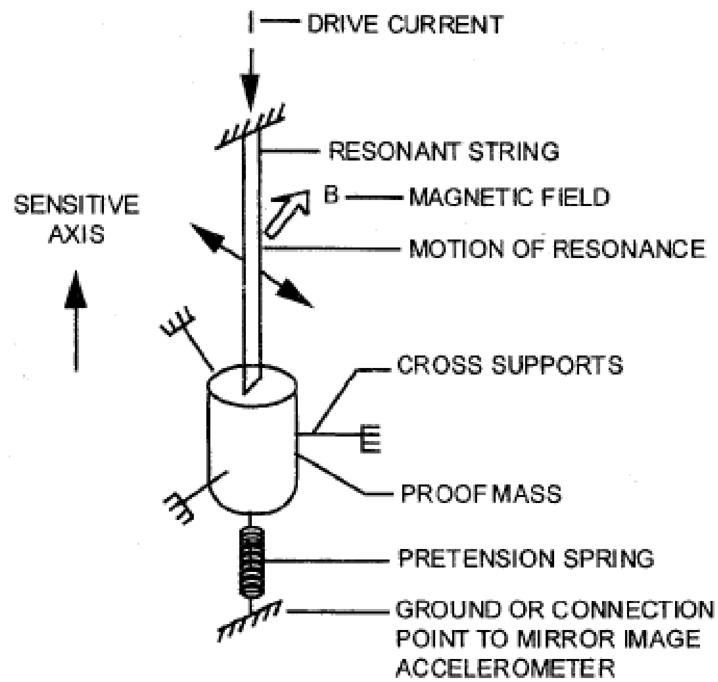

Figure D.1—Schematic view of vibrating string accelerometer (see Norling [B38])

D.3 VBA—Theory of operation

D.3.1 Quartz resonator

The vibrating string accelerometer was an elegant device, and the differential output was well suited to the limited data-processing capabilities of the day. However, the large spring preload produced microcreep in the ribbon attachments, which resulted in a continuous drift in bias. The thrust of present research has shifted to the VBA.

The VBA is based on the technology of crystal-controlled oscillators, which was developed in the 1920s primarily with crystalline quartz. The piezoelectric properties and excellent mechanical stability of quartz made it a natural material for high-performance resonators. Piezoelectricity is a reciprocal property that permits the crystal to function both as a motor and as a generator so that oscillation can be achieved simply by using it to close a loop around an amplifier having suitable gain and phase response.

The excellent mechanical properties of quartz include great stability and low losses due to mechanical hysteresis. The result is an oscillator with a stable output under fixed load conditions and with a high-quality factor Q. High Q means that the phase response of the resonator changes rapidly with changes in frequency near resonance, so that its oscillation frequency is nearly insensitive to changes in the characteristics of the feedback electronics. In a frequency output accelerometer, a key feature of quartz is that it is stiff, comparable to aluminum, so that as a force sensor, it can accommodate compression as well as tension. It needs no pretensioning spring, and it has the potential to be simple in design.

Development has not been that obvious, however. The quartz oscillators that were developed as frequency standards were designed specifically for shapes and modes of operation that are insensitive to extraneous stresses. A useful VBA requires a crystal oscillator element that is not only stable when unstressed, but also sensitive to a particular component of stress, which can be made proportional to acceleration by the sensor designer.

D.3.2 Single tine resonator

An optimal or near-optimal combination of stability and the desired sensitivity is offered by a transversely vibrating beam, hence, the name, VBA. An example is shown schematically in Figure D.2. The natural frequency of such a beam is determined partly by the elastic properties of the quartz and partly by the guitar-string tension (or compression) effect. When the vibrating beam is loaded in tension, for example, the curvature of the deflected beam turns part of the axial force into a transverse restoring force, which adds to the elastic restoring force and, therefore, raises the resonant frequency. The following equations show to a good approximation how these forces combine to cause the shift:

$$f_0 = \frac{1}{2\pi}\sqrt{\frac{K}{m}} \qquad f_n = \frac{1}{2\pi}\sqrt{\frac{K+\alpha Ma}{m}} = f_0\sqrt{1+\frac{\alpha Ma}{K}} = f_0\sqrt{1+\frac{Ma}{C}} \tag{D.1}$$

where

K	is the beam stiffness
m	is the beam equivalent mass
α	is a constant,
M	is the suspended mass
f_0	is the zero load frequency
f_n	is the beam natural frequency
a	is the input acceleration
C	is the Euler buckling load

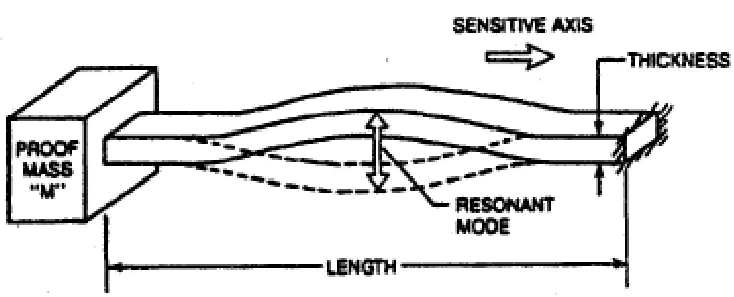

Figure D.2—Schematic drawing of VBA (see Norling [B38])

Compression corresponds to negative *Ma,* so the frequency goes down. When *Ma* equals the constant C, the frequency is zero, and any further force will cause the beam to become unstable and collapse.

Clearly C, the factor that determines the scaling of the accelerometer, is the classic Euler buckling load of the beam.

The usual design of a VBA limits the input force to a fraction of C so that buckling never really occurs. The magnitude of the fraction is a trade-off between sensitivity and nonlinearity, among other things. The optimal fraction for most applications is about ±20% of C, which causes the frequency to deviate approximately ±10% from the zero load natural frequency f_0. This scaling gives ~5% nonlinearity, primarily second order, at full scale. For loads much greater than the designed full scale, the proof mass is typically mechanically caged to limit the stress due to a shock overload.

The stiffness of the quartz element in such a VBA is usually sufficient to produce mechanical resonance of the resonator/proof-mass combination on the order of a few kilohertz. In particular, its stiffness can easily be made many times greater than that of the suspension elements that provide constraint of other DOF. The accelerometer is, in fact, an open-loop sensor but one in which the force sensor that provides the principal constraint is comparable in stiffness and accuracy to the electromagnet that is used to close the loop in inertial-quality servoed accelerometers.

Two features are missing from the schematic drawing of Figure D.2. One is the suspension needed to restrain the proof mass to a single DOF; the other is a means to prevent energy from the transverse vibration from coupling into the base and proof mass of the accelerometer. Bending or shear energy, which can leave the beam and be dissipated in the structure, reduces the *Q* of the resonator and reduces accuracy. It can also cause frequency shifts by coupling energy into nearby resonant modes.

The need to contain the resonant energy in a VBA has led to two distinct paths of development of the VBA: single tine and dual tine. Those who favor the single tine approach appreciate the simplicity of a single vibrating element but accept the need for an effective vibration isolator to contain the energy. In high-performance accelerometers, the design of effective isolators can lead to a different kind of complexity, as illustrated in Figure D.3.

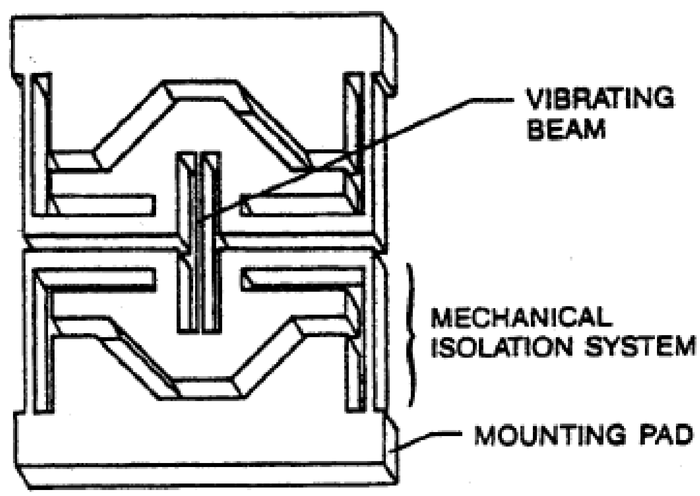

Figure D.3—Single vibrating beam with isolators (see Norling [B38])

D.3.3 Dual tines—Double-ended tuning fork (DETF)

The alternative approach is to cancel, rather than isolate, the vibration energy trying to leave the resonator. This cancelation is done by providing two adjacent tines, which are connected at the ends, and driven 180° out of phase. The result is like a doctor's tuning fork, except that it has a handle at each end to permit application of the axial forces being measured. An example is shown in Figure D.4. The theory is that, if the two tines are balanced, both the bending stresses and the shear stresses combine in the end regions and cancel each other out within a few tine widths. The end mounting pad, being a mode of the vibration of the two tines, eliminates the need for vibration isolators but substitutes a need to match the paired tines in mass and stiffness. Advocates of single tines believe that the matching requirements for high *Q* crystals are impossibly tight. Those who favor the DETF point to models that show small mismatches lead only to a small shift in mode shape, not two separate modes, and to photolithographic etching techniques that have a strong tendency toward balanced parts.

The argument is by no means settled at this time, but actual lab and production data tend to support the viability of the DETF approach. That makes possible the use of small elements to produce small accelerometers. The DETF shown in Figure D.4 is similar in size and in production techniques to the single-ended tuning fork used in digital watches: less than 0.6 cm long and etched from a quartz wafer only 0.01 cm thick.

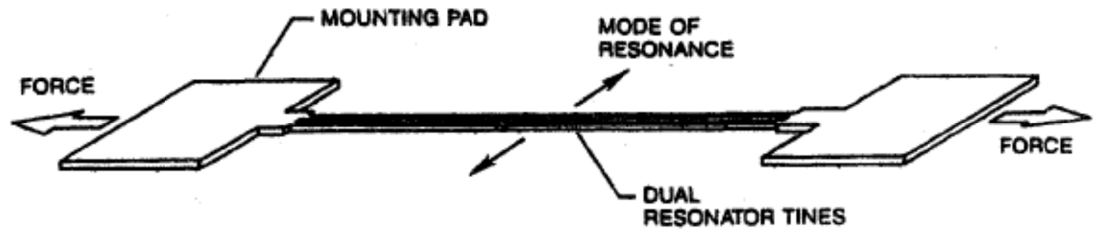

Figure D.4—DETF (see Norling [B38])

D.3.4 Push–pull mechanization

In principle, a single proof mass and a single resonator, either single or double tine, is sufficient to produce a working accelerometer. In practice, such an accelerometer is medium precision at best because of a list of error sources that tend to be somewhat larger than the corresponding terms in servo accelerometers, for example, temperature effects, aging effects, and rectification effects from the inherent nonlinearity. Frequently, the largest single error in a single-resonator-per-axis accelerometer is the inaccuracy of the system clock. Fortunately, many of these error sources turn out to be quite similar in accelerometers of a given design or fabricated in a given lot. By using two resonators, arranged so that acceleration causes one to increase in frequency when the other decreases, these common mode errors can be made to cancel in the difference frequency. Clock errors, in particular, can be made comparable to those in other types of accelerometers, allowing the use of a simple and inexpensive system clock.

The push–pull arrangement is shown schematically in Figure D.5. This mechanization has become the standard form of the VBA: a single accelerometer case containing two resonators and producing two output frequencies, which are processed in a single algorithm to produce a signal representing instantaneous acceleration or velocity change. In high-precision systems, a second resonator is accepted as the cost of the performance. In low-precision systems, the cost of the extra channels of information is generally offset by being able to use a cheaper clock.

In some applications, there may be three frequency outputs, with the third being a measure of sensor internal temperature, for modeling.

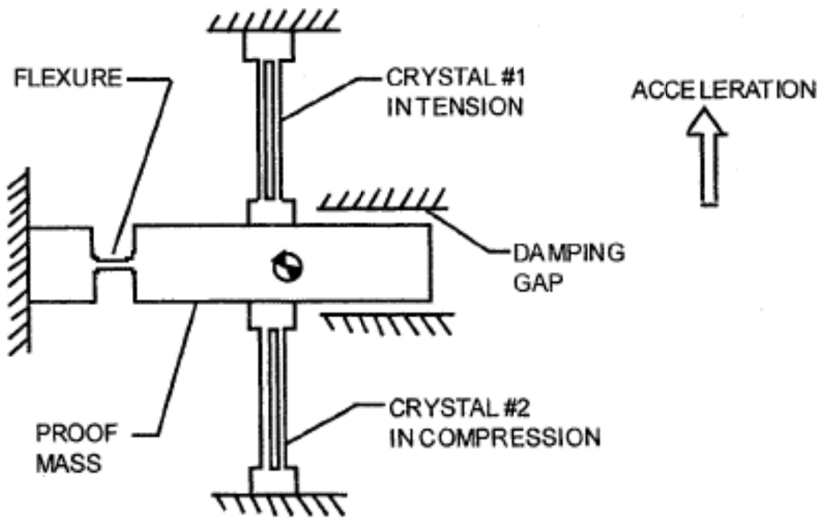

Figure D.5—Schematic drawing of push–pull mode (see Norling [B38])

D.3.5 Gas damping

For some applications, damping can be required on a VBA proof mass. Proof-mass damping is usually accomplished by introducing a gas into the VBA enclosure. A trade-off exists between the pressure and type of gas employed to obtain adequate squeeze film proof-mass damping while minimizing the resulting diminution of the resonator *Q*.

D.4 VBA signal processing

D.4.1 Frequency counting

Each output of a VBA is a frequency that exhibits a change approximately proportional to acceleration. There is a certain amount of nonlinearity, whose magnitude depends on the fractional shift, ηf_0, which occurs at full-scale input. For 10% maximum frequency deviation, for example, $\eta = 0.1$.

Several useful observations can be made by examining first the ideal linear case. For each output frequency f under acceleration a, the indicated acceleration A_{ind} is derived to be

$$f = f_0 + K_1 a\,; \qquad A_{ind} = \frac{f - f_0}{K_1} \tag{D.2}$$

The obvious way to measure f is simply to count cycles over a sample period t_s, or for contiguous samples, at a frequency $f_s = 1/t_s$, with an uncertainty of up to 1 count in each sample. This simple scheme requires two counters: one to count f and one to count the number of clock cycles that defines t_s. The quantization error due to such a scheme is the change ΔA_{ind} in indicated acceleration for a one-count change

$$f_{\mathrm{ind}} = \frac{f_0 t_{\mathrm{s}} \pm 0.5}{t_{\mathrm{s}}} = f_0 \pm 0.5 f_{\mathrm{s}}$$

$$\Delta f_{\mathrm{ind}} = f_{\mathrm{s}}$$

$$\Delta A_{\mathrm{ind}} = \frac{f_{\mathrm{s}}}{K_1} = \frac{f_{\mathrm{s}}}{\eta f_0} * \text{ fullscale} \tag{D.3}$$

As an example, suppose f_0 = 40 kHz (a typical figure), f_s = 200 samples per second, full scale = 100 *g*, and η = 0.1. Then ΔA_{ind} = 5 *g*. This gross resolution can be improved by averaging readings over time, but many samples are needed. If contiguous samples are taken with no lost counts, the resolution improves as $1/n$, where *n* is the number of samples averaged, and it would take 5000 samples, or 25 s, to achieve 0.001-*g* resolution. If there is dead time in the sampling process, as there can be between the outputs of a commercial frequency counter, then the correlation of the samples is reduced, as is the rate of improvement. For completely uncorrelated samples, the improvement is only $1/\sqrt{n}$, which is clearly much worse. Even for the more favorable case of triangular filtering, for which the improvement is $1/n^{3/2}$, it takes 3 s to achieve 0.001-*g* resolution (see I.3).

D.4.2 Period

For this reason, VBA outputs are generally counted by some process equivalent to period measurement, that is, by counting the number of clock cycles from one rising zero crossing of *f* to another. The resolution improves dramatically. In the equation for ΔA_{ind}, the crystal frequency f_0 is replaced by the clock frequency f_c. In the example just seen, if f_c = 50 MHz, the quantization error drops from 5 *g* to 0.004 *g*, and with no lost counts, it takes only 20 ms to average to 0.001 *g*.

Period measurements that run exactly from one zero crossing to the next are synchronous with the output frequency *f* but asynchronous with the system computer data frames. In static testing, such nonequal time sampling does not matter, and laboratory tests are often conducted exactly that way. This count also requires two counters or a commercial laboratory counter that performs the equivalent function.

For dynamic measurements, with actual systems, asynchronism adds noise to the signal. Systems generally are synchronized to the actual frame edges by using the high-frequency clock to interpolate from the nearest zero crossings to the actual frame edges. This count requires a third counter. When done correctly, with no lost counts, the scheme will not accumulate errors from the interpolation process, as each such estimation is added to the present frame and then subtracted from the following one.

D.4.3 Phase processing

If $$f = f_0 + K_1 g$$

Then $$\int_t^{t+\Delta t} f\,dt = f_0 \Delta t + K_1 \int_t^{t+\Delta t} g\,dt$$

$$= f_0 \Delta t + K_1 \Delta V$$

Thus $$\Delta V = \frac{1}{K_1}\left[\int_t^{t+\Delta t} f\,dt - f_0 \Delta t\right]$$

$$= \frac{1}{K_1}\left[\Phi(t+\Delta t) - \Phi(t) - f_0 \Delta t\right] \tag{D.4}$$

If *f* is in Hz, and K_1 in Hz/*g*, Φ will be in cycles, and Δ*V* in *g*·s. If *f* is in rad/s, and K_1 in rad/s/*g*, Δ*V* will be the same, but Φ will be in rad. Either way, Δ*V* can be converted to m/s, or whatever is required, by multiplying by either the value of standard or local gravity.

As in the case of frequency/acceleration processing, phase/velocity can be counted simply by counting cycles, but the results show either poor quantization error or serious asynchronism, depending on point of view. Once again, the answer is to use the system clock and a third higher rate counter to interpolate fractional cycles of phase with no lost counts.

This phase processing technique can also be done with a hardware device called a phase-locked loop (PLL), where the higher frequency phase interpolation function is accomplished with a high-frequency voltage-controlled oscillator (VCO). The VCO control voltage is adjusted at each positive going zero voltage-controlled oscillator (VCO). The VCO control voltage is adjusted at each positive going zero crossing of a resonator's oscillator circuit output to maintain phase synchronism. The count output of the VCO is sampled at equal time intervals. Unequal time interval samples of a period readout (higher frequency counts between positive going zero crossings of a resonator's oscillator circuit output) can be converted to equal-time phase samples with software interpolation (see Ash et al. [B5]).

D.4.4 Dual resonators

When considered as an ideal linear sensor, the dual-resonator push–pull VBA has the following two advantages compared to a single resonator implementation:

a) Calculating acceleration or velocity change from the difference of two counts doubles the scale factor, with a corresponding reduction in quantization error.
b) Differencing two identical resonators (or taking an appropriately weighted difference if the f_0 frequencies are not quite equal) provides nearly perfect common mode rejection of bias errors due to clock instabilities. This gain by itself usually is sufficient reason to use dual resonators.

With real resonators, which depart significantly from both perfect linearity and perfect stability, dual push–pull resonators provide useful common mode rejection of several other error sources, as well. These are discussed in D.5.

D.4.5 Algorithms

The most straightforward algorithms for dealing with single resonators are derived from a polynomial model in acceleration, similar to that used in servo accelerometer model equations

$$f = \frac{f - f_0}{K_1} = a + K_2 a^2 + K_3 a^3 + \cdots \tag{D.5}$$

The nonlinear coefficients are larger than those seen in a servo accelerometer, but they are stable and, therefore, modelable. The precise values arise from details of the geometry of the etched quartz resonators and are also affected by the geometry of the remainder of each individual sensor. However, their magnitudes are mainly determined by the classic equations of a rectangular beam with built-in end conditions. For the square root approximation cited earlier, the following are good approximations:

$$K_1 \approx \frac{f_0}{2\mathrm{C}}$$
$$K_2 \approx \frac{1}{4\mathrm{C}}$$
$$K_3 \approx \frac{1}{8\mathrm{C}^2} \tag{D.6}$$

where

C is the number of g for Euler buckling

For a VBA with a ±10% frequency deviation, C is five times full scale. For example, a sensor that deviates 10% at 100-g full scale will have a K_2 value of approximately 500 μg/g^2. Nonlinearities of this magnitude are inherent in any scheme that uses inertial forces to modulate the effective elastic restoring force of a resonator.

The inverse of the square root approximately is simply

$$A_{\text{ind}} = \mathrm{C}\left[1 - \frac{f^2}{f_0^2}\right] \tag{D.7}$$

This approximation, used with a single resonator, is suitable only for the simplest kinds of medium-precision systems, but it suggests a family of good dual-resonator algorithms that take the form

$$A_{\text{ind}} = A_1 f_1^2 - A_2 f_2^2 - A_0 \tag{D.8}$$

These algorithms correct for nonlinearity in the following two ways:

- At low frequencies up to approximately half the Nyquist frequency associated with the data sampling, they correct for the resonator nonlinearities directly and in real time.
- At higher frequencies, they apply common mode rejection to the residual even order nonlinearities to minimize rectification errors.

These algorithms work well enough for most medium-precision applications and even many high-precision systems. The effectiveness of common mode rejection of the dominant even order effects can be seen in the fact that an even simpler algorithm is found to work almost as well

$$A_{\text{ind}} = A_1 f_1 - A_2 f_2 - A_0 \tag{D.9}$$

This last algorithm can be rewritten into a phase/velocity algorithm that has useful properties

$$\Delta V_{\text{ind}} = A[\Delta\Phi + B\Sigma\Phi + F\Delta t]$$

with

$$\Delta\Phi = \Phi_1 - \Phi_2$$
$$\Sigma\Phi = \Phi_1 + \Phi_2 \tag{D.10}$$

where A, B, F are constants and $\Phi_1 - \Phi_2$ is the difference of the phase changes of the two resonators across the time interval Δt.

A useful feature of this algorithm is that it allows a VBA to be treated almost like the more familiar quasi-linear servoed accelerometers. The major nonlinearities of the sensor are corrected almost entirely by the *B* coefficient. Once *B* has been evaluated by a multipoint tumble or, for more demanding applications, by a centrifuge test, it can be considered to be a known constant of the accelerometer. Further testing only needs to update the *A* coefficient, for scale factor, and the *F* coefficient, for bias. These tests can be accomplished by such familiar procedures as ±1-*g* tumble tests.

This overview has concentrated on the low- to medium-accuracy applications of VBAs, which also dominate the world of servoed accelerometers. In this realm, VBAs can be treated very much like their analog predecessors. Laboratory testing has revealed that VBAs may also be capable of operating in the very high accuracy realm of high-performance sensors, such as pendulous integrating gyroscopic accelerometers (PIGAs) and specific force integrating receivers (SFIRs). Those applications are much more demanding and require much more demanding analysis. They are beyond the scope of this document.

D.5 VBA error sources

D.5.1 Scale factor stability

The scale factor of a VBA is determined almost exclusively by resonator elastic properties, a feature that has inherently high stability. Experience has shown that a VBA must be very poorly designed and/or built before scale-factor stability becomes a problem.

a) Aging effects: typically less than 5 ppm/yr
b) Temperature sensitivity: typically less than 5 ppm/ºC and almost always less than 10 ppm/ºC

D.5.2 Bias stability

VBA bias stability is adequate for a wide range of applications, but it depends on common mode error rejection. Factors that common-mode-reject well include

a) Clock error
b) Temperature effects, including hysteresis
c) Outgassing
d) Aging
e) Vibration rectification

Creep effects do not common-mode-reject to any useful degree, but they are seldom a problem.

Because of the anisotropic properties of quartz, the orientation of the crystal lattice can be chosen so that a resonator's bias frequency temperature sensitivity is zero at a point near room temperature called the "zero temperature coefficient (ZTC) temperature." Temperature-controlled operation near this temperature yields the best performance. Temperature-controlled and/or temperature-compensated performance away from this temperature benefits from common mode rejection in the difference frequency of the two resonators, especially if care is taken to match ZTC temperatures and temperature sensitivities in the two resonators during fabrication.

D.5.3 Effect of clock errors

The measurement of an individual resonator's frequency is sensitive to clock errors, being of the order of 1 μ*g* per part per billion of clock error. Hence, if individual frequencies are being recorded for engineering analysis and even if the difference frequency is being used, an atomic frequency reference should be used in laboratory testing for timing the equal time samples from a phased-locked loop readout or for high-frequency counting in a period readout.

If the bias frequency f_{0i} and scale factor K_{1i} of the two resonators match (i = 1,2), then the measured difference frequency $f_1 - f_2$ of the two resonators has about a 1-μ*g*/ppm sensitivity to clock error about the same as for any other accelerometer. A crystal-controlled laboratory or guidance system frequency reference can be employed in acquiring data.

If the bias and scale factor of the two resonators do not match, then the weighted difference of the two measured resonator frequencies f_i,

$$\Gamma_1 f_1 - \Gamma_2 f_2, \qquad \Gamma_1 + \Gamma_2 = 1, \quad \Gamma_i > 0 \tag{D.11}$$

has the minimal sensitivity to clock errors, where

$$\Gamma_1 = \frac{f_{02}/K_{12}}{f_{01}/K_{11} + f_{02}/K_{12}}, \qquad \Gamma_2 = \frac{f_{01}/K_{11}}{f_{01}/K_{11} + f_{02}/K_{12}} \tag{D.12}$$

Even for several milliradian misalignments, the effective input axis (IA) for the weighted difference frequency measurement of acceleration is essentially the bisector of the IA_1 and $-IA_2$ of the almost antiparallel resonators 1 and 2.

D.5.4 Quantization noise

In D.4.1 and D.4.2, quantization error is discussed in terms of the change in indicated acceleration for a single count change in the measurement of frequency or period of a single resonator. For a classic analysis of the effect of quantization on system error or to make sense of the quantization effect in the case of dual resonators, it is necessary to consider the statistics of these errors, specifically the root-mean-square (rms) value due to random steps and its frequency response, as indicated by the associated power spectral density (PSD).

For a single resonator, the variation of indicated acceleration about the mean is uniformly distributed in the interval $-0.5\ \Delta A_{\text{ind}}$ to $+0.5\ \Delta A_{\text{ind}}$ since all such errors are equally probable. The rms value is thus given by

$$\Delta A_{\text{rms}} = \sqrt{\int_{-0.5\Delta A_{\text{ind}}}^{+0.5\Delta A_{\text{ind}}} \frac{x^2 dx}{\Delta A_{\text{ind}}}} = \frac{\Delta A_{\text{ind}}}{\sqrt{12}} \tag{D.13}$$

Since the individual sample errors are uncorrelated variations in phase (or velocity), it is intuitively reasonable (and can, in fact, be shown) that quantization noise can be represented by a white phase (or velocity) spectrum in the frequency range from zero to the Nyquist frequency associated with the sampling process. The magnitude is defined by observing that the frequency integral of the PSD from zero to the Nyquist frequency is equal to ΔA_{rms}.

For dual resonators, two sets of uncorrelated sample errors root-sum-square (rss) to give

$$\Delta A_{\text{rms}}(2) = \frac{\Delta A_{\text{ind}}}{\sqrt{24}} \tag{D.14}$$

The largest change that can be induced by a worst-case step in quantization error is ΔA_{ind} for either one or two resonators, but in the case of two, it requires that both resonators make the appropriate errors in the appropriate directions at the same time. The probability of the larger errors is correspondingly reduced.

Similar reductions in the rms error due to quantization may be accomplished by digital low-pass filtration of the sampled data, often by sampling at a very high frequency and then decimating after filtering (see Annex H). Knowledge of the PSD is an aid in understanding this process.

D.5.5 Vibration rectification compensation

If the K_2 coefficients of the two resonators match, then the difference frequency or weighted difference frequency is a measure of indicated acceleration that is mainly free of the effects of vibration rectification. If the K_2 coefficients do not match, then vibration rectification compensation can be accomplished by converting each measured frequency to acceleration at a high rate (at least twice the highest frequency vibration in the application) and then taking the weighted difference of the individual resonator indicated accelerations to obtain the acceleration measurement of the VBA as a whole. This acceleration then has digital filtering applied before decimating to the output rate of the application. If the individual resonator frequency measurements were filtered and decimated to the lower rate and then weighted-differenced and converted to acceleration, the result would be affected by vibration rectification because of the very nonlinear VBA model.

Because of the highly nonlinear VBA model, the conversion of the individual resonator frequencies to acceleration at a high rate puts stringent requirements on the size of the quantization error that can be tolerated in the VBA readout. Hence, a PLL's VCO or a period readout's counter have to operate at a high frequency. Exactly how high would have to be worked out using the K_2 mismatch of the two resonators, the acceleration environment of the application, and the amount of vibration rectification rejection that is required.

D.5.6 Aliasing

VBA outputs are digital, and they interface with sampled data systems. They will, therefore, alias. Furthermore, they are directly digital, so antialiasing filters are neither simple nor straightforward. They have an inherent aliasing characteristic that makes them manageable for most systems, however.

a) The counting processes that are used to measure VBA output are essentially integrations, so high-frequency aliasing is inherently attenuated.
b) The output will not alias at dc if all data points are equally weighted, and no counts are missed.

D.5.7 Inversion transients

A finite settling time following an input step from +1 *g* to –1 *g* can cause problems in high-performance systems. With careful attention to packaging, temperature control, and temperature sensitivity of resonator electronics, VBAs have demonstrated transients consistently less than 1 μ*g*. This performance is comparable to competing accelerometers, but it remains a topic for further research.

D.5.8 Dual-pendulum effects

Some VBAs acquire dual resonators by the simple expedient of housing dual pendulums. This approach has a desirable effect on pendulous cross-coupling errors if they are oriented correctly, but it may require special correction for use in strapdown systems since the pendulums are at different locations. The effect may be particularly noticeable during centrifuge testing, where the pendulums may be at different radii.

In addition, many applications may impose tight constraints on matching the two pendulums to achieve acceptable dynamic common mode rejection.

D.5.9 Frequency lock and activity dips

Frequency lock and activity dips are localized nonlinearities that can alter the frequency and amplitude of crystal resonator oscillators (see Bottom [B10] and Heising [B25]). Both of these events result from the coupling of resonator energy into another resonant mode in the system (see Heising [B25]). In the case of frequency lock, the other resonant system is the other resonator in a dual-resonator VBA. In the case of activity dip, the other resonant system may be a structural resonance in the accelerometer or it may be another mode in the resonator itself. These deleterious phenomena were first detected in the field of quartz frequency standard resonators. There the nonlinearities appear primarily as difficulties in achieving crystal resonator oscillations when an adverse phase relationship draws energy out of the resonator, hence, the name "activity dip" (see Heising [B25]).

Frequency lock may occur when two variable frequency resonators occupy a common housing and are allowed to approach a common frequency. Energy exchange between resonant systems will cause the lower frequency resonator to be drawn upward in frequency and the higher one downward, giving rise to a localized disturbance in the apparent acceleration, which is typically the difference frequency.

D.5.9.1 Static behavior versus dynamic behavior

Frequency lock is difficult to eliminate entirely, but by careful selection of resonators, it can be placed at a spot in the accelerometer range where it does little harm. In particular, it can be placed outside the range of +1 *g* to –1 *g*, where the input is likely to dwell. Energy transfer between resonant systems does not occur instantaneously, and elimination of the dwell condition can dramatically reduce the magnitude as well as the duration of the associated frequency shift. In any case, its effects can be easily confirmed because they are easy to find. The approach, crossover, and separation of two output frequencies are easily observed and can even be predicted to reasonable accuracy when two scale factors and two biases have been measured.

Activity dips, on the other hand, can occur almost anywhere and are easily missed in most search routines. Their saving grace is that they are amenable to design changes with the aid of finite element model analysis. They should not be a problem in a robust production design that has demonstrated generous margins during development.

D.5.9.2 Test procedures

The nonlinearities typically have magnitudes of several m*g*. For accelerometers of unknown characteristics, determining the presence of these phenomena may pose testing problems. Several test configurations can be used to test for frequency lock and activity dip.

D.5.9.2.1 Frequency lock

Frequency lock is easy to confirm since the point where it can occur can be estimated when the bias and scale factors are measured. The effect can be experimentally measured by using the following procedures, which are straightforward and effective:

a) By calculation from the biases and scale factors, or simply by observing the proximity and rate of change of the two frequencies, determine approximately where frequency crossover will occur.
b) If crossover occurs within the range of –1 *g* to +1 *g*, mount the accelerometer to a dividing head and take a series of closely spaced digital readings, for example, 20 readings over a range of a m*g* or so. Refine the sampling plan as required to define the location and magnitude of the maximum peak-to-peak deviations from local linearity.
c) If crossover occurs at higher or lower acceleration, the same test can be conducted, but it will be necessary to use a centrifuge, varying the speed as required, to obtain the necessary inputs.

D.5.9.2.2 Activity dip

Activity dips are difficult to locate because they can occur almost anywhere in the accelerometer range, and the effects may extend over a few m*g* or less. There is no easy way to know where to look.

a) On a dividing head, with 4-s samples to get useful resolution, a half rotation between +1 *g* and –1 *g* at 50-μ*g* steps will take about a day. Bigger steps can be used for screening for large effects. This procedure gives useful coverage for less than 1 *g*. It is slow but may not be totally impractical for evaluation testing of small quantities of accelerometers.
b) With a centrifuge, another possibility has been used successfully. Instead of taking digital readings, which may require an elaborate system to get adequate resolution at a useful sample rate, connect each resonator output to an analog phase-locked loop, to get an analog output voltage. Connect this voltage to a chart recorder; then spin the centrifuge at a rate sufficient to produce full-scale input. Open the centrifuge control loop, and allow the centrifuge to coast down to a stop. The *g*-to-voltage transfer function need not be linear, as long as it is smooth. Activity dips will show as transient disturbances on the output trace. If the centrifuge is sufficiently quiet, sensitivity can be improved by bandpass filtering the analog signal to suppress the dc term.

Activity dip research is time consuming and sometimes ambiguous. The centrifuge coast-down test has provided a reasonable way of identifying the locations of activity dips; however, the magnitude of the activity dip cannot be accurately measured. Accurate measurement requires digital inspection of the nonlinearity over a narrow acceleration range with the proper sampling rate.

The accelerometer design will affect the magnitude and locations of activity dip and frequency lock (see ErNiesse [B18]). If proper design techniques are used and sufficient development testing is pursued, it may not be necessary to do comprehensive testing for activity dip and frequency lock during production testing.

D.6 Related developments

The VBA is adaptable to most of the applications that have been claimed by pendulous servo accelerometers over the past few decades and possibly all of those that require interface with a digital system. It requires adaptation to a significantly different set of idiosyncrasies than preceding designs, but different does not necessarily imply worse. For example, VBA mechanisms require significant mechanical redesign to change their scaling or dynamic response. However, since they are generally stiff, wide-band devices, such redesign usually will not be a problem. Most of the characteristics already are close to what a designer would aim for if designing a servoed accelerometer to satisfy a broad spectrum of applications.

Two applications in particular stand out, however: Coriolis rate sensors and silicon micromachining technology.

D.6.1 Coriolis rate sensors

Many Coriolis rate sensors require synchronous demodulation of dithered linear accelerometers or their functional equivalent. For those that require interface with a digital system, and especially those that require both angular rate and linear acceleration as outputs, the VBA has much to offer, such as follows:

a) Accelerometers can be made small to minimize dithered mass.
b) Phase output, corresponding to $\Delta\theta$, is easily achieved by counting output pulses.
c) The combination of frequency output and a high bias frequency gives near zero threshold and good resolution.
d) Inherently digital processing permits production trims to be made in software rather than hardware with sealed cases and no debris.

D.6.2 Silicon micromachining technology

The structures required for a micrometer-scale accelerometer are conveniently fabricated by state-of-the-art, three-dimensional micromachining. The resulting accelerometers face the same thermal noise limits as other technologies, but otherwise their scaling laws are favorable for miniature devices. The structural characteristics of silicon have been shown to be at least as good as those of quartz. Silicon is not piezoelectric, but several other physical principles have been demonstrated to drive resonant structures. See F.3.

Annex E

(informative)

VBA resonator frequency as a function of applied acceleration

E.1 Geometry and elastic properties of vibrating beam

Consider the elastic vibrating beam or tuning fork tine depicted in Figure D.2 with a rectangular cross section and subjected to fixed–fixed boundary conditions. The beam is loaded by an axial force, *F*, as depicted in Figure E.1. The parameters of the beam are

L	is the length of the beam (cm)
F	is the axial tension (dynes = g·cm/s^2)
m	is the mass per unit length (g/cm)
E	is the Young's modulus (isotropic) (dynes/cm^2)
I	is the $\frac{b^3h}{12}$ area moment of inertia (cm^4)

The nonisotropic nature of quartz and the surface piezoelectric forces are being ignored. The density of α crystalline quartz (the transition to β quartz is at 570 ºC) is

$$\rho = 2.64 \quad \text{g/cm}^3 \tag{E.1}$$

so that the mass per unit length is

$$m = \rho\, b\, h \quad \text{g/cm} \tag{E.2}$$

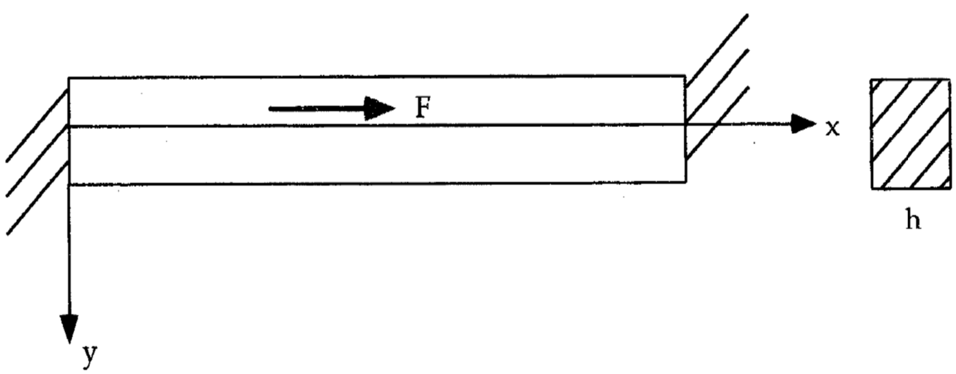

Figure E.1—Axial force on beam with rectangular cross section

In Figure E.1, the *x* crystallographic axis of the quartz beam or tine is almost in the *y* direction and the *y* crystallographic axis is almost in the *x* direction. There is a manufacturer-specific small rotation θ about the *x* crystallographic axis rotating y toward *z*. The values of *L*, *b*, *h*, and θ are chosen by the manufacturer to give desired frequency and thermal sensitivity values. That the *y* crystallographic axis is almost along the length axis of the beam or tine is because of the possible ways that electrode plating can be put on the beam or tine to excite flexure mode vibration in the *x*–*y* plane using the axes specific piezoelectric properties of quartz.

By Nye [B40] for the trigonal quartz system, the Young's modulus E along the beam or tine length axis is related to the compliance s'_{11} along the rotated crystallographic length axis by

$$\frac{1}{E} = s'_{11} = \left(1 - \ell_3{}^2\right)s_{11} + \ell_3{}^2\left(1 - \ell_3{}^2\right)(2s_{13} + s_{44}) \tag{E.3}$$

where

$$\ell_3 = \sin\theta, \quad \ell_1 = \cos\theta, \quad \ell_2 = 0 \quad \text{(singly rotated)} \tag{E.4}$$

and where in units of 10^{-12} cm^2/dyne

$$\begin{aligned} s_{11} &= 1.27, \; s_{12} = -0.17, \; s_{44} = 2.01 \\ s_{33} &= 0.97, \; s_{13} = -0.15, \; s_{14} = -0.43 \end{aligned} \tag{E.5}$$

If $\theta = 0$,

$$E = \frac{1}{s_{11}} = 7.87 \times 10^{11} \text{dynes/cm}^2 = 1.14 \times 10^7 \text{ psi} \tag{E.6}$$

E.2 Square-root relationship derived from energy considerations

E.2.1 Internal energy of beam

The energy of the beam is (see Clough and Penzier [B15])

$$J_{pm}(t) = \frac{1}{2}\int_0^L M(x,t)\, k(x,t)\, dx \tag{E.7}$$

where $M(x, t)$ is the moment distribution throughout the beam and $k(x, t)$ is the curvature of the beam center line $y(x, t)$. The beam curvature is

$$k(x,t) = \frac{\partial^2 y/\partial x^2}{\sqrt{1 + (\partial y/\partial x)^2}} \tag{E.8}$$

Assume that the deformed beam has small slopes

$$\left|\frac{\partial y(x,t)}{\partial x}\right| \ll 1 \tag{E.9}$$

which is consistent with fixed–fixed boundary conditions but not necessarily with others (such as pinned–pinned). With this assumption,

$$k(x,t) = \frac{\partial^2 y(x,t)}{\partial x^2} \tag{E.10}$$

From the moment-curvature relationship in linear beam theory (see Clough and Penzier [B15]),

$$M(x,t) = EI\,k(x,t) \tag{E.11}$$

giving the internal energy of the beam as

$$J_{pm}(t) = \frac{1}{2}\int_0^L EI\left[\frac{\partial^2 y(x,t)}{\partial x^2}\right]^2 dx \tag{E.12}$$

E.2.2 Effect of axial force

The axial force potential energy due to the axial load *F* is the force *F* times the change of length (*ds* – *dx*)

$$J_{pf}(t) = \int_0^L F(ds - dx) \tag{E.13}$$

where

$$\begin{aligned} ds &= \sqrt{(dx)^2 + \left[\frac{\partial y(x,t)}{\partial x}dx\right]^2} \\ &= dx\sqrt{1 + \left[\frac{\partial y(x,t)}{\partial x}\right]^2} \end{aligned} \tag{E.14}$$

The series approximation to the square root is

$$ds = dx\left\{1 + \frac{1}{2}\left[\frac{\partial y(x,t)}{\partial x}\right]^2 + \cdots\right\} \tag{E.15}$$

Substituting Equation (E.15) into Equation (E.13) gives the following expression for the potential energy of the beam due to the axial load:

$$J_{pf}(t) = \frac{F}{2}\int_0^L \left[\frac{\partial y(x,t)}{\partial x}\right]^2 dx \tag{E.16}$$

The linear kinetic energy of an incremental mass *dm* is one half of the mass times the square of the linear velocity

$$dK(t) = \frac{1}{2}dm\left[\frac{\partial y(x,t)}{\partial t}\right]^2 \tag{E.17}$$

But for the beam element $dm = \rho\, b\, h\, dx$. Therefore,

$$dK(t) = \frac{1}{2}\rho\, b\, h\left[\frac{\partial y(x,t)}{\partial t}\right]^2 dx \tag{E.18}$$

and the kinetic energy of the beam can be expressed as

$$K(t) = \frac{1}{2}\rho\, b\, h\int_0^L \left[\frac{\partial y(x,t)}{\partial t}\right]^2 dx \tag{E.19}$$

At any time t,

$$J_{pm}(t) + J_{pf}(t) + K(t) = \text{constant} \tag{E.20}$$

Since the beam is experiencing harmonic motion with

$$y(x,t) = Y(x)\sin(\omega t + \text{phase}) \tag{E.21}$$

assume that

$$\max_t\left[J_{pm}(t) + J_{pf}(t)\right] = \max_t K(t) \tag{E.22}$$

$$\max_t\left[\frac{\partial y(x,t)}{\partial t}\right] = \omega \max_t[y(x,t)] \tag{E.23}$$

Following Clough and Penzier [B15], the beam resonant frequency is determined by inserting Equation (E.12), Equation (E.16), Equation (E.19), and Equation (E.23) into Equation (E.22) and solving for ω:

$$\omega^2 = \frac{A}{B} \tag{E.24}$$

where

$$A = \max_t\left\{\frac{1}{2}\int_0^L EI\left[\frac{\partial^2 y(x,t)}{\partial x^2}\right]^2 dx + \frac{F}{2}\int_0^L \left[\frac{\partial y(x,t)}{\partial x}\right]^2 dx\right\} \tag{E.24a}$$

$$B = \frac{1}{2}\rho\, b\, h \max_t \int_0^L y(x,t)^2\, dx \tag{E.24b}$$

The maximum of the sum of the terms in Equation (E.24a) is the sum of the maximums of the terms because the terms are nonnegative.

The unstressed bias circular frequency ω_0 is determined from Equation (E.24) by the condition $F = 0$, so Equation (E.24) can be rewritten as

$$\omega = \omega_0\sqrt{1 + FS} \tag{E.25}$$

where

$$S = \frac{1}{2B{\omega_0}^2}\max_t \int_0^L \left[\frac{\partial y(x,t)}{\partial x}\right]^2 dx \tag{E.26}$$

Assumptions used in deriving Equation (E.25) were that the amplitudes are small, the approximations of linear beam theory apply, and Equation (E.9) and Equation (E.14) are valid. Equation (E.25) gives an expression for the frequency variation about the bias frequency where the variations under axial load stay in the same vibration mode as the bias frequency.

E.2.3 Taylor series expansion for square root expression

In Equation (E.25), replace the circular frequency ω by frequency $f = \omega/2\pi$ and write $FS = a_{\mathrm{i}}s$, where the acceleration a_{i} along the IA of the VBA causes axial force F on the beam. The quantity s depends on the manufacturer-specific size of the proof mass and geometry of the beam and on the elasticity properties of quartz. The Taylor series expansion of Equation (E.25) is

$$f = f_0 \left[\begin{array}{c} 1 + \frac{1}{2} a_i s - \frac{1}{8} a_i^2 s^2 + \frac{1}{16} a_i^3 s^3 - \frac{5}{128} a_i^4 s^4 + \frac{7}{256} a_i^5 s^5 \\ - \frac{21}{1024} a_i^6 s^6 + \frac{33}{2048} a_i^7 s^7 - \frac{429}{32768} a_i^8 s^8 + \frac{2145}{196608} a_i^9 s^9 - \cdots \end{array} \right]$$

$$= f_0 + K_1 a_i + K_2 a_i^2 + K_3 a_i^3 + K_4 a_i^4 + K_5 a_i^5 + K_6 a_i^6 + K_7 a_i^7 + K_8 a_i^8 + K_9 a_i^9 + \cdots \quad \text{(E.27)}$$

where

$$K_n = b_n K_1^n / f_0^{n-1} \quad \text{Hz}/g^n$$

$$K_n / K_1 = b_n K_1^{n-1} / f_0^{n-1} \quad g/g^n, \; n = 2,3,4,5,6,7,\ldots \quad \text{(E.28)}$$

$b_2 = -1/2 = -0.5$
$b_3 = +1/2 = +0.5$
$b_4 = -5/8 = -0.625$
$b_5 = +7/8 = +0.87$
$b_6 = -21/16 = -1.3125$
$b_7 = +33/16 = +2.0625$
$b_8 = -429/128 = -3.3515625$
$b_9 = +2145/384 = +5.5859375$

The value of (K_1/f_0) is determined by the size of the proof mass and is a design choice of the VBA manufacturer. Table E.1 gives the coefficients predicted by Equation (E.28) with two different design choices. It is clear that increasing the Hz/g scale factor to gain sensitivity places an increased burden on the number of terms that have to be carried along in the VBA nonlinear model and the accuracy to which they have to be known.

Table E.1—Value of nonlinear coefficients predicted by square-root model

	$\frac{K_1}{f_0} = 1 \times 10^{-3} g^{-1}$		$\frac{K_1}{f_0} = 3 \times 10^{-3} g^{-1}$	
Coefficient	Value $\mu g/g^n$	Effect at 30 g μg	Value $\mu g/g^n$	Effect at 30 g μg
K_2/K_1	-500	450 000	-1500	1 350 000
K_3/K_1	0.5	13 500	4.5	121 500
K_4/K_1	-6.3×10^{-4}	510	-1.7×10^{-2}	13 770
K_5/K_1	8.8×10^{-7}	21	7.1×10^{-5}	1725
K_6/K_1	-1.3×10^{-9}	0.95	-3.2×10^{-7}	233
K_7/K_1	2.1×10^{-12}	0.046	1.5×10^{-9}	33
K_8/K_1	-3.4×10^{-15}	0.0022	-7.3×10^{-12}	4.8
K_9/K_1	5.6×10^{-18}	0.00011	3.7×10^{-14}	0.73

E.3 Direct frequency versus force relation

Now return to first principles to derive a more accurate expression for the vibration frequency of a quartz resonator using the direct force equation.

E.3.1 Vibrating beam partial differential equation

The motion of a uniform beam resonator of rectangular cross section can be expressed as a single partial differential equation as outlined in Church [B14], Clough and Penzier [B15], and Timoshenko and MacCollough [B58]. The same equation can be used for the vibration of one of the two tines in a double-ended tuning fork (DETF) resonator. The two tines vibrate $180°$ out of phase. The interaction of one tine with the other is determined through the elastic boundary conditions.

The beam (tine) is kept vibrating at its natural frequency by piezoelectric forces on the surface. However, the effects of surface forces are ignored and the elastic boundary conditions are assumed to be fixed–fixed boundary conditions.

The following analysis seeks to establish the analytical relation between the axial force generated in the beam and the corresponding beam frequency. Consider an elastic beam having a rectangular cross section and subjected to fixed–fixed boundary conditions and loaded by an axial force F, as depicted in Figure E.1.

The equation of the vibrating beam with fixed-fixed boundary conditions is

$$F\frac{\partial^2 y}{\partial x^2} - EI\frac{\partial^4 y}{\partial x^4} = m\frac{\partial^2 y}{\partial t^2} \tag{E.29}$$

$$y(0,t) = \frac{\partial y(0,t)}{\partial x} = 0 \tag{E.29a}$$

$$y(L,t) = \frac{\partial y(L,t)}{\partial x} = 0 \tag{E.29b}$$

where $y(x,t)$ is the transverse displacement and the units of length and time are centimeters and seconds, respectively. The nonisotropic nature of quartz and the surface piezoelectric forces are ignored in this equation.

E.3.2 Reduction to ordinary differential equations

The solution of Equation (E.29) begins by using the technique of separation of variables. Let

$$y(x,t) = Y(x)T(t) \tag{E.30}$$

where the dimensions of Y are centimeters and T is dimensionless. Inserting Equation (E.30) into Equation (E.29) gives

$$FT\,\frac{d^2Y}{dx^2} - EIT\,\frac{d^4Y}{dx^4} = mY\,\frac{d^2T}{dt^2} \tag{E.31}$$

Dividing by YT yields

$$\frac{F}{Y}\frac{d^2Y}{dx^2} - \frac{EI}{Y}\frac{d^4Y}{dx^4} = \frac{m}{T}\frac{d^2T}{dt^2} \tag{E.32}$$

The left side of this equation is a function of x only, and the right side is a function of t only. Therefore, each side must be a constant $-\lambda$, where $\lambda > 0$ yields the bounded solutions

$$\frac{F}{Y}\frac{d^2Y}{dx^2} - \frac{EI}{Y}\frac{d^4Y}{dx^4} = -\lambda \tag{E.33}$$

$$\frac{m}{T}\frac{d^2T}{dt^2} = -\lambda \tag{E.34}$$

which yields

$$F\frac{d^2Y}{dx^2} - \frac{EI}{Y}\frac{d^4Y}{dx^4} + \lambda Y = 0 \tag{E.35}$$

$$m\frac{d^2T}{dt^2} + \lambda T = 0 \tag{E.36}$$

The dimensions of the constant λ are $\frac{\text{g}}{\text{cm}\cdot\text{s}^2} = \frac{\text{dynes}}{\text{cm}^2}$.

E.3.3 Solution by separation of variables

The general solution to Equation (E.36) is

$$T(t) = A\sin\left[\sqrt{\frac{\lambda}{m}}\,t\right] + B\cos\left[\sqrt{\frac{\lambda}{m}}\,t\right] \tag{E.37}$$

where A, B are found by time initial conditions (initial phase and amplitude of the beam vibration). The beam circular frequency is

$$\omega = \left[\sqrt{\frac{\lambda}{m}}\right] \text{rad/s} \tag{E.38}$$

where λ is unknown.

Let $Y = \text{c}e^{\alpha x}$ in Equation (E.35), which yields the characteristic equation

$$F\alpha^2 - EI\alpha^4 + \lambda = 0 \tag{E.39}$$

This equation gives the general solution

$$Y(x) = a_1\sin\alpha_1 x + a_2\cos\alpha_1 x + a_3\sinh\alpha_2 x + a_4\cosh\alpha_2 x \tag{E.40}$$

where the solutions of Equation (E.39) to give the trigonometric and hyperbolic arguments are

$$\alpha_1(\lambda) = \sqrt{\sqrt{\left(\frac{F}{2EI}\right)^2 + \frac{\lambda}{EI}} - \frac{F}{2EI}} \quad \text{cm}^{-1} \tag{E.41}$$

$$\alpha_2(\lambda) = \sqrt{\sqrt{\left(\frac{F}{2EI}\right)^2 + \frac{\lambda}{EI}} + \frac{F}{2EI}} \quad \text{cm}^{-1} \tag{E.42}$$

or since $\omega = \sqrt{\lambda/\text{m}}$

$$\alpha_j(\omega) = \sqrt{\sqrt{\left(\frac{F}{2EI}\right)^2 + \frac{m\omega^2}{EI}} + (-1)^j\frac{F}{2EI}} \quad \text{cm}^{-1}\ , \qquad j = 1,2 \tag{E.43}$$

where ω is unknown.

E.3.4 Application of the boundary conditions

To apply the boundary conditions [(Equation (E.29a) and Equation (E.29b)], evaluate Equation (E.40) and its first derivative at both ends of the beam when $x = 0$ and $x = L$. The resulting set of equations have the form

$$D\,a = 0 \tag{E.44}$$

where a is the column vector $(a_1, a_2, a_3, a_4)^T$ and

$$D(\omega) = \begin{bmatrix} 0 & 1 & 0 & 1 \\ \alpha_1 & 0 & \alpha_2 & 0 \\ \sin\alpha_1 \mathrm{L} & \cos\alpha_1 \mathrm{L} & \sinh\alpha_2 \mathrm{L} & \cosh\alpha_2 \mathrm{L} \\ \alpha_1\cos\alpha_1 \mathrm{L} & -\alpha_1\sin\alpha_1 \mathrm{L} & \alpha_2\cosh\alpha_2 \mathrm{L} & \alpha_2\sinh\alpha_2 \mathrm{L} \end{bmatrix} \tag{E.45}$$

In order for Equation (E.44) to have nonzero solutions, the determinate of D must be zero. Evaluating the determinant of D yields the characteristic equation

$$({\alpha_2}^2 - {\alpha_1}^2)\sin\alpha_1 L \sinh\alpha_2 L + 2\alpha_1\alpha_2(1 - \cos\alpha_1 L\cosh\alpha_2 L) = 0 \tag{E.46}$$

By Equation (E.43)

$${\alpha_2}^2 - {\alpha_1}^2 = \frac{F}{EI} \tag{E.47}$$

$$\alpha_1\alpha_2 = \omega\sqrt{\frac{m}{EI}} \tag{E.48}$$

Inserting these relations in Equation (E.46) yields

$$2\omega\sqrt{mEI}\{1 - \cos[\alpha_1(\omega)L]\cosh[\alpha_2(\omega)L]\} + F\sin[\alpha_1(\omega)L]\sinh[\alpha_2(\omega)L] = 0 \tag{E.49}$$

which is the fundamental equation relating the axial force F with the circular frequency ω of an axially loaded fixed-fixed beam.

E.3.5 Frequency of beam under no axial load

Let ω_0 the circular frequency when $F = 0$. Then, by Equation (E.43)

$$\alpha_1 = \alpha_2 = \sqrt[4]{\frac{m}{EI}}\sqrt{\omega_0} \quad \mathrm{cm}^{-1} \tag{E.50}$$

so that using Equation (E.49)

$$1 - \cos\left[\alpha_j(\omega_0)L\right]\cosh\left[\alpha_j(\omega_0)L\right] = 0\,, \quad j = 1,2 \tag{E.51}$$

The solution of Equation (E.51) gives the bias circular frequency ω_0.

The function

$$g(z) = 1 - \cos z\,\cosh z \tag{E.52}$$

has infinitely many zeros above $z = 0$. The first one at

$$z_0 = 4.7300407448627 \tag{E.53}$$

corresponds to the first vibration mode of the fixed–fixed beam or tine, that is, the mode shape that has no zero crossings of $Y(x)$ between $x = 0$ and $x = L$. Higher modes can have multiple such zero crossings, but the oscillator circuit of the quartz resonator suppresses those modes and only excites the desired mode.

Using this zero of $g(z)$, the unstressed bias circular frequency of the beam or tine is

$$\omega_0 = \frac{22.373285448061}{L^2}\sqrt{\frac{EI}{m}} \quad \mathrm{rad/s} \tag{E.54}$$

and the unstressed bias frequency is

$$\begin{aligned} f_0 = \frac{\omega_0}{2\pi} &= \frac{3.56081897722649}{L^2}\sqrt{\frac{EI}{m}} \quad \mathrm{Hz} \\ &= 5.613 \times 10^5 \frac{b}{L^2} \quad \mathrm{Hz} \end{aligned} \tag{E.55}$$

by Equation (E.1) to Equation (E.6). The values of b and L in centimeters are specific to a given manufacturer's design. Depending on the design, the bias frequency is between about 10 kHz and 100 kHz.

E.3.6 Frequency of beam with axial load

Equation (E.43) can be expressed as

$$\alpha_j(\omega) = \sqrt{\sqrt{\left(\frac{F}{2EI}\right)^2 + \frac{{z_0}^4}{L^4}\left(\frac{\omega}{\omega_0}\right)^2} + (-1)^j \frac{F}{2EI}} \quad \mathrm{cm}^{-1} \tag{E.56}$$

and Equation (E.49) as

$$2\frac{{z_0}^2}{L^2}\frac{\omega}{\omega_0}\{1 - \cos[\alpha_1(\omega)L]\cosh[\alpha_2(\omega)L]\} + \frac{F}{EI}\sin[\alpha_1(\omega)L]\sinh[\alpha_2(\omega)L] = 0 \tag{E.57}$$

Consider the Taylor series expansion

$$\omega = \omega_0 + \left.\frac{d\omega}{dF}\right|_{F=0} F + \cdots \tag{E.58}$$

Differentiating Equation (E.57) gives

$$\begin{aligned} &\frac{2{z_0}^2}{L^2\omega_0}\frac{d\omega}{dF}\,[1 - \cos(\alpha_1 L)\cosh(\alpha_2 L)] \\ &+ \frac{2{z_0}^2}{L}\frac{\omega}{\omega_0}\,\left[\sin(\alpha_1 L)\cosh(\alpha_2 L)\frac{d\alpha_1}{dF} - \cos(\alpha_1 L)\sinh(\alpha_2 L)\frac{d\alpha_2}{dF}\right. \\ &+ \frac{1}{EI}\sin(\alpha_1 L)\sinh(\alpha_2 L) \\ &+ \frac{FL}{EI}\,\left[\cos(\alpha_1 L)\sinh(\alpha_2 L)\frac{d\alpha_1}{dF} + \sin(\alpha_1 L)\cosh(\alpha_2 L)\frac{d\alpha_2}{dF}\right. \\ &= 0 \end{aligned} \tag{E.59}$$

where by Equation (E.56)

$$\frac{d\alpha_j}{dF} = \frac{1}{4\alpha_j}\left[\frac{\frac{F}{2E^2I^2} + \frac{2{z_0}^4}{L^4}\frac{\omega}{{\omega_0}^2}\frac{d\omega}{dF}}{\sqrt{\left(\frac{F}{2EI}\right)^2 + \frac{{z_0}^4}{L^4}\left(\frac{\omega}{\omega_0}\right)^2}} + \frac{(-1)^j}{EI}\right] \tag{E.60}$$

Let $F = 0$ with $\omega = \omega_0$, so that Equation (E.60) becomes

$$\begin{aligned}\frac{d\alpha_j}{dF} &= \frac{1}{4\alpha_j}\left[\frac{L^2}{{z_0}^2}\frac{2{z_0}^4}{L^4\omega_0}\frac{d\omega}{dF} + \frac{(-1)^j}{EI}\right] \\ &= \frac{z_0}{2L\omega_0}\frac{d\omega}{dF} + \frac{(-1)^j L}{4z_0 EI}\end{aligned} \tag{E.61}$$

since $\alpha_j L = z_0$ Equation (E.59) becomes by Equation (E.52)

$$\begin{aligned}&\frac{2{z_0}^2}{L^2\omega_0}\frac{d\omega}{dF}g(z_0) + \frac{2{z_0}^2}{L}\left[\sin(z_0)\cosh(z_0)\frac{d\alpha_1}{dF} - \cos(z_0)\sinh(z_0)\frac{d\alpha_2}{dF}\right] \\ &+ \frac{1}{EI}\sin(z_0)\sinh(z_0) = 0\end{aligned} \tag{E.62}$$

which by Equation (E.61) and the fact that $g(z_0) = 0$ becomes

$$\begin{aligned}\left.\frac{d\omega}{dF}\right|_{F=0} &= \frac{L^2\omega_0}{{z_0}^3 EI}\frac{\frac{z_0}{2}[\sin(z_0)\cosh(z_0) + \cos(z_0)\sinh(z_0)] - \sin(z_0)\sinh(z_0)}{\sin(z_0)\cosh(z_0) - \cos(z_0)\sinh(z_0)} \\ &= 1.2288759317432 \times 10^{-2}\frac{L^2\omega_0}{EI}\end{aligned} \tag{E.63}$$

Let F_1 be the force in dynes exerted on the beam or tine under an acceleration of 1 g, and let a_i be the acceleration in g. Since $\omega = 2\pi f$, Equation (E.58) and Equation (E.63) imply

$$f = f_0 + K_1 a_\mathrm{i} + \cdots \tag{E.64}$$

where

$$\frac{K_1}{f_0} = 1.2288759317432 \times 10^{-2}\frac{L^2 F_1}{EI} \quad \mathrm{Hz}/g \tag{E.65}$$

E.4 Frequency versus force numerical evaluation

E.4.1 Generation of curve

Look for the solution to Equation (E.57) that gives the first vibration mode of the beam or tine, that is, the mode shape that has no zero crossings of $Y(x)$ between $x = 0$ and $x = L$. Higher modes can have multiple such zero crossings, but the oscillator circuit of the quartz resonator suppresses those modes and only excites the desired mode. The frequency with no axial load for this mode is given by Equation (E.55).

Suppose

$$\frac{K_1}{f_0} = 3 \times 10^{-3} \tag{E.66}$$

so that 10% frequency deviation exists at 33 g. Different manufacturers would have different choices of proof mass and hence scale factor. By Equation (E.65), the axial force at 1 g acceleration is

$$F_1 = 2\,\lambda\frac{EI}{L^2} \tag{E.67}$$

where

$$\lambda = 0.122062769825116 \tag{E.68}$$

The axial force at acceleration level a_i in g is

$$F = a_i F_1 \tag{E.69}$$

Inserting Equation (E.67) and Equation (E.69) into Equation (E.56) yields

$$\theta_j = \alpha_j(f)L = \sqrt{\sqrt{(\lambda\, a_i)^2 + {z_0}^4\left(\frac{f}{f_0}\right)^2} + (-1)^j \lambda a_i} \tag{E.70}$$

Equation (E.57) can be expressed as

$${z_0}^2\frac{f}{f_0}[1 - \cos\theta_1 \cosh\theta_2] + \lambda a_i \sin\theta_1 \sinh\theta_2 = 0 \tag{E.71}$$

Create a table of f/f_0 versus a_i using the direct frequency versus force relation for $-30\,g \le a_i \le +30\,g$ in increments of Δa_i. Start at $a_i = 0$ with $f/f_0 = 1$ and $\theta_1 = \theta_2 = z_0$. Having determined f/f_0 at a value a_i, let the first guess at a new value $a_i \pm \Delta a_i$ be $(f/f_0)_1 =$ value of f/f_0 at a_i.

Given a value $(f/f_0)_k$ at iteration k in a Newton–Raphson solution for f/f_0 at new acceleration level a_i, do the following steps:

a) Calculate θ_1, θ_2 by Equation (E.70).

b) Calculate

$$H\left[\left(\frac{f}{f_0}\right)_k\right] = {z_0}^2\frac{f}{f_0}[1 - \cos\theta_1\cosh\theta_2] + \lambda a_i \sin\theta_1 \sinh\theta_2$$

$$H'\left[\left(\frac{f}{f_0}\right)_k\right] = {z_0}^2[1 - \cos\theta_1\cosh\theta_2]$$
$$+{z_0}^2\frac{f}{f_0}[\theta_1'\sin\theta_1\cosh\theta_2 - \theta_2'\cos\theta_1\sinh\theta_2]$$
$$+\lambda a_i[\theta_1'\cos\theta_1\sinh\theta_2 + \theta_2'\sin\theta_1\cosh\theta_2]$$

where

$$\theta_j' = \frac{1}{2\theta_j}\frac{1}{\sqrt{(\lambda\, a_i)^2 + {z_0}^4\left(\frac{f}{f_0}\right)^2}}\,{z_0}^4\left(\frac{f}{f_0}\right), \quad j = 1,2$$

c) Adjust

$$\left(\frac{f}{f_0}\right)_{k+1} = \left(\frac{f}{f_0}\right)_k - \frac{H\left[\left(\frac{f}{f_0}\right)_k\right]}{H'\left[\left(\frac{f}{f_0}\right)_k\right]}$$

d) Repeat Step a) to Step c) with the new value $(f/f_0)_{k+1}$ until H is sufficiently close to 0.

In this manner, a table of $\frac{f-f_0}{f_0}$ can be constructed over ±30 g every $\Delta a_i = 0.01\,g$, for example.

E.4.2 Least-squares fit

Let y_k be tabular point k in the table at acceleration level $a_{\mathrm{i},k}$. Do a least-squares fit to the data in this table to determine the coefficients K_n in the model

$$y_k = \sum_{n=1}^{9} \frac{K_n}{f_0} a_{\mathrm{i},k}^n \tag{E.72}$$

where the coefficient estimates are such that

$$\sum_{k=1}^{N} [y_k - \mathrm{model}]^2 = \mathrm{minimum} \tag{E.73}$$

From these coefficient estimates, the b_n coefficients are calculated using Equation (E.28).

The standard least-squares maximum likelihood fitting algorithm also gives the uncertainties of the coefficient estimates based on the root-mean-square (rms) of the postfit residuals to the data.

E.5 Comparison of fit coefficients and square-root Taylor coefficients

The b_n coefficients [Equation (E.28)] with the K_1/f_0 ratio in Equation (E.66) are given in Table E.2 for the Taylor series coefficients for the square-root model and for the least-squares fit coefficients for the square root and force versus frequency models. The rms and maximum of the residuals over the ±30 *g* fit interval every 0.01 *g* are also given in each case.

The coefficient uncertainties are for the least-squares fit to the force-versus-frequency model. The uncertainties for the fit to the square-root model are slightly less. The b_1 coefficient should be 1; the fit estimates differ from the value 1 by slightly more than 1 standard deviation.

The square-root model using Taylor series coefficients has a larger rms postfit residual than does the same model using the least-squares fit coefficients, although only slight differences exist between the two sets of coefficients.

The least-squares fit coefficients to the force-versus-frequency model differ significantly from those in the square-root model. The latter set of b_n coefficients should better represent the quartz resonator model, if the resonator truly has fixed–fixed boundary conditions and if the other assumptions used in deriving the force versus frequency table are valid.

For the assumed value in Equation (E.66), the K_2/K_1 coefficient in the square root model is $-1500\ \mu g/g^2$, whereas in the force-versus-frequency model, it is $-1649\ \mu g/g^2$. The comparison for K_3/K_1 is $4.5\ \mu g/g^3$ versus $5.14\ \mu g/g^3$, and so on. The two models differ in acceleration prediction by $144\ \mu g$ at 1 *g* and by 9.96 mg at 10 *g*. Taking the 0.5-weighted difference of anti-parallel resonator acceleration measurements lowers this discrepancy. For instance, if the two resonator bias frequencies differed by 1.5% (so no frequency overlap is less than 5 *g*) and the scale factors also differed by 1.5%, then the worst-case discrepancy would be $2.2\ \mu g$ at 1 *g* and 0.15 m*g* at 10 *g*.

Table E.2—Nonlinear coefficient scaling predicted by square-root model and least-squares fit to square root and force versus frequency models over ±30 g with $\frac{K_1}{f_0} = 3 \times 10^{-3}\ g^{-1}$

Coefficient	Square root	Least-squares fit		Uncertainty
		Square root	Force versus frequency	
b_1	1.0000000	0.9999999999972	0.9999999999983	1.5×10^{-12}
b_2	–0.5000000	–0.499999997618	–0.549839111238	3.4×10^{-11}
b_3	0.5000000	0.50000000132	0.5709369961	2.1×10^{-9}
b_4	–0.6250000	–0.6250030524	–0.732040391	2.4×10^{-8}
b_5	0.8750000	0.875002649	1.05078465	9.2×10^{-7}
b_6	–1.3125000	–1.31129552	–1.6169395	5.4×10^{-6}
b_7	2.0625000	2.0608760	2.612723	1.6×10^{-4}
b_8	–3.3515625	–3.536606	–4.63058	3.7×10^{-4}
b_9	5.5859375	5.87939	7.9490	9.1×10^{-3}
f/f_0 rms		7.49×10^{-11}	4.79×10^{-13}	6.63×10^{-13}
f/f_0 max		3.92×10^{-10}	2.60×10^{-12}	3.53×10^{-12}

Annex F

(informative)

Micromechanical accelerometers

F.1 Micromachining

Silicon micromechanical accelerometers are fabricated by the photolithographic and chemical etching process used in the integrated circuit industry. The micromechanical sensor, or micro electro mechanical systems (MEMS), manufacturing process is an extension beyond the conventional silicon microelectronic circuit technology in that the integrated circuit (IC) chip batch fabrication methods are used to build miniature mechanical structures. Typical microsensors have active areas on the order of 0.1 mm^2 to 10 mm^2.

Microfabrication is also applicable to quartz wafer processing to create miniature vibrating beam accelerometers (VBAs) as well as the quartz resonators used in macro-sized VBAs. Since VBAs are discussed in Annex D, only silicon accelerometers will be discussed here.

Chemicals that etch doped or undoped silicon isotropically and anisotropically exist, and undercut structures can be etched. Micromechanical structures can be made from chemically vapor-deposited poly (or amorphous) silicon and from crystalline silicon.

Silicon bonds to silicon and to low expansion glass, allowing assembly of diverse piece parts. The conductivity of silicon allows electrostatic devices. Proximity electronic components and circuits can be created on the same silicon wafer as the sensing device.

An open-loop silicon micromechanical accelerometer can sense proof-mass displacement piezoelectrically, piezoresistively, or electrostatically. Piezoelectric sensing of the strain in the proof-mass support restricts measurement to ac (above about 5 Hz) rather than to dc inputs because of leakage of the piezoelectric generated charge and, therefore, will not be considered.

Open-loop piezoresistive silicon micromechanical accelerometers are first described. Then electrostatically sensed open-loop and electrostatically driven closed-loop silicon micromechanical accelerometers are discussed. Finally, electrostatically driven silicon (replacing piezoelectrically driven quartz) VBAs are discussed.

F.2 Micromachined silicon accelerometer—flexured-mass configurations

F.2.1 Design features of the piezoresistive flexured-mass accelerometer

Figure F.1 is a conceptual drawing of an open-loop pendulous piezoresistive accelerometer. The piezoresistive element on the silicon proof-mass flexure is created with appropriate doping. For a translational proof-mass design, the piezoresistive element would be on the translational proof-mass support. The structure around the proof mass provides stops for proof-mass displacement.

The resistance to current flowing through the piezoresistive element varies with the strain of the proof-mass flexure or support caused by acceleration along input axis (IA), so the amount of current flow for a constant voltage is the measure of acceleration. Piezoresistive sensing of proof-mass displacement has higher temperature sensitivity than does electrostatic sensing.

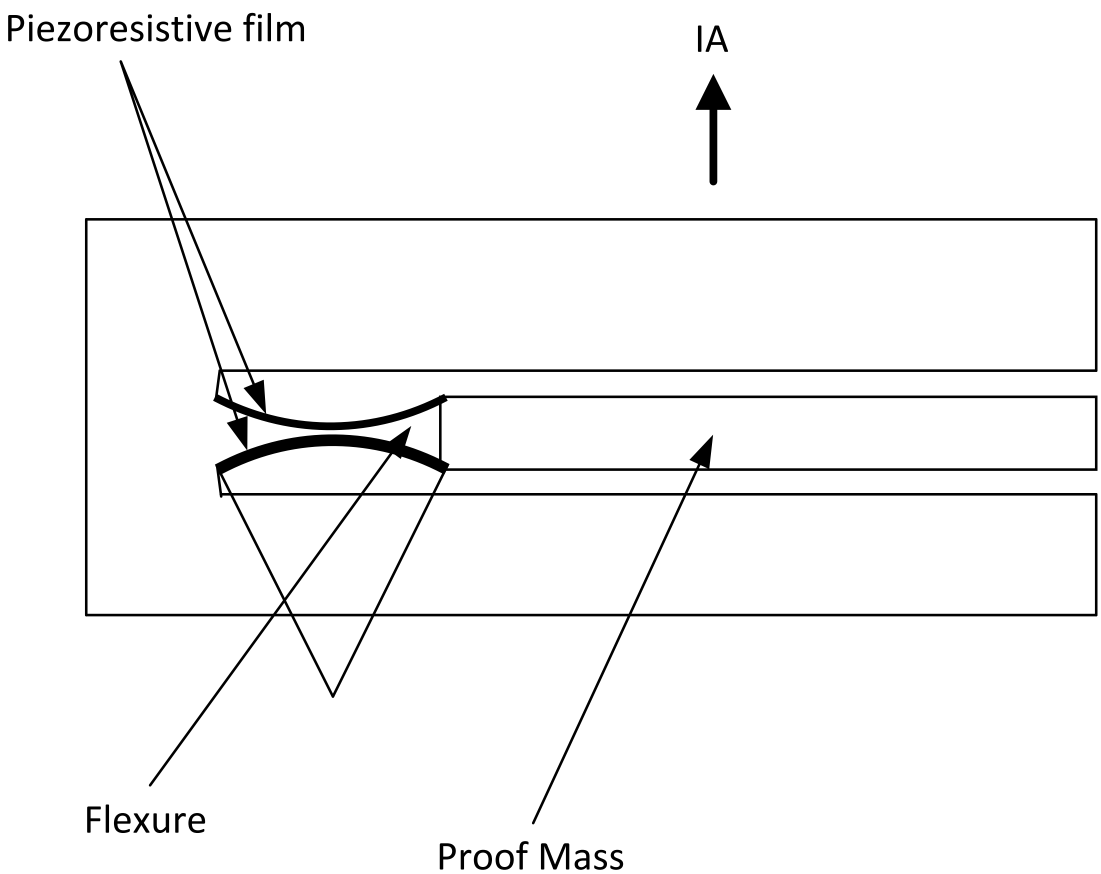

Figure F.1—Flexured-pendulous-mass accelerometer with piezoresistive sensing of proof-mass displacement

F.2.2 Design features of the capacitive pickoff and forcer flexured-mass accelerometer

Design architectures commonly used in electrostatically or capacitively forced and/or sensed silicon micromechanical accelerometers have the proof mass supported via a set of compliant flexures between or above reference electrodes plated on case-fixed substrates. Input acceleration rotates or translates the proof mass causing an air-gap change that is proportional to acceleration. The case-fixed substrates provide stops for proof-mass movement as well as support for the electrodes.

Usually two case-fixed, position-sensing pickoff electrodes are employed to furnish a differential measurement of the proof-mass deflection for open- or closed-loop operation. In closed-loop operation, two additional forcer or torquer electrodes are also required, or the forcer/torquer and pickoff electrodes could be combined into one pair. Four generic flexured-mass capacitive micromechanical accelerometer configurations are shown in Figure F.2a through Figure F.2d.

a) In Figure F.2a, the pendulous proof mass is sandwiched between the two pickoff capacitor plates so that the top air gap opens while the bottom gap closes under acceleration in the +IA direction. As depicted, the torquer electrodes have little mechanical advantage, but this and the other figures are only conceptual drawings. The electrodes could be plated on Pyrex glass anodically bonded to the rest of the silicon structure, or the whole structure could be poly or single crystal silicon.
b) In Figure F.2b, the proof mass is supported so that it translates on its flexure supports under acceleration to open and close the gaps with the top and bottom pickoff capacitor plates, rather than rotating as in Figure F.2a and Figure F.2d.
c) In Figure F.2c, the proof mass is supported so that it translates on its flexure supports under acceleration to vary the gaps with many more comb capacitor plates than are shown in the figure.

The gaps vary side to side rather than vary in and out as in Figure F.6. Figure F.2c depicts an open-loop accelerometer with sensing provided by appropriate wiring of the silicon proof mass and silicon fixed combs (see F.2.3). A support other than the folded flexure depicted in Figure F.2c could be used for a translational proof-mass accelerometer with comb capacitor plates.

d) In Figure F.2d, the proof mass is supported as a teeter-totter on a pair of torsional flexures above an electrode plane. It is mounted off-center to introduce pendulosity for sensitivity to acceleration along the IA. The gaps with the two case-fixed pickoff capacitor electrodes in the same plane on either side of the flexure axis open and close under acceleration.

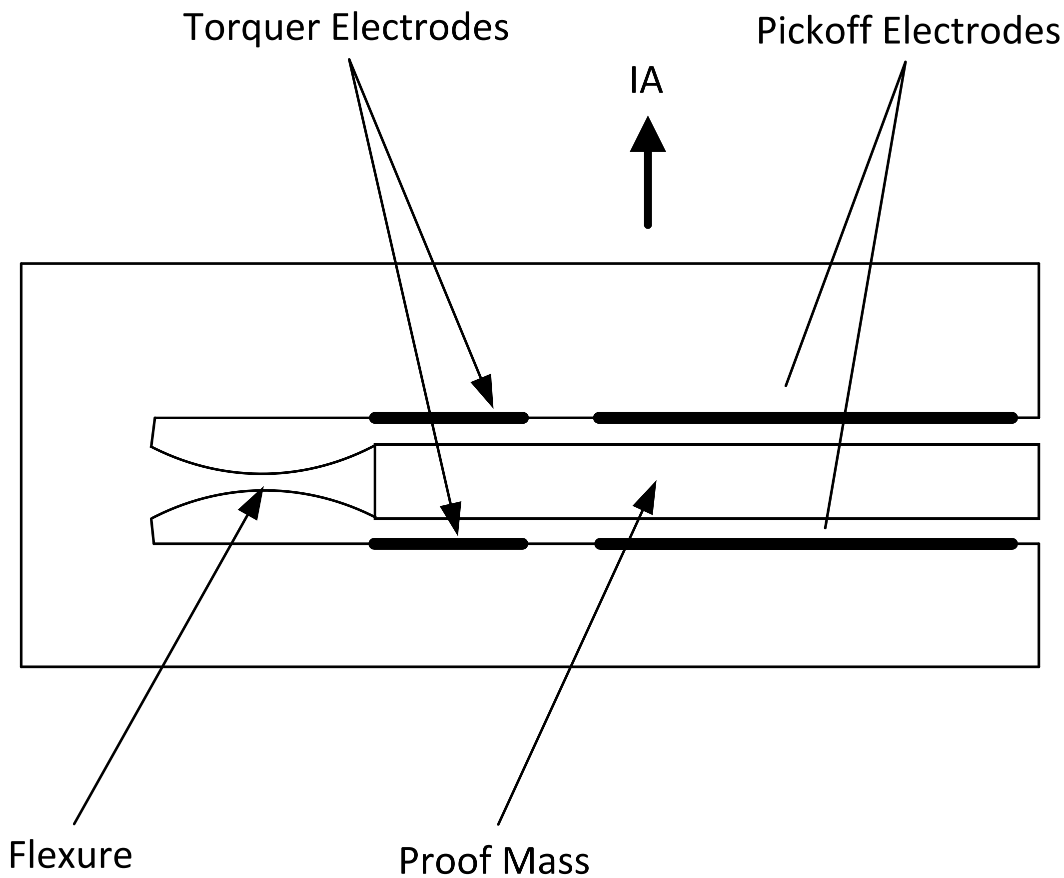

Figure F.2a—Flexured-pendulous-mass accelerometer with top and bottom electrodes

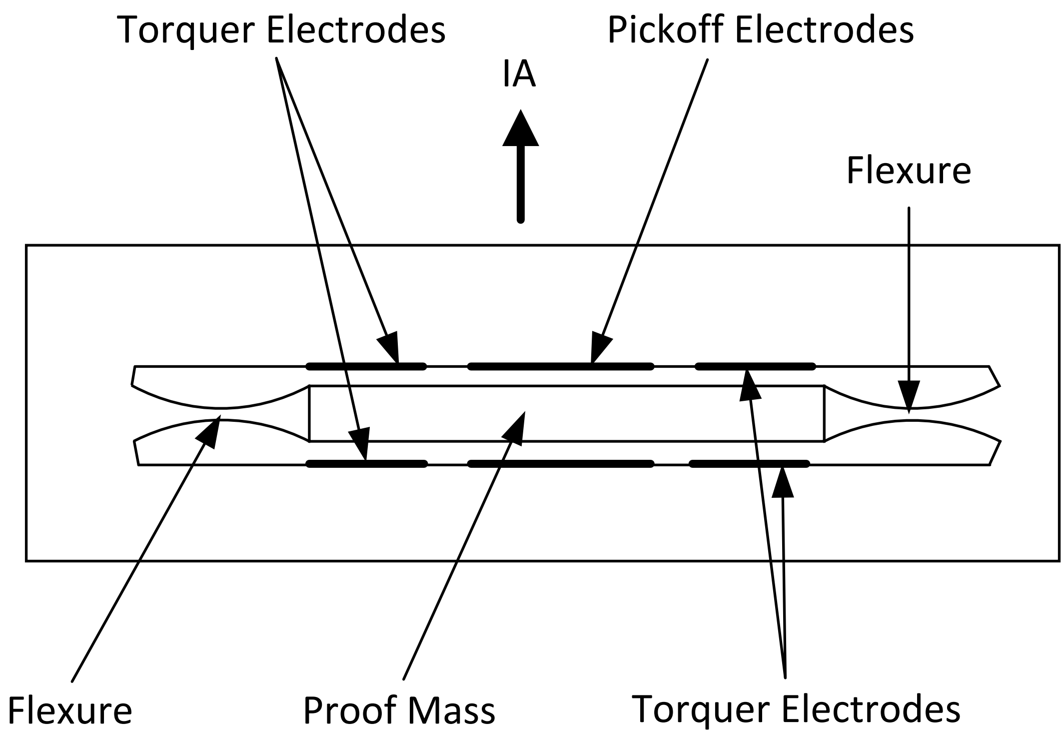

Figure F.2b—Flexured-translational-mass accelerometer with top and bottom electrodes

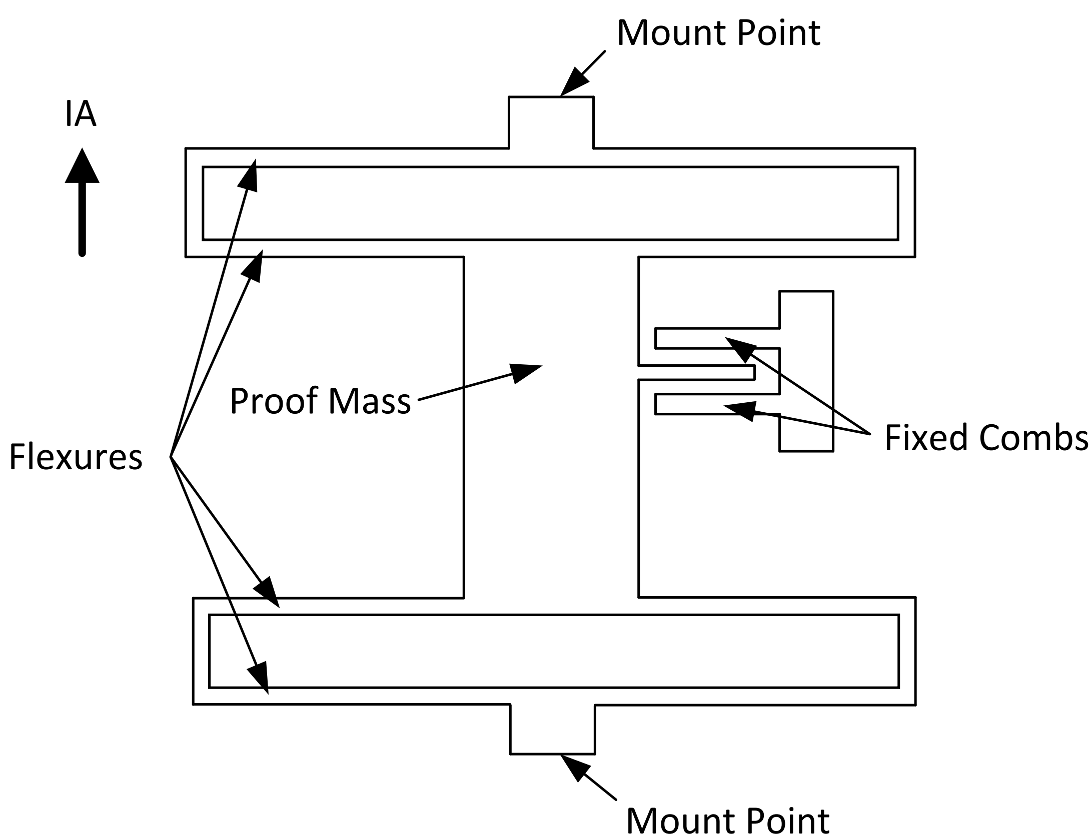

Figure F.2c—Flexured-translational-mass accelerometer with comb electrodes

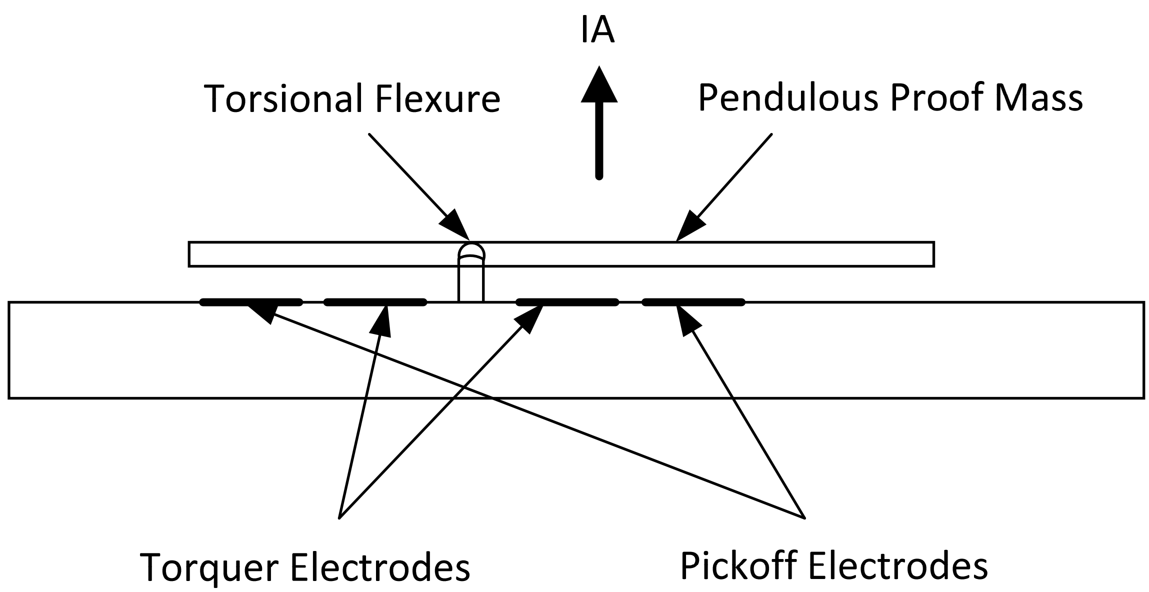

Figure F.2d—Flexured-mass-accelerometer—Teeter-totter configuration

F.2.3 Circuit diagrams for capacitive sensing and forcing

Figure F.3 shows an electrical schematic of a closed-loop micromechanical accelerometer. For notation, see Equation (F.5), Equation (F.7), and Equation (F.19).

The pickoff electrodes are excited with an ac voltage; the two plates are excited out of phase to get a differential measurement. Under proof-mass rotation, the capacitance between the proof mass and pickoff electrodes is unbalanced, and current flows through the proof-mass flexure into a pre-amplifier. The pre-amp output is demodulated and passed through a low-pass filter. The resulting dc voltage signal is proportional to the proof-mass angle and, hence, to the input acceleration.

The schematic also shows servo loop blocks for torque rebalance of the proof mass using torquer electrodes.

F.2.4 Open-loop operation

The variation in capacitor gaps in an open-loop teeter-totter implementation using the differential readout is shown in Figure F.4, where input axis (*IA), pendulous axis* (*PA),* and *flexure axis (FA) = –out put axis (OA)* are the input, pendulous, and flexure (or negative output) axes, respectively, with the convention that *IA* × *PA* = –*FA*. The signal generator differential capacitance change for this or any of the configurations in Figure F.2a to Figure F.2d is given by

$$\Delta C = C^{+} - C^{-} = \frac{\varepsilon_0 A}{h^{+}} - \frac{\varepsilon_0 A}{h^{-}} \qquad \text{(F.1)}$$

where

ε_0	is the permittivity of air or enclosure gas (8.85×10^{-12} *F/m)*
A	is the pickoff electrode area (one plate)
h^{+}	is the positive pickoff gap
h^{-}	is the negative pickoff gap

Designating the displacement of the rigid plate as Δh, the two capacitance gaps can be written as $h + \Delta h$ and $h - \Delta h$, or

$$\Delta C = \frac{\varepsilon_0 A}{h\left(1+\frac{\Delta h}{h}\right)} - \frac{\varepsilon_0 A}{h\left(1-\frac{\Delta h}{h}\right)} \qquad \text{(F.2)}$$

Expanding the two denominators in a Taylor series expansion and subtracting the plus and minus signals gives the pickoff output as

$$\Delta C = -2C_{\text{pick}}\left[\frac{\Delta \text{h}}{\text{h}} + \left(\frac{\Delta \text{h}}{\text{h}}\right)^3 + \left(\frac{\Delta \text{h}}{\text{h}}\right)^5 + \ \ldots\right] \qquad \text{(F.3)}$$

where

$C_{\text{pick}} = \varepsilon_0 A/h$ is the nominal pickoff capacitance (one plate)

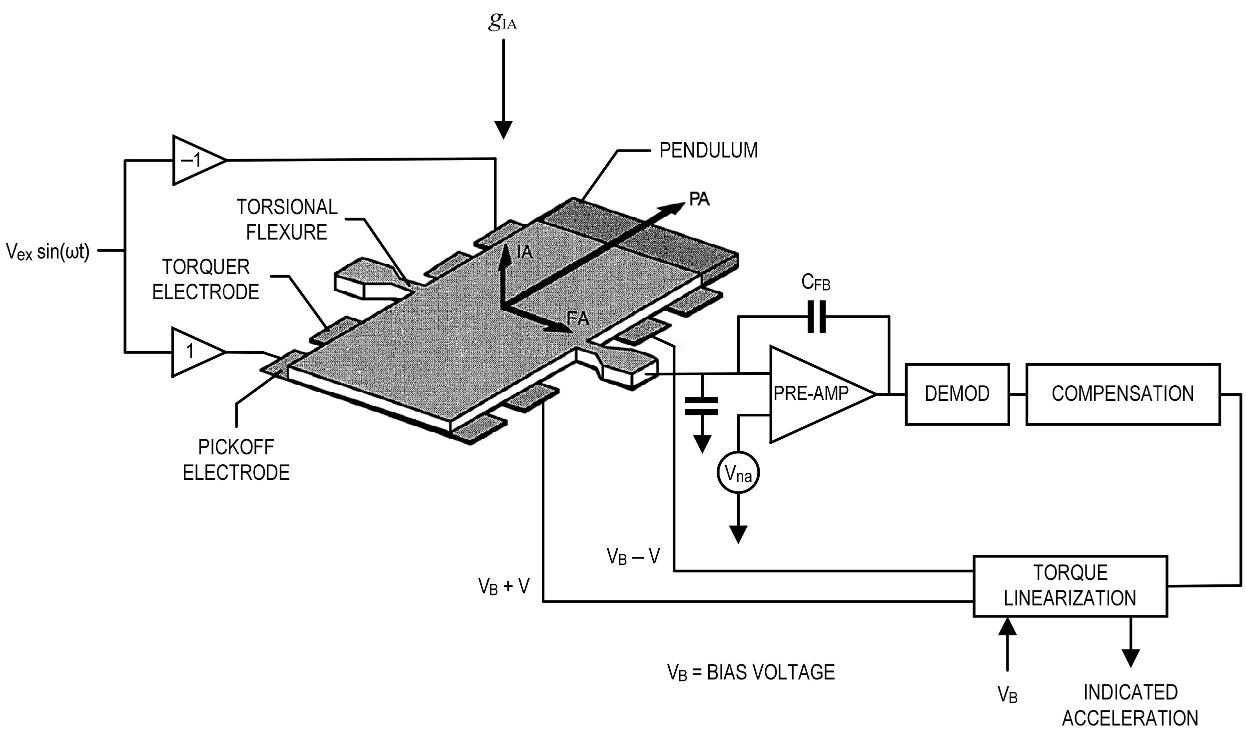

Figure F.3—Circuit diagrams for capacitive sensing and forcing—Teeter-totter configuration

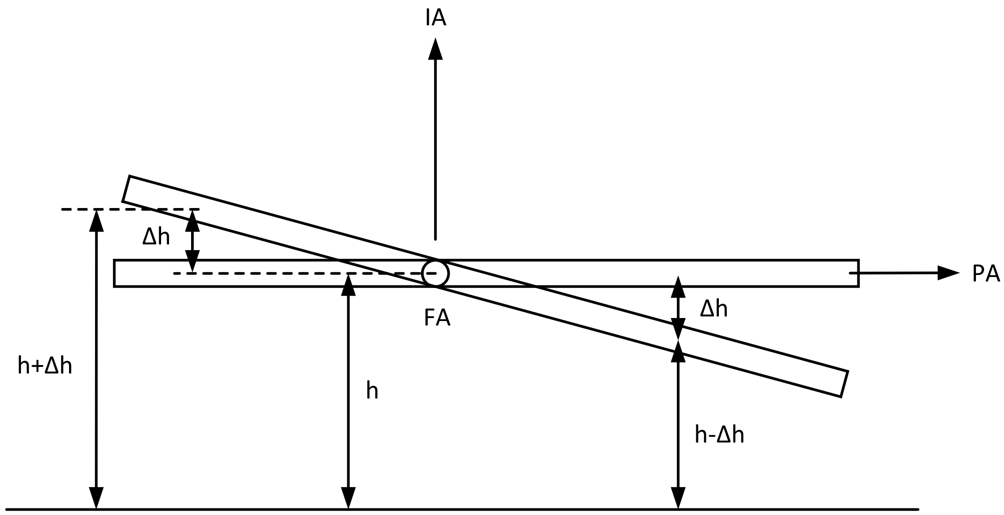

Figure F.4—Variation in capacitor gaps in teeter-totter open-loop operation

This pickoff output signal is nonlinear in the gap change Δh, and Δh is proportional to acceleration a_i along the IA

$$\Delta h = -K_h\, a_\mathrm{i} \tag{F.4}$$

where K_h is pendulosity divided by flexure stiffness for a rotational proof mass or mass divided by flexure stiffness for a translational proof mass, with appropriate unit changes to allow a_i to be in g. Thus, the pickoff output signal has a linear g term and higher order g^3, g^5, and so on, terms.

The output pre-amp converts the capacitance change into a voltage proportional to the proof-mass position, which is in turn proportional to input acceleration. The pre-amp output passes through an ac gain stage, is demodulated, and is low-pass-filtered to give the final indicated acceleration output as a dc voltage. The pre-amplifier output voltage is related to the pickoff capacitance change by

$$V_\mathrm{o} = V_\mathrm{ex}\left(\frac{\Delta C}{C_{FB}}\right) \tag{F.5}$$

where

V_o	is the pre-amp output voltage
V_ex	is the pre-amp ac excitation voltage amplitude
ΔC	is the pickoff capacitance change
C_FB	is the pre-amp feedback capacitance

F.2.5 Closed-loop operation

A closed-loop operation can also be employed to force-rebalance the proof mass under the action of applied input acceleration. In this case, the force or torque loop holds the proof mass at a null position; the force or torque signal is proportional to acceleration.

For electrostatic forcing or torquing, the applied net force or torque from a pair of electrodes is given by

$$T = \frac{\varepsilon_0 A (V_1^2 - V_2^2)d}{2h^2} \tag{F.6}$$

where

ε_0	is the permittivity of air (8.85×10^{-12} F/m)
A	is the forcer or torquer capacitor area
V_1	is the left forcer or torquer voltage
V_2	is the right forcer or torquer voltage
h	is the air gap
d	is $\begin{cases} \text{torquer lever arm if a pendulous design} \\ \text{1 if a translational proof mass design} \end{cases}$

Equation (F.6) indicates that the applied force or torque is proportional to the square of the applied voltage. The forcing or torquing action can be linearized by applying a dc bias voltage to both forcer or torquer plates; that is,

$$V_1 = V_\mathrm{B} + V$$

$$V_2 = V_\mathrm{B} - V$$

In this case, the net force or torque is given by

$$T = 2\, C_\mathrm{torq}\, \frac{d}{h} V_B V \tag{F.7}$$

where

C_torq	is the forcer or torquer capacitance = $\varepsilon_0 A\, /\, h$
V_B	is the forcer or torquer bias voltage
V	is the applied differential forcer or torquer voltage

The forcer or torquer scale factor is proportional to the bias voltage. Hence, the stability of the forcer or torquer bias voltage directly affects the accelerometer scale-factor stability.

F.2.6 Scale-factor, bias, and second-order nonlinearity

F.2.6.1 Open-loop operation

Equation (F.3) and Equation (F.4) indicate that the accelerometer output is nonlinear for open-loop operation. The magnitude of the nonlinearity depends on the excursion of the proof mass under maximum acceleration. Equation (F.4) also indicates that the open-loop nonlinearity has only odd orders of acceleration (i.e., 3rd, 5th, etc.). Side-to-side mismatch of the pickoff capacitor areas introduces even order terms to the pickoff output, most significantly a second-order, or g/g^2 term, as well as a bias term.

Consider the following model equation for the output voltage V_o of an open-loop micromechanical accelerometer:

$$V_\mathrm{o} = K_{0,\mathrm{open}} + K_{1,\mathrm{open}}\, a_\mathrm{i} + K_{2,\mathrm{open}}\, a_\mathrm{i}^2 + \cdots \quad \mathrm{V} \tag{F.8}$$

From Equation (F.8) and Equation (F.4), the open-loop linear scale factor is given by

$$K_{1,\mathrm{open}} = 2\, C_\mathrm{pick} \frac{K_h}{h} \quad \mathrm{V}/g \tag{F.9}$$

By introducing a dimensionless area mismatch parameter ε, Equation (F.3) can be modified to show that the bias is

$$K_{0,\mathrm{open}} = \varepsilon C_\mathrm{pick} \quad \mathrm{V} \tag{F.10}$$

and the second-order term is

$$K_{2,\text{open}} = \varepsilon\, C_{\text{pick}} \left[\frac{K_h}{h}\right]^2 \qquad \text{V}/g^2 \tag{F.11}$$

or in terms of the maximum design acceleration g_{max}

$$\frac{K_{2,\text{open}}}{K_{1,\text{open}}} = \frac{\varepsilon}{2g_{\text{max}}} \left[\frac{\Delta h}{h}\right]_{\text{max}} \qquad g/g^2 \tag{F.12}$$

F.2.6.2 Closed-loop operation

Using model Equation (F.8) for $V_{\text{o}} = V$ with closed-loop instead of open-loop parameters, the closed-loop linear forcer or torquer scale factor is given from (F.7) with $T = Pa_{\text{i}}$, as

$$K_{1,\text{closed}} = \frac{P}{2\, C_{\text{torq}} \frac{d}{h} V_{\text{B}}} \qquad \text{V}/g \tag{F.13}$$

where

P is the pendulosity of rotational proof mass or mass of translational proof mass acted on by acceleration in g

Area mismatch between torquers also introduces a bias and second-order nonlinearity, which from Equation (F.7) are given by

$$K_{0,\text{closed}} = \frac{\varepsilon\, V_B}{4\, C_{\text{torq}} \frac{d}{h}} \qquad \text{V} \tag{F.14}$$

$$K_{2,\text{closed}} = \frac{\varepsilon\, K_{1,\text{closed}}{}^2}{4\, V_{\text{B}}} \qquad \text{V}/g^2 \tag{F.15}$$

or in terms of the maximum design acceleration g_{max} for restoring voltage $V = V_{\text{B}}$

$$\frac{K_{2,\text{closed}}}{K_{1,\text{closed}}} = \frac{\varepsilon}{4g_{\text{max}}} \qquad g/g^2 \tag{F.16}$$

F.2.7 Performance considerations

The error mechanisms affecting the performance of silicon microfabricated accelerometers fall into the general categories of

— Sensitivities/stability of accelerometer dimensions
— Sensitivities/stability of electronics

As is typical of inertial sensors, thermal effects are a primary driver of these general error sources.

Equation (F.5) can be generalized to

$$V_0 = \frac{-V_1 C_1 + V_2\, C_2}{C_{\text{FB}}} \tag{F.17}$$

where

V_{o} is the pickoff pre-amp output voltage
C_1 is the nominal value of left pickoff capacitance

C_2	is the nominal value of right pickoff capacitance
V_1	is the left pickoff excitation voltage
V_2	is the right pickoff excitation voltage
C_{FB}	is the pre-amp feedback capacitance

The sensitivity of the accelerometer output to common-mode thermal expansion of the pickoff capacitance can be trimmed to null by adjusting the left and right pickoff excitation voltages so that $C_1V_1 = C_2V_2$. It is instructive to look at the case where the pickoff capacitances are mismatched and the pickoff excitations are not trimmed, so that $V_1 = V_2 = V_{EX}$. In this case, the sensitivity to temperature can be estimated by simplifying Equation (F.17) to

$$\frac{\Delta a_{\mathrm{i}}}{\Delta T} = \frac{V_{\mathrm{EX}}(C_1 - C_2)}{K_{1,\mathrm{open}} C_{\mathrm{FB}}} \frac{\Delta C/C}{\Delta T} \tag{F.18}$$

where

Δa_i	is the change in sensed acceleration along the IA due to temperature change ΔT
$K_{1,open}$	is the accelerometer open-loop scale factor (V/g)
C_1	is the nominal value of left pickoff capacitance
C_2	is the nominal value of right pickoff capacitance
$\Delta C/C/\Delta T$	is the nominal capacitance gap temperature sensitivity

The difference between the nominal left and right capacitances produces a nonzero accelerometer bias. Assuming that the accelerometer is operating under this bias residual, the bias temperature sensitivity is simply the nominal bias value times the $\Delta C/C/\Delta T$ capacitance sensitivity.

The $\Delta C/C/\Delta T$ term can be used generically to represent errors from both mechanical capacitance gap instability and electrical instability. Hence, the net accelerometer bias error described by Equation (F.18) is a combination of thermal expansion effects and electrical effects, such as pickoff pre-amplifier gain sensitivity or pickoff excitation voltage sensitivity.

The thermal sensitivities discussed earlier are typically the predominant bias stability sensitivities in micro accelerometers. Scale-factor temperature sensitivity generally is governed by a lumped effect of the electronics (e.g., pickoff pre-amp gain) sensitivity and the mechanical sensitivity of the proof-mass elastic restraint. The −100 ppm/°C sensitivity of the Young's modulus of silicon is one of the contributors to accelerometer scale-factor sensitivity.

The accelerometer signal-to-noise ratio, or acceleration resolution capability, is limited by the noise floor of the pickoff pre-amplifier (and forcer or torquer readout if closed loop) and Brownian motion of the accelerometer proof-mass ambient atmosphere. The root-mean-square (rms) noise equivalent acceleration of pickoff noise is given by

$$G_{rms} = \frac{1}{Pg\left(\frac{\Delta C}{\Delta g}\right)} V_{\mathrm{na}} \left(\frac{C_{\mathrm{N}}}{V_{\mathrm{ex}}}\right) \left\{ f \left[K_{\theta}^2 + \frac{1}{3}(2\pi f)^2 (D^2 - 2K_{\theta} I) + \frac{1}{5}(2\pi f)^4 I^2 \right] \right\}^{\frac{1}{2}} \tag{F.19}$$

where

G_{rms}	is the rms resolution (g, 1 g = 9.8 m/s^2)
$\Delta C/\Delta g$	is the open-loop scale factor (F/g)
V_{na}	is the pre-amp white noise square root PSD level (V/$\sqrt{\mathrm{Hz}}$ single-sided)
C_N	is the input node capacitance (F)
V_{ex}	is the pickoff excitation voltage (V)
f	is the frequency bandwidth (Hz)
D	is the proof-mass damping (N·m·s for a rotational proof mass or N·s/m for a translational proof mass)
K_θ	is flexure spring constant (N·m/rad for a rotational proof mass or N/m for a translational proof mass)

I	is the rotational proof-mass inertia (kg·m^2) or translational proof mass (kg)
P	is the rotational proof-mass pendulosity (kg·m) or translational proof mass (kg)

Brownian motion is a white noise process, whose power spectral density (PSD) is given by

$$G = \frac{1}{Pg}\sqrt{4\,\kappa\, DT} \tag{F.20}$$

where

G	is the acceleration white noise square root PSD level ($g/\sqrt{\text{Hz}}$ single-sided)
P	is the rotational proof-mass pendulosity (kg·m) or translational proof mass (kg)
g	is the 9.8 m/s^2 (approximate value of local acceleration due to gravity)
κ	is Boltzman's constant (1.38×10^{-23} N·m/K),
D	is proof-mass damping (N·m·s for a rotational proof mass or N·s/m for a translational proof mass)
T	is the absolute temperature (K)

Brownian motion is usually not a significant effect unless the proof-mass inertia were very small or the damping very high. Damping can be controlled by ventilating the proof mass or operating at reduced ambient pressure.

Torque generator readout noise is also a white noise process. The following equation can be used to project resolution over the frequency band of interest:

$$G = \frac{V_\text{n}}{K_\text{torq}} \tag{F.21}$$

where

G	is the acceleration white noise square root PSD level ($g/\sqrt{\text{Hz}}$ single-sided)
V_n	is the forcer or torquer readout white noise square root PSD level (V/$\sqrt{\text{Hz}}$ single-sided)
K_torq	is the forcer or torquer scale factor (V/g)

F.3 Micromachined silicon VBAs

F.3.1 Design features

The familiar VBA uses the frequency shift from applied load in vibrating elements to detect acceleration. Many manufacturers have developed VBAs based on quartz resonators, which are excited via the piezoelectric effect by applying the proper waveform through electrodes on the resonator surface (see Annex D).

Typically a self-oscillator drive loop is employed to excite the natural frequency of the resonator. To first order, the frequency sensitivity of the resonator to acceleration loading is given by

$$f = \sqrt{\frac{2}{m}\left(\frac{12EI}{L^3} + \frac{6P}{5L}\right)} \tag{F.22}$$

where

f	is the resonator frequency
m	is the resonator mass
E	is Young's modulus
I	is the resonator beam inertia
L	is the resonator beam length
P	is the load applied to the resonator

The emergence of the silicon microfabrication technology has initiated development of silicon-based VBAs. The elastic stability of silicon makes it an attractive material for use in a precision VBA. In contrast to quartz, a silicon VBA requires capacitive forcing and sensing to actuate and readout the resonator frequencies.

Possible configurations for a silicon VBA include ribbon resonators that are driven by electrodes either above or below on an adjacent substrate (Figure F.5) or beam resonators that use a lateral comb drive actuator (Figure F.6).

F.3.2 Drive force and position sensing

For a ribbon resonator, the electrostatically applied drive force and position sensing equations are essentially the same as the force and sense relationships for a flexure-supported, proof-mass accelerometer. The difference here is that the drive force is applied via a combination of a dc bias and an ac drive signal at the resonator natural frequency to sustain oscillation. To maximize the drive force and to improve accelerometer sensitivity, the resonator is designed to have a high *Q* at its natural frequency. For a silicon resonator, high *Q* is generally achieved by operating at reduced ambient pressures.

Comb drive resonators use the same principle of combining dc bias and an ac drive signal for force actuation. However, the comb actuators feature a sliding face capacitance sensitivity, rather than the closing gap relationship in ribbon resonators.

The capacitance across a set of engaged comb drive fingers is given by

$$C = 2\,N\,\alpha\,\varepsilon_0\,\frac{w}{h}\,L \tag{F.23}$$

where

C	is the capacitance
ε_0	is the permittivity of air (8.85×10^{-12} F/m)
N	is the number of teeth per side
α	is the fringing factor (≈1.5)
w	is the comb finger thickness
h	is the air gap between fingers
L	is the engaged length of fingers

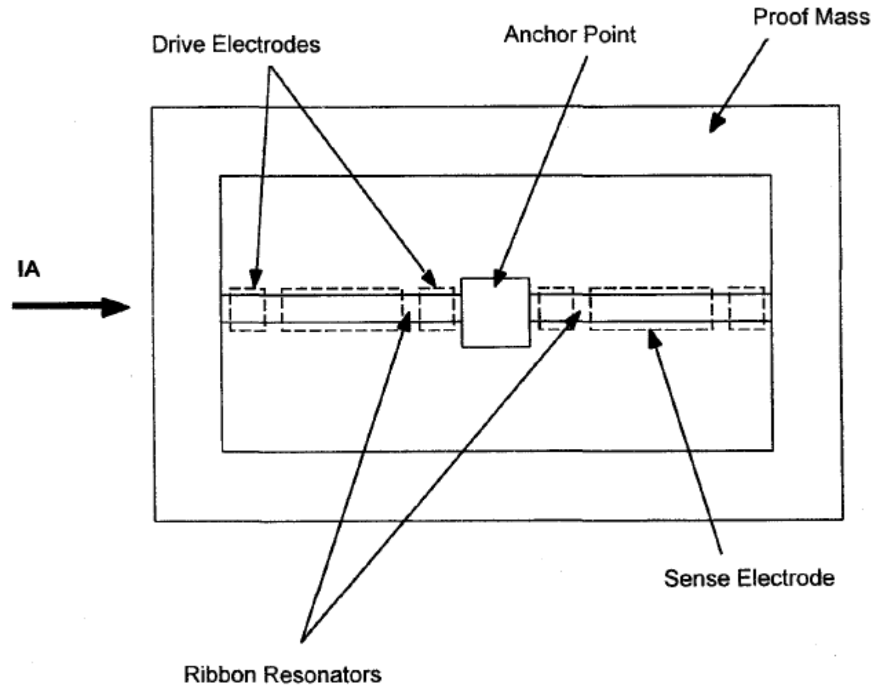

Figure F.5—Ribbon silicon VBA

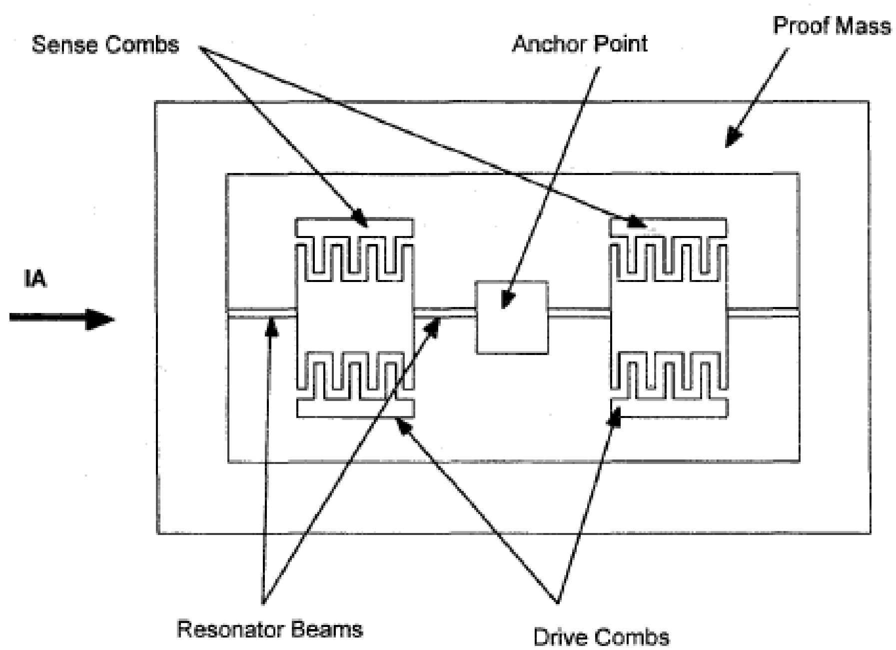

Figure F.6—Comb drive silicon VBA

The capacitance sensitivity to position (i.e., engaged length) is given by

$$\frac{dC}{dx} = 2\,N\,\alpha\,\varepsilon_0\,\frac{w}{h} \tag{F.24}$$

where

$\frac{dC}{dx}$ is the capacitance sensitivity to position

The drive force is given by

$$F_{\mathrm{D}} = 4\,N\,\alpha\,\varepsilon_0\,\frac{w}{h}\,V_{\mathrm{B}}\,V_{\mathrm{D}} \tag{F.25}$$

where

F_{D} is the drive force
V_{B} is the comb drive bias voltage
V_{D} is the applied drive voltage

F.3.3 Oscillator drive loop

In either the ribbon or the comb drive configurations, a self-oscillator drive loop is used to track the resonant frequency shift with acceleration. The high Q of the resonator furnishes a large electric phase sensitivity to frequency change. At resonance the phase angle sensitivity to frequency change is given by

$$\Delta\phi = 2\,Q\,\frac{\Delta f}{f} \tag{F.26}$$

where

$\Delta\phi$ is the phase change
Δf is the frequency shift
f is the nominal resonant frequency
Q is the resonator quality factor

Hence, a high Q resonator produces a large electric phase sensitivity to small changes in the nominal resonant frequency.

F.3.4 Error mechanisms

Two primary error mechanisms in silicon VBAs are frequency shift sensitivities to

— Temperature
— Drive amplitude instability

The VBA thermal sensitivity is the combined effect of thermal expansion strains loading the resonator and the Young's modulus sensitivity of silicon (−100 ppm/°C) changing the resonator stiffness. Since frequency is proportional to the square root of stiffness, the net effect of the silicon modulus is −50 ppm/°C of frequency change with temperature.

The axial load on a resonator element with temperature is given by

$$P = [\alpha_{\mathrm{si}}(T_{\mathrm{si}} - T_0) - \alpha_{\mathrm{sub}}(T_{\mathrm{sub}} - T_0)]\left(\frac{L_s}{L}\right) EA \tag{F.27}$$

where

P	is the axial load
α_{si}	is the temperature coefficient of expansion (TCE) of silicon
α_{sub}	is the TCE of the substrate
T_{si}	is the resonator temperature
T_{sub}	is the substrate temperature
T_0	is the initial temperature
E	is Young's modulus of silicon
A	is the resonator beam cross-sectional area
L	is the resonator length
L_s	is resonator mounting spacing

This sensitivity added to the Young's modulus sensitivity gives the net steady-state thermal sensitivity of a silicon VBA.

Automatic gain control is used to control the amplitude of the drive frequency. Drive amplitude control is essential because of the well-known nonlinear relationship between amplitude and resonant frequency for vibrating beams. Nonlinear perturbation analysis shows that the frequency amplitude relationship for a vibrating beam is given by

$$f = f_0\left[1 + \frac{3}{8}\frac{K_3}{K}x^2\right] \tag{F.28}$$

where

f	is the resonator frequency
f_0	is the resonator nominal frequency
K	is the linear stiffness of resonator beam
K_3	is the cubic stiffness coefficient of resonator beam
x	is the drive amplitude

At a given drive amplitude, the resonator frequency shifts above the nominal, "zero displacement" linear resonant frequency. The nominal shift in itself is not an error source, but variations in the drive amplitude are.

Annex G

(informative)

Outline of error sources in accelerometers

G.1 Introduction

This standard covers moderate- to high-precision accelerometers of the sort commonly associated with leveling or guidance and control. It specifically excludes super-precision gyroscopic sensors and low-precision vibration sensors (e.g., open-loop piezoelectric sensors having a bandpass, as opposed to low-pass, frequency response characteristic). Even with these limitations, the range of possibly significant sources of error is too large to treat in detail in an annex of practical size. The following outline is offered as a useful alternative.

G.2 Sensor characterization by mechanization

Sensors may be characterized by their mechanization as follows:

a) Proof-mass constraint
  1) Pendulous
    i) Metallic, fused or crystalline quartz, or silicon flexure hinge
    ii) Pivot and jewel hinge
    iii) Magnetic, gas film, or ceramic ball bearing
    iv) Taut band
    v) Gas, liquid, or servo phase lead damping on pendulum rotation degrees of freedom (DOF)
  2) Translational
    i) Parallelogram or compound (folded) flexures
    ii) Multiple DOF servo
      – Electrostatic
      – Superconducting magnetic levitation
  3) Floated
    i) Temperature controlled
    ii) Electromagnetic or electrostatic vernier for off-buoyancy
    iii) Pendulous rotation countered by additional DOF in servo
b) Operating mode
  1) Open loop
    i) Passive elastic restraint with separate proof-mass displacement pickoff
    ii) VBA, stress-sensitive resonator
      – Piezoelectrically driven quartz
      – Capacitively driven silicon
  2) Closed loop
    i) Electromagnetic force or torque to balance
    ii) Electrostatic force or torque to balance
    iii) Piezoelectric force [can be dc]
  3) Passive stops for overload protection in either case
c) Operating environment
  1) Instrument level
  2) System level

d) Proof-mass displacement pickoff
   1) Optical
   2) Capacitive
   3) Inductive
   4) Piezoresistive
   5) Laser interferometer
   6) Microwave
   7) Quantum tunneling
   8) Piezoelectric (however, not dc)
e) Readout
   1) Electromagnetic current or current pulse
   2) Electrostatic voltage or charge pulse
   3) VBA or microwave frequency output
   4) Superconducting magnetometer

G.3 Typical sensor characterization by manufacturing process

Sensors may be characterized by their manufacturing process as follows:

a) Macroscopic
   1) Electromagnetic torque rebalance
      i) Analog output
      ii) Digital output
         – Pulse rebalance
         – Analog with current-to-frequency, voltage-to-frequency, or analog-to-digital converter
   2) Vibrating beam accelerometer (VBA)
b) Micromachined
   1) Open loop
      i) Piezoresistive readout
      ii) Capacitive readout
      iii) Piezoelectric readout [ac > 5 Hz, not dc]
   2) Electrostatic force rebalance
      i) Analog output
      ii) Digital output
         – Pulse rebalance
         – Analog with current-to-frequency, voltage-to-frequency, or analog-to-digital converter
   3) Resonant structure accelerometer (RSA, includes silicon VBA)

G.4 Error categories

Errors may be stated in terms of a model equation, which is in the same form as in 8.3 but may include additional or different terms. Implementation of error coefficients and compensation depends on application requirements and other appropriate considerations. Modeled and unmodeled error categories may be grouped as follows:

a) Bias
   1) Magnitude
   2) Drift
   3) Thermal effects, including thermal hysteresis, gradients, and self-heating

   4) Case stresses, including mounting stresses
   5) Shift across environments and transient following environments
   6) Elastic restraint torque
   7) Special topics (e.g., pivot and jewel torques)
- b) Scale factor
   1) Magnitude
   2) Drift
   3) Aging
   4) Thermal effects, including thermal hysteresis, gradients, and self-heating
   5) Shift across environments and transient following environments
   6) Special topics (e.g., scale-factor rectification from cubic term in VBA)
- c) IA misalignment
   1) Magnitude
   2) Drift
   3) Thermal effects, including thermal hysteresis, gradients, and self-heating
   4) Shift across environments and transient following environments
   5) Remount repeatability
   6) Pivot flop
- d) Frequency response errors
   1) Amplitude and phase response
   2) Open-loop dynamics
   3) Closed-loop dynamics
   4) Squeeze film damping
   5) Second-order time lag (normal velocity storage)
- e) Input axis (IA) nonlinearity
   1) Rectification errors
   2) Static sources (e.g., magnetic effects, VBA frequency versus applied stress)
   3) Dynamic sources (e.g., gas film damping rectification)
- f) Nonlinearities in other axes
   1) Cross-coupling (e.g., K_{ip})
   2) Quadratic and cubic cross-axis sensitivity (e.g., K_{oo} and K_{ppp})
- g) Pendulous effects in rotating environments (see Annex C)
   1) Angular velocity and acceleration effects
   2) Size effect
- h) Noise sources
   1) Thermal (Brownian motion) noise associated with lossy elements
   2) Electronic noise
   3) Readout quantization and other measurement noise

G.5 Sensor physics

Physics effects that may influence the operation of the sensor include the following:

- a) Material effects
   1) Suspension compliances
   2) Elastic deflection of strain isolation elements

3) Case-mounting strain
4) S-bending of flat flexures (static and dynamic)
5) Anisoelastic effects
6) Anelastic, creep, and diffusion effects
7) Thermal hysteresis effects
8) Processing strains and stress relaxation
9) Aging

b) Magnetic effects
   1) Magnetic return path interactions
   2) Coil motions along IA through IA magnetic field gradients
   3) Deflections of flexure support structure through output axis (OA) and pendulous axis (PA) magnetic field gradients
   4) Permanent magnet thermal effects
   5) Magnet return path thermal effects
   6) External magnetic fields (ac or dc)
   7) Aging

c) Thermal effects
   1) Temperature effects on density, size, and elastic coefficients
   2) Thermal strains and thermal stresses
   3) Thermal gradients
   4) Self-heating effects

d) Damping effects
   1) Gas damping, including Bernoulli Law and compressibility effects
   2) Fluid damping, with thermal and density gradients, and non-Newtonian effects

e) Electrical effects
   1) Intentional and unintentional electrostatic torques and forces
   2) Stray impedances, especially with separate electronics

f) Dynamic effects
   1) Open-loop dynamics
   2) Servo dynamics
   3) Rectification errors
   4) Modal analysis and interactions
   5) Pendulum asymmetries
   6) Vibration power spectral density (PSD)
   7) Shock spectra
   8) Vibrating beam frequency equations

Part IV—Filtering, noise, and transient analyses

Annex H

(informative)

Digital filtering

H.1 Types of filtering and decimation

If the output of an inertial sensor is digitized for input to a computer, it is desirable to perform higher rate digital filtering on the data to reduce noise before doing lower rate navigation, guidance, or other computations.

If $x(n)$ is a digital word read by a computer (possibly a preprocessor before the final applications computer) at time $t(n)$, a causal finite-impulse-response (FIR) filter applied to the data stream has output $y(n)$ (see Rabiner and Gold [B45])

$$y(n) = \sum_{i=0}^{N} a_i \; x(n-i) \tag{H.1}$$

where the a_i are the filter weighting coefficients. If the array of weighting coefficients is symmetric about its midpoint, the FIR filter has linear phase; and the time tag associated with the output data point $y(n)$ is at time $t(n - N/2)$. If the sum of the weighting coefficients is not unity because of, for instance, using fixed-point computations, the output $y(n)$ could be divided by this sum in order to have unit gain through the filter.

A casual infinite-impulse-response (IIR) recursive filter applied to the data stream has the form (see Rabiner and Gold [B45])

$$y(n) = \sum_{i=0}^{N} a_i \; x(n-i) - \sum_{i=1}^{M} b_i \; y(n-i) \tag{H.2}$$

The behavior of an analog filter (using capacitors, inductors, etc.) can be emulated digitally with an IIR filter.

A properly chosen low-pass filter attenuates the higher frequency content (including noise content) of a data stream. Thus, if application computations are carried out at a lower rate, a high-rate data stream can be filtered and then decimated to obtain a lower rate data stream for the application computations; that is, instead of sending every filtered output $y(n)$ to the application computation, only every mth output is sent. It is very important to filter before decimation; otherwise the decimated data stream will contain the effects of aliasing of high-frequency noise in the low-frequency output.

A system design could have a cascade of filters. For example, an analog filter could be applied to a voltage signal before it is converted and sampled by a digital processor. Then the digital processor could apply a cascade of digital filters (e.g., an IIR filter followed by an FIR filter) before the decimated output goes to the application computation.

An IIR filter can be less computationally intensive than an FIR filter for a desired noise attenuation performance, so it is often used for high-rate applications. However, the linear phase, constant time delay characteristics of a symmetric FIR filter are desirable for navigation and guidance applications. Hence, only symmetric FIR filters for such applications will be discussed.

H.2 Rectangular filtering

If a counter is sampled from the pulsed torque or other output of an inertial instrument, then rectangular averaging (constant FIR filter weights $a_i = 1$ with output divided by $N + 1$) has essentially been applied to the data. It is important that the counter be continuous so that a pulse missed in one sampling interval will appear in the next interval. Continuity can be accomplished by latching the counter into a register to be read by the computer without affecting the counter or, if the counter is reset when it is read, without missing the next pulse during the reset.

The results obtained from a low-rate, sampled, continuous-reset counter are the same as if the sampling were done at a high rate and the high-rate readings added or averaged to get the low-rate, full-width decimated output. The relative quantization error associated with such rectangular counter averaging is proportional to T^{-1}, where T is the averaging or count interval (width of the rectangular filter).

The pattern of slightly larger or smaller incremental counts in each high-rate sampling interval is lost by rectangular averaging. Faster attenuation of quantization noise can be accomplished if account is taken of this pattern, as happens with the triangular filter.

H.3 Triangular filtering

Triangular filtering for an odd number of sample points $2m$-1 uses the following FIR filter weights:

$$a_i = \begin{cases} \dfrac{i+1}{m^2} & i = 0, \cdots, m-1 \\ \dfrac{2m-i-1}{m^2} & i = m-1, \cdots, 2m-2 \end{cases} \tag{H.3}$$

The triangular filter can be implemented using fixed-point arithmetic double-running sums s_n and u_n

$$s_n = \sum_{j=0}^{m-1} x(n-j) \tag{H.4}$$

$$u_n = \sum_{k=0}^{m-1} s_{n-k} = \sum_{k=0}^{m-1}\sum_{j=0}^{m-1} x(n-k-j)$$
$$= \sum_{i=0}^{2m-2} (m^2 a_i) x(n-i) \tag{H.5}$$

A circular buffer of length m is kept for the last m data points x. After an initial start-up transient, a new running sum s_n of length m is expressed in terms of the old running sum s_{n-1} of length m by

$$s_n = s_{n-1} + x(n) - x(n-m)$$

A u_n running sum can be reset at its decimation output time if two u_n running sums are simultaneously accumulated if half-width decimation is used, for example.

The computations can be done using fixed-point arithmetic additions. The double-running sum filter output is divided by m^2 to obtain unit gain. If half-width decimation is employed, every raw data point is used with equal weight, partly in one output point and partly in another.

If Q is the quantization error in $x(n)$, then the quantization error is s_n/m in Q/m. The quantization error in s_n occurs in the last $\Delta t = t(n) - t(n-1)$ time interval, which is independent of the quantization error in the last Δt time interval in s_{n-1}. The quantization error in the normalized triangular filter output is, therefore, reduced by a further factor of $m^{1/2}$ since this output is the average of m independent s_n/m. Thus, the triangular filter reduced continuous counter or other quantization errors by $T^{-3/2}$, where T is the filter width.

To summarize, triangular filtering of high-rate continuous counter data obtains higher accuracy in shorter time than does low-rate sampling (rectangular filtering) of the continuous counter data.

H.4 Higher order filtering

If curvature exists in the data, the triangular filter will misestimate the inertial instrument output at the midpoint time tag of the filter width interval. Because of this misestimation, and to improve pass-band, transition-band, and stop-band performance, a higher order than a triangular FIR filter can be used, although at the cost of having to do multiplications as well as additions rather than just additions in the signal processing computer.

Of particular interest for inertial instrument applications are polynomial-passing digital filters with decimation, which faithfully represent accelerometer output at the midpoint time tag of the filter width interval, even in the face of jerk or higher order changes in acceleration. The filter design technique described in Wilkinson [B66] yields polynomial-passing FIR filters with high fidelity at low frequencies and good stop-band attenuation and can even contain a notch (zero of the transfer function) at a known corrupting frequency, such as due to dither.

Annex I

(informative)

Noise characterization

I.1 Stochastic processes

The noise in measurements $x(t)$ arising from accelerometer or other inertial instrument testing can usefully be characterized by modeling $x(t)$ as a stochastic process and applying power spectral density and other noise estimation techniques.

A stochastic process consists of a family of (possibly vector-valued) random variables that are taken from a probability space Ω and indexed by a parameter t (see Parzen [B43]). A stochastic process is written as $x(t,\omega)$ or simply $x(t)$, where ω is a point in Ω and t is the time variable.

A sample path or realization of a stochastic process is the time function $x(t, \omega)$ for a fixed value of ω. Different sample paths of the same stochastic process will not, in general, be identical. The set of all possible sample paths of the process is called its ensemble.

I.2 Autocorrelation function of a stochastic process

The correlation function of two stochastic processes $x(t)$ and $y(t)$ is defined to be the expected value of their product at different times t_1, t_2 (see Brown [B11])

$$\phi_{xy}(t_1,t_2) \equiv E\{x(t_1)\, y(t_2)^T\} \tag{I.1}$$

where the superscript ^{T} denotes the matrix transpose of the column vector y and where the expected value E is calculated by integrating over the probability space (ensemble averaging). In general, ϕ_{xy} is a matrix with the element $[\phi_{xy}]_{ij}$ given by the scalar correlation function

$$[\phi_{xy}(t_1,t_2)]_{ij} = E\{x_i(t_1) y_j(t_2)\} \tag{I.2}$$

The units of a correlation function are equal to the product of the units of the signals of interest.

The correlation function of a stochastic process with itself is called its autocorrelation function and is given by

$$\phi_{xx}(t_1,t_2) = E\{x(t_1)\, x(t_2)^T\} \tag{I.3}$$

In this special case, the diagonal terms are the autocorrelations of the scalar processes that make up the vector $x(t)$, and the off-diagonal terms are known as the cross correlations between the individual scalar processes. The autocorrelation function of a stochastic process is essentially a measure of the dependence of the value of the process at one time with its value at other times.

The covariance function of a stochastic process is found by subtracting the mean from the process and calculating the autocorrelation of the resulting signal

$$\mathrm{cov}[x(t_1,t_2)] = E\{[x(t_1) - \mu(t_1)]\, [x(t_2) - \mu(t_2)]^T\} \tag{I.4}$$

where

$$\mu(t) = E\{x(t)\} \tag{I.5}$$

A stochastic process is called stationary if its probability density is not a function of time (see Brown [B11]), so that none of the process statistics are functions of absolute time. The autocorrelation function of such a process depends only on the difference between the time indices $\tau = t_1 - t_2$. The autocorrelation function of a stationary process is even, that is, $\phi_{xx}(\tau) = \phi_{xx}(-\tau)$, as shown by the change of variable $s = t + \tau$

$$\phi_{xx}(\tau) = E\{x(t+\tau)x(t)\} = E\{x(s)x(s-\tau)\} = \phi_{xx}(-\tau) \tag{I.6}$$

Note also for a stationary process with $s = t + \frac{\tau}{2}$

$$\phi_{xx}(\tau) = E\{x(t+\tau)x(t)\} = E\left\{x\left(s+\frac{\tau}{2}\right)x\left(s-\frac{\tau}{2}\right)\right\} \tag{I.7}$$

An ergodic process is a stationary process that has the additional property that time averaging over a particular realization is equivalent to ensemble averaging, so that in particular

$$\phi_{xx}(\tau) = \lim_{T\to\infty} \frac{1}{2T} \int_{-T}^{T} x(t+\tau)x(t)\, dt \tag{I.8}$$

for any realization $x(t)$ (see Bendat and Piersol [B8] and [B9]).

I.3 Estimation of the autocorrelation function

For a scalar, ergodic, stochastic process, given a span of data $x(t)$ where $-T \leq t \leq T$, a change of variables in Equation (I.8) shows that an estimator for the autocorrelation function is given by (see Bendat and Piersol [B8])

$$\tilde{\phi}_{xx}(\tau) = \frac{1}{2T} \int_{-T+\frac{|\tau|}{2}}^{T-\frac{|\tau|}{2}} x\left(t+\frac{\tau}{2}\right)x\left(t-\frac{\tau}{2}\right) dt, \quad |\tau| < 2T \tag{I.9}$$

If $p(\omega)$ is the probability density of the stationary, ergodic process $x(t)$, then the expected value of the estimate in Equation (I.9) is given by (see Bendat and Piersol [B8])

$$\mathrm{E}\{\tilde{\phi}_{xx}(\tau)\} = \int_{-\infty}^{\infty}\left[\frac{1}{2T}\int_{-T+\frac{|\tau|}{2}}^{T-\frac{|\tau|}{2}} x\left(\mathrm{t}+\frac{t}{2}\right)\mathrm{x}\left(\mathrm{t}-\frac{t}{2}\right)\mathrm{dt}\right]\mathrm{p}(\omega)\mathrm{d}\omega$$

$$= \frac{1}{2T}\int_{-T+\frac{|\tau|}{2}}^{T-\frac{|\tau|}{2}}\left[\int_{-\infty}^{\infty} x\left(\mathrm{t}+\frac{\tau}{2}\right)\mathrm{x}\left(\mathrm{t}-\frac{\tau}{2}\right)\mathrm{p}(\omega)\mathrm{d}\omega\right]\mathrm{dt}$$

$$= \frac{1}{2T}\int_{-T+\frac{|\tau|}{2}}^{T-\frac{|\tau|}{2}} \phi_{xx}(\tau)\mathrm{dt} \qquad \text{by Equation (I.7)}$$

$$= \left(1-\frac{|\tau|}{2T}\right)\phi_{xx}(\tau) \tag{I.10}$$

Equation (I.10) shows that the estimate of the autocorrelation function given by Equation (I.9) is unbiased in the limit as T becomes very large with respect to τ (see Bendat and Piersol [B9]). Multiplying $\tilde{\phi}_{xx}(\tau)$ by $(1-|\tau|/2T)^{-1}$ will also make the estimate unbiased.

I.4 Power spectral density (PSD) of a stationary stochastic process

The PSD of a stationary stochastic process is defined to be the Fourier transform of its autocorrelation function (see Brown [B11])

$$\phi_{xx}(\mathrm{f}) \equiv \int_{-\infty}^{\infty} \phi_{xx}(\tau)e^{-2\pi\mathrm{i}\mathrm{f}\tau}\mathrm{d}\tau, \quad -\infty < \mathrm{f} < \infty \tag{I.11}$$

where

f	is the frequency in Hz
i	is $\sqrt{-1}$

The PSD has units equal to (units^2)/Hz if the process $x(t)$ is measured in units.

Because the autocorrelation function of a stationary stochastic process is even, the PSD is also even so that the one-sided PSD is equal to (see Papoulis [B41] and [B42])

$$\phi_{\mathrm{xx}}^{1}(\mathrm{f}) \equiv 2\int_{-\infty}^{\infty} \phi_{\mathrm{xx}}(\tau)\mathrm{e}^{-2\pi\mathrm{i}\mathrm{f}\tau}\mathrm{d}\tau, \quad \mathrm{f} \geq 0 \tag{I.12}$$

$$\phi_{\mathrm{xx}}^{1}(\mathrm{f}) = \phi_{\mathrm{xx}}(f) + \phi_{\mathrm{xx}}(-\mathrm{f}), \quad \mathrm{f} \geq 0 \tag{I.13}$$

The one-sided PSD is often used in analyzing data where it is convenient to regard frequency f as being positive, whereas the two-sided PSD is more convenient for mathematical proofs.

I.5 Estimation of the PSD

I.5.1 Continuous data

It is often desirable to determine the PSD of a stationary, scalar, ergodic, stochastic process from a finite sample path of that process. One way of calculating the PSD from a finite sample path is to take the Fourier transform of the estimate of the autocorrelation function defined by Equation (I.9) (see Bendat and Piersol [B8] and [B9])

$$\tilde{\Phi}_{xx}(f) = \int_{-2T}^{2T} \tilde{\phi}_{xx}(\tau) e^{-2\pi i f \tau} d\tau \tag{I.14}$$

or

$$\tilde{\Phi}_{xx}(f) = \int_{-2T}^{2T} \left[\frac{1}{2T} \int_{-T+\frac{|\tau|}{2}}^{T-\frac{|\tau|}{2}} x\left(t+\frac{\tau}{2}\right) x\left(t-\frac{\tau}{2}\right) dt \right] e^{-2\pi i f \tau} d\tau \tag{I.15}$$

This integral is only evaluated between $-2T$ and $2T$ because the estimate of the autocorrelation function is only defined in this region and is assumed to be zero outside of it.

If $X(f)$, $Y(f)$ are the Fourier transforms of $x(t)$, $y(t)$, it is easily verified that

$$\text{Fourier transform of } \int_{-\infty}^{\infty} x(t+\tau) y(t)\, dt = X(f)\, \overline{Y(f)} \tag{I.16}$$

where the integral is called the time domain correlation of $x(t)$, and $y(t)$, and $\overline{Y}$ is the complex conjugate of Y.

Since by the ergodic hypothesis $\tilde{\phi}_{xx}$ is a time-domain autocorrelation of $x(t)$ [Equation (I.8) and Equation (I.9)], Equation (I.14) may be expressed as

$$\tilde{\Phi}_{xx}(f) = \frac{1}{2T} X(f)\overline{X(f)} = \frac{1}{2T} |X(f)|^2 \tag{I.17}$$

where the finite Fourier transform of $x(t)$ is given by

$$X(f) = \int_{-T}^{T} x(\tau) e^{-2\pi i f \tau} d\tau \tag{I.18}$$

since $x(t)$ is assumed zero outside the interval $-T \leq t \leq T$.

The one-sided PSD estimate is given by

$$\tilde{\Phi}^{1}_{xx}(f) = \frac{1}{T} |X(f)|^2, \qquad f \geq 0 \tag{I.19}$$

and the expected value of the estimate of the PSD is given by

$$\begin{aligned} E\{\tilde{\Phi}_{xx}(f)\} &= \int_{-\infty}^{\infty} \left[\int_{-2T}^{2T} \tilde{\phi}_{xx}(\tau) e^{-2\pi i f \tau} d\tau \right] p(\omega) d\omega \\ &= \int_{-2T}^{2T} E\{\tilde{\phi}_{xx}(\tau)\} e^{-2\pi i f \tau} d\tau \\ &= \int_{-2T}^{2T} \left(1 - \frac{|\tau|}{2T}\right) \phi_{xx}(\tau) e^{-2\pi i f \tau} d\tau \end{aligned} \tag{I.20}$$

Equation (I.20) shows that the estimate of the PSD will be unbiased as T becomes large, that is, as the span of available data becomes large

$$\lim_{T\to\infty} E\{\tilde{\Phi}_{xx}(f)\} = \int_{-\infty}^{\infty} \phi_{xx}(\tau) e^{-2\pi i f \tau} d\tau = \Phi_{xx}(f) \tag{I.21}$$

I.5.2 Interpretation of the PSD as a power spectrum

The power in a time function $x(t)$ is

$$\text{Total Power} = \lim_{T\to\infty} \int_{-T}^{T} |x(t)|^2 dt \tag{I.22}$$

$$\text{Average Power} = \lim_{T\to\infty} \frac{1}{2T} \int_{-T}^{T} |x(t)|^2 dt \tag{I.23}$$

The Fourier transform $X(f)$ and the inverse Fourier transform with frequency f in Hz are (see Papoulis [B42])

$$X(f) = \int_{-\infty}^{\infty} x(t) e^{-2\pi i f t} dt\,, \quad x(t) = \int_{-\infty}^{\infty} X(f) e^{2\pi i f t} df \tag{I.24}$$

The Fourier transform $X_\omega(\omega)$ and the inverse Fourier transform in terms of circular frequency $\omega = 2\pi f$ in rad/s are

$$X_\omega(\omega) = \int_{-\infty}^{\infty} x(t) e^{-i\omega t} dt\,, \quad x(t) = \frac{1}{2\pi} \int_{-\infty}^{\infty} X_\omega(\omega) e^{i\omega t} d\omega \tag{I.25}$$

Plancherel's formula is (see Strang [B54])

$$\int_{-\infty}^{\infty} |x(t)|^2 dt = \int_{-\infty}^{\infty} |X(f)|^2 df \tag{I.26}$$

Thus, the total power in the time signal $x(t)$ is the same as the total power in the Fourier transform $X(f)$, so $|X(f)|^2$ may be interpreted as giving the power split up into frequency components or as giving the power density as a function of frequency.

If $x(t)$ is real, then $X(f) = X(-f)$. In this case, the power over all frequencies is equal to twice the power in the positive frequencies

$$\int_{-\infty}^{\infty} |X(f)|^2 df = 2\int_{0}^{\infty} |X(f)|^2 df \tag{I.27}$$

so that no information is lost in using the one-sided PSD.

The PSD as the Fourier transform of the expected value of the autocorrelation function is estimated by Equation (I.17), so that

$$\Phi_{xx}(f) \cong \tilde{\Phi}_{xx}(f) = \frac{1}{2T}|X(f)|^2 \tag{I.28}$$

= average power in $x(t)$ broken into frequency components

I.5.3 Discrete data

It is most common for data to be taken at discrete times using a digital computer. Assuming that the samples of the continuous process $x(t)$ are evenly spaced in time from $-T$ to T, Equation (I.18) is approximated by

$$X(f) \cong \sum_{k=0}^{N-1} x\left[\left(k+\frac{1}{2}\right)\Delta t - T\right] e^{-2\pi i f[(k+.5)\Delta t - T]}\Delta t \tag{I.29}$$

where

$$\Delta t = \frac{2T}{N} s \tag{I.30}$$

Define the discrete function

$$x_k = x\left[\left(k+\frac{1}{2}\right)\Delta t - T\right] \ , \ k = 0, 1, \cdots N-1 \tag{I.31}$$

and the discrete Fourier transform

$$X_j = \sum_{k=0}^{N-1} x_k e^{-2\pi i jk/N} \ , \ j = 0, 1, \cdots, N-1 \tag{I.32}$$

Equation (I.32) has a rigorous discrete inverse Fourier transform (see Bendat and Piersol [B9])

$$x_k = \frac{1}{N}\sum_{j=0}^{N-1} X_j \, e^{2\pi i jk/N} \ , \ k = 0, 1, \cdots, N-1 \tag{I.33}$$

For $j = 0$, Equation (I.32) shows that X_0/N is the average or mean of the data. For numerical reasons, the mean is often removed from the data without affecting the remaining Fourier transform coefficients, in which case, the dc term becomes $X_0 = 0$.

The discrete equivalent to Plancherel's theorem is Parseval's theorem (see Strang [B54])

$$\sum_{j=0}^{N-1} |X_j|^2 = N \sum_{k=0}^{N-1} |x_k|^2 \tag{I.34}$$

This theorem shows that the power density interpretation of the continuous PSD holds for the discrete PSD.

Substituting Equation (I.31) into Equation (I.29) yields

$$X(f) \cong e^{-2\pi i f(\Delta t/2 - T)} \sum_{k=0}^{N-1} x_k e^{-2\pi i f k \Delta t} \, \Delta t \tag{I.35}$$

so that, except for the phase change from the complex exponential in front of the summation sign due to the shift in the time origin (which does not affect the PSD), the discrete Fourier transform of Equation (I.32) approximates the continuous Fourier transform at discrete frequencies f_j by

$$X(f_j) \cong X_j \Delta t \tag{I.36}$$

with

$$f_j = \frac{j}{N\Delta t} = \frac{j}{2T} \ \text{Hz} \tag{I.37}$$

Using sampled data over a time span $2T$ with time spacing Δt and $2T = N\Delta t$, the discrete Fourier transform is thus computed at a frequency spacing of

$$\Delta f = \frac{1}{2T} \ \text{Hz} \tag{I.38}$$

If $x(t)$ for $-\infty < t < \infty$ is a band-limited signal so that $X(f) = 0$ for $\lfloor f \rfloor > F$ and if X_j is the discrete Fourier transform of samples of $x(t)$ at a sampling interval Δt with

$$N\Delta f = \frac{N}{2T} = \frac{N}{N\Delta t} = \frac{1}{\Delta t} \geq 2F \tag{I.39}$$

Then $x(t)$ can be exactly reconstructed from X_j (see Eshback and Sanders [B19]). Thus, the finite Fourier transform given by X_j will contain all of the information about the time series $x(t)$ only if the sampling frequency is greater than $2F$. The requirement to sample faster than twice the highest frequency content of the data is the Nyquist criterion. If the time series $x(t)$ is not band-limited, then the lower frequency discrete Fourier transform values will contain energy from the higher frequency components of the signal. This phenomenon is known as aliasing (see Papoulis [B41]).

If the data x_k are real, Equation (I.32) shows that

$$X_{N-j} = \bar{X}_j\,, \quad j = 1, 2, \cdots, \left[\frac{N}{2}\right] \tag{I.40}$$

where $\left[\frac{N}{2}\right]$ is the largest integer less than or equal to $\frac{N}{2}$. This relationship and the fact that the discrete Fourier transform has been defined for positive frequencies is consistent with the Nyquist criterion in limiting the range of available frequency information to $0 \le f \le \frac{1}{2\Delta t}$.

Thus, by Equation (I.19) and Equation (I.36), the estimate from a finite span of sampled data of the one-sided PSD at frequency f_j is

$$\widetilde{\Phi}^1_{xx}(f_j) = \frac{\Delta t^2}{T}\left|X_j\right|^2, \quad j = 0, 1, \cdots, \left[\frac{N}{2}\right] - 1 \tag{I.41}$$

$$\widetilde{\Phi}^1_{xx}(f_{[N/2]}) = \begin{cases} \dfrac{\Delta t^2}{T}\left|X_{[N/2]}\right|^2 & \text{if N is odd} \\ \dfrac{\Delta t^2}{2T}\left|X_{[N/2]}\right|^2 & \text{if N is even} \end{cases} \tag{I.42}$$

The discrete Fourier transform can be evaluated using the Cooley–Tukey fast Fourier transform (FFT) algorithm if N is a power of 2 (see Bendat and Piersol [B9]). This well-known algorithm greatly reduces the computational burden of calculating the discrete Fourier transform. The number of computations is proportional to $N \log_2 N$ rather than the N^2 required for the brute force evaluation of Equation (I.32) (see Bendat and Piersol [B9]).

I.6 Numerical evaluation and plotting of the PSD

Let x_k $(k = 0, \cdots, N-1)$ be experimental data collected at uniform time intervals Δt corrupted by stationary, ergodic noise. Let N be a power of 2. Either the sampling rate should be at least twice as fast as the highest frequency noise or deterministic signal in the data, or a prefilter should be applied to the data to minimize aliasing of such high-frequency noise or signal into the sampled data. The prefilter could be an analog prefilter if a voltage is read by an analog-to-digital converter, or a digital prefilter could be applied to high-rate data with lower rate decimated output x_k at the Δt time interval (see Annex H).

The FFT is then computed and the $\left[\frac{N}{2}\right] + 1$ points in the PSD are calculated using Equation (I.41) and Equation (I.42). Use of double precision floating-point computations reduces roundoff accumulation. The PSD is then plotted using logarithmic PSD and frequency axes with the dc zero frequency point deleted.

The data can be multiplied by tapering or window function before the FFT and PSD are calculated in order to minimize distortion caused by nonexact periodicities between the first and last data points (see Bendat and Piersol [B8]).

As shown in I.5.1, the thus computed estimate of the PSD is unbiased. However, the standard deviation of estimate (I.41) and (I.42) of the PSD at a given frequency is equal to the actual value of the PSD at that frequency (see Bendat and Piersol [B9], Hestrom [B27], and Papoulis [B41]). The variance of the estimate may be decreased by either averaging several estimates or averaging adjacent frequencies of a given estimate. The former method is known as ensemble averaging, while the latter is called frequency averaging.

Ensemble averaging is often employed in commercial spectral analysis software, where a series of, for example, N = 1024 or 4096 measurements are made and the PSDs calculated, averaged, and then plotted.

An alternative technique is to calculate a single PSD for, as an example, N = 32 768 or 65 536 measurements, and then to average the adjacent frequency values according to the scheme in Table I.1. The low-frequency part of the PSD plot has high uncertainty but still conveys some information. The high-frequency part of the PSD plot has the uncertainty obtained by ensemble averaging and is conveniently plotted with the low-frequency data because the frequency averaging prevents bunching of the high-frequency data points in the log–log plot. This technique reduces the number of points in the PSD to approximately 50 points per decade.

Table I.1—Logarithmic frequency averaging of 32 768 points

Data interval	Points in interval	Number of points Per average	Number of Points to plot
1–32	32	1	32
33–64	32	2	16
65–128	64	4	16
129–256	128	8	16
257–512	256	16	16
513–1024	512	32	16
1025–2048	1024	64	16
2049–4096	2048	128	16
4097–8192	4096	256	16
8193–16 384	8192	512	16
16 385–32 768	16 384	1024	16

I.7 Characteristic PSD noise slopes

I.7.1 Deterministic signals

The PSD of a single-frequency sinusoid is a spike. However, if the sinusoid frequency does not coincide with one of the discrete PSD frequencies, the spike will be smeared into several adjacent PSD frequencies, which is a phenomenon known as “leakage.”

Consider the Fourier transform of any finite segment of a trend $x(t) = \alpha t$

$$X(f) = \int_{-T}^{T} \alpha t e^{-2\pi i f t} dt \tag{I.43}$$

Equation (I.30) and Equation (I.37) motivate the change of variables

$$f = j\frac{1}{2T}, \qquad t = n\Delta t = n\frac{2T}{N} \tag{I.44}$$

where, for the moment, *j* and *n* are allowed to vary continuously. Equation (I.43) becomes

$$X(j) = \int_{-N/2}^{N/2} \alpha\, n\Delta t e^{-2\pi i j n/N} \Delta t\, dn \tag{I.45}$$

Using integration by parts, Equation (I.45) becomes

$$X(j) = \alpha\Delta t^2 \left[\frac{-N^2}{4\pi i j}(e^{-\pi i j} + e^{\pi i j}) + \frac{N^2}{4\pi^2 j^2}(e^{-\pi i j} - e^{\pi i j})\right] \tag{I.46}$$

If *j* is restricted to take on only integer values as it would in the discrete Fourier transform, this equation reduces to

$$X(j) = \frac{\alpha\Delta t^2 N^3}{2\pi j}(-1)^j i = \frac{2\alpha T^2}{\pi j}(-1)^j i \tag{I.47}$$

Therefore, by Equation (I.17), the value of the PSD at frequencies spaced $\frac{1}{2T}$ Hz apart is given by

$$\Phi_{XX}(f) = \frac{2\alpha^2 T^3}{\pi^2 j^2} \tag{I.48}$$

which will have a –2 log–log slope.

Because both random walk (see I.7.2) and trend have a –2 log–log PSD slope, they cannot be distinguished using frequency domain analysis. However, they can be distinguished in the time domain with the Allan variance described in I.8 or the maximum likelihood estimator described in I.9.3.

I.7.2 White, random walk, and flicker noise

White noise has by definition constant power at all frequencies and is represented by a zero slope line parallel to the frequency axis. Integration by parts in the Fourier transform shows that

$$\text{PSD (derivative of data)} = (2\pi)^2 f^2 \quad \text{PSD (data)} \tag{I.49}$$

$$\text{PSD (integral of data)} = \frac{1}{(2\pi)^2 f^2} \quad \text{PSD (data)}$$

Since random walk is the integral of white noise, the PSD of random walk is represented by a –2 slope line in a log–log plot.

The flicker noise that is often seen in experimental data has by definition a –1 slope in a log–log PSD plot (see Hooge [B28] and Solo [B52]). The non-Markov fractional Brownian motion stochastic process has many of the characteristics of flicker noise (see Flandrin [B20] and Mandlebrot and Van Ness [B35]).

I.7.3 Quantization noise

If accelerometer output is being measured by a continuous counter, the accumulated count value is the integrated velocity truncated to the quantization resolution of the counter. Under the assumption that the value of the signal is changing rapidly with respect to the level of quantization, the counter output is equivalent to subtracting a uniformly distributed random variable $n(t)$ from the true value of the signal. The probability distribution of n is given by

$$p[n(t)] = \begin{cases} \dfrac{1}{q} & \text{if } 0 \le n \le q \\ 0 & \text{otherwise} \end{cases} \tag{I.50}$$

where q is the resolution of the measurement device. Quantization noise is assumed to be uncorrelated in time so that

$$\phi_{nn}(\tau) = E\{n(t+\tau)n(t)\} = E\{n(t)^2\}\ \delta(\tau) = \frac{q^2}{3}\ \delta(\tau) \tag{I.51}$$

where $\delta(\tau)$ is the delta function.

The PSD of quantization noise in the velocity domain is

$$\Phi_{nn}(f) = \int_{-\infty}^{\infty} \phi_{nn}(\tau) e^{-2\pi i f t} d\tau = \frac{q^2}{3} \tag{I.52}$$

since the Fourier transform of the delta function is the constant 1. Therefore, in the acceleration domain with the accumulated count difference observable, quantization noise has a +2 log–log PSD slope by Equation (I.49).

I.7.4 Typical log–log PSD plot

The quietest accelerometer data are usually taken with IA vertical, where the output is insensitive to tilt variations. The integrated velocity from such an experiment has a large trend, unless the ramp is removed by a least-squares fit. However, such a procedure could also remove some random walk noise. In order to conform more closely to the stationary ergodic hypothesis implicit in PSD noise analysis, an acceleration domain PSD is typically computed for an accelerometer. Similarly, an angle rate domain PSD is typically computed for a gyroscope.

The characteristic slopes in an accelerometer or gyroscope PSD are shown in Figure I.1, where the actual units (μ*g* or m*g*, perhaps, for an accelerometer) and frequency range are hypothetical. With real data, gradual transitions would exist between the different PSD slopes, rather than the sharp transitions in Figure I.1; and the slopes might be different than the –2, –1, 0, and +2 values in Figure I.1. A certain amount of noise or hash would exist in the plot curve due to the uncertainty of the measured PSD.

The logarithm of the PSD is plotted versus the logarithm of the frequency, but the tick marks on the plot are labeled with the value of the quantity rather than the logarithm of the value. The PSD units are units^2/Hz, for which the integral with respect to frequency (area under PSD curve as a linear–linear plot) is the mean square noise in the accelerometer output about the average output (since the zero frequency dc point is not plotted).

The PSD in Figure I.1 represents a combination of the environmental noise input to the accelerometer and the inherent noise in the accelerometer. Seismic environmental noise is typically above 1 Hz and might have discrete spikes due to resonances in the local geology and test table (see M.2). The low-frequency end of the PSD is probably representative of the noise characteristics of the accelerometer itself for IA vertical testing if care is taken to prevent aliasing from high-frequency seismic noise and except for any 0.1-Hz earthquake vibrations and the 0.1-μ*g*, 12.4-h period earth tides (see M.4). Cross-PSD analysis (see Bendat and Piersol [B8]) or the difference in accelerometer outputs could be used in dual IA-parallel accelerometer testing to separate the inherent noise in the accelerometers from the effects of common environmental inputs (e.g., seismic, thermal, and magnetic).

The quantization noise line in Figure I.1 is an artifact of the readout system. It can be moved to the right by greater readout resolution and/or by higher rate sampling, prefiltering, and decimation to the output rate (20 Hz in Figure I.1, since the highest frequency point in a PSD is half the output frequency).

The sampling frequency should be at least twice the frequency of the highest rate noise or deterministic signal in the data to prevent aliasing into the lower rate portion of the PSD plot. If this required sampling frequency is higher than the desired output frequency, the data should either be analog-filtered to the output frequency before sampling at the output frequency or sampled at this higher frequency, digitally filtered, and decimated to the output frequency (see Annex H).

The white noise portion of the PSD indicates the noise floor of the instrument, where root-mean-square (rms) noise is reduced as the square root of the averaging time. In the flicker noise portion of the spectrum, rms noise is not reduced by increased averaging time. In the random walk portion of the spectrum, rms noise is, in fact, made worse by increased averaging time (see I.8). The flicker and random walk processes are due to thermal and other environmental variations and to long-term changes in the instrument itself (stress relaxation, creep, contamination buildup, fluid stratification, deterioration, wear, magnetic and other aging, etc.).

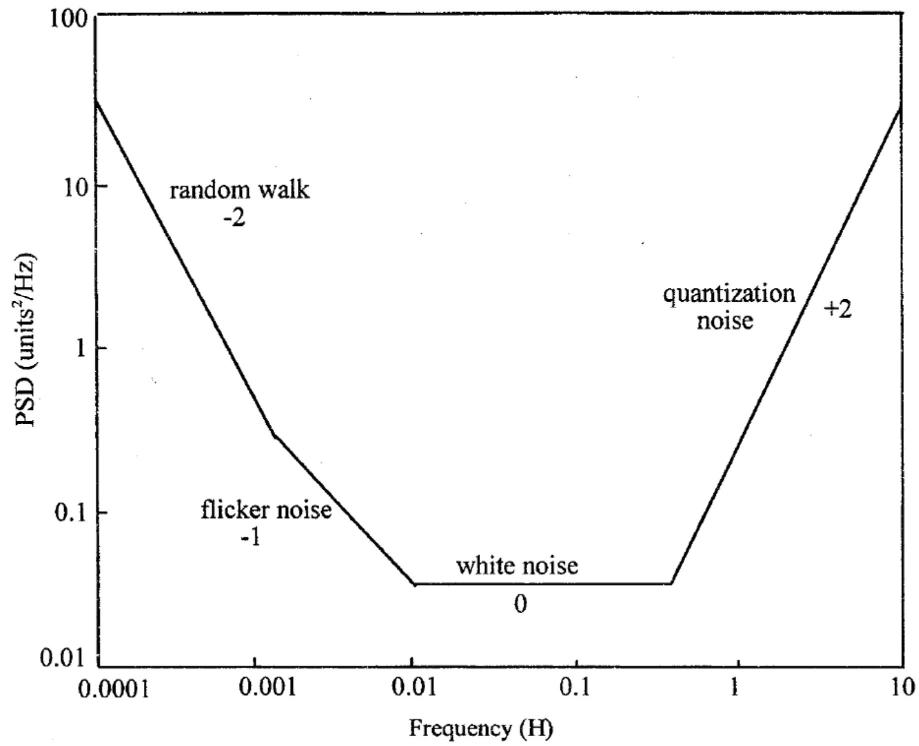

Figure I.1—Typical slopes in $\log_{10}$-$\log_{10}$ plot of one-sided PSD versus frequency (accelerometer acceleration data or gyroscope angle rate data)

The various slopes in a log–log PSD plot can be estimated by eye or a least squares fit of the function

$$\frac{A_1}{f^2} + \frac{A_2}{f} + A_3 + A_4 f^2 \tag{I.53}$$

can be made to the PSD. However, the spectral estimation technique described in I.9.3 has a sounder theoretical basis if combined with judicious analysis of PSD plots to see whether anything unexpected is in the data.

As an example of unexpected behavior, spikes in the PSD plot would be indicative of sinusoidal variations due to the accelerometer device itself, harmonics in the readout system, seismic or other environmental input, or aliasing into the frequency range of the PSD plot from higher frequency versions of these mechanisms. Discontinuities in the data would cause ringing (scallops) in the PSD due to the frequency content in the Fourier transform of a step function.

I.7.5 Noise specification

The noise specification for an accelerometer could state the allowed levels for each type of noise process in given frequency ranges. In particular, it could state the frequency range over which a white noise spectrum should exist and the level below which it should lie, expressed in $\mu g/\sqrt{\text{Hz}}$ if desired rather than $\mu g^2/\text{Hz}$. The specification requirements for the low-frequency end of the noise PSD could be expressed in terms of long-term stability requirements on bias, scale factor, and misalignment.

By Equation (I.26) and Equation (I.27), the noise specification could also be expressed as an integrated noise over a given frequency bandwidth

$$\text{rms noise } f_1 \text{ to } f_2 = \sqrt{\int_{f_1}^{f_2} \text{PSD(f) df}} \quad \mu g \tag{I.54}$$

where the area under the PSD curve is evaluated from a linearly scaled plot rather than from a log–log scaled plot. PSD software should plot and print the integrated PSD along with the PSD, so that the integrated PSD between given limits can be calculated as the difference of the total integrated PSD at the two limits. Alternatively, if the PSD has log–log slope m from f_a to f_b, then

$$\int_{f_a}^{f_b} Af^m \, df = \begin{cases} A[\ell n f_b - \ell n f_a] & \text{if } m = -1 \\ \dfrac{A}{m+1}[f_b^{m+1} - f_a^{m+1}] & \text{otherwise} \end{cases} \tag{I.55}$$

and the integrated PSD in the bandwidth f_1 to f_2 is the sum of the integrated PSDs between sub-bandwidths with constant log–log slope.

I.8 Characteristic Allan variance noise slopes

The variance of two data points x_{j-1}, x_j relative to their mean is

$$\left[x_{j-1} - \frac{x_{j-1} + x_j}{2}\right]^2 + \left[x_j - \frac{x_{j-1} + x_j}{2}\right]^2 = \frac{\left(x_j - x_{j-1}\right)^2}{2} \tag{I.56}$$

Equation (I.56) motivates the definition of the Allan variance of data x_0, x_1, ..., x_{N-1} taken at time interval Δt to be the average of the variances of the data pairs x_{j-1}, x_j

$$\sigma_a^2(\Delta t) = \frac{1}{2(N-1)} \sum_{j=1}^{N-1} \left(x_j - x_{j-1}\right)^2 \tag{I.57}$$

Define a new sequence

$$y_j = \frac{x_{2j} + x_{2j+1}}{2}, \quad j = 0, 1, ..., \left[\frac{N}{2}\right] - 1 \tag{I.58}$$

and compute the Allan variance $\sigma_a^2(2\Delta t)$ for this sequence. Iterating, the Allan variance $\sigma_a^2(n\Delta t)$ is calculated for longer and longer averaging times $\tau = n\Delta t$, n = 1, 2, 4, 8, ... The square root of the Allan variance is then plotted versus averaging time τ with log–log scales.

IEEE Std 952™-1997 [B29] contains a thorough discussion of Allan variance noise characterization. The summary results along with those for the PSD derived earlier are given in Table I.2.

Table I.2—Slopes in PSD and square root of Allan variance log–log plots (accelerometer acceleration data or gyroscope angle rate data)

Signal	PSD versus frequency	Square root of Allan variance versus averaging time
Trend	–2	+1
Random walk	–2	+1/2
Flicker noise	–1	0
White noise	0	–1/2
Quantization noise	+2	–1

I.9 Estimation of Markov noise parameters

I.9.1 Stochastic linear dynamic systems

A stochastic linear dynamic system model is of the form

$$dx(t) = A\,x(t)\,dt + B\,u(t)\,dt + L\,d\beta(t), \quad t \geq t_0 \tag{I.59}$$

$$z(t_k) = Hx(t_k) + \theta(t_k), \;\; k = 1, 2, \ldots \tag{I.60}$$

where

$x(t)$	is dynamic system state vector
$u(t)$	is control or environmental input
$\beta(t)$	is zero mean Gaussian Wiener stochastic process (mathematical model of the Brownian motion or random walk process)
$z(t_k)$	is observables vector
$\theta(t_k)$	is zero mean white measurement noise with covariance matrix $R(t_k)$
A,B,L,H,R	are matrices that depend on parameters α

The state vector $x(t)$ can be estimated from the observables $z(t_k)$ using a Kalman filter (see Jazwinski [B30]).

The differential notation in Equation (I.59) stands for the integral equation

$$x(t_k) - x(t_0) = \int_{t_0}^{t_k} A\,x(t)dt + \int_{t_0}^{t_k} B\,u(t)dt + \int_{t_0}^{t_k} L\,d\beta(t) \tag{I.61}$$

where the last integral is the Ito stochastic integral with respect to the Wiener process $\beta(t)$. Given a random initial condition vector $x(t_0)$, it can be proved that there is a unique Markov stochastic solution $x(t)$ to Equation (I.61) (see Jazwinski [B30]).

A Markov stochastic process $x(t)$ is a stochastic process in which the expected value of the future given the present and the past is equal to the expected value of the future given the present

$$E(x(t_{n+1})|x(t_n), x(t_{n-1}), \ldots) = E(x(t_{n+1})|x(t_n)) \tag{I.62}$$

where $t_{n+1} > t_n > t_{n-1} > \ldots$ and where $E(A|B)$ is the conditional expectation of A given B. The Markov property is the stochastic equivalent of the principal of causality, where the solution of a differential equation expressing the time evolution of a physical system just depends on the initial conditions and not on the past behavior of the system that arrived at those initial conditions.

Since inertial guidance and navigation system models are of the form [Equation (I.59) and Equation (I.60)] with gyroscope and accelerometer biases, scale factors, misalignments, and other parameters as Kalman filter states, inertial instrument noise models have to be put into this form to be usable in guidance and navigation system applications.

I.9.2 Stochastic linear dynamic system noise models

I.9.2.1 Random walk and white noise model for accelerometer velocity and gyroscope angle observables

For guidance and navigation system applications, it is natural to use accelerometer-integrated velocity and gyroscope-integrated angle as observables $z(t_k)$ since the quantization noise in accelerometer acceleration and gyroscope angle rate measurements becomes white measurement noise $\theta(t_k)$ in the integrated observables $z(t_k)$. The following analysis is applicable to both accelerometers and gyros; however, the derivation herein only applies to accelerometers. A similar derivation may be done for gyroscopes. If there were random walk as well as white measurement noise in the integrated output signal $z(t_k)$ from an accelerometer, add a state x_b to the dynamic system state vector with dynamic equation

$$dx_b(t) = (K_0 + K_1 a_i(t) + \ldots)\, dt + b\, d\beta_1 \qquad \text{(I.63)}$$

$$z(t_k) = x_b(t_k) + \theta(t_k) \quad \text{m/s} \qquad \text{(I.64)}$$

where

$K_0, K_1, \ldots$	are bias (m/s^2), scale factor (m/s^2/g), and other model parameters (could be states in the guidance system calibration Kalman filter)
$a_i(t)$	is applied acceleration along the input axis
b	is random walk standard deviation (m/s/$\sqrt{\text{s}}$)
θ	is white measurement noise with standard deviation r (m/s) for sampling interval $\Delta t = t_{k+1} - t_k$ s

The standard deviation of Δt increments of the Wiener Brownian motion process $b\, d\beta_1$ is $b\sqrt{\Delta t}$.

Let the accelerometer one-sided acceleration PSD versus frequency f in Hz be of the form

$$\text{one sided acceleration PSD} = \begin{cases} \text{A (m/s}^2)^2/\text{Hz} & \text{f} < \text{f}_0 \text{ white noise} \\ \dfrac{\text{A}}{\text{f}_0^2}\text{f}^2 & \text{f} > \text{f}_0 \text{ quantization noise} \end{cases} \qquad \text{(I.65)}$$

By Equation (I.12), Equation (I.24), Equation (I.27), and Equation (I.49), the two-sided PSD white noise levels versus frequency f in Hz (1/s) that generate the one-sided PSD are

two-sided velocity white noise (acceleration quantization) in velocity domain	$\dfrac{\text{A}}{2(2\pi)^2\text{f}_0^2}\ (\text{m/s}^2)^2/\text{Hz}$
two-sided velocity random walk (acceleration white noise) in acceleration domain	$\dfrac{\text{A}}{2}(\text{m/s}^2)^2/\text{Hz}$

The Fourier transform of two-sided white noise level σ^2 units^2/Hz in the frequency domain is the autocorrelation function $\sigma^2\delta(t)$ units^2 in the time domain, where $\delta(t)$ is the delta impulse function. The dynamic system variable $x(t)$ whose unit time increments have this autocorrelation function satisfies the Itô stochastic differential equation $dx = \sigma\ d\beta(t)$, where $\beta(t)$ is a unit Wiener Brownian motion process. Therefore, the relation between the accelerometer dynamic noise model parameters b and r in Equation (I.63) and Equation (I.64) and the PSD noise parameters are

$$b = \sqrt{\frac{A}{2}} \qquad \text{(m/s)}/\sqrt{s} \tag{I.66}$$

$$r = \frac{1}{2\pi f_0}\sqrt{\frac{A\Delta t}{2}} \qquad \text{m/s}$$

I.9.2.2 Velocity and angle random walk per root hour

If A is the one-sided acceleration PSD white noise level in $(\text{m/s}^2)^2$/Hz of an accelerometer, then by Equation (I.66) the accelerometer's velocity random walk coefficient in m/s/$\sqrt{\text{h}}$ is

$$b = 60\sqrt{\frac{\text{A}}{2}} \qquad \text{m/s}/\sqrt{\text{h}} \tag{I.67}$$

Similarly, if A is the one-sided angle rate white noise level in $(\text{deg/h})^2$/Hz of a gyroscope, then by Equation (I.66), the gyroscope's angle random walk coefficient in deg/$\sqrt{\text{h}}$ is

$$b = \frac{1}{60}\sqrt{\frac{\text{A}}{2}} \qquad \text{deg}/\sqrt{\text{h}} \tag{I.68}$$

Expressing the angle or velocity random walk in units per root hour is useful for inertial navigation systems because it shows how much of an error accumulates after 1 h of inertial navigation due to white noise instability in a gyroscope's angle rate bias or in an accelerometer's acceleration bias. The standard deviation of the angle or velocity error after 4 h is twice as large, and after 0.25 h, it is half as large as it is after 1 h. It is important to include the conversion from one-sided to two-sided PSD as well as the conversion from seconds to hours in the random walk computation.

The angle or velocity error caused by an initial error in the inertial instrument angle rate or acceleration bias (due for instance to the bias calibration having been done some time in the past) will grow linearly with time, in contrast to the square root in time angle or velocity error growth due to white process noise in the angle rate or acceleration bias.

I.9.2.3 Flicker noise modeled as sum of exponentially correlated noises

Flicker noise can be modeled by a combination of Markov noise states (see Keshner [B31]). To see how this is possible, consider the exponentially correlated noise state x_c satisfying (see Jazwinski [B30], p. 122])

$$dx_c(t) = -c_1 x_c(t)\,dt + c_1 c_2 d\beta_2 \tag{I.69}$$

$$z(t_k) = x_b(t_k) + x_c(t_k) + \theta(t_k) \tag{I.70}$$

where the state x_b comes from Equation (I.63) and

c_1 is the inverse time constant of exponentially correlated noise
c_2 is the scaling parameter of exponentially correlated noise

The effects of the accelerometer bias, scale factor, and other model coefficients and of the random walk, exponentially correlated, and white noise parameters are now combined into the observable.

The autocorrelation function of exponentially correlated or colored noise is (see Jazwinski [B30], p. 122])

$$E[x_c(t_k)x_c(t_k+\tau)] = \frac{c_1 {c_2}^2}{2} e^{-c_1|\tau|} \tag{I.71}$$

and the two-sided power spectral density as a function of circular frequency ω is (see Jazwinski [B30], p. 83])

$$PSD(\omega) = \frac{c_2^2}{1+\left(\frac{\omega}{c_1}\right)^2} \tag{I.72}$$

At low frequencies, this PSD has 0 log–log slope, and at high frequencies, it has –2 log–log slope. In between there is a region where the slope approximates –1. Thus, flicker noise over a given bandwidth can be approximated as a sum of exponentially correlated noises.

The information in the PSD and/or Allan variance plots of gyroscope and accelerometer data indicates how an inertial guidance and navigation linear dynamic system model can be augmented with states to approximate the noise spectrum of the inertial instrument outputs. Having correct noise models in the guidance and navigation model leads to better performance for the calibration, alignment, and guidance Kalman filters.

I.9.3 Estimating parameters in stochastic linear dynamic systems

Instead of estimating noise parameters from the slopes and levels in log–log PSD or Allan variance plots, these parameters can be estimated along with the states from the dynamic system model [Equation (I.59) and Equation (I.60)].

The parameters $\alpha = (\alpha_1, ..., \alpha_m)$ enter into the dynamic system model in the matrices *A, B, L, H,* and *R.* If the state vector $x(t)$ is augmented with the parameters α with the added state equations

$$d\alpha = 0 + \text{noise} \tag{I.73}$$

then both $x(t)$ and α can be estimated with a Kalman filter. However, the augmented state dynamic equations might no longer be linear since the α could multiply the x through the matrix A and the Wiener process β through the matrix L. Therefore, an extended Kalman filter might have to be used.

A more theoretically correct approach to simultaneously estimating the parameters α and the states $x(t)$ is to employ maximum likelihood system identification (see Sandell and Yared [B48]), a technique that is also used in adaptive control (see Maybeck [B36]). A first guess is made for the values of the parameters α

— Mean x_0 of state initial conditions
— Dynamic parameters (e.g., trends, scale factors, and biases)
— Noise parameters (e.g., white, random walk, and exponentially correlated)

Then the Kalman filter is run to estimate the states $x(t_k)$ and at the same time calculate quantities associated with the likelihood function (probability density) of the observables $z^N = (z_N, ..., z_1)$

$$p(z^N) = p(z_N|z^{N-1}, x_0)p(z_{N-1}|z^{N-2}, x_0) \dots p(z_2|z_1, x_0)p(z_1|x_0)p(x_0) \tag{I.74}$$

where

$p(z_k|z^{k-1}, x_0)$ is the Gaussian probability density of Kalman filter pre-update residual (innovation) at time t_k

The partial derivatives of the negative log likelihood $\zeta(z^N) = -\ell n[p(z^N)]$ with respect to the parameters α are computed, and a maximum likelihood adjustment is made to the parameters toward the values that minimize the negative log likelihood. Using the adjusted values α, the Kalman filter is rerun and further adjustments made, and the process is continued until convergence is obtained.

Maximum likelihood system identification can successfully separate trend from random walk and estimate white, random walk, and exponentially correlated noise parameters (see Ash and Skeen [B6] and Skeen [B50]).

Annex J

(informative)

Characterization of transient behavior

J.1 Types of transient behavior

There can be a transient in an accelerometer's output after inversion between +1 *g* and –1 *g*; after shock, vibration, or other environmental exposures; and after a turn-on and warm-up to operating temperature after a previous shutdown. This transient could be increasing or decreasing with overshoot and undershoot oscillations about the final steady-state output. There could also be changes in the steady-state trend and a shift in the data from before to after the event.

The specifications in 5.3.12, 5.3.16, and 5.3.18 require that the accelerometer output be within specified limits within a specified time after a turn-on or inversion. The repeatability requirements of 5.3.5.5, 5.3.7.5, and 5.3.8.5 require that variations in the accelerometer bias, scale factor, and misalignment be within certain bounds across environmental exposures. The various specifications could be stated in terms of the allowable shift in output across an event and the allowable change in trend from before to after the event at a given time after the event.

The nature of the transient in reaching steady-state output can give insight into the physical mechanisms involved in the accelerometer responding to an event, which can help in designing error sources out of the device. The shift and transient across an event are separate characteristics from the hysteresis behavior of the accelerometer through a thermal cycle or a pendulum movement cycle although the physical mechanisms in transient and hysteresis effects could be related.

J.2 Second-order ordinary differential equation transient

Consider the second-order ordinary differential equation

$$\frac{1}{\omega^2}\frac{d^2Y}{dT^2}+\frac{2\zeta}{\omega}\frac{dY}{dT}+Y=R \quad \text{(J.1)}$$

where

ω	is the natural circular frequency of undamped system
ζ	is the damping ratio
R	is the input

The response $Y(T)$ to a unit step input R subject to zero initial conditions at time $T = 0$ is (see D'Azzo and Houpis [B17])

$$Y(T)=1-\frac{\mathrm{e}^{-\zeta\omega T}}{\sqrt{1-\zeta^2}}\sin\left(\omega\sqrt{1-\zeta^2}T+\cos^{-1}\zeta\right) \quad \text{(J.2)}$$

The damped sinusoidal response with ζ= 0.3 is given in Figure J.1.

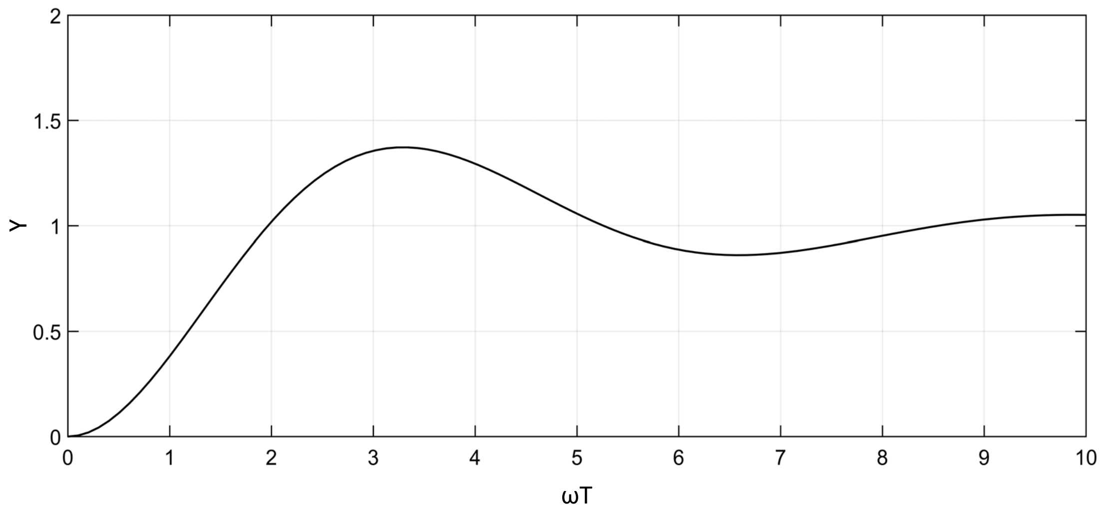

Figure J.1—Second-order system transient (ζ = 0.3)

The transient response in Figure J.1 could arise, for instance, during the warm-up of an accelerometer to operating temperature where the temperature control loop initially overshoots the amount of heat put in the accelerometer and then settles out at the control point. However, a second-order ordinary differential equation model of the behavior of the temperature control loop and the physical response of the accelerometer to temperature variations could be overly simplistic.

J.3 Exponential, square root, and logarithmic transients

Exponential-in-time transient behavior often occurs with thermal effects. Logarithmic-in-time transient behavior is often associated with anelastic, stress relaxation, creep, and magnetic and other aging effects in the materials used in fabricating the accelerometer.

Logarithmic transient behavior could be difficult to distinguish from square-root-in-time transient behavior, which is characteristic of diffusion effects.

Figure J.2 plots the following curves:

Exponential Transient: $\mathrm{Y} = 1 - \mathrm{e}^{-bT}$, $b = \ln 2$ (J.3)

Square Root in Time Transient: $\mathrm{Y} = b\sqrt{T}$, $b = 0.5$ (J.4)

Logarithmic Transient: $\mathrm{Y} = \ln(1 + bT)$, $b = \mathrm{e}^{0.5} - 1$ (J.5)

where the coefficients b are chosen so that the curves coincide at time $T = 0$ and time $T = 1$ to the values 0 and 0.5, respectively. Increasing transient examples are plotted; the negative of the these functions gives decreasing transient examples.

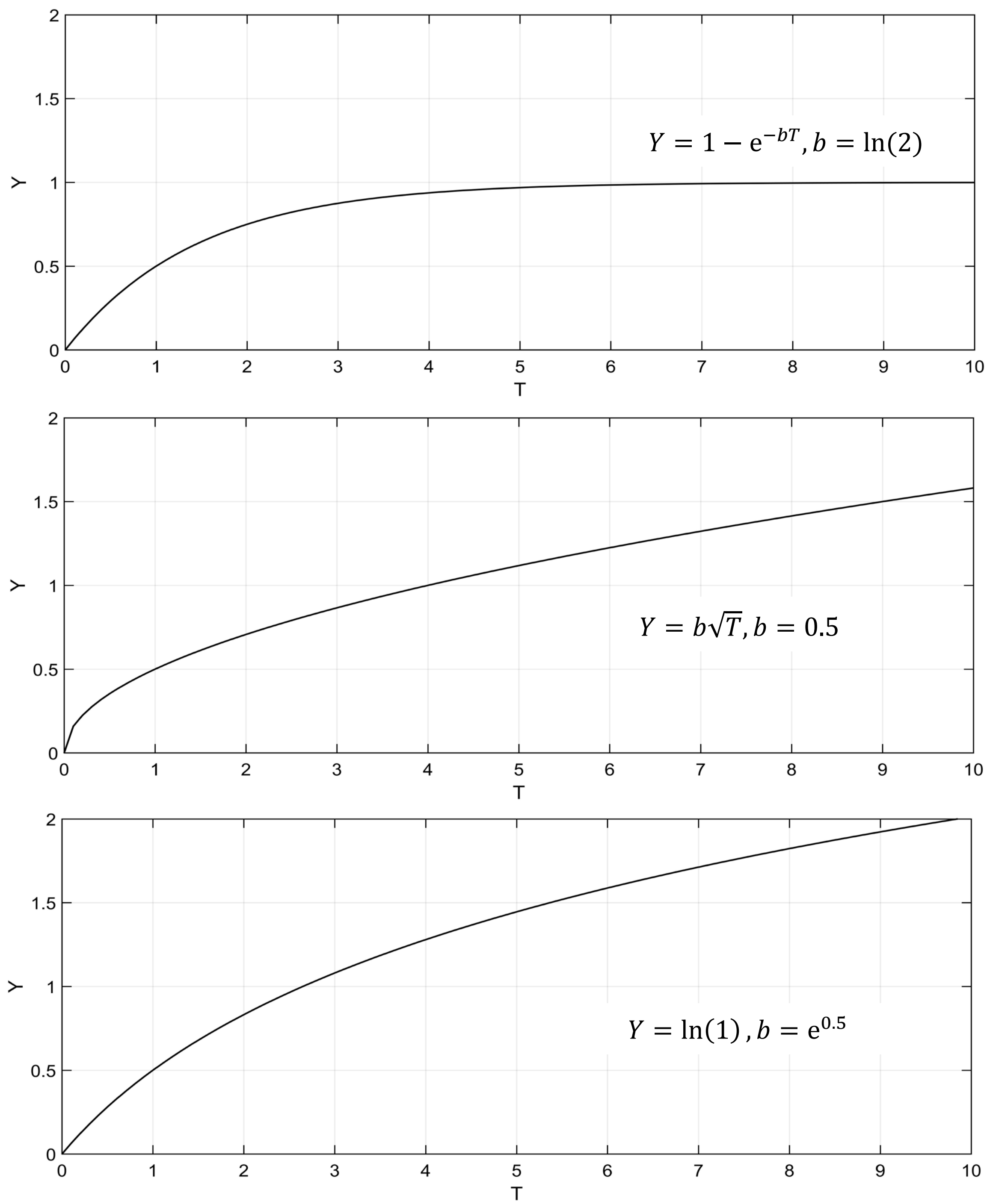

Figure J.2—Exponential, square root, and logarithmic transients

The exponential decay response is the unit step response solution of the following first-order ordinary differential equation with zero initial condition:

$$\frac{1}{b}\frac{dY}{dT} + Y = R \tag{J.6}$$

The exponential transient eventually dies out, whereas the square root and logarithmic transients increase in magnitude without bound. However, even the latter effects could be self-limiting. For instance, diffusion effects go as the square root of time multiplied by the difference between the concentrations of the diffused quantity between different parts of the system, where the latter eventually goes to 0.

Several mechanisms could be involved in a transient, each with its own functional form, magnitude, and time constant.

J.4 Estimation of transient parameters

Let t_0 be the starting time of a transient with the following possible functional forms:

Exponential: $$A\mathrm{e}^{-B(t-t_0)} + \text{bias or trend} \tag{J.7}$$

Square Root: $$A\sqrt{t-t_0} + \text{bias or trend} \tag{J.8}$$

Logarithmic: $$A\ln[1+B(t-t_0)] + \text{bias or trend} \tag{J.9}$$

Once an intelligent guess is made at what seems to be the functional form of a transient, an iterative, nonlinear, least-squares estimation can be used to determine the coefficients of the given model *(A, B,* and the bias or trend parameters). Convergence might not be obtained if an incorrect model is chosen or if the first guesses at the parameter values are not close enough to the true values.

If several error mechanisms are occurring simultaneously, two or more exponential decay terms, for example, might be required in the model with different time constants. Multiple exponential transients could appear like a square root or logarithmic transient.

Part V—Calibration and modeling techniques

Annex K

(informative)

Calibrating accelerometer model coefficients from static multipoint tumble data

K.1 Multipoint tumble test and analysis procedures

K.1.1 Purpose of multipoint tumble testing

In a discrete multipoint tumble test, an accelerometer is rigidly attached in a mounting fixture on a dividing head (see 11.2.2.3), and its input axis (IA) is sequentially placed at discrete orientations relative to the local gravity vector with output data recorded at each dividing-head position.

The goals of multipoint tumble data analysis are

- Calibration of the accelerometer model coefficients
- Determination of model coefficient stability from tests spread over time
- Determination of model coefficient sensitivities from varying temperature and other test condition set points
- Determination of the existence and signature of unmodeled effects from any systematic rather than random behavior in the postfit data residuals

K.1.2 Analysis procedures

The estimation (i.e., calibration) technique employed in a multipoint tumble test for an inertial guidance system is typically a sequential Kalman filter, whereas for accelerometer level tests, it is typically a batch least-squares maximum likelihood estimator. Either technique yields the same estimates of the model coefficients if the model is linear and the measurement noise is additive and Gaussian (see Gelb [B22]). A discussion of fitting models to data using least-squares maximum likelihood estimation is given in K.6.

Using more dividing-head positions than required for estimating known model coefficients can better reveal the signature of unmodeled effects in the postfit data residuals and help infer possible physical causes for the unmodeled effects. However, the estimation of the known model coefficients from the tumble data is aliased by the presence of unmodeled effects, and the true signature of the unmodeled effect in the postfit residuals is distorted.

As an extreme example, consider an unmodeled thermal effect that has the same shape tumble signature as a modeled quadratic acceleration sensitivity; that is, the two effects are perfectly correlated. The only way to differentiate the two is to use a calibration test that excites one physical mechanism and not the other. For instance, the quadratic acceleration sensitivity could be calibrated in a vibration test (see Annex L) where the thermal effect is not excited with average zero acceleration. Then the quadratic acceleration sensitivity coefficient is held fixed at the vibration-calibrated value in estimating other model coefficients from tumble data, so that the magnitude and signature of the unmodeled thermal effect can better be discerned in the tumble postfit data residuals.

K.1.3 Setup of dividing head and mounting fixture

The accelerometer is attached to an aluminum (or other such material) mounting fixture or block with (nonmagnetic if required) bolts with a specified wrench torquing level. If the mounting fixture were a cube, for example, there could be mounting surfaces with the bolt hole pattern of the accelerometer mounting flange on five of the six cube faces. A free surface of the mounting fixture is attached to the face plate of the dividing head with bolts, perhaps with the use of an adapter plate.

The mounting fixture might be thermally controlled (see 11.1.2.2), in which case, a thermal shim or spacer might be required between the mounting fixture and the dividing head or adapter plate. The parallelism and perpendicularity of the mounting-fixture faces are toleranced to have the mounting surfaces parallel or perpendicular to the dividing-head rotation axis within specified limits.

The dividing-head angle at which a given mounting surface is perpendicular to the gravity vector can be determined by placing a horizontal precision bubble level approximately perpendicular to the dividing-head rotation axis on the mounting surface in the up orientation. For a fine resolution angle readout, the angle reading at bubble level null defines the up position of the dividing head for a tumble test. For a discrete angle readout, such as every 1°, the dividing head could have a vernier adjustment to bring the nearest 1° angle position to the up position.

The bubble level rotated 90° on the given mounting surface in the up orientations (so that the horizontal bubble level is approximately parallel to the dividing-head rotation axis) can be adjusted to null by putting shims under the dividing head. In this manner, the dividing-head rotation axis can be made horizontal within required tolerances.

It is assumed that an appropriate bias angle is subtracted from the dividing-head readout so that 0° and 180° define the IA horizontal orientations, 90° the IA up orientation (accelerometer output indicating +1 *g*), and 270° the IA down orientation (accelerometer output indicating –1 *g*), except for residual mounting block alignment errors, misalignments between the accelerometer's mounting flange and IA, dividing-head and fixture coning, dividing-head positioning error, and so on. If these misalignments are ignorable in the IA up and down positions (because their cosines are essentially 1) and allow small-angle approximations in other positions, then they are accounted for in analyzing the test data.

K.1.4 Test and data acquisition scenarios

K.1.4.1 Angle sequences

A sequence of dividing-head positions θ_1, ….., θ_n is chosen. A discrete set of positions is assumed rather than a continuous tumble, although the latter might be used for the calibration of some guidance systems.

The number and spacing of the dividing-head positions are a trade-off between obtaining accurate estimates of the coefficients in the accelerometer model, giving visibility into any unmodeled effects, and not having the tumble test extend over too long a time, both to minimize cost and to minimize corruption from trends or other phenomena.

One commonly used angle sequence scenario is to have uniform angle spacing $\Delta\theta = 360°/n$ (see 12.3.5.4). For some accelerometers, it might be necessary to avoid positions having IA exactly horizontal ($\theta_j = 0°$, 180°) because of, for example, bias, scale-factor, or misalignment asymmetries. An angle sequence scenario for most economically obtaining accurate estimates for coefficients sensitive to along-IA acceleration is at uniform increments of sensed acceleration but not necessarily so for cross-IA and other coefficients. The data at the IA up and down positions are particularly important to include in a fit because they are insensitive to the effect of dividing-head angle-setting and tilt errors.

The dividing head could be automatically or manually rotated between positions. It could be locked into position with no possibility of movement, except from seismic inputs and tilt variations in the pad on which the dividing head rests, or there could be servo control at each position. In the latter case, if high accuracy is required, applying a brake at each position might be necessary to prevent servo control limit cycling from corrupting the accelerometer data.

K.1.4.2 Data averaging or filtering at a position

When the dividing head is moved to an angle θ_j, any transients are allowed to die out. The data are then accumulated over an appropriate time and averaged or higher ordered filtered to obtain a measurement E_j with required accuracy. If outliers exist in the data being averaged or filtered at a given position (more than 3 or so standard deviations from the average of the data), they can be left out or interpolated across in the averaging or filtering computations, especially if there is a seismic or other cause for their deviation. The uncertainty of a measurement E_j at a position, which can be used as a weighting w_j in the least-squares estimation process, is the root-mean-square (rms) of the raw data about E_j.

One method of filtering the data at a tumble position is to do a least-squares fit of a straight line to the accumulated velocity increments output from the accelerometer. The acceleration measurement is then the slope of this line, and its uncertainty is provided by the standard deviation of the slope estimate (see K.6.6).

K.1.4.3 Single versus multiple accelerometer testing

If a single accelerometer is being tested, or if multiple IA parallel or antiparallel accelerometers are being tested, then the angle-setting error and repeatability of the dividing head and the tilt variation during the test have to be less than the accuracy being sought in the accelerometer-tumble calibration. Since dividing heads have at best no better than μrad angle-setting accuracy and repeatability, and tilt variations could be of the order of a μrad or more over the course of a test, when single or multiple IA parallel or antiparallel accelerometers are being tested, one cannot expect to obtain better than μ*g*, ppm, and μrad estimation accuracies for bias, scale factor, and misalignment, respectively. However, data from multiple IA parallel or antiparallel accelerometers can help distinguish between data anomalies due to a problem in one of the accelerometers versus anomalies due to instrumentation or environmental problems that are common to all the accelerometers, besides increasing productivity by testing more accelerometers in a given period of time.

If the accelerometer is more accurate than the dividing head on which it is tested, then dual orthogonal accelerometer testing should be employed. Dual orthogonal accelerometer testing allows for the estimation of angle-setting and tilt errors simultaneously with that of the accelerometer model coefficients and nonorthogonality. Alternatively, the magnitude-squared-of-*g* observable (sum-of-squares of orthogonal accelerometer outputs, commonly used in guidance system calibrations) can be employed to estimate accelerometer model coefficients and nonorthogonality since it is insensitive to angle-setting and tilt errors.

K.1.5 Test orientations

K.1.5.1 OA rotation mounting position

For a tumble test with the OA along the dividing-head rotation axis, the components of the specific acceleration reaction to gravity are taken to be

$$a_i = G\sin(\theta + \delta\theta + \delta_o), \quad a_p = G\cos(\theta + \delta\theta + \delta_o), \quad a_o = 0 \tag{K.1}$$

where

G	is the vertical acceleration reaction to plumb bob gravity (taken to be the value 1 plus often ignorable effects from the lunar–solar earth tide and the gravity gradient during a tumble; see K.2.5.2)
$\delta\theta$	is the dividing-head and mounting-fixture angle-setting and tilt error relative to the local vertical at dividing-head position θ

δ_o is the misalignment about the output axis (OA) of the accelerometer IA relative to its mounting flange (the sign of δ_o relative to θ depends on whether the OA is inward or outward along the dividing-head rotation axis and is ignored)

Since the scale factor estimated in a multipoint tumble test uses the local value of plumb bob gravity as a reference, its value has to be converted into a standard unit for use in a guidance system mission or for comparisons with calibrations at different test sites.

The acceleration component a_o is $G(\delta_p + \delta_a + \delta_b)$, where sign phasing is ignored and the sine of a small angle is set equal to the angle. Here, δ_p is the misalignment about the pendulous axis (PA) of the accelerometer IA relative to its mounting flange, δ_a is the misalignment of the mounting flange relative to the dividing-head rotation axis, and δ_b is the misalignment of the dividing-head rotation axis from horizontal.

The values of $\delta\theta$ and $\delta_a + \delta_b$ at the $\theta = 90°$ up position can be made small (less than 10 μrad or so) with bubble leveling (see K.1.3). The values of $\delta\theta$ will vary at other positions, but for a good dividing head, they could be of the order of a few μrad relative to its value at $\theta = 90°$. The value of δ_b can also vary at other positions due to dividing-head coning or wobble relative to the mean rotation axis, but it could be less than 10 μrad for a good dividing head. However, because of manufacturing tolerances, the accelerometer internal misalignments δ_o, δ_p could be of the order of 1 mrad.

The component a_o is ignored in analyzing multipoint tumbles about OA because its effect cannot be separated from that of bias for constant $\delta_p + \delta_a + \delta_b$ and from scale factor for coning δ_b. Remounting the accelerometer on the mounting fixture affects misalignment estimates. Hence, the coefficients estimated in tumbles about OA and PA with accelerometer remounts between tests cannot be directly compared. However, the comparison of the results of a sequence of tumbles about a given axis with no remounts in between is directly comparable as far as stability of coefficients is concerned.

The magnitude of G is reduced by a factor of the cosine of $\delta_p + \delta_a + \delta_b$ in Equation (K.1). For 1-mrad misalignment, G is reduced by a factor of 5×10^{-7}. This reduction again is of no concern in comparing the results of a sequence of instrument-level multipoint tumbles, but it does affect the absolute estimate of scale factor, as does the ignored value of a_o. However, scale factor, bias, and misalignments are typically estimated at the guidance system level before a mission from tumbles about several axes without remounts in order to have the most current values of these coefficients (see K.2.6.2).

K.1.5.2 PA rotation mounting position

For a tumble test with the PA along the dividing-head rotation axis, the components of the specific acceleration reaction to gravity are taken to be

$$a_i = G\sin(\theta + \delta\theta + \delta_p), \quad a_o = G\cos(\theta + \delta\theta + \delta_p), \quad a_p = 0 \qquad \text{(K.2)}$$

where the sign of δ_p relative to θ depends on whether the PA is inward or outward along the dividing-head rotation axis and is ignored. The same comments as in K.1.5.1 about assuming $a_o = 0$ for a tumble about OA apply to assuming $a_p = 0$ for a tumble about PA.

K.1.5.3 IA rotation mounting position

A sequence of multipoint tumbles with IA along the dividing-head rotation axis could be used to determine stability of bias and two IA misalignment angles simultaneously if dividing-head coning is repeatable, rather than only one misalignment at a time as with tumbles about OA or PA. The IA along dividing-head rotation axis orientation should not be used if the accelerometer has scale-factor, bias, or IA misalignment asymmetries. Multipoint tumbles about IA will not be considered further in this annex.

K.2 Model equation for multipoint tumble analysis

K.2.1 Choice of model coefficients

Let the scale factor in the model equation of 8.3 be expressed as

$$K_1 = K_1^{\circ}(1 + k_1) \tag{K.3}$$

where

K_1°	is a nominal scale factor
k_1	is a small correction or error

The nominal scale factor could be determined, for example, from an IA up–down test [see e) of 12.3.4.4]. It is then desired to estimate the remaining model coefficients k_1, K_x (x = 0, 2, 3, *oq, ip, pp,* etc.) and misalignments in 8.3 from the tumble data. After the scale-factor error k_1 has been estimated, the scale factor K_1 in output units/g is calculated from Equation (K.3).

It can be assumed that squares and products of k_1, and the K_x $(x \neq 1)$ are small enough to ignore.

K.2.2 Estimating model coefficients

Write the model equation in 8.3 for the indicated accelerometer output $A_{\text{ind},j}$ at angle position θ_j in the form

$$A_{\text{ind},\,j} = E_j/(K_1^{\circ}) = f(\theta_j, \alpha) + \varepsilon_j \quad , \quad j = 1, \ldots, n \tag{K.4}$$

where

E_j	is the averaged or filtered value of the measurements at position θ_j
ε_j	is the assumed random measurement noise at position θ_j
$\alpha = (\alpha_1, \ldots, \alpha_m)$	are the parameters k_1, K_x, and misalignments to be estimated (x = 0, 2, 3, *oq, ip, pp,* etc.)

Employing the model equation for the raw observable E_j rather than the quantity $A_{\text{ind},j}$ would be desirable if K_1 were brought inside the curly brackets in the model equation in 8.3 and the parameters were considered to be K_1 and (K_1K_x) for x = 0, 2, 3, *oq, ip, pp,* and so on. However, in deriving the theoretical value of the magnitude-squared-of-g observable, the model equation has to be written in terms of $(l + k_1)$, with k_1 being the scale factor error whose square and product with the other model terms can be ignored. Therefore, model equation (K.4) is assumed in order to handle all three approaches to tumble test parameter estimation (single accelerometer, dual orthogonal accelerometers, and magnitude-squared-of-g) in a unified manner.

In 8.3, ε_j includes process noise and unmodeled error as well as measurement noise. Since this annex does not employ a Kalman filter for which process noise within the accelerometer (characterized by Allan variance or PSD analysis, see Annex I) is modeled by augmented Markov noise states, process noise is ignored. If least-squares estimation is employed, ε_j can include unmodeled error. However, to obtain the maximum likelihood formula for parameter estimate covariance, it is necessary to ignore unmodeled error and assume that ε_j is zero mean Gaussian random measurement noise, uncorrelated from position to position. (The uncorrelated assumption is not strictly necessary.)

Insofar as measurement noise is the sum of many small errors, the central limit theorem implies that the measurement noise will tend to be Gaussian. Sufficiently long averaging or filtering time at a tumble position will ensure that quantization noise can be ignored (see K.1.4.2).

Let w_j be the uncertainty of the scaled measurement $A_{\text{ind},j}$ (standard deviation of ε_j). The method of least squares seeks values $\hat{\alpha}$ of the parameters α for which

$$\sum_{j=1}^{n} \frac{\left[A_{\text{ind},j} - f\left(\theta_j, \hat{\alpha}\right)\right]^2}{w_j^2} = \text{minimum} \tag{K.5}$$

As a practical matter, if the accuracy of the data varies little at each position, the weights can be taken as $w_j = 1$.

The technique for solving Equation (K.5) for the parameter estimates $\hat{\alpha}$ is described in K.6.2. If the model function $f(\theta_j, \alpha)$ is nonlinear in the parameters α, then an iterative technique is required, whereas one iteration suffices to determine the estimates $\hat{\alpha}$ for a linear model.

Since least-squares estimation is the same as maximum likelihood estimation if the measurement errors ε_j have Gaussian probability distributions, uncertainties and correlations can be assigned to the parameter estimates $\hat{\alpha} = (\hat{\alpha}_1, \ldots, \hat{\alpha}_m)$ (see K.6.6).

There have to be at least as many tumble positions as there are coefficients to be estimated. Having more than the minimum number of necessary positions is desirable to increase estimation accuracy and discern unmodeled error signatures. Some parameters cannot be simultaneously estimated in a 1 *g* tumble because of perfect correlations no matter how many positions are used, such as K_2 and K_{pp} in a tumble about OA (see K.2.4).

Sometimes the indicated acceleration at a position has a postfit residual much larger than the residuals at other positions. Leaving such a "wild" point out of the fit could yield more valid estimation results, especially if there were a reason for the average of data at a position to be corrupted or if repetitions of the tumble test did not have that behavior at that position.

K.2.3 Single accelerometer model equation

K.2.3.1 Tumble about OA

Combining the model equation in 8.3 and Equation (K.1) with $\delta\theta = 0$ and $G = 1$, the model equation in (K.4) takes the form

$$\begin{aligned} f\left(\theta_j, \alpha\right) = \quad & K_0 + \frac{1}{2}K'_0 \operatorname{sign}\left[\sin\left(\theta_j + \delta_o\right)\right] + (1 + k_1)\sin\left(\theta_j + \delta_o\right) \\ & + \frac{1}{2}K'_1\left|\sin\left(\theta_j + \delta_o\right)\right| + K_{oq}\sin\left(\theta_j + \delta_o\right)\left|\sin\left(\theta_j + \delta_o\right)\right| \\ & + K_2\sin^2\left(\theta_j + \delta_o\right) + K_3\sin^3\left(\theta_j + \delta_o\right) \\ & + K_{ip}\sin\left(\theta_j + \delta_o\right)\cos\left(\theta_j + \delta_o\right) + K_{pp}\cos^2\left(\theta_j + \delta_o\right) \end{aligned} \tag{K.6}$$

where the parameters α are δ_o, k_1, and the K_x (x = 0, 2, 3, *oq, ip, pp,* etc.). If model equation (K.6) is used with no small-angle approximation made for the misalignment δ_o, then iterative, nonlinear, least-squares parameter estimation has to be used.

If a small-angle approximation is made with the misalignment δ_o, then linear least-squares parameter estimation can be used with the model equation

$$f(\theta_j,\alpha) = K_0 + \frac{1}{2}K'_0 \mathrm{sign}[\sin\theta_j] + (1+k_1)\sin\theta_j + \delta_o\cos\theta_j + \frac{1}{2}K'_1|\sin\theta_j| + K_{oq}\sin\theta_j|\sin\theta_j| + K_2\sin^2\theta_j + K_3\sin^3\theta_j + K_{ip}\sin\theta_j\cos\theta_j + K_{pp}\cos^2\theta_j \quad \text{(K.7)}$$

K.2.3.2 Tumble about PA

Combining the model equation in 8.3 and Equation (K.2) with $\delta\theta = 0$ and $G = 1$ leads to an equation similar to (K.6) with no small-angle approximation for δ_p and similar to (K.7) with a small-angle approximation for δ_p, with K_{pp} replaced by K_{oo}, K_{ip} replaced by K_{io}, and δ_o replaced by δ_p. The small misalignment angle approximation version is

$$f(\theta_j,\alpha) = K_0 + \frac{1}{2}K'_0 \mathrm{sign}[\sin\theta_j] + (1+k_1)\sin\theta_j + \delta_p\cos\theta_j + \frac{1}{2}K'_1|\sin\theta_j| + K_{oq}\sin\theta_j|\sin\theta_j| + K_2\sin^2\theta_j + K_3\sin^3\theta_j + K_{io}\sin\theta_j\cos\theta_j + K_{oo}\cos^2\theta_j \quad \text{(K.8)}$$

where the sign of δ_p is arbitrary, depending on whether PA is inward or outward along the dividing-head rotation axis.

K.2.4 Fourier coefficients and parameter correlations

The Fourier expansion of the accelerometer model Equation (K.7) for a tumble about OA is

$$f(\theta_j,\alpha) = b_0 + \sum_{\ell\geq 1} b_\ell\cos\ell\theta_j + \sum_{\ell\geq 1} c_\ell sinl\theta_j \quad \text{(K.9)}$$

where by the standard integral formulas for Fourier coefficients

$$b_\ell = \frac{1}{\pi}\int_0^{2\pi}(\text{model equation})\cos\ell\theta\ d\theta \qquad (1/2\pi \text{ if } \ell = 0)$$

$$c_\ell = \frac{1}{\pi}\int_0^{2\pi}(\text{model equation})\sin\ell\theta\ d\theta$$

so that

$$b_0 = K_0 + K_2 + \frac{1}{2}(K_{pp} - K_2) + \frac{1}{\pi}K'_1$$

$$b_1 = \delta_o$$

$$c_1 = (1 + k_1) + \frac{3}{4}K_3 + \frac{2}{\pi}K'_0 + \frac{8}{3\pi}K_{\mathrm{oq}}$$

$$b_2 = \frac{1}{2}\left(K_{pp} - K_2\right) - \frac{2}{3\pi}K'_1$$

$$c_2 = \frac{1}{2}K_{\mathrm{ip}}$$

$$c_3 = -\frac{1}{4}K_3 + \frac{2}{3\pi}K'_0 - \frac{8}{15\pi}K_{\mathrm{oq}}$$

$$b_{2\ell} = -\frac{2}{(4\ell^2 - 1)\pi}K'_1, \quad \ell > 1$$

$$c_{2\ell+1} = \frac{2}{(2\ell + 1)\pi}K'_0 + \frac{1}{\pi}\left[\frac{2}{2\ell + 1} - \frac{1}{2\ell - 1} - \frac{1}{2\ell + 3}\right]K_{\mathrm{oq}}, \quad \ell > 1 \qquad \text{(K.10)}$$

The formulas for a tumble about PA are the same with K_{pp} replaced by K_{oo}, K_{ip} replaced by K_{io}, and δ_{o} replaced by δ_{p}.

The Fourier coefficients are listed to illustrate correlations (i.e., similar tumble signatures) between model coefficients. Estimation of model coefficients should make use of the original model equation with least-squares estimation since some terms such as K_{oq} and asymmetries lead to an infinite number of Fourier coefficients.

From the Fourier coefficients b_2 and b_0, it is clear that, when K_0 is estimated, only the difference ($K_{\mathrm{pp}} - K_2$) can also be estimated in a tumble about OA and only the difference ($K_{\mathrm{oo}} - K_2$) can be estimated in a tumble about PA, with the individual K_2 lumped in with K_0. The estimates of K_2 and K_{pp} or K_{oo} individually are perfectly correlated in a 1-*g* tumble test because the sum of the squares of orthogonal components of gravity acceleration is equal to 1 *g*. To estimate all the quadratic acceleration sensitivity coefficients, vibration (Annex L) or centrifuge (IEEE Std 836™) tests are needed along various axes at various acceleration levels.

Some quadratic acceleration sensitivity coefficients could be estimated in such high-*g* tests, and the others estimated in a 1-*g* tumble test using the previously calibrated values in the model equation. However, extremes of accuracy are needed to estimate quadratic and higher order acceleration sensitivities in a 1-*g* tumble test (see K.3.4 and K.4.2).

If K_3 were not estimated, but rather set to 0, for instance, then the estimate of scale-factor error k_1 would be biased by three fourths of the value of K_3. Similarly, if principal second-order nonlinearities were not estimated but rather set to 0, then the estimate of bias K_0 would be biased by one half the sum of some of the principal nonlinearities, depending on which axis the tumble is about.

This biasing is unimportant if stability of parameter estimates is being determined from tumble tests made over a period of time without remounts on the tumble fixture. Besides biasing parameter estimates, nonestimated parameters as well as unmodeled effects contribute to systematic postfit data residuals unless they are included in the model equation using calibrated values from other tests.

K.2.5 Model equation with dual orthogonal accelerometers

K.2.5.1 Estimating model coefficients and angle-setting errors

Consider two accelerometers ($\lambda = 1, 2$) tested simultaneously with model equations

$$A_{\mathrm{ind},\lambda_j} = f_\lambda\left(\theta_j, \alpha\right) + \varepsilon_{\lambda j}\ , \qquad j = 1, \ldots, n \qquad \text{(K.11)}$$

where, as in Equation (K.4), $\varepsilon_{\lambda j}$ is the random measurement error. Assume that the accelerometers are oriented nearly orthogonal on the dividing head with their OAs along the dividing-head rotation axis and that their measurement accuracies are greater than the angle-setting accuracy of the dividing head. Assume

- η is the nonorthogonality error between the IAs of accelerometers 1 and 2 about OA
- $\delta\theta_j$ is the angle-setting error for the IA of accelerometer 1 at position θ_j (including the effect of misalignment δ_o of accelerometer 1 and the instantaneous tilt of the test platform relative to the local vertical direction)
- $K_{\lambda x}$ is the model parameter for accelerometer λ (x = 0, 2, 3, *oq, ip, pp*, etc.)
- $k_{\lambda 1}$ is the scale factor correction or error for accelerometer λ

Let G_λ be the vertical acceleration reaction to gravity on accelerometer λ, differing from 1 only because of the lunar-solar earth tide and gravity gradient corrections. Assume that the variation of G_λ from 1 is ignorable in products with all model terms $k_{\lambda 1}$, $K_{\lambda x}$. Model equation (K.6) for accelerometer 1 for a tumble about OA is then

$$\begin{aligned} f_1(\theta_j, \alpha) = \quad & K_{10} + \frac{1}{2}K'_{10}\text{sign}\left[\sin(\theta_j + \delta\theta_j)\right] + (G_1 + k_{11})\sin(\theta_j + \delta\theta_j) \\ & + \frac{1}{2}K'_{11}\left|\sin(\theta_j + \delta\theta_j)\right| + K_{1oq}\sin(\theta_j + \delta\theta_j)\left|\sin(\theta_j + \delta\theta_j)\right| \\ & + K_{12}\sin^2(\theta_j + \delta\theta_j) + K_{13}\sin^3(\theta_j + \delta\theta_j) \\ & + K_{1\text{ip}}\sin(\theta_j + \delta\theta_j)\cos(\theta_j + \delta\theta_j) + K_{1\text{pp}}\cos^2(\theta_j + \delta\theta_j) \end{aligned} \tag{K.12}$$

The model equation for accelerometer 2 rotated 90° + η on the dividing head is

$$\begin{aligned} f_2(\theta_j, \alpha) = \quad & K_{20} + \frac{1}{2}K'_{20}\text{sign}\left[\cos(\theta_j + \delta\theta_j + \eta)\right] \\ & + (G_2 + k_{21})\cos(\theta_j + \delta\theta_j + \eta) + \frac{1}{2}K'_{21}\left|\cos(\theta_j + \delta\theta_j + \eta)\right| \\ & + K_{2\text{oq}}\cos(\theta_j + \delta\theta_j + \eta)\left|\cos(\theta_j + \delta\theta_j + \eta)\right| \\ & + K_{22}\cos^2(\theta_j + \delta\theta_j + \eta) + K_{23}\cos^3(\theta_j + \delta\theta_j + \eta) \\ & - K_{2\text{ip}}\cos(\theta_j + \delta\theta_j + \eta)\sin(\theta_j + \delta\theta_j + \eta) \\ & + K_{2\text{pp}}\sin^2(\theta_j + \delta\theta_j + \eta) \end{aligned} \tag{K.13}$$

Let m model coefficients for each accelerometer be estimated in fitting to the tumble data, where nonestimated coefficients come from some other calibration test, such as must be done for one of $K_{\lambda 2}$ or $K_{\lambda\text{pp}}$, for example. Also the $K_{\lambda\text{ip}}$ and $K_{\lambda 3}$ cannot be estimated in this test (see K.5.2). In addition, n angle-setting errors $\delta\theta_j$ and one nonorthogonality η have to be estimated, for a total of $2m + n + 1$ parameters from $2n$ measurements at the n positions. If n is chosen so that $2n > 2m + n + 1$ or $n > 2m + 1$, then the model coefficients can in principle be estimated with the effect of angle-setting errors removed if parameter estimate correlations allow. Just how well the parameters can in fact be estimated is discussed in K.4.

The model equations for a tumble about PA are similar to those for a tumble about OA and will not be written out.

K.2.5.2 Effect of lunar-solar earth tide and gravity gradient

In units of local plumb-bob-gravity acceleration g, the magnitude of the vertical acceleration reaction of gravity acting on accelerometer λ is

$$G_\lambda = 1 + G_{\text{tide}} + G_{\text{grad},\lambda} \quad g \tag{K.14}$$

where the vertical component G_{tide} of the lunar–solar earth tide acceleration varies up to ±0.15 μg every 12.4 h (see Annex M) and where the gravity gradient correction $G_{\text{grad},\lambda}$ is

$$G_{\text{grad, 1}} = 0.00314\rho_1 \sin\theta_j \quad \mu g$$

$$G_{\text{grad, 2}} = 0.00314\rho_2 \cos\theta_j \quad \mu g \tag{K.15}$$

with ρ_λ being the distance in centimeters of the accelerometer λ proof mass from the dividing-head rotation axis. For example, if the distance of an accelerometer's proof mass from the dividing-head rotation axis is 10 cm, then the height of the accelerometer in the gravity field varies by ±10 cm in a tumble test and the gravity acceleration varies by ±0.0314 μg.

The horizontal component of the tidal acceleration varies the tilt of the local vertical direction relative to inertial space or the earth rotation axis by up to ±0.15 µrad (see Annex M), which is not of concern for accelerometer testing because the estimated angle-setting errors $\delta\theta_j$ are relative to the instantaneous local vertical direction.

K.2.6 Magnitude-squared-of-*g* model equation

K.2.6.1 Dual orthogonal accelerometer dividing-head tumble

Assume that squares and products of all model coefficients $k_{\lambda 1}$, $K_{\lambda x}$ (x = 0, 2, 3, *oq, ip, pp*, etc.), nonorthogonality η, and angle-setting errors $\delta\theta_j$ are ignorable. Consider the following model equation for the observable $A^2_{\text{ind},1j} + A^2_{\text{ind},2j} - 1$ for a tumble about OA:

$$\begin{aligned}
f(\theta_j,\alpha) = {} & f_1(\theta_j,\alpha)^2 + f_2(\theta_j,\alpha)^2 - 1 \\
= {} & 2\left[G_{\text{tide}} + \left(G_{\text{grad, 1}} + k_{11}\right)\sin^2\theta_j + \left(G_{\text{grad, 2}} + k_{21}\right)\cos^2\theta_j\right] \\
& +2\sin\theta_j\left[K_{10} + \frac{1}{2}K'_{10}\text{sign}(\sin\theta_j) + \frac{1}{2}K'_{11}\left|\sin\theta_j\right|\right. \\
& +K_{1\text{oq}}\sin\theta_j\left|\sin\theta_j\right| + K_{12}\sin^2\theta_j + K_{13}\sin^3\theta_j \\
& \left.+K_{1\text{ip}}\sin\theta_j\cos\theta_j + K_{1\text{pp}}\cos^2\theta_j\right] \\
& +2\cos\theta_j\left[K_{20} + \frac{1}{2}K'_{20}\text{sign}(\cos\theta_j) + \frac{1}{2}K'_{21}\left|\cos\theta_j\right|\right. \\
& +K_{2\text{oq}}\cos\theta_j\left|\cos\theta_j\right| + K_{22}\cos^2\theta_j + K_{23}\cos^3\theta_j \\
& \left.+K_{2\text{ip}}\cos\theta_j\sin\theta_j + K_{2\text{pp}}\sin^2\theta_j - \eta\sin\theta_j\right]
\end{aligned} \tag{K.16}$$

If m model coefficients for each accelerometer and the nonorthogonality η are being estimated from this observable at n positions, then if $n > 2m + 1$, the model parameters can be estimated without being corrupted by angle-setting errors $\delta\theta_j$ if parameter estimate correlations allow. For example, $K_{\lambda 2}$ and $K_{\lambda\text{pp}}$ cannot be simultaneously estimated. Also, $K_{\lambda\text{ip}}$ and $K_{\lambda 3}$ cannot be estimated in this test (see K.5.2).

To have squares and products ignorable, the angle-setting errors must be less than, for example, 0.1 mrad to 1 mrad. Suppose that the squares and products of some of the model parameters are not ignorable, such as bias being more than a m*g*. Let $\bar{f}_\lambda(\theta_j)$ be the model equation for accelerometer $\lambda = 1, 2$ with nominal values of the parameters so that the squares and products of the differences between the true and nominal parameter values are ignorable. Take the magnitude-squared-of-*g* observable to be

$$\left[A_{\text{ind},\,1j} - \bar{f}_1(\theta_j)\right]^2 + \left[A_{\text{ind},\,2j} - \bar{f}_2(\theta_j)\right]^2 \qquad \text{(K.17)}$$

The model equation for this observable is the same as the right side of Equation (K.16), where the parameters now represent adjustments to the nominal values of the parameters.

The model equation for a tumble about PA is similar to that for a tumble about OA and will not be written out.

K.2.6.2 Guidance system tumble with three orthogonal accelerometers

Consider an inertial guidance system with three nearly orthogonal accelerometers and also gyroscopes. A continuous or discrete multiaxis guidance system tumble scenario is chosen to excite gyroscope as well as accelerometer model coefficients. With the sum-of-squares accelerometer observable, tumbles are traversed without corruption of the accelerometer parameter estimates from angle-setting errors. For individual gyroscope observables, tumbles or slews about each gyroscope IA parallel or antiparallel to the earth rotation vector excite gyroscope model terms without corruption from angle-setting errors.

The accelerometer frame is defined with *X* axis along the IA of the first accelerometer, with *Y* axis orthogonal to the *X* axis in the plane of the IAs of the first and second accelerometers nearly along the IA of the second accelerometer, and with Z axis orthogonal to the *X* and *Y* axes nearly along the IA of the third accelerometer. Three accelerometer IA misalignments or nonorthogonalities have to be estimated along with the accelerometer model coefficients. Two misalignment angles relative to the accelerometer frame for each gyroscope IA have to be estimated along with the gyroscope model coefficients.

A real-time sequential Kalman filter estimator or a batch least-squares maximum likelihood estimator is employed to calibrate the model coefficients and nonorthogonalities or misalignments from the tumble or slew data with quadratic and higher order acceleration sensitivities probably being used from instrument-level vibration or centrifuge tests.

If the individual accelerometer observables have white Gaussian measurement noise, then the sum of the squares of the accelerometer observables does not have this property; and thus, the fundamental assumption used in deriving maximum likelihood and Kalman filter estimation formulas is not true. Using power spectral density (PSD) or other such techniques, the error statistics for individual accelerometer and sum-of-squares observables after passing through prefilters should be determined, and the appropriate modifications made to the estimation techniques if necessary. For example, the Kalman filter states could be augmented with Markov noise states.

As a practical matter, however, estimating model coefficients from individual accelerometer (with angle-setting errors estimated) or sum-of-squares observables lead to essentially the same results, even with different error statistics for the different observables.

K.3 Multipoint tumble analysis with a single accelerometer observable

K.3.1 Solving for bias, scale factor, and misalignment

K.3.1.1 Linear model with small misalignment angle assumption

Consider a multipoint tumble about OA or PA with bias K_0, scale-factor error k_1, and misalignment δ ($=\delta_o$ or δ_p) to be estimated with the small misalignment angle approximation model equation [Equation (K.7) or Equation (K.8)]

$$f(\theta_j) = K_0 + (1 + K_1)\sin\theta_j + \delta\cos\theta_j \tag{K.18}$$

The normal equations [Equation (K.33) to Equation (K.35)] with equally weighted data at the n positions $\theta_1, \ldots, \theta_n$ are

$$\begin{bmatrix} n & \sum_{j=1}^{n}\sin\theta_j & \sum_{j=1}^{n}\cos\theta_j \\ \sum_{j=1}^{n}\sin\theta_j & \sum_{j=1}^{n}\sin^2\theta_j & \sum_{j=1}^{n}\sin\theta_j\cos\theta_j \\ \sum_{j=1}^{n}\cos\theta_j & \sum_{j=1}^{n}\sin\theta_j\cos\theta_j & \sum_{j=1}^{n}\cos^2\theta_j \end{bmatrix} \begin{bmatrix} \hat{K}_0 \\ \hat{k}_1 \\ \hat{\delta} \end{bmatrix} = \begin{bmatrix} \sum_{j=1}^{n}(A_{ind,j} - \sin\theta_j) \\ \sum_{j=1}^{n}(A_{ind,j} - \sin\theta_j)\sin\theta_j \\ \sum_{j=1}^{n}(A_{ind,j} - \sin\theta_j)\cos\theta_j \end{bmatrix} \tag{K.19}$$

The solution of these equations gives the least-squares maximum likelihood estimates $\hat{K}_0, \hat{k}_1, \hat{\delta}$ directly (one iteration away from the initial guess 0 since the model equation is linear in the parameters with the small misalignment angle approximation). The covariance of the parameter estimates is the inverse of the coefficient matrix of the normal equations times the rms of the postfit residuals (see K.6.6).

K.3.1.2 Nonlinear model without small misalignment angle assumption

Now suppose no small misalignment angle assumption is made; and, therefore, the model equation is nonlinear in the parameters by Equation (K.6)

$$f(\theta_j) = K_0 + (1 + k_1)\sin(\theta_j + \delta) \tag{K.20}$$

Let K_0, k_1, δ be first guesses at the values of the parameters with equally weighted data at the *n* positions θ_1, ..., θ_n, and let ΔK_0, Δk_1, $\Delta\delta$ be adjustments to the first guesses. The normal equations [Equation (K.33) to Equation (K.35)] are

$$\begin{bmatrix} n & \sum_{j=1}^{n}\sin(\theta_j+\delta) & \sum_{j=1}^{n}(1+k_1)\cos(\theta_j+\delta) \\ \sum_{j=1}^{n}\sin(\theta_j+\delta) & \sum_{j=1}^{n}\sin^2(\theta_j+\delta) & \sum_{j=1}^{n}(1+k_1)\sin(\theta_j+\delta)\cos(\theta_j+\delta) \\ \sum_{j=1}^{n}(1+k_1)\cos(\theta_j+\delta) & \sum_{j=1}^{n}(1+k_1)\sin(\theta_j+\delta)\cos(\theta_j+\delta) & \sum_{j=1}^{n}(1+k_1)^2\cos^2(\theta_j+\delta) \end{bmatrix}$$
$$\times \begin{bmatrix} \Delta K_0 \\ \Delta k_1 \\ \Delta\delta \end{bmatrix} = \begin{bmatrix} \sum_{j=1}^{n}[A_{ind,j} - f(\theta_j)] \\ \sum_{j=1}^{n}[A_{ind,j} - f(\theta_j)]\sin(\theta_j+\delta) \\ \sum_{j=1}^{n}[A_{ind,j} - f(\theta_j)](1+k_1)\cos(\theta_j+\delta) \end{bmatrix} \tag{K.21}$$

The solutions of these equations give adjustments to the parameters K_0, k_1, δ. Using the new values of the parameters, the normal equations are reformed and solved. The process continues until convergence is obtained to the least-squares maximum likelihood estimates $\hat{K}_0$, $\hat{k}_1$, $\hat{\delta}$ for which the model equation best fits the data.

The covariance of the parameter estimates is the inverse of the coefficient matrix of the normal equations times the rms of the postfit residuals (see K.6.6). Convergence has been obtained when the last iteration's adjustments are small fractions of the parameter estimate standard deviations (square roots of the diagonal elements of the covariance matrix).

K.3.1.3 Information in postfit residuals

If the postfit observed minus theoretical residuals $A_{\text{ind},j} - f(\theta_j)$ show systematic rather than random behavior as a function of dividing-head angle θ_j or, better, of input acceleration sin θ_j, then either the error model is incomplete or systematic errors exist in the test equipment. If proper care is taken to eliminate test equipment errors, then the signature of the postfit residuals gives the form of the unmodeled accelerometer error (see Fuhrman [B21]), although modified by aliasing of the unmodeled error into the estimates of known model parameters. The physical mechanisms leading to systematic postfit residuals should be sought (see Annex G).

K.3.2 Effect of asymmetries

K.3.2.1 Asymmetry in bias

If the bias, scale-factor, and misalignment postfit data residuals are distributed as in Figure K.1 as a function of input acceleration, then bias asymmetry is indicated. Take the model equation with no small misalignment angle approximation to be

$$f(\theta_j) = K_0 + (1 + k_1)\sin(\theta_j + \delta) + \frac{1}{2}K'_0 \operatorname{sign}\left[\sin(\theta_j + \delta)\right] \tag{K.22}$$

As explained in a boxed note in 8.3, the bias asymmetry model equation could be equivalently written as

$$f(\theta_j) = (1 + k_1)\sin(\theta_j + \delta) + \begin{cases} K_{0+} & \text{if} \sin(\theta_j + \delta) > 0 \\ K_{0-} & \text{if} \sin(\theta_j + \delta) < 0 \end{cases} \tag{K.23}$$

where either model equation is ambiguous when the dividing-head angle θ_j is closer to the horizontal values 0° or 180° than the misalignment angle δ.

The same fit to the data is obtained solving either for k_1, δ, K_0, K'_0 or for k_1, δ, K_{0+}, K_{0-}, with

$$K_0 = \frac{1}{2}(K_{0+} + K_{0-})$$

$$K'_0 = K_{0+} - K_{0-} \tag{K.24}$$

Even if the test shows that the apparent bias is different for the two polarities of input acceleration, they are only statistically significantly different at the 95% confidence level if the difference $K_{0+} - K_{0-}$ is greater in absolute value than twice the standard deviation of the estimate of K_{0+} or K_{0-}.

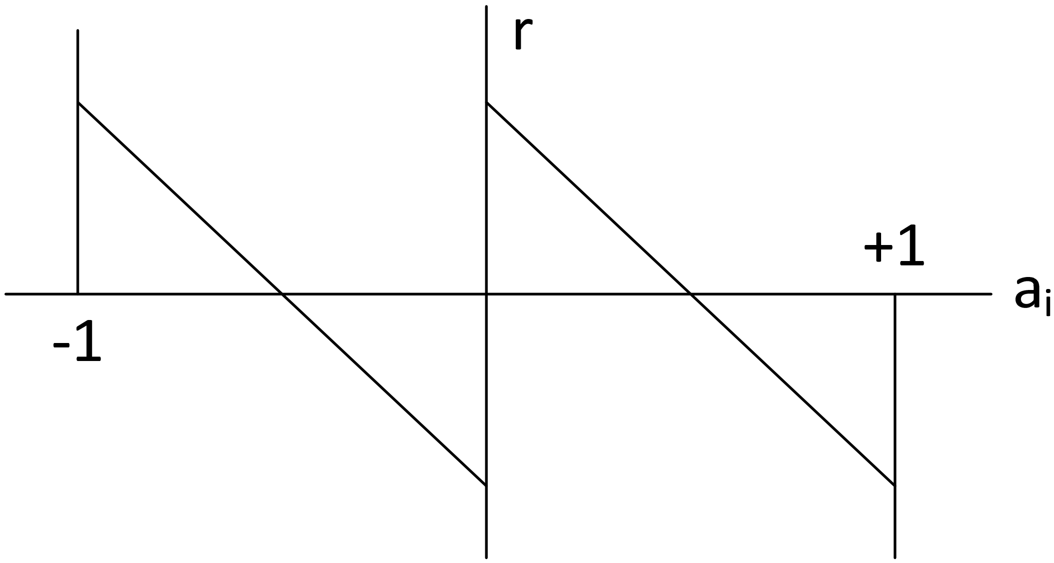

Figure K.1—Residuals due to bias asymmetry

K.3.2.2 Asymmetry in scale factor

If the bias, scale-factor, and misalignment postfit data residuals are distributed as in Figure K.2 as a function of input acceleration, then scale-factor asymmetry is indicated. Take the model equation with no small misalignment angle approximation to be

$$f(\theta_j) = K_0 + (1 + k_1)\sin(\theta_j + \delta) + \frac{1}{2}K'_1\left|\sin(\theta_j + \delta)\right| \qquad \text{(K.25)}$$

As explained in a boxed note in 8.3, the bias asymmetry model equation could be equivalently written as

$$f(\theta_j) = K_0 + \begin{cases} (1 + k_{1+})\sin(\theta_j + \delta) & \text{if } \sin(\theta_j + \delta) > 0 \\ (1 + k_{1-})\sin(\theta_j + \delta) & \text{if } \sin(\theta_j + \delta) < 0 \end{cases} \qquad \text{(K.26)}$$

The same fit to the data is obtained solving either for δ, K_0, k_1, K'_1 or for δ, K_0, k_{1+}, k_{1-}, with

$$k_1 = \frac{1}{2}(k_{1+} + k_{1-})$$

$$K'_1 = k_{1+} - k_{1-} \qquad \text{(K.27)}$$

Even if the test shows that the apparent scale-factor deviation from nominal is different for the two polarities of input acceleration, they are only statistically significantly different at the 95% confidence level if the difference $k_{1+} - k_{1-}$ is greater in absolute value than twice the standard deviation of the estimate of k_{1+} or k_{1-}.

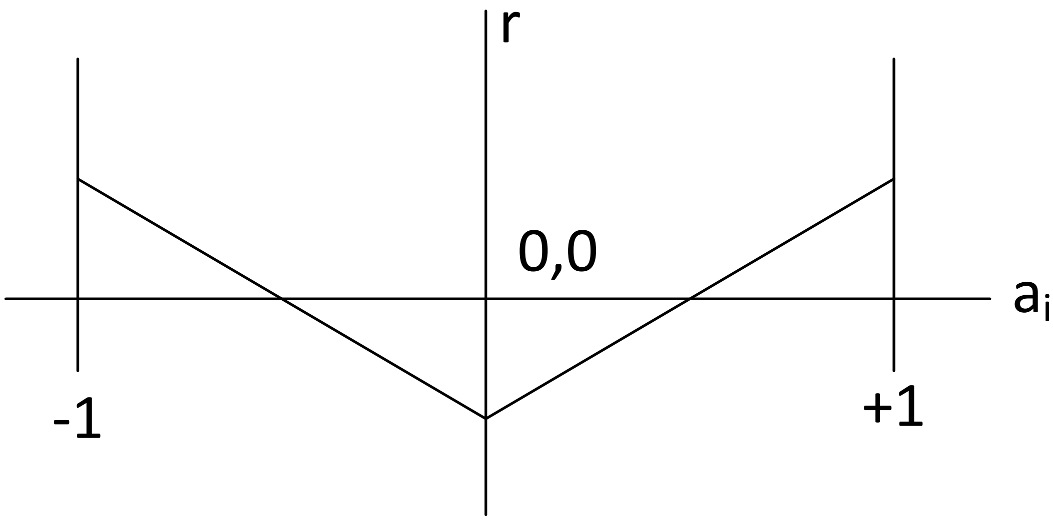

Figure K.2—Residuals due to scale-factor asymmetry

K.3.2.3 Asymmetry in misalignment as well as in bias and scale factor

Assume misalignment is held at 0 and the bias and the scale factor are determined from up–down data. If the data residuals at all the positions are distributed as in Figure K.3a, then the misalignment error is the same for positive and negative accelerations. If the residuals have a crossover as indicated in Figure K.3b even after convergence with bias, scale factor, and misalignment estimated from the data at all the positions, then misalignment asymmetry is indicated. Both drawings in Figure K.3 include the effect of some scale-factor error as indicated by the tilt of the ellipse. The misalignment asymmetry is only statistically significant at the 95% confidence level if the absolute value of the difference between the misalignments estimated for positive and negative accelerations is greater than twice the misalignment asymmetry standard deviation.

If adding several asymmetry or other terms to the model equation is necessary, the number of multipoint tumble positions should be increased to retain necessary statistical accuracy in the parameter estimates as well as to reveal any remaining systematic signature in the postfit residuals.

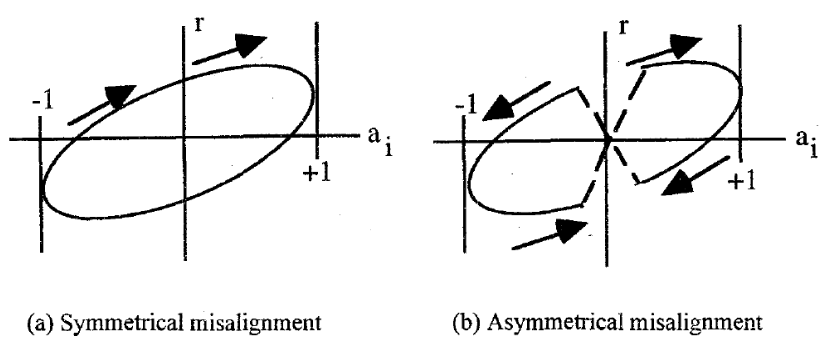

Figure K.3—Residuals due to misalignment

K.3.3 Effect of quadratic and cubic acceleration sensitivities

K.3.3.1 Effect of K_3 and Koq

The effect of not estimating K_3 or K_{oq} in the model equation would contribute the sloping line *AB* in Figure K.4a to the estimate of scale-factor error k_1. The postfit residuals with the k_1 estimate thus aliased would look like Figure K.4b.

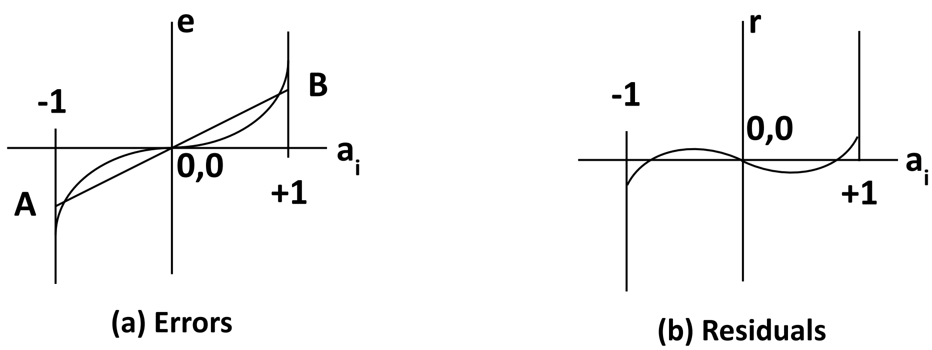

Figure K.4—Errors and residuals due to K_3 and K_{oq}

K.3.3.2 Effect of K_2

The effect of not estimating K_2 in the model equation has an error shown in Figure K.5. An aliased estimate of bias K_0 results, with postfit residuals looking like the curve in Figure K.5 shifted downward to have equal deviations above and below the acceleration axis.

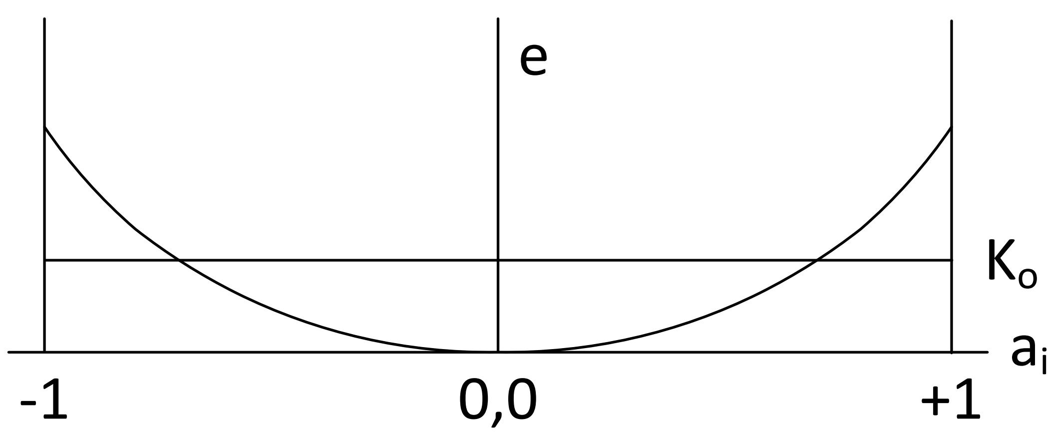

Figure K.5—Errors due to K_2

K.3.4 Difficulty of estimating quadratic and cubic acceleration sensitivities in a single accelerometer multipoint tumble

Assume the model equation

$$f(\theta_j, \alpha) = K_{oq} \sin\theta_j |\sin\theta_j| + K_2 \sin^2\theta_j + K_3 \sin^3\theta_j + K_{ip} \sin\theta_j \cos\theta_j$$

$$+\delta\cos\theta_j + \begin{cases} K_{0+} + (1+k_{1+})\sin(\theta_j+\delta) & \text{if } \sin(\theta_j) > 0 \\ K_{0-} + (1+k_{1-})\sin(\theta_j+\delta) & \text{if } \sin(\theta_j) < 0 \end{cases} \quad \text{(K.28)}$$

Consider the following positions in a multipoint tumble test:

0°	90°	180°	270°
5°	95°	185°	275°
15°	105°	195°	285°
25°	115°	205°	295°
45°	135°	225°	315°
65°	155°	245°	335°
75°	165°	255°	345°
85°	175°	265°	355°

with the data at the 0° and 180° horizontal positions not included, because of assumed model asymmetries, so that there are 30 positions. With 1-μ*g* accuracy data at each position, a covariance analysis (see K.6.6) yields the first column of standard deviations in Table K.1 for the estimates of the nine parameters in the model equation. Since K_{oq} and K_3 were correlated –0.989, the second column of standard deviations was computed with K_{oq} left out of the simulated fit; and then the third column, with K_3, was left out as well. The final column had no bias or scale-factor asymmetry, with the positive parameter being also the negative parameter.

Because of angle-setting and possibly other systematic errors at the several μ*g* level, it is probably unreasonable to estimate quadratic and cubic acceleration sensitivities in a single accelerometer multipoint tumble test, especially for the cubic term, even for μ*g* accuracy accelerometers.

Table K.1—Standard deviations of parameter estimates in a single accelerometer multipoint tumble (30 positions, 1-μ*g* accuracy measurements)

Parameter		Units	Standard deviations			
Positive bias	K_{0+}	μ*g*	1.2	0.9	0.8	0.3
Negative bias	K_{0-}	μ*g*	1.2	0.9	0.8	
Positive scale factor error	k_{1+}	ppm	8.3	3.4	2.9	0.3
Negative scale factor error	k_{1-}	ppm	8.3	3.4	2.9	
Misalignment	δ	μrad	0.3	0.3	0.3	0.3
Quadratic sensitivity	K_2	$\mu g/g^2$	2.5	2.5	2.5	0.5
Cross coupling	K_{ip}	$\mu g/g^2$	0.6	0.6	0.6	0.6
Cubic sensitivity	K_3	$\mu g/g^3$	10.2	1.5		
Odd quadratic sensitivity	K_{oq}	$\mu g/g^2$	16.7			

K.4 Multipoint tumble analysis with dual orthogonal accelerometer observables

K.4.1 Simultaneous estimation of angle-setting and tilt errors, nonorthogonality, and accelerometer model coefficients

Sub-μ*g* accuracy accelerometers are more accurate than the dividing head on which they are tested. Therefore, to estimate bias, scale-factor error, misalignment, and quadratic and higher order acceleration sensitivities with the accuracy implied by the accuracy of the accelerometer itself, the effect of angle-setting and tilt errors has to be eliminated if more than just the IA up and IA down data are to be used. As explained in K.2.5.1, a technique that has been successfully used is to solve for angle-setting errors simultaneously with accelerometer model coefficients and nonorthogonality in a dual orthogonal accelerometer multipoint tumble. Iterative nonlinear least-squares estimation is employed if no small-angle approximations are made for the angle-setting errors and nonorthogonality.

Suppose there were two accurate accelerometers and a third accelerometer with an unmodeled error effect whose signature is corrupted by angle-setting and tilt errors when analyzing data from a single accelerometer multipoint tumble test. A three-accelerometer multipoint tumble test can be done with two IA orthogonal accurate accelerometers and with the third accelerometer having IA parallel or antiparallel with the IA of one of the first two.

The dual orthogonal accelerometer data is analyzed to estimate angle-setting errors along with the accelerometer model coefficients and nonorthogonality. These angle-setting errors are then used in estimating the model coefficients and misalignment of the third accelerometer. The resulting model coefficient estimates and postfit data residuals are free of the corrupting effects of angle-setting and tilt errors.

K.4.2 Covariance simulation

As an example of estimating angle-setting errors along with accelerometer coefficients, consider the 32 positions in a multipoint tumble test listed in K.3.4 (including the 0° and 180° positions). Let there be 0.1-μ*g* accuracy measurements from two nearly orthogonal accelerometers at each position, including when an accelerometer is horizontal. If no horizontal accelerometer data exist, an angle-setting error would not have to be estimated at that position because the vertical accelerometer data is insensitive to angle-setting error.

Let bias, scale-factor error, and K_2 be estimated for each of the two accelerometers, plus the nonorthogonality between the accelerometers and the 32 angle-setting errors. Assume that the accelerometer data do not display unmodeled errors such as bias, scale-factor, or misalignment asymmetries and that K_{oq}, K_{ip}, K_{pp}, and K_3 are not present or have calibrated values from other tests. A covariance analysis (see K.6.6) yields the parameter estimate uncertainties in Table K.2 assuming 0.1-μ*g* measurement errors.

Bias and K_2 for a given accelerometer have –0.96 correlations. Otherwise, the correlations among the 39 parameters estimated from 64 measurements are less than 0.67 in magnitude. The effect of correlations is fully reflected in the parameter estimate uncertainties.

Thus, under the assumptions made, the K_2 quadratic acceleration sensitivity can be estimated in a l-*g* tumble test for an accurate accelerometer, although for lesser accuracy devices test acceleration levels up to those encountered in a mission are typically required. The K_2 thus estimated in a multipoint tumble test should be checked for consistency with the value estimated in centrifuge or vibration tests on a sample of accelerometers to see whether K_2 can be calibrated with an inexpensive tumble test for a family of accurate accelerometers without aliasing from unmodeled effects.

Table K.2—Standard deviations of parameter estimates in a dual orthogonal accelerometer multipoint tumble (32 positions, 0.1-μ*g* accuracy accelerometer measurements)

Parameter		Units	Standard deviation
Bias	K_0	μ*g*	0.091 (each accelerometer)
Scale-factor errors	k_1	ppm	0.028 (each accelerometer)
Quadratic sensitivities	K_2	$\mu g/g^2$	0.11 (each accelerometer)
Nonorthogonality	η	μrad	0.061
Angle-setting errors	$\delta\theta_j$	μrad	0.15

K.5 Multipoint tumble analysis with orthogonal accelerometer magnitude-squared-of-*g* observable

K.5.1 Comparison with solving for angle-setting errors with individual accelerometer observables

For an *n* position multipoint tumble test, estimating *m* model coefficients for each of two orthogonal accelerometers plus the nonorthogonality angle from *n* accelerometer sum-of-squares observables yields essentially the same model coefficient estimates as when those $2m + 1$ parameters are estimated simultaneously with *n* angle-setting errors from $2n$ individual accelerometer observables. Thus, if only model coefficient estimates are desired, little distinguishes the two estimation procedures, and, in fact, the sum-of-squares observable is typically used for guidance system calibrations.

However, if unmodeled effects are being sought, the individual accelerometer postfit data residuals might be more revealing than the sum-of-squares data residuals. Also, if angle-setting errors are estimated with two orthogonal accurate accelerometers, they can be applied in estimating the model coefficients of a third accelerometer. Finally, large angle-setting errors (such as 1°) can be estimated in the dual orthogonal separate accelerometer approach of K.2.5.1, whereas the magnitude-squared-of-*g* approach as formulated in K.2.6 assumes angle-setting errors less than about 0.1 mrad to 1 mrad for which the squares and products with other coefficients are ignorable. On the other hand, the magnitude-squared-of-*g* observable is ideally suited for guidance system calibration with three orthogonal accelerometers.

The relevancy of systematic postfit data residuals for revealing unmodeled effects only applies to batch least-squares maximum likelihood estimation. For a sequential Kalman filter estimator, the existence of unmodeled errors is revealed by variations in the Kalman filter estimates during the course of (perhaps several) tumbles after start-up transients have died out, since the Kalman filter tries to zero out the observed minus model residual at each tumble position.

K.5.2 Covariance simulations

A covariance analysis (see K.6.6) for estimating the parameters in the first four rows of Table K.2 for all 32 positions listed in K.3.4 using the magnitude-squared-of-*g* observable yields the same standard deviations for the parameter estimates as in Table K.2 (without angle-setting errors) if use is made of the fact that, if the standard deviations of the independent individual accelerometer observables are $\Delta = 0.1\ \mu g$, then the standard deviation of the magnitude-squared-of-*g* observable is $2\Delta(\cos^2\theta + \sin^2\theta) = 0.2\ \mu g$.

When K_{ip} is added to the covariance simulation, the K_0 and K_2 of one accelerometer correlates perfectly with the K_{ip} of the other accelerometer. When K_3 is added to the covariance simulation, perfect correlations are revealed among the four parameters $K_{\lambda 1}$ and $K_{\lambda 3}$ ($\lambda = 1, 2$). Applying trigonometric identities to Equation (K.16) shows that these perfect correlations indeed exist. Therefore, neither K_{ip} nor K_{pp} can be estimated simultaneously with K_2 and K_0, and K_3 cannot be estimated simultaneously with K_1, in dual orthogonal accelerometer testing with either the magnitude-squared-of-*g* observable or the individual accelerometer observables with angle-setting errors estimated.

Thus the quadratic, cubic, and higher order acceleration nonlinearities in the model equation must be estimated in vibration and centrifuge tests with perhaps only the K_2 coefficient estimated in 1-*g* tumble tests along with scale factor and bias for very accurate accelerometers.

Covariance simulations with the model parameters that are not perfectly correlated yields the results in the first column of Table K.3. All 32 positions are used (even the horizontal ones) because with the magnitude-squared-of-*g* observable the partial derivatives with respect to asymmetries are unambiguously zero at these positions. Because of high correlations involving K_{oq}, the second column of standard deviations was computed with K_{oq} left out of the simulated fit. The final column had no bias or scale factor asymmetry, with the positive parameter being also the negative parameter, and agrees with Table K.2.

Table K.3—Standard deviations of parameter estimates in a dual accelerometer multipoint tumble (32 positions, 0.2-μ*g* accuracy magnitude-squared-of-*g* measurements)

Parameter		Units	Standard deviations		
Positive biases	K_{0+}	μ*g*	1.0	0.44	0.091
Negative biases	K_{0-}	μ*g*	1.0	0.44	
Positive scale factor errors	k_{1+}	ppm	5.8	1.0	0.028
Negative scale factor errors	k_{1-}	ppm	5.8	1.0	
Nonorthogonality	η	μrad	0.61	0.61	0.061
Quadratic sensitivities	K_2	$\mu g/g^2$	0.69	0.69	0.11
Odd quadratic sensitivities	K_{oq}	$\mu g/g^2$	9.7		

K.6 Least-squares maximum likelihood estimation

K.6.1 Likelihood function and maximum likelihood estimates

For model Equation (K.4) with Gaussianly distributed zero mean uncorrelated additive measurement errors ε_j with standard deviations w_j, the likelihood function is the joint probability density $p(z;\alpha)$ of the measurements $z_j = A_{\text{ind},j}$ $(j = 1, \ldots, n)$ given the parameters α

$$p(z;\alpha) = (2\pi)^{-n/2}[w_1 \ldots w_n]\mathrm{e}^{-\Sigma[z_j - f(\theta_j,\alpha)]^2/(2w_j^2)} \quad \text{(K.29)}$$

The maximum likelihood estimates $\hat{\alpha}$ of the parameters α are those that maximize $p(z;\alpha)$. In other words, they make it most likely that the measurements that did occur would have occurred. Maximizing $p(z;\alpha)$ is the same as minimizing the negative log likelihood

$$\zeta(z;\alpha) = -\ln\big(p(z;\alpha)\big) \quad \text{(K.30)}$$

which is the same as Equation (K.5) if constant terms are deleted. Hence, under the assumptions stated, least-squares estimates are the same as maximum likelihood estimates, and all the good theoretical properties of maximum likelihood estimates apply to least-squares estimates (asymptotically unbiased, consistent, efficient, and sufficient; see Cramer [B16]).

K.6.2 Iterative determination of least-squares maximum likelihood estimates

The condition for a minimum of the negative log likelihood (K.5) or (K.30) with $z_j = A_{\mathrm{ind},j}$ is

$$\sum_{j=1}^{n} \frac{\left[A_{ind,j} - f(\theta_j, \alpha)\right]}{w_j^2} \left.\frac{\partial f(\theta_j, \alpha)}{\partial \alpha_i}\right|_{\alpha = \hat{\alpha}} = 0\,, \quad i = 1, \ldots, m \qquad \text{(K.31)}$$

Let $\alpha_0 = (\alpha_{10}, \ldots, \alpha_{m0})$ be first guesses for the values of the parameters, with

$$\Delta\alpha_k = \hat{\alpha}_k - \alpha_{k0}\,, \quad k = 1, \ldots, m \qquad \text{(K.32)}$$

Assume that

$$f(\theta_j, \hat{\alpha}) = f(\theta_j, \alpha_0) + \sum_{k=1}^{m} \frac{\partial f(\theta_j, \alpha_0)}{\partial \alpha_k} \Delta\alpha_k$$

$$\frac{\partial f(\theta_j, \hat{\alpha})}{\partial \alpha_i} = \frac{\partial f(\theta_j, \alpha_0)}{\partial \alpha_i}$$

Then the following linear equations (called the "normal equations") are obtained for the adjustments $\Delta\alpha_k$ to the first guesses α_{k0}:

$$\sum_{k=1}^{m} A_{\mathrm{ik}} \Delta\alpha_k = B_{\mathrm{i}} \quad , \quad i = 1, \ldots, m \qquad \text{(K.33)}$$

$$B_i = \sum_{j=1}^{n} \frac{\left[A_{ind,j} - f(\theta_j, \alpha)\right]}{w_j^2} \left.\frac{\partial f(\theta_j, \alpha)}{\partial \alpha_i}\right|_{\alpha = \alpha_0} \qquad \text{(K.34)}$$

$$A_{ik} = \sum_{j=1}^{n} \frac{1}{w_j^2} \frac{\partial f(\theta_j, \alpha)}{\partial \alpha_i} \left.\frac{\partial f(\theta_j, \alpha)}{\partial \alpha_k}\right|_{\alpha = \alpha_0} \qquad \text{(K.35)}$$

The normal equations are solved and then reformed with the adjusted values of the parameters. The process is continued until convergence is obtained. If the model function $f(\theta_j, \alpha)$ is linear in the parameters α_k (as it is in this annex when the small misalignment angle approximation is made), then only one iteration is required to obtain convergence.

K.6.3 Postfit data residuals

The rms of the weighted postfit data residuals is

$$\text{residual rms} = \sqrt{\frac{1}{n} \sum_{j=1}^{n} \frac{\left[A_{ind,j} - f(\theta_j, \hat{\alpha})\right]^2}{w_j^2}} \qquad \text{(K.36)}$$

It can be shown that division by *(n – m)* rather than *n* would more realistically represent the goodness of a fit when *m* parameters are being estimated. Only the relative values of the measurement standard deviations matter in the least-squares fitting process. For uniform weighting of the measurements, all the w_j could be assumed to be 1, and the postfit rms value is then a measure of the standard deviations of the measurements if there are a large number of positions and no unmodeled effects.

K.6.4 Fisher information matrix

The $m \times m$ covariance matrix of the least-squares maximum likelihood estimates will be shown to be the inverse of the coefficient matrix of the normal equations multiplied by the rms of the postfit residuals if the w_j are relative weights rather than measurement standard deviations. The first step is to prove in K.6.4 by straightforward integration over probability densities that the coefficient matrix of the normal equations is the Fisher information matrix. Then in K.6.5 the Cramer-Rao lower bound is proved in the one-dimensional case with a reference to the proof in the *m*-dimensional case. This result states that the covariance matrix of any unbiased parameter estimates is bounded from below by the inverse of the Fisher information matrix for the estimates. Finally, a reference is given in K.6.6 to the result that, in the limit of a large number of observations, maximum likelihood estimates are unbiased and the Cramer-Rao lower bound is attained.

The probability density $p(z;\alpha)$ of the observations satisfies

$$\int p(z;\alpha)dz = 1 \tag{K.37}$$

Taking partial derivatives of both sides of the above equation yields

$$\int \frac{\partial p(z;\ \alpha)}{\partial\alpha_i}dz = 0, \quad \int \frac{\partial^2 p(z;\ \alpha)}{\partial\alpha_i\partial\alpha_k}dz = 0 \tag{K.38}$$

The Fisher information matrix **I** is defined to be the expected value of the Hessian of second partial derivatives of the negative log-likelihood function with respect to the parameters

$$\mathbf{I}_{ik} = E\left\{\frac{\partial^2\zeta(z;\alpha)}{\partial\alpha_i\partial\alpha_k}\right\} \tag{K.39}$$

where $E\{\ \}$ denotes expectation (integration over the probability density of the random variable z). By Equation (K.37) and Equation (K.38)

$$\begin{aligned}
\mathbf{I}_{ik} &= -\int \frac{\partial^2 \ell n[p(z;\alpha)]}{\partial\alpha_i\partial\alpha_k}p(z;\alpha)dz \\
&= -\int \frac{\partial}{\partial\alpha_i}\left[\frac{1}{p(z;\alpha)}\frac{\partial p(z;\alpha)}{\partial\alpha_k}\right]p(z;\alpha)dz \\
&= -\int \frac{\partial^2 p(z;\alpha)}{\partial\alpha_i\partial\alpha_k}dz + \int \frac{1}{p(z;\alpha)^2}\frac{\partial p(z;\alpha)}{\partial\alpha_i}\frac{\partial p(z;\alpha)}{\partial\alpha_k}p(z;\alpha)dz \\
&= E\left\{\frac{\partial \ell n[p(z;\alpha)]}{\partial\alpha_i}\frac{\partial \ell n[p(z;\alpha)]}{\partial\alpha_k}\right\} \\
&= E\left\{\frac{\partial\zeta(z;\alpha)}{\partial\alpha_i}\frac{\partial\zeta(z;\alpha)}{\partial\alpha_k}\right\}
\end{aligned} \tag{K.40}$$

By Equation (K.29), Equation (K.30), Equation (K.34), and Equation (K.40), the Fisher information matrix **I** for least-squares maximum likelihood estimation is the coefficient matrix [Equation (K.35)] of the normal Equation (K.33)

$$\mathbf{I}_{ik} = \sum_{j=1}^{n} \frac{1}{w_j^4} \frac{\partial f(\theta_j, \alpha)}{\partial \alpha_i} \frac{\partial f(\theta_j, \alpha)}{\partial \alpha_k} E\left\{\left[z_j - f(\theta_j, \alpha)\right]^2\right\} = A_{ik} \tag{K.41}$$

K.6.5 Cramer-Rao lower bound

An estimate $\tilde{\alpha}_j$ of a parameter α_j is a function of the measurements

$$\tilde{\alpha}_j = h_j(z_1, \ldots, z_n) \tag{K.42}$$

As a function of the measurement random variables, it is also a random variable. The function h_j cannot be arbitrarily chosen if the parameter estimate is to have good properties. One desirable property of an estimator is that it be unbiased

$$E\{\tilde{\alpha}_j\} = \text{true value of } \alpha_j \tag{K.43}$$

Another desirable property is that its variance be small, although there is a lower bound as to how small it can be.

In the case of a scalar parameter, if $\tilde{\alpha}$ is an estimate of the parameter α then

$$\int (\tilde{\alpha} - \alpha) p(z; \alpha) dz = b(\alpha) \tag{K.44}$$

where $b(\alpha)$ is the bias associated with the estimate. Assuming that $p(z; \alpha)$ has a first derivative and taking the partial derivative of each side gives

$$\int \frac{\partial}{\partial \alpha} [(\tilde{\alpha} - \alpha) p(z; \alpha)] dz = b'(\alpha) \tag{K.45}$$

where $b'(\alpha)$ is the derivative of the bias with respect to α. Taking the derivative of the product gives

$$-\int p(z; \alpha) dz + \int (\tilde{\alpha} - \alpha) \frac{\partial}{\partial \alpha} p(z; \alpha) dz = b'(\alpha) \tag{K.46}$$

$$\int (\tilde{\alpha} - \alpha) \left\{\frac{\partial}{\partial \alpha} \ell n[p(z; \alpha)]\right\} p(z; \alpha) dz = 1 + b'(\alpha) \tag{K.47}$$

At this point, the Schwarz inequality for integration with respect to the measure $p(z; \alpha)\, dz$ may be applied to give

$$\int (\tilde{\alpha} - \alpha)^2 p(z; \alpha)\, dz \int \left\{\frac{\partial}{\partial \alpha} \ell n[p(z; \alpha)]\right\}^2 p(z; \alpha) dz \geq [1 + b'(\alpha)]^2 \tag{K.48}$$

Finally, using the definition of the expected value operator and the scalar form of Equation (K.40) gives a lower bound for the variance of an estimate

$$E\{(\tilde{\alpha}-\alpha)^2\} \geq \frac{[1+b'(\alpha)]^2}{\mathbf{I}} \tag{K.49}$$

This lower bound is known as the Cramer-Rao lower bound. Equation (K.49) shows that for an unbiased scalar estimator, the Cramer-Rao lower bound is equal to the inverse of the Fisher information matrix, which is reduced to a scalar.

In the case of an unbiased estimate of m unknown parameters, this lower bound generalizes to (see Wilks [B67])

$$E\{(\tilde{\alpha}-\alpha)^2\} \geq \mathbf{I}^{-1} \tag{K.50}$$

which means that every element of the covariance of the estimate must be greater than the corresponding element of the inverse of the Fisher information matrix.

K.6.6 Covariance of parameter estimates

Since the symmetric $m \times m$ coefficient matrix A_{ik} of the normal equations for least-squares maximum likelihood estimation is the Fisher information matrix, the Cramer-Rao lower bound says that the covariance matrix σ_{ik} of the parameter estimates is bounded below by the inverse of A_{ik} multiplied by the square of the rms of the postfit residuals if the w_j are relative weights rather than measurement standard deviations

$$\sigma_{ik} \geq (A^{-1})_{ik} \times (\text{residual rms})^2 \tag{K.51}$$

It can be shown that the Cramer-Rao lower bound is more of an equality (≈ instead of ≥) if division by n is replaced by division by $(n - m)$ in Equation (K.36) for the postfit residual rms. If the number of measurements were the same as the number of parameters, the fit could be perfect with zero postfit residual rms. Maximum likelihood estimates are asymptotically normally distributed and unbiased and the Cramer-Rao lower bound is asymptotically attained in the limit of a large number of measurements for zero mean additive random measurement errors and no unmodeled effects (see Cramer [B16]).

Because of small sample sizes and unmodeled effects, a more realistic indication of the parameter estimate uncertainties is the variation in the parameter estimates in repetitions of the multipoint tumble test if the time between tests is not so long that the resulting comparisons are corrupted by trends or other parameter instabilities. Another indication of the uncertainties of higher order acceleration sensitivities (such as K_2) is provided by comparison of the tumble results with those of centrifuge, vibration, or other tests. Keep in mind that unmodeled effects can bias estimates as well as cause variations in estimates in repetitions of the test.

The standard deviation σ_k of the estimate of α_k is

$$\sigma_k = \sqrt{\sigma_{kk}} \tag{K.52}$$

The correlation between parameter estimates is

$$\varepsilon_{ik} = \frac{\sigma_{ik}}{\sigma_i \sigma_k}, \qquad -1 \leq \varepsilon_{ik} \leq 1 \tag{K.53}$$

If two parameters are perfectly correlated –1 or +1, such as for certain accelerometer quadratic coefficient as revealed by tumble test Fourier series (see K.2.4), then only one of the parameters can be estimated with the other held fixed (at zero or at a vibration or centrifuge test value, for example) with the understanding that, if the other parameter is held at 0, then the estimated parameter value contains the lumped effect of both parameters.

A covariance analysis can be done before a test is performed by calculating the $m \times m$ coefficient matrix A of the normal equations for assumed estimated parameter m-vector α, angle sequence scenario $\theta_1, ..., \theta_n$, and measurement standard deviations w_j. The inverse of A is then the covariance that will be obtained in estimating the vector α from real data. The right side of the normal equations B depends on the data, whereas the coefficient matrix A does not and, therefore, can be precomputed for a given test scenario.

Annex L

(informative)

Vibration test equipment, test procedures, and analysis techniques

L.1 Test equipment and test fixtures

L.1.1 Mounting fixture

For linear vibration tests, an accelerometer is mounted in a fixture that is attached to a vibrator's face plate, possibly with different choices of mounting bolt hole patterns, so that vibration inputs can be applied along any cardinal instrument axis [input axis (IA), pendulous axis (PA), or output axis (OA)] or along a noncardinal axis, such as a bisector. The fixture is typically a fairly massive block to avoid having resonance frequencies near the vibration frequencies or harmonics of the frequencies used in the test.

Fixtures are typically made of a material having good internal damping, such as a magnesium alloy, and verified before use by a frequency sweep with a dummy test article. If the fixture were temperature controlled, thermal isolation would have to be used between the fixture and the face plate.

L.1.2 Electrodynamic vibrator

The vibration exciter is most commonly electrodynamic, producing oscillatory forces by driving appropriate currents through a coil immersed in a magnetic field. The magnetic field is produced by a large permanent magnet assembly or by fixed conductive coils within a magnetic return structure. Electrodynamic exciters can produce useful acceleration waveforms within the frequency range from approximately 20 Hz to greater than 2000 Hz, although some vibrators have upper limits reaching 10 kHz to 100 kHz for small masses.

Low-frequency operation is limited by the available travel of the exciter armature within the constant part of the magnetic field. Peak-to-peak travel is typically limited to 1 cm to 1.5 cm on small shakers and rarely more than 2.5 cm on large ones, limiting acceleration to ~10-*g* peak at 20 Hz. Low-frequency vibration may also be limited by the bandwidth of the power amplifier or by waveform distortion introduced by imperfections in the suspension that constrains the armature motion to a single axis.

At high frequencies, acceleration amplitude is limited by the force rating or the voltage limits of the exciter. For example, with a suspended mass of 30 kg, including the tare weight of the armature and fixture, a 30 000-N exciter is limited to 100-*g* peak, or ~30-*g* root-mean-square (rms) random. At very high frequencies, above 1000 Hz in the example of Figure L.1, additional limits related to voltage capability and inductance may apply.

L.1.3 Hydraulic vibrator

For special applications that require larger acceleration at very low frequency, such as mimicking rigid body motions of a missile, hydraulic exciters are available that operate below 1 Hz, at 50 cm peak to peak. These shakers are generally limited by valve operating speeds and fluid line compliances to operation at high frequencies of at most a few hundred hertz.

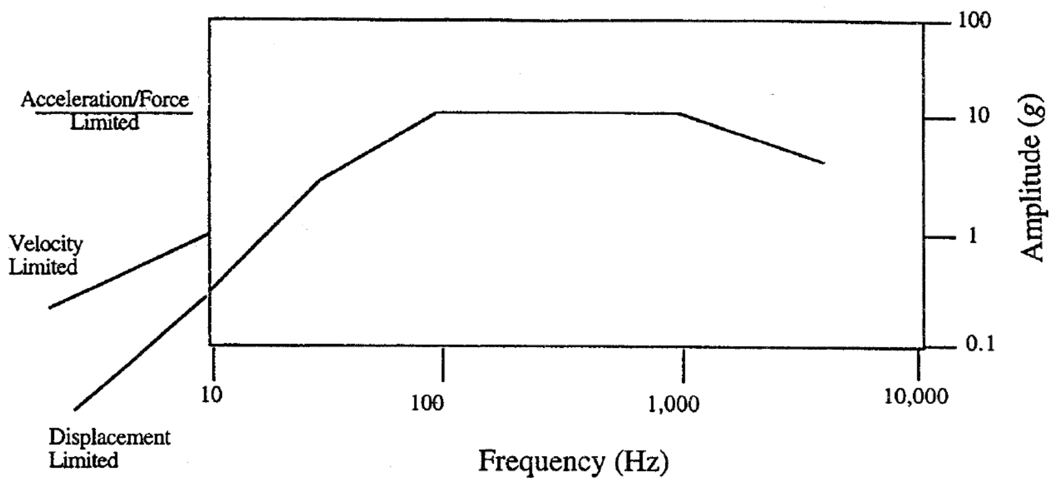

Figure L.1—Example of electrical vibrator's maximum acceleration capability versus frequency

L.1.4 Vibrator orientation, slip tables, and attachment to floor

Electromagnetic vibration exciters are usually operated with the vibration axis vertical to eliminate side loading on the suspension and to minimize tilt effects (see Figure L.2). They can be operated horizontally by coupling them to a slip plate supported by an oil film, as illustrated in Figure L.3. The accelerometer under test in Figure L.2 and Figure L.3 has IA vertical, but other orientations are possible (see Figure L.4).

Vibrators are most commonly restrained by simply bolting them to a concrete floor. In high-precision applications, where cross-axis and especially rocking motions must be minimized, the vibrator, and slip table if used, may be mounted to a large, pneumatically suspended, steel reaction mass (concrete is not rigid enough) with the vibration axis passed through the center of mass.

As depicted in Figure L.2 and Figure L.3, the motion applied to the test fixture is determined by a signal generator through a servo loop, which uses a piezoelectric accelerometer for feedback. These accelerometers are typically accurate to ~3%, but they can be calibrated to 0.5% by comparing to a specially calibrated piezoelectric or other accelerometer or by using laser interferometer techniques.

Because of the wide range of mechanical impedances represented by the test fixtures and test items that may be attached to a general-purpose shaker, it is impractical to provide a high-frequency, high-gain servo that attempts to servo directly to the applied wave form; instability would be a constant problem. Instead, a simple, robust servo is created by simply controlling the rms amplitude of the motion and allowing the drive to run otherwise open loop.

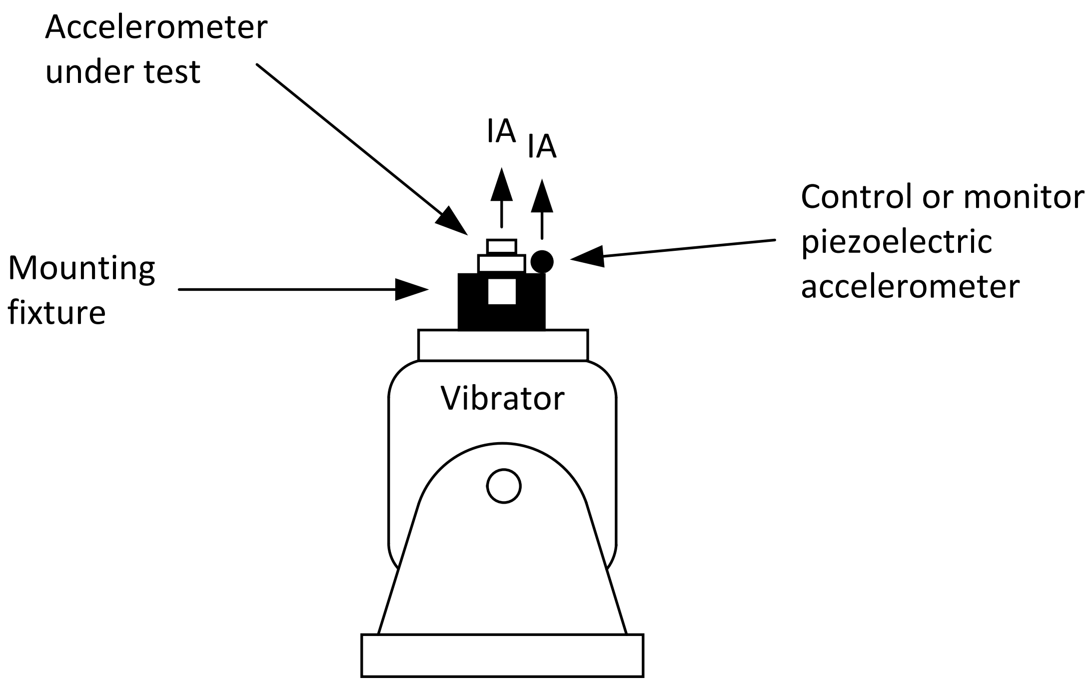

Figure L.2—Vertically oriented vibrator

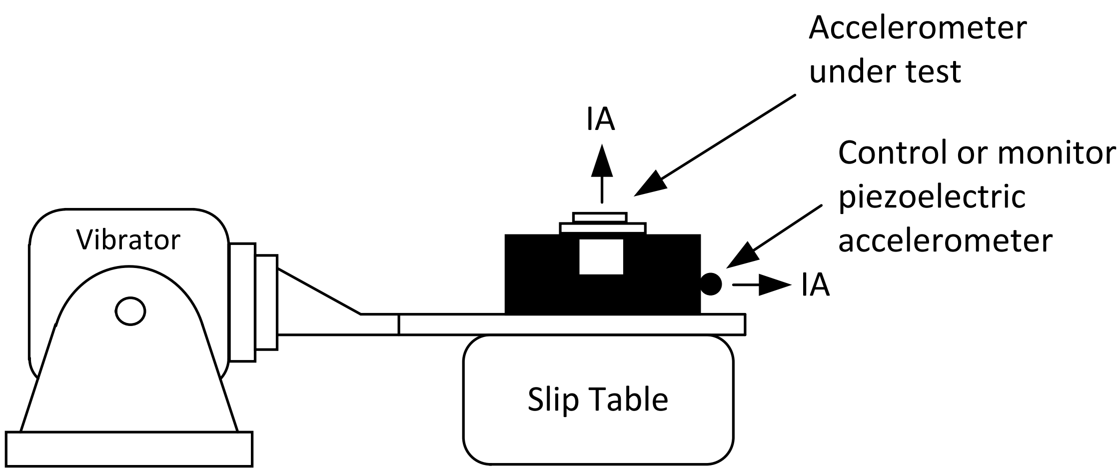

Figure L.3—Horizontally oriented vibrator with slip table

L.1.5 Measurement and control of vibration

It is important to design the system for few or no resonances, to place the controlling accelerometer on the fixture as close to the test item as possible, and to run resonance searches slowly enough to allow high Q resonances to build up. These precautions guard against application of damaging vibration amplitudes during actual testing.

A piezoelectric or other accelerometer can be used for monitoring and controlling vibration, although the piezoelectric accelerometer is not in the class of accelerometers considered in this document since it does not measure low-pass and dc accelerations. The piezoelectric accelerometer is calibrated by the manufacturer and/or the user with laser interferometer or other such motion-monitoring techniques. The calibration at higher frequency is likely to be less precise because of the smaller amplitude of motion.

Large-amplitude vibrations are used to calibrate small nonlinearities (relative to performance requirements) with a few percent accuracy in the accelerometers considered in this document using the piezoelectric accelerometer or some other accelerometer or displacement monitor as a reference (see L.6.3). Then the calibrated nonlinearities are used in compensating low-pass and dc acceleration measurements in a mission. Although not discussed in this annex, vibration and shock can be used to calibrate accelerometer scale factor for some applications using a laser interferometer motion monitor (see 12.3.18).

Additional premission tests are the application of random vibration and shock as controlled by a piezoelectric accelerometer. The tests determine whether there are any shifts in the tested accelerometer across mission-level or qualification-level environments. They also determine whether the accelerometer performs through mission-level random vibration and shock generally with the assumption that the nonlinear terms are small enough to ignore for mission-level vibration and shock even though compensation might be used for dc and low-pass acceleration inputs. If nonlinearities are not ignorably small for mission-level random vibration, then vibration rectification compensation would be required at higher as well as lower frequencies.

L.2 Test scenarios

L.2.1 Vibration tests

L.2.1.1 Types of vibration input

The vibration waveform can be a constant amplitude sinusoid at a constant frequency, or at a varying frequency, swept at some rate, such as 4-Hz/s linear variation or 1-octave/min logarithmic variation. A frequency sweep can be used to evaluate resonances in the accelerometer's structure or incipient instabilities in a servo loop. A constant frequency vibration with amplitude started and stopped, or varied in amplitude, for example, between 1 *g* and 20 *g* every few minutes, can be used to calibrate nonlinear coefficients.

A white noise generator and a real or virtual filter bank can be used to apply random motion to a test item with any desired spectral shape. The controller for a desired input spectrum is first developed with a dummy mass in the fixture. Then with the real test article, the preprogrammed controller will typically apply a low level of vibration for several seconds to standardize the filter bank for resonances or notches in the test package frequency response before applying the full rms amplitude requested.

Many spectra are possible, depending on the application and the standards cited, but a common spectrum for navigation grade accelerometers simulates the effect of a vibration isolator by rising to a peak in the range of 50 Hz to 100 Hz, and then declining to a low level at higher frequencies.

L.2.1.2 Types of vibration tests

Besides this breakdown by the kind of motion applied, shaker use may be discussed in terms of the *reasons* for each test. The principal test categories are as follows:

a) *Resonance search* of the test article, in which a frequency sweep is performed, after first verifying with a dummy mass that no resonances exist in the fixture.

b) *Calibration,* in which vibration is used to evaluate certain accelerometer coefficients either to assign values for future data correction or to ensure that they are within guaranteed limits (see L.6 and 12.3.17 for nonlinear model terms and 12.3.18 for scale factor and bias). Rectification testing described in L.6 is an important special case of calibration in which coefficients of certain critical nonlinear processes are evaluated in a sensitive way by separating a dc term from an ac term.

c) *Environmental testing,* in which specified kinds and magnitudes of motion are applied, and the test items are then examined to ensure that they still meet their performance specifications.

d) *Performance through environment testing,* in which a random vibration or other environment, such as shock, is applied for a specified time. It is determined whether the velocity integral of the accelerometer output does not deviate by more than a specified amount from the line joining the before and after velocity integral lines (since there is zero average motion on the shaker). Usually the nonlinear acceleration model terms are required to be small enough that the accelerometer meets performance requirements through the random vibration or shock environment encountered in a mission without compensation for nonlinear effects even though compensation may be used for the dc acceleration levels encountered in the mission. Alternatively, the accelerometer output can be acquired at least twice as fast as the highest significant vibration or shock frequency in a mission, and the output converted to acceleration before averaging or filtering to the output frequency used in the navigation or guidance application in order to compensate for vibration rectification.

e) *Shift across environment (SAE) testing,* in which certain specific accelerometer coefficients are evaluated (e.g., by a tumble test) before and after exposure to specified vibration or other environment, such as shock, to verify whether these specific coefficients have not changed by more than a specified amount. The accelerometer output while on the shaker should not shift from before to after the environmental exposure by more than the lumped effect of the allowed variations in, for example, scale factor and bias.

L.2.2 Shock tests

L.2.2.1 Types of shock input

Processor-controlled electromagnetic shakers can also be programmed to apply a limited but useful range of shock inputs: full sine, sinusoidal with decaying exponential amplitude, and an approximation to half sine, among others. Their principal limitation in this area is their inability to produce shocks that entail a net change of velocity.

As with random vibration tests, the programming of the shock spectrum is developed with a dummy mass. Then with the real test article, the preprogrammed controller applies a low-level shock of the specified spectrum for calibration before applying the full amplitude requested.

Nonzero displacement shocks can be generated with other techniques, such as drops from a specified height with controlled stopping elements to set the shape, peak value, and duration of the shock (see 11.2.2.4). For a more complete description of shock tests and procedures, see ISO 5347.

L.2.2.2 Types of shock tests

The principal test categories are the same as in c), d), and e) of L.2.1.2, namely environmental testing, performance through environment testing, and SAE testing. In addition, calibration tests using shock input can be performed using laser interferometer and other motion monitoring techniques (see ISO 5347, Umeda and colleagues [B60] to [B64], and 12.3.18).

L.3 Error sources

The following list of error sources associated with vibration testing is encouragingly short and for the most part specific to certain tests:

a) *Reference accelerometer.* Calibration accuracy of the piezoelectric reference limits the accuracy of amplitude measurements and, therefore, the accuracy of transfer function measurements; fortunately those measurements seldom require great precision. Reference accelerometer accuracy has little effect on rectification measurements, allowing many nonlinear coefficients to be evaluated with precision comparable to a good centrifuge. The most damaging errors that may arise from the reference are due to improper placement relative to the test package. If a resonance is encountered, this error can cause severe local errors in indicated transfer functions as well as damaging vibration levels. Calibration errors in amplitude and phase response are generally not critical, although the possibility that a piezoelectric accelerometer (which lacks dc response) may have significant phase lead at low frequencies is often overlooked.

b) *Waveform distortion.* Waveform distortion may affect transfer function measurements, but the effect is generally small. Since the distortion is inherently zero mean, it has little or no effect on rectification testing.

c) *Sculling.* Sculling is a form of synchronized linear and angular motion that may appear to be an accelerometer error but is in reality a test setup problem. It only affects rectification testing and is only severe at or near low-frequency shaker resonances. Such resonances generally are not difficult to identify and avoid. Low-level sculling can be canceled by two-position testing so that test and accelerometer errors add in one position and cancel in the other, for example, IA up and IA down on a horizontal slip table.

d) *Self-heating*. Heating due to ac current in the torque coil and load resistor of a force-balance servo accelerometer can cause an apparent cubic nonlinearity during rectification testing for the K_3 coefficient. The effect is similar to that encountered during centrifuge testing but only one third as large.

e) *Frequency-sensitive rectification error terms*. Frequency-sensitive rectification error terms may cause difficulty in extrapolating nonlinear coefficients to near dc, but such terms generally occur only in fluid-filled instruments having substantial internal asymmetry.

f) *Ac magnetic fields.* Ac magnetic inductions of the order of 25 G may be found near the face plate of typical electromagnetic vibration exciters during operation. Most accelerometers are well shielded against such fields at 10 Hz or higher, but the possibility of error should be checked in critical cases.

L.4 Test instrumentation and procedures

L.4.1 Data acquisition

Test instrumentation for vibration testing is basically that required to monitor the output of the accelerometer and present it in a form suitable for processing. Processing generally requires analysis of an ac signal to modest accuracy (a percent or so) while separating a dc component that may need to be evaluated to <1 ppm of full scale. Systems may be broadly classified as analog, digital, or hybrid and are used with accelerometers that are either analog or digital.

The simplest systems use analog processing of an analog output. These systems may be considered as analog, even though the final voltage or phase measurements may be made digitally, because the ac and dc components are separated by a simple process of analog low-pass filtering. This process provides sub-ppm accuracy with averaging times on the order of 10 s.

Digital systems are, of course, much more flexible and are the most natural format for digital accelerometers [e.g., vibrating beam accelerometers (VBAs)]. For ac processing, accuracy requirements are not great, but the sample rate must be high enough that the sample process itself does not define the transfer function in the region of interest. The dc component presents more obstacles. First, the sampling process itself must not alter the dc value, which requires, as a minimum, that it contain no dead time. In the case of a frequency analog accelerometer such as a VBA, that requirement means no lost counts. Second, the averaged output must not alias significantly at low frequencies. For simple boxcar (running average) filters, that goal may require averaging times in excess of 100 s even for low-to-medium performance assessment. More elaborate filters having shaped windows (the simplest is triangular) may permit more practical averaging times, but at the cost of a custom processor that runs computationally intensive algorithms at rates in excess of 10 000 samples/s.

Hybrid processing is a third alternative that may allow the simplicity of analog processing (e.g. for a one-of-a-kind test or a very limited test series) when testing a digital accelerometer. Its simplest form may be used with a frequency analog output such as that of a VBA. The output frequency is applied to the input of a phase-locked loop (PLL). The voltage signal that is fed back to the voltage-controlled oscillator (VCO) of the PLL then becomes an analog output that can be processed in the usual analog way as long as two conditions are met. For transfer function measurements, the loop closure frequency must be high enough so that the PLL does not become the dominant transfer function in the frequency range of interest. For rectification testing, the VCO must not introduce significant nonlinearity to the system.

L.4.2 Test procedures

Test procedures vary widely depending on the facility available and the precise purpose of the test. Transfer function measurements are ac only and do not require high precision; therefore, those tests can be quite flexible. Rectification testing to evaluate nonlinear coefficients requires great stability of the dc signal; therefore, these tests are generally run with the accelerometer IA vertical. Tilt effects are minimized when the IA is vertical. Vibration testing with the IA vertical and with vibration along the IA has low-tilt sensitivity and also has the virtue of being almost insensitive to shaker sculling error. Other positions should be carefully evaluated as they arise.

Testing on a slip table with vibration axis horizontal and accelerometer IA vertical (a setup used to evaluate cross-axis sensitivity terms) is inherently sensitive to sculling if the load is not perfectly balanced and may require two-position testing (IA up and IA down) to cancel sculling effects. For the rectification testing used to evaluate super precision accelerometers, it may be necessary to use fixtures that allow testing of pairs of similar accelerometers with IAs parallel and antiparallel as well as up and down. The analysis is similar to the corresponding centrifuge tests and is an extension of the multiposition testing described in L.6.

Many accelerometers have significant sensitivity to the temperature variations encountered during rectification testing and SAE testing. These effects may be compensated by modeling the accelerometer output against a temperature sensor, which may be internal to the accelerometer or part of the setup. Temperature drifts may also cancel approximately from well-designed test sequences, for example, by measuring accelerometer output with low (or no) vibration before and after the high-vibration measurement during a rectification test. In SAE testing, the setup needed to calibrate the coefficient whose repeatability is being evaluated should be as close to the vibration facility as possible: preferably on the shaker and certainly in the same room.

L.5 General comments on analysis techniques

Vibration test data analysis falls broadly into the two categories of transfer function development and rectification testing. Transfer function development can be as brute force as stepping manually through a series of sinusoidal frequencies and recording the readings on two true rms voltmeters and a phase meter at each frequency or as elegant as applying a broadband white random spectrum and plotting the phase and amplitude Fourier response spectra. The choice depends on the nature of the test (e.g., laboratory evaluation versus production).

Rectification testing is basically a matter of recording the change in dc level of an accelerometer output when a zero mean vibration is applied and dividing by the square of the rms vibration, in g^2_{rms} to obtain a coefficient. The input can be a sinusoid at a single defined frequency, several sinusoids applied sequentially, or a defined random spectrum; but the coefficient must always be defined by the *rms* input. Beyond that, many possible test sequences correspond to many possible coefficients, usually with the need to incorporate compensation for temperature effects. A classic example, for the case of evaluating K_2 and K_3, can be found in Peters and Foote [B44].

L.6 Calibration of nonlinear coefficients from vibration along different instrument axes

L.6.1 Introduction

This subclause discusses vibration testing for estimating accelerometer nonlinearities. The basic measurements are average (dc) indicated accelerations in both static and vibration environments. The difference between the static and dynamic measurements gives an indication of nonlinear coefficients via rectification. The various nonlinear terms can be separated with vibrations along appropriate axes.

Estimating nonlinear parameters with vertically and horizontally oriented electrodynamic vibrations is discussed in L.6.2. Estimating nonlinear parameters with horizontally oriented hydraulic vibrations is discussed in L.6.3. The effects of shaker compliance, test package jitter, and short-term instabilities are discussed in L.6.4.

L.6.2 Calibration with vertical and horizontal electrodynamic vibrations

Let the vibration amplitude of a vertically or horizontally oriented electrodynamic vibrator be controlled with a piezoelectric accelerometer at, for example, 20 Hz, 50 Hz, or 100 Hz, as in Figure L.2 and Figure L.3.

L.6.2.1 Model equation

When subjected to a vibration $A \sin \omega t$, the accelerometer output E is modeled as

$$E = K_1 \Big\{ K_0 + (a_\mathrm{i} + g_\mathrm{i}) + K_2 (a_\mathrm{i} + g_\mathrm{i})^2 + K_3 (a_\mathrm{i} + g_\mathrm{i})^3 + K_\mathrm{pp} \big(a_\mathrm{p} + g_\mathrm{p}\big)^2$$
$$+ K_\mathrm{oo} (a_\mathrm{o} + g_\mathrm{o})^2 + K_\mathrm{ip} (a_\mathrm{i} + g_\mathrm{i}) \big(a_\mathrm{p} + g_\mathrm{p}\big) + K_\mathrm{io} (a_\mathrm{i} + g_\mathrm{i})(a_\mathrm{o} + g_\mathrm{o}) + \varepsilon \Big\} \qquad \text{(L.1)}$$

where

E	is the accelerometer output
K_1	is the accelerometer scale factor
K_0	is the bias
K_2	is the second-order nonlinearity
K_3	is the third-order nonlinearity
K_pp, K_oo	are the second-order cross-axis nonlinearities
K_io, K_ip	are the cross-coupling coefficients
a_i, a_p, a_o	are the IA, PA, OA acceleration components due to vibration = $A_j \sin\omega t$, $j = i, p$, o
g_i, g_p, g_o	are the IA, PA, OA acceleration reaction to gravity components
ε	is the measurement noise

This model is adequate for many accelerometers. For some high-precision accelerometers, it may be required to add other terms such as bias and scale-factor asymmetries, third-order cross-axis terms, and so on (see L.6.3.1).

L.6.2.2 Measurements

During vibration calibration tests, the accelerometer output is averaged, and the mean values of the acceleration are as follows:

$$\overline{(a_i + g_i)} = g_i \qquad \overline{(a_i + g_i)^2} = \frac{A_i^2}{2} + g_i^2 \qquad \overline{(a_i + g_i)^3} = \frac{3A_i^2 g_i}{2} + g_i^3$$

$$\overline{\left(a_p + g_p\right)^2} = \frac{A_p^2}{2} + g_p^2 \qquad \overline{(a_o + g_o)^2} = \frac{A_o^2}{2} + g_o^2$$

$$\overline{(a_i + g_i)\left(a_p + g_p\right)} = \frac{A_i A_p}{2} + g_i g_p \qquad \overline{(a_i + g_i)(a_o + g_o)} = \frac{A_i A_o}{2} + g_i g_o \qquad \text{(L.2)}$$

Care must be taken in the averaging process, especially for low frequencies, so that the mean values of a_i, a_p, a_o are really 0. Thus, in the general case, the averaged accelerometer output is

$$\begin{aligned}\bar{E} \quad = \quad & K_1 \left\{ K_0 + g_i + K_2\left(\frac{A_i^2}{2} + g_i^2\right) + K_3\left(\frac{3A_i^2 g_i}{2} + g_i^3\right)\right. \\ & + K_{pp}\left(\frac{A_p^2}{2} + g_p^2\right) + K_{oo}\left(\frac{A_o^2}{2} + g_o^2\right) \\ & \left. + K_{ip}\left(\frac{A_i A_p}{2} + g_i g_p\right) + K_{io}\left(\frac{A_i A_o}{2} + g_i g_o\right)\right\} \qquad \text{(L.3)}\end{aligned}$$

L.6.2.3 Test orientations

Axis configurations considered are given in Figure L.4. The orientation to measure K_{po} with IA horizontal is not included in the vibration calibration because of the increased sensitivity of the accelerometer average output to the dynamic orientation of the shaker relative to the local vertical. However, see L.6.3 for means to better control the shaker dynamic orientation.

L.6.2.4 Test results

For each configuration and amplitude of vibration, the averaged output is given in Table L.1 assuming that $g = 1$.

For a given axis configuration, it is more useful to consider the averaged output as the difference between the actual averaged measurement (during vibration) and the static measurement (without vibration applied but with the field still on in an electromagnetic vibrator to prevent alignment shifts). Let the "unbiased" measurements in orientation C_k be

$$E_{Ck}{}^{*} = \overline{(E_{Ck})} - K_1 \text{Bias}_{Ck} \qquad \text{(L.4)}$$

Then the different parameters can be readily calculated for a given vibration amplitude

$$K_2 = \frac{1}{K_1}\frac{(E_{\mathrm{CI}}{}^* + E_{\mathrm{C2}}{}^*)}{A^2}$$

$$K_3 = \frac{1}{K_1}\frac{(E_{\mathrm{CI}}{}^* - E_{\mathrm{C2}}{}^*)}{3A^2}$$

$$K_{\mathrm{pp}} = \frac{2}{K_1}\frac{E_{\mathrm{C3}}{}^*}{A^2} \qquad K_{oo} = \frac{2}{K_1}\frac{E_{\mathrm{C4}}{}^*}{A^2} \tag{L.5}$$

$$K_{\mathrm{ip}} \approx \frac{2}{K_1}\frac{(E_{\mathrm{C5}}{}^* - E_{\mathrm{C3}}{}^* - E_{\mathrm{C1}}{}^*)}{A^2} \qquad K_{io} \approx \frac{2}{K_1}\frac{(E_{\mathrm{C6}}{}^* - E_{\mathrm{C4}}{}^* - E_{\mathrm{C1}}{}^*)}{A^2}$$

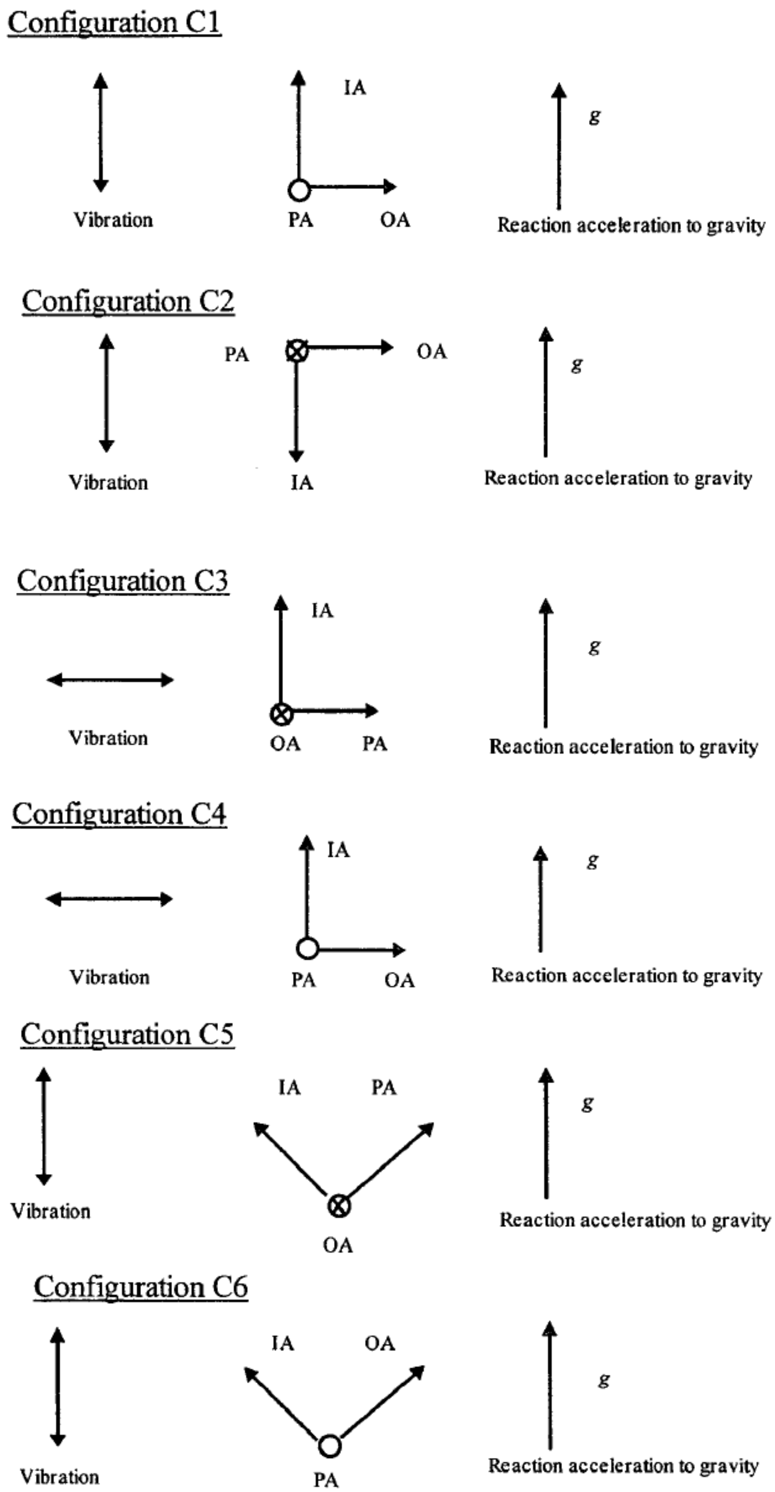

Figure L.4—Accelerometer orientations on vertical and horizontal electrodynamic vibrator for calibrating nonlinear terms

Table L.1—Averaged accelerometer output versus orientation and vibration amplitude

Axes config.	Vibration amplitude	Averaged output
C1	$A \sin \omega t$	$\overline{E_{C1}} = K_1\left(\text{Bias}_{C1} + K_2\frac{A^2}{2} + K_3\frac{3A^2}{2}\right)$
C2	$A \sin \omega t$	$\overline{E_{C2}} = K_1\left(\text{Bias}_{C2} + K_2\frac{A^2}{2} - K_3\frac{3A^2}{2}\right)$
C3	$A \sin \omega t$	$\overline{E_{C3}} = K_1\left(\text{Bias}_{C3} + K_{pp}\frac{A^2}{2}\right)$
C4	$A \sin \omega t$	$\overline{E_{C4}} = K_1\left(\text{Bias}_{C4} + K_{oo}\frac{A^2}{2}\right)$
C5	$A\sqrt{2} \sin \omega t$	$\overline{E_{C5}} = K_1\left[\text{Bias}_{C5} + \left(K_2 + \frac{3}{\sqrt{2}}K_3 + K_{pp} + K_{ip}\right)\frac{A^2}{2}\right]$
C6	$A\sqrt{2} \sin \omega t$	$\overline{E_{C6}} = K_1\left[\text{Bias}_{C6} + \left(K_2 + \frac{3}{\sqrt{2}}K_3 + K_{oo} + K_{io}\right)\frac{A^2}{2}\right]$

In fact,

$$\frac{2}{K_1}\frac{E_{C5}{}^* - E_{C3}{}^* - E_{C1}{}^*}{A^2} = K_{ip} + 3K_3\left(\frac{1}{\sqrt{2}} - 1\right) \approx K_{ip} - 0.88K_3 \qquad \text{(L.6)}$$

Since K_3 is usually less than 1 μg/g^3, 0.88K_3 can be neglected in most applications. If this approximation is not acceptable, 0.88K_3 can then be added to each value of K_{ip} calculated. This comment is also valid for K_{io}.

The scale factor K_1 is taken from the tumble test value. Instead of subtracting the zero vibration bias, least-squares fits to data at different vibration amplitudes (as measured by a piezoelectric accelerometer) can separate the coefficients of interest from the biases at the different orientations. The measurements for each configuration can be repeated for different frequencies or during a frequency sweep if the averaging process allows.

Repeating the estimation technique at different frequencies determines the dependence of the coefficients on frequency. For example, the apparent value of K_2 can change with frequency due to internal resonances of the pendulum or the accelerometer structure. The same phenomenon can appear with K_{ip} (often called "vibropendulosity" in the frequency domain), K_{io}, K_{pp}, and K_{oo}.

L.6.3 High-precision calibration with horizontal hydraulic vibrations

A horizontally oriented hydraulic vibrator with V-groove or other such bearing or slip table can provide precise large-amplitude linear vibration motion at 10 Hz, 15 Hz, and 20 Hz. Control of the vibration motion has been accomplished using a linear variable differential transformer (LVDT) as a displacement monitor combined with pendulous torque-rebalance monitor accelerometer measurements with IA along the horizontal vibration axis. The lower vibration frequencies employed with a hydraulic vibrator make the use of a torque-rebalance accelerometer as a monitor a better solution than the use of a piezoelectric accelerometer.

The following test procedure employs this instrumentation to estimate nonlinear model coefficients for the accelerometer under test.

L.6.3.1 Model equation

Expand the model equation in L.6.2.1 with the following terms:

$$\frac{K_0'}{2}\,\mathrm{sign}(a_\mathrm{i}+g_\mathrm{i})+\frac{K_1'}{2}|a_\mathrm{i}+g_\mathrm{i}|+K_\mathrm{oq}(a_E+g_\mathrm{i})|a_\mathrm{i}+g_\mathrm{i}|+K_\mathrm{po}(a_\mathrm{p}+g_\mathrm{p})(a_\mathrm{o}+g_\mathrm{o})$$
$$+K_\mathrm{ppp}(a_\mathrm{p}+g_\mathrm{p})^3+K_\mathrm{ooo}(a_\mathrm{o}+g_\mathrm{o})^3 \qquad \text{(L.7)}$$

where the scale-factor and bias asymmetry coefficients K'_0 and K'_1, the odd quadratic coefficient K_{oq}, and the cross-coupling coefficient K_{po} are as in 8.3. The cubic cross-axis model coefficients K_{ppp} and K_{ooo} are new.

Dynamic moment of inertia effects (K_{spin} and $K_{ang.accel}$) are negligible error contributions in vibration testing and are, therefore, ignored for test purposes. Also not included in the model (because they are presumed to be small) are any additional cubic nonlinearities, such as $K_{iip,}$ $K_{ppo,}$ and so on.

Shaker compliance effects resulting from the deflection of the accelerometer triad from the nominal position during vibration are considered in L.6.4.1.

L.6.3.2 Measurements

The measurements processed by the estimation algorithm are differences in average indicated accelerations between the static and vibration environments. The manner in which the various nonlinear coefficients are reflected into this difference depends on the orientation of the accelerometer IA, OA, and PA relative to gravity and the vibration axis. Consider the examples illustrated in Figure L.5 for horizontal vibrations with θ being the angle above the horizontal.

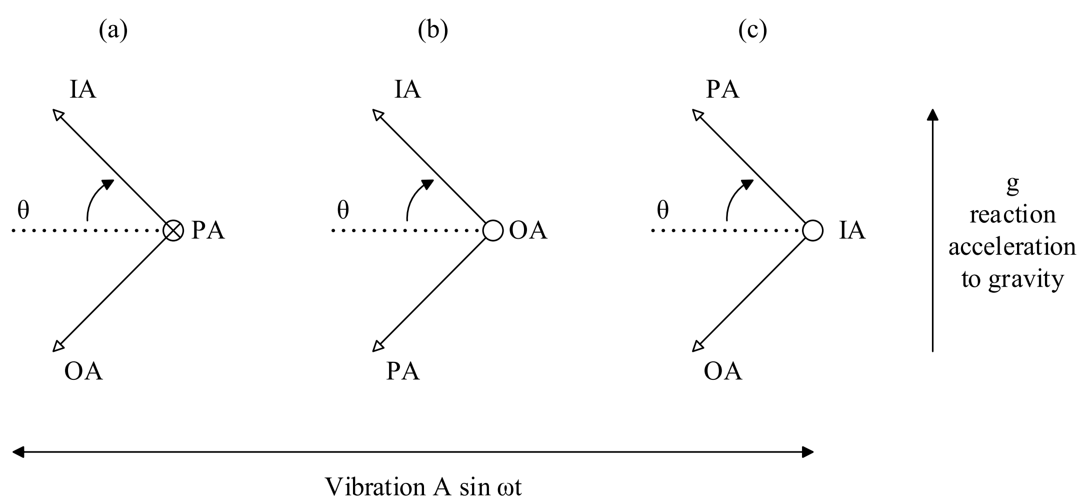

Figure L.5—Accelerometer orientations on horizontal hydraulic vibrator for calibrating nonlinear terms

For Case (a) in Figure L.5, the components of acceleration along the accelerometer axes assuming that $g = 1$ are

$$a_{\mathrm{i}} = A\cos\theta\sin\omega t \qquad a_{\mathrm{o}} = A\sin\theta\sin\omega t \qquad a_{\mathrm{p}} = 0$$

$$g_{\mathrm{i}} = \sin\theta \qquad g_{\mathrm{o}} = -\cos\theta \qquad g_{\mathrm{p}} = 0 \tag{L.8}$$

In a static environment, the indicated acceleration A_{ind} for Case (a) in Figure L.5 is

$$\frac{E(\text{static})}{K_1} = A_{ind}(\text{static})$$

$$= K_0 + \frac{K'_0}{2}\operatorname{sign}(\sin\theta) + (1 + k_1)\sin\theta + \frac{K'_1}{2}|\sin\theta|$$

$$+K_{oq}\sin\theta\,|\sin\theta| + K_2\sin^2\theta + K_3\sin^3\theta - K_{io}\sin\theta\cos\theta$$

$$+K_{oo}\cos^2\theta + K_{ooo}\cos^3\theta + \varepsilon \tag{L.9}$$

where k_1 is the error in the nominal scale factor K_1. In the vibration environment, the indicated acceleration is

$$A_{ind}(vib) = K_0 + \frac{K'_0}{2}\operatorname{sign}(\sin\theta + A\cos\theta\sin\omega t) + (1 + k_1)(\sin\theta + A\cos\theta\sin\omega t)$$

$$+\frac{K'_1}{2}|\sin\theta + A\cos\theta\sin\omega t|$$

$$+K_{oq}(\sin\theta + A\cos\theta\sin\omega t)|\sin\theta + A\cos\theta\sin\omega t|$$

$$+K_2(\sin\theta + A\cos\theta\sin\omega t)^2 + K_3(\sin\theta + \cos\theta\sin\omega t)^3$$

$$-K_{io}(\sin\theta + A\cos\theta\sin\omega t)(\cos\theta + A\sin\theta\sin\omega t)$$

$$+K_{oo}(\cos\theta + A\sin\theta\sin\omega t)^2$$

$$+K_{ooo}(\cos\theta + A\sin\theta\sin\omega t)^3 + \varepsilon \tag{L.10}$$

The rectified portion (average) of Equation (L.10) is

$$\begin{aligned}\overline{A_{\mathrm{ind}}(vib)} &= K_0 + \frac{K'_0}{2}\frac{(\pi + \xi_1 - \xi_2)}{\pi} + (1 + k_1)\sin\theta \\ &+ \frac{K'_1}{2\pi}\{(\pi + \xi_1 - \xi_2)|\sin\theta| + A(\cos\xi_2 - \cos\xi_1)|\cos\theta|\} \\ &+ \frac{K_{oq}}{2\pi}\Big\{2(\pi + \xi_1 - \xi_2)\sin^2\theta + 4A(\cos\xi_2 - \cos\xi_1)\sin\theta\cos\theta \\ &+ \frac{A^2\cos^2\theta}{2}[2\xi_1 - 2\xi_2 + \sin(2\xi_2) - \sin(2\xi_1)]\Big\} \\ &+ K_2\left\{\sin^2\theta + \frac{A^2\cos^2\theta}{2}\right\} \\ &+ K_3\left\{\sin^3\theta + \frac{3}{2}A^2\sin\theta\cos^2\theta\right\} + K_{\mathrm{io}}\left\{\frac{A^2\sin\theta\cos\theta}{2} - \sin\theta\cos\theta\right\} \\ &+ K_{\mathrm{oo}}\left\{\cos^2\theta + \frac{A^2\sin^2\theta}{2}\right\} + K_{\mathrm{ooo}}\left\{\frac{3}{2}A^2\cos\theta\sin^2\theta - \cos^3\theta\right\} + \bar{\varepsilon}\end{aligned} \tag{L.11}$$

where ξ_1 and ξ_2, are the angles (ωt) at which the acceleration along IA crosses 0

$$\xi_1 = \pi + \sin^{-1}\left\{\frac{\sin\theta}{A\cos\theta}\right\}, \qquad \xi_2 = 2\pi - \sin^{-1}\left\{\frac{\sin\theta}{A\cos\theta}\right\} \tag{L.12}$$

The measurement for the vibration test data processing for Case (a) in Figure L.5 is the difference between the rectified vibration measurement and the static measurement

$$\begin{aligned}\Delta A_{\mathrm{ind}} &= \frac{K'_0}{2}\frac{(\xi_1 - \xi_2)}{\pi} + \frac{K'_1}{2\pi}\{(\xi_1 - \xi_2)|\sin\theta| + A(\cos\xi_2 - \cos\xi_1)|\cos\theta|\} \\ &+ \frac{K_{\mathrm{oq}}}{\pi}\Big\{(\xi_1 - \xi_2)\sin^2\theta + 2A(\cos\xi_2 - \cos\xi_1)\sin\theta\cos\theta \\ &+ \frac{A^2\cos^2\theta}{4}[2\pi + 2\xi_1 - 2\xi_2 + \sin(2\xi_2) - \sin(2\xi_1)]\Big\} \\ &+ K_2\frac{A^2\cos^2\theta}{2} + K_3\left\{\frac{3}{2}A^2\sin\theta\cos^2\theta\right\} + K_{\mathrm{io}}\frac{A^2\sin\theta\cos\theta}{2} \\ &+ K_{\mathrm{oo}}\frac{A^2\sin^2\theta}{2} + K_{\mathrm{ooo}}\left\{\frac{3}{2}A^2\cos\theta\sin^2\theta\right\} + \text{ noise}\end{aligned} \tag{L.13}$$

If $|A\cos\theta| < |\sin\theta|$, then the IA nongravitational acceleration never crosses 0, and K'_0 and K'_1 have no net signature, whereas K_{oq} has the same signature as K_2. The IA nongravitational acceleration not crossing 0 can be modeled simply by setting $\xi_1 = \xi_2 = 0$. K_0, k_1 and any error in the angle θ never have any net signature.

Analogous expressions can be derived for Case (b) and Case (c) in Figure L.5 for the difference between the rectified vibration measurement and the static measurement.

L.6.3.3 Test orientations

A carefully planned combination of θs and vibration planes (e.g., IA/OA, IA/PA, PA/OA as in Figure L.5) will make any combination of nonlinear coefficients observable (limited only by available fixturing). If estimation of all modeled nonlinear and asymmetry error terms is desired, then a minimum of 14 positions would be necessary, although estimation or common mode rejection of fixture/table compliance coefficients may necessitate additional positions.

L.6.4 Error sources

L.6.4.1 Sculling error driven by compliance

The compliance of the shaker can cause a dc shift (due to rectification) in measured acceleration and corrupt the estimation of the parameters. Consider the situation illustrated in Figure L.6. The vibration acceleration along the accelerometer IA is

$$a_i = A \sin \omega t \sin \theta(t) \tag{L.14}$$

where the shaker acceleration is $A \sin \omega t$, and

$$\theta(t) \approx \beta A \sin \omega t \quad (\beta = \text{compliance coefficient}) \tag{L.15}$$

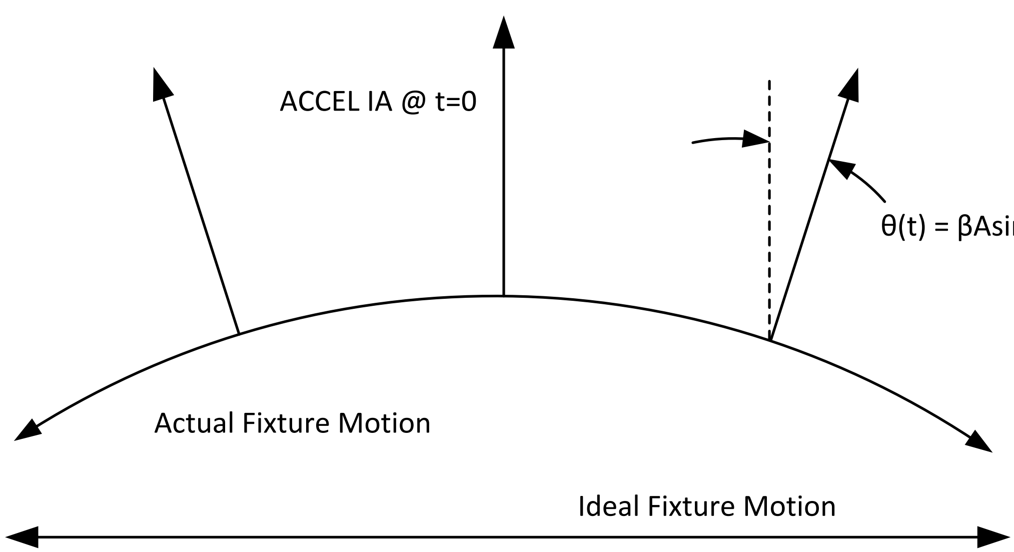

Figure L.6—Shaker compliance effects

Thus, for small $\beta A \sin \omega t$ angles,

$$a_i \approx A \sin \omega t \, (\beta A \sin \omega t) \tag{L.16}$$

If this phenomenon causes too large an error compared with the desired estimation accuracy, one could simply add other axis configurations by adapting the configurations in Figure L.4 such as C3’ with IA down and C4’ with IA down. If the fixture symmetry is such that the sculling motion is unchanged by rotation about the vibration axis, axis configurations C3’ and C4’ invert the sculling output term while leaving all else the same in those positions. Then in L.6.2.4, the correct estimation for K_{pp} is obtained by averaging E_{C3}* and $E_{C3'}$* and the correct estimation for K_{oo} is obtained by averaging E_{C4}* and $E_{C4'}$*.

L.6.4.2 Error in average acceleration due to jitter

Noise can be present in the measured acceleration due to any number of causes, such as the instrument under test, the measurement device(s), and harmonic distortion in the shaker. For sampled data, however, an important noise source is sampling jitter.

Assume that acceleration data are taken at a frequency = l/Δ*T* for *N* × 60/Δ*T* minutes and averaged and that the vibration and data collection are synchronized so that an integer number of vibration cycles are sampled. Then the error in estimated dc acceleration is determined primarily by the sampling jitter. That is,

$$\begin{aligned}\hat{a}_{dc} &= \frac{1}{N}\sum_{i=1}^{N} A\sin\omega(i\Delta t + \delta t_i)\\ &\approx \frac{1}{N}\sum_{i=1}^{N} A[\sin\omega i\Delta t + (\omega\delta t_i)\cos\omega i\Delta t]\\ &\approx \frac{1}{N}\sum_{i=1}^{N} A(\omega\delta t_i)\cos\omega i\Delta t \end{aligned} \qquad \text{(L.17)}$$

Then, for pure jitter (independent δt_i's),

$$\begin{aligned}\sigma_a^2 &= \frac{A^2}{N^2}\omega^2 \mathrm{E}\left\{\sum_{i=1}^{N}\delta t_i\cos\omega i\Delta t\sum_{j=1}^{N}\delta t_j\cos\omega j\Delta t\right\}\\ &\approx \frac{\omega^2 A^2}{2N}\sigma_{\delta t}^2\end{aligned} \qquad \text{(L.18)}$$

where *E*{ } denotes the expectation operator, and where

δt_i	is the *i*th jitter
$\sigma_{\delta t}^2$	is the rms jitter
N	is the total number of samples
A	is the vibration level
ω	is the vibration frequency (rad/s)

L.6.4.3 Accelerometer short-term instabilities

To provide a worst-case bound for their effects, short-term instabilities of accelerometer bias and scale factor may be treated for analysis purposes as if the error coefficient changes in an uncorrelated fashion from the nonvibration data collection period to the vibration data collection period at each fixture orientation, vibration level, and frequency. Thus, in addition to the noise errors discussed, the modeled Δ-acceleration measurement includes a noise term with an rms value, σ, given by

$$\sigma^2 = \sigma_{\mathrm{AB}}^2 + g^2\sin^2\theta\sigma_{\mathrm{SFE}}^2 \qquad \text{(L.19)}$$

where θ is the angle of the accelerometer IA above horizontal.

The duration of vibration and shock tests is short enough that long-term stability considerations, such as aging, are not a concern. However, a trend across the test sequence due to thermal or other such variations could be estimated and compensated for.

L.7 Summary

Vibration and shock testing can be used as a form of environmental stress or as a means to characterize the dynamic behavior of inertial sensors. When used to excite and measure rectification errors, it can provide a powerful and efficient tool for evaluating nonlinear characteristics across a wide range of frequencies, starting from near dc.

By using multiple orientations of the accelerometer under test relative to the vibration axis and the gravity vector, vibration can be used to perform calibrations that would normally be done with a centrifuge but often can do so more quickly with equal or better accuracy and with less uncertainty due to self-heating effects.

The orientations chosen will depend on the coefficients to be evaluated and on error sources that may sometimes be excited. Small amounts of shaker compliance can contribute large errors to tests for cross-axis sensitivity, but careful selection of test positions can cause this error to cancel out or even allow it to be estimated as one of the test outputs.

Annex M

(informative)

Geophysical effects in inertial instruments testing

M.1 Introduction

Gyroscopes, accelerometers, and other inertial instruments are sensitive to seismic disturbances, lunar–solar earth and ocean tides, tilts, azimuth motions, and variations in the rotation of the earth. Such geophysical effects can be regarded as

- A corrupting influence in testing or using inertial instruments, to be modeled out if possible
- A reference against which to judge an instrument's sensitivity
- Something to be measured by inertial instruments

Measurement of geophysical effects is best accomplished by devices specifically designed for the task (such as a seismometer or gravimeter) rather than by an instrument designed for guiding a vehicle, for example. However, an indication of the capabilities of a vehicle guidance instrument is whether it can detect geophysical phenomena such as lunar–solar earth tides.

M.2 Seismic environment

An inertial instrument test station receives vibration input from local cultural activity and from the general seismic background of the earth. The frequency spectrum of this vibration input depends on the particular site and whether it is in an urban or isolated location. It is generally above 1 Hz, possibly with discrete spikes due to resonances in the local geology and test table. Earthquake frequencies can be below 0.1 Hz.

Local cultural activity (automobile and other traffic, rotary equipment in the building in which the test station is housed, and even people walking by the test station) cause horizontal and vertical vibration inputs and lower frequency tilts. Effects can be amplified or damped by local geologic conditions, such as landfill over bedrock, where surface vibrations are reflected from the bedrock to cause constructive interference at certain frequencies and damping at others. The upper floors of a building generally have higher vibration levels; as a result inertial instrument test laboratories should be located at or below ground level, utilizing test piers or slabs isolated from the structure of the building.

The general seismic background of the earth includes phenomenon such as the vibrations from ocean waves striking the sea shore. The surface and solid body seismic waves from an earthquake thousands of kilometers away can cause disturbances in inertial instrument test data. The different modes of vibration have different arrival times because of differing paths through the earth and differing speeds of travel. There can be considerable ringing in the earth for several hours after an earthquake, in addition to the initial and after-shock disturbances.

A test station should be in as seismically quiet a location as possible. However, the seismic input averages zero over the averaging time of many types of measurements, either as a natural consequence of the measurement system itself (such as low-rate counter readings) or because high-rate sampling followed by digital filtering is employed. But such averaging cannot eliminate all seismic aliasing and other corruption, such as that due to earthquakes or from a parking lot speed bump. Some tests, such as noise measurements, might require use of a site remote from the usual facility.

M.3 Tilt and azimuth variations

A test table on a pier or laboratory floor will have diurnal, seasonal, and long-term tilt variations relative to the local vertical due to temperature, solar heating, ground water, and other local geophysical effects. There could be several microradians of tilt variation over a day and tens of microradians of tilt variation over weeks.

The data from an input axis (IA) vertical accelerometer test are insensitive to such tilt variations, whereas the data from off-vertical positions in a tumble test are sensitive to them. Tilt meters could be monitored during a test in order to correct the tumble test angle readings for tilt errors. Alternatively, the orthogonal accelerometer tumble test analysis technique described in Annex K can be used to correct for tilt errors, if accuracy warrants.

Tilt variations also affect the results of gyroscope testing in that they change the orientation of the gyroscope IA relative to the earth-rotation vector. Azimuth variations of the test station can be of the same order of size as tilt variations and similarly affect the results of gyroscope testing but not those of accelerometer testing. Optical monitoring of test station azimuth variations by sighting on an external target can be corrupted by movements of the target due to the same geophysical causes (temperature, etc.) that cause the test station to rotate in azimuth and tilt.

The technique of gyro compassing uses a gyroscope's output to determine the direction of the earth-rotation vector and hence the azimuth variations of a tilt stabilized platform. Rotating a gyroscope's horizontally oriented IA 180° alternately between nearly east and west allows the separation of azimuth and gyroscope bias variations.

M.4 Effect of lunar–solar earth tides

The difference between gravitational attractions of the moon and sun at a point on the earth's surface and the attraction averaged over the volume of the earth is the tide producing force. The solid, elastic earth partially yields to this force and, therefore, rises and falls about ±30 cm approximately every 12.4 hours. The following three solid earth equilibrium tide effects combine to vary the gravity vector at a test site:

— The direct attraction of the moon and sun minus this attraction at the center of the earth (same as the attraction averaged over the volume of the earth)

— The direct attraction of the tidal bulge

— The variation in the direct attraction of the whole earth caused by the variation in distance of the test site from the center of the earth

Let $\overrightarrow{r_m}$ and $\vec{\rho}$ be the vectors from the center of mass of the earth to the moon and to a point on the surface of the earth, respectively. Let γ_m be the gravitational constant times the mass of the moon. The lunar-tide producing acceleration is

$$\overrightarrow{g_m} = \gamma_m \left[\frac{\overrightarrow{r_m} - \vec{\rho}}{|\overrightarrow{r_m} - \vec{\rho}|^3} - \frac{\overrightarrow{r_m}}{|\overrightarrow{r_m}|^3} \right] \quad \text{(M.1)}$$

with a similar formula for the solar-tide-producing acceleration with the subscript *m* being replaced by *s*. The total direct-tide-producing acceleration is

$$\overrightarrow{g_t} = \overrightarrow{g_m} + \overrightarrow{g_s} \quad \text{(M.2)}$$

Mean orbit formulas for the moon and sun transformed from ecliptic coordinates to those referred to the equinox and equator of date can be used in evaluating $\overrightarrow{r_m}$ and $\overrightarrow{r_s}$.

Let ρ be the distance of the test site from the center of mass of the earth, ϕ' the geocentric latitude, λ the east longitude, and s the sidereal time (angle between the Greenwich meridian and the vernal equinox). Then the coordinates of the test site referred to the equinox and equator of data are

$$\rho_1 = \rho\cos\phi'\cos(\lambda + s)$$
$$\rho_2 = \rho\cos\phi'\sin(\lambda + s) \tag{M.3}$$
$$\rho_3 = \rho\sin\phi'$$

If ϕ is the geodetic latitude, the unit normal $\vec{n}$ to the geoid has components

$$n_1 = \cos\phi\cos(\lambda + s)$$
$$n_2 = \cos\phi\sin(\lambda + s) \tag{M.4}$$
$$n_3 = \sin\phi$$

The unit vector $\vec{m}$ along the meridian to the north is

$$m_1 = -\sin\phi\cos(\lambda + s)$$
$$m_2 = -\sin\phi\sin(\lambda + s) \tag{M.5}$$
$$m_3 = \cos\phi$$

The unit vector $\vec{q} = \vec{m} \times \vec{n}$ to the east is

$$q_1 = -\sin(\lambda + s)$$
$$q_2 = \cos(\lambda + s) \tag{M.6}$$
$$q_3 = 0$$

The vertical component of the tide producing acceleration is (see Melchoir [B37])

$$\Delta g = G\overrightarrow{g_t}\cdot\vec{n} \tag{M.7}$$

where the gravimetric factor G alters the direct tide producing acceleration for the effects of the elasticity of the earth. In terms of the Love numbers h and k (see Melchoir [B37] and Tomaschek [B59])

$$G = 1 + h - \frac{3}{2}k \approx 1.16 \tag{M.8}$$

Let the tidal tilt of the local vertical be

α_1 = tilt about north (positive vertical to east)

α_2 = tilt about east (positive north to vertical)

Let $\bar{g}$ be the average acceleration due to gravity at the site and let (see Melchoir [B37] and Tomaschek [B59])

$$\Lambda = 1 + k - \ell \approx 1.13 \tag{M.9}$$

where ℓ is Shida's constant. Then (see Melchoir [B37] and Tomaschek [B59])

$$\alpha_1 = \Lambda \frac{\vec{g}_t \cdot \vec{\mathrm{q}}}{\bar{g}} \tag{M.10}$$

$$\alpha_2 = -\Lambda \frac{\vec{g}_t \cdot \vec{\mathrm{m}}}{\bar{g}} \tag{M.11}$$

The three tidal components $\Delta g, \alpha_1, \alpha_2$ are plotted in Figure M.1 for a month and a half at a northern latitude test site. The variations are as much as ±140 n*g* in the vertical component and ±33 milliarcsec (±0.16 µrad) in each horizontal component. These values could be slightly larger at the peak of the 18.6-year lunar cycle.

The tidal tilt affects the orientation of the local vertical relative to the earth-rotation axis. The local geophysical tilt measured by a tilt meter gives the motion of the test table relative to the local vertical. The combination of the two, plus azimuth variation is needed in determining the angles between a gyroscope's IA and the earth-rotation vector. The angle between the local vertical and an accelerometer's IA depends only on the tilt-meter-measured local geophysical tilt, and not on the tidal tilt or azimuth variation.

The vertical component of the tidal acceleration is needed for interpreting a sub-µ*g*-accuracy accelerometer's output. Even if the tidal signature were not directly visible, a signal detection could be attempted by least-squares fitting a coefficient times the tidal model to several days of IA vertical accelerometer data and determining whether the estimated coefficient had the value 1 within the experimental uncertainty.

Since an accelerometer on a test table responds to the upward specific acceleration reaction to gravity pulling down, the vertical component of the tidal acceleration must be negated before comparing with an accelerometer's output.

M.5 Effect of ocean tides

The tide-producing force acting on the water in deep ocean basins creates resonances that depend on shoreline shape and builds up the water tide to a greater height than the equilibrium tide in the solid earth. The effect of the water tide on the gravity vector at a land-based test site is due to

- The direct attraction of the water tidal bulge
- The change in the direct attraction of the whole earth caused by the change of the distance of the test site from the center of the earth due to water tide loading of the local plate
- The tilt due to water tide loading of the local plate

The water tide effect on the gravity vector at a coastal test site could be as much as ±4 n*g* in the vertical component and ±0.016 µrad in test table tilt relative to the local vertical (see Melchoir [B37]).

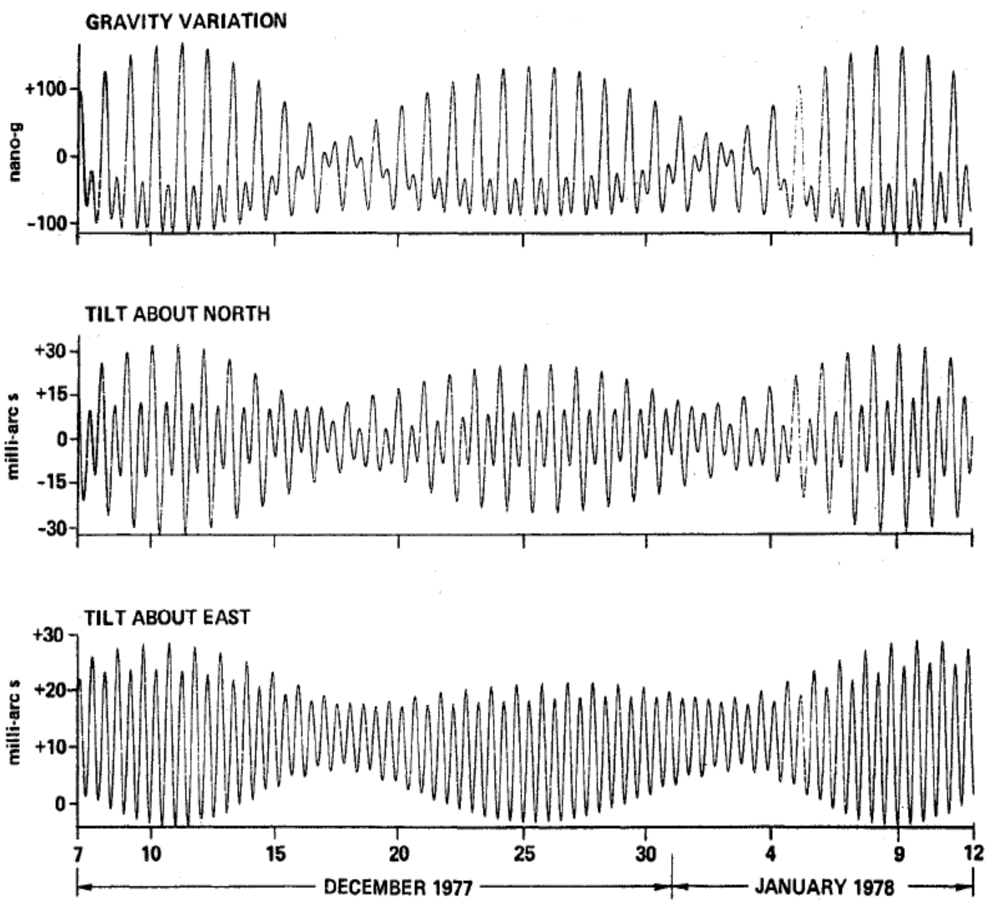

Figure M.1—Lunar–solar earth tide gravity variation and tilt (λ = 71.0919°, φ 42.3640°) (see Ash [B3])

M.6 Variations in earth rotation

The 7.292115 × 10^{-5} rad/s earth-rotation angular velocity has seasonal variations that can amount to ±0.028 seconds-of-time-accumulated angle over 6 months. The 14-month Chandler wobble of the earth axis of figure relative to the earth-rotation axis (or motion of the pole of figure relative to the pole of rotation) has 0.3-arcsec amplitude.

The earth-rotation axis is inclined about 23° to the pole of the ecliptic (plane of the orbit of the earth around the sun). The astronomical precession is a 26 000-year coning motion of the earth-rotation axis around the pole of the ecliptic due to the gravitational attractions of the moon and sun acting on the earth's equatorial bulge. Superimposed on this average motion are forced nutational motions with half-weekly to 18.6-year periods (20 arcsec and smaller amplitudes).

The angular velocity and centripetal acceleration effects of these phenomena are listed in Table M.1. The local value of gravity used as a reference in accelerometer testing includes the earth-rotation centripetal acceleration at the latitude and altitude of the test site. The angular velocity due to seasonal variations in the uniform rotation is parallel to the uniform rotation angular velocity, whereas the parts of the wobble, precession, and nutation angular velocities that are not absorbed into the uniform rotation rate are perpendicular to the uniform rotation angular velocity.

The variations in the uniform centripetal acceleration due to the earth precession, nutation, wobble, and seasonal rotation variations are ignorable when analyzing conventional accelerometer data, but they should be considered when analyzing superconducting gravimeter data. The departures from uniform earth-rotation angular velocity are generally ignorable in terrestrial gyroscope testing, except perhaps for future super-accurate instruments. However, the position of the pole of figure relative to the pole of rotation should be taken into account when interpreting accurate gyrocompass data.

Table M.1—Effect of variations in earth rotation (see Ash [B3])

Phenomenon	Angular velocity		Maximum centripetal acceleration (g)
	Fraction of earth rate	Deg/hour	
Uniform rotation	1.0	15.04106	0.00346 cos(lat)[a]
Seasonal rotation variation	5.0×10^{-9}	7.5×10^{-8}	3.4×10^{-11}
Wobble	5.0×10^{-9}	7.5×10^{-8}	1.7×10^{-11}
Precession	4.2×10^{-8}	6.4×10^{-7}	1.4×10^{-10}
Nutation	4.2×10^{-8}	6.4×10^{-7}	1.4×10^{-10}

[a]Pointed toward the earth rotation axis; the vector subtraction of this from the acceleration due to the earth gravitational attraction is included in the local value of gravity.

Annex N

(informative)

Bibliography

Bibliographical references are resources that provide additional or helpful material but do not need to be understood or used to implement this standard. Reference to these resources is made for informational use only.

[B1] Albert, W. C., “Force sensing using quartz flexure resonators,” *38th Annual Frequency Control Symposium*, 1984.

[B2] Albert, W. C., “Vibrating quartz crystal accelerometer,” *ISA 28th International Instrumentation Symposium*, vol. 28, no. 1, pp. 33–44, 1982.

[B3] Ash, M. E., “Detecting geophysical motions with inertial instruments,” *IEEE 1978 National Aerospace and Electronics Conference*, pp. 789–797, May 1978.

[B4] Ash, M. E., and P. A. DeBitetto, “Kalman filter nonlinear control law for an inertial instrument pulse width modulation torque loop,” *Joint Services Data Exchange for Guidance, Navigation, and Control*, Oct. 1992.

[B5] Ash, M. E., M. F. Luniewicz, P. C. L. Leung, and M. A. Bates, “Coherent high-speed frequency measurement and signal processing,” *International Conference on Signal Processing Applications and Technology*, pp. 661–670, Nov. 1992.

[B6] Ash, M. E., and M. E. Skeen, “Maximum likelihood estimation of fractional Brownian motion and Markov noise parameters,” *AIAA Journal of Guidance, Control, and Dynamics*, vol. 18, pp. 379–382, 1995,

[B7] Barbour, N., et al. “Micro-electromechanical instrument and systems development at Draper Laboratory,” *3rd St. Petersburg International Conference on Integrated Navigation Systems*, May 1996.

[B8] Bendat, J. S., and A. G. Piersol, *Engineering Applications of Correlation and Spectral Analysis*. New York: John Wiley and Sons, 1971.

[B9] Bendat, J. S., and A. G. Piersol, *Random Data: Analysis and Measurement Procedures*. New York: John Wiley and Sons, 1971.

[B10] Bottom, V. E., *Introduction to Quartz Crystal Unit Design*. New York: Van Nostrand Reinhold, 1982.

[B11] Brown, R. G., *Introduction to Random Signal Analysis and Kalman Filtering*. New York: John Wiley and Sons, 1983.

[B12] Burns, D. W., et al., with the Honeywell Technology Center, University of Wisconsin, “Resonant microbeam accelerometers,” *Transducers ‘95-Eurosensors IX*, pp. 659–662, June 1995.

[B13] Chau, K. H., et al., with Analog Devices, Inc. and University of California, Berkeley, “An integrated force-balanced capacitive accelerometer for low-g applications,” *Transducers ‘95-Eurosensors IX*, pp. 593–596, June 1995.

[B14] Church, A. A., *Mechanical Vibrations*. New York: John Wiley and Sons, 1957.

[B15] Clough, R., and J. Penzier, *Dynamics of Structures*. New York: McGraw-Hill, 1975.

[B16] Cramer, H., *Mathematical Methods of Statistics*, 9th ed. Princeton, NJ: Princeton University Press, 1961.

[B17] D’Azzo, J. J., and C. H. Houpis, *Feedback Control System Analysis and Synthesis*, 2nd ed. New York: McGraw-Hill, 1966.

[B18] ErNiesse, E. P., et al., United States Patent #4,372,173, Feb. 8, 1983.

[B19] Eshback, O. W., and M. Sauders, eds., *Handbook of Engineering Fundamentals*. New York: John Wiley and Sons, 1975.

[B20] Flandrin, P., "On the spectrum of fractional Brownian motions," *IEEE Transactions on Information Theory*, vol. 35, pp. 197–199, 1989.

[B21] Fuhrman, T. A., "An improved technique for estimating accelerometer linearity from multipoint data," *AIAA Guidance and Control Conference Proceedings*, p. 530, Aug. 1977.

[B22] Gelb, A., *Applied Optimal Estimation*. Cambridge, MA: M. I. T. Press, 1974.

[B23] Harris, C. M., ed., *Shock and Vibration Handbook*, New York: McGraw-Hill, 1995.

[B24] Hartog, D. J., ed., *Mechanical Vibrations*, 4th ed. New York: McGraw-Hill, 1956.

[B25] Heising, R. A., *Quartz Crystals for Electrical Circuits Their Design and Manufacture*. New York: D. Van Nostrand, 1946.

[B26] Henrion, W., et al., with Triton Technologies, "Wide dynamic range direct digital accelerometer," *IEEE IC Sensors Conference*, Paper CH2783-9/90/0000-0153, 1990.

[B27] Hestrom, C. W., *Probability and Stochastic Processes for Engineers*. New York: Macmillan, 1984.

[B28] Hooge, F., "Discussion of recent experiments in l/f noise," *Physica*, vol. 60, pp. 130–144, 1972.

[B29] IEEE Std 952™-1997, IEEE Standard Specification Format Guide and Test Procedure for Single-Axis Interferometric Fiber Optic Gyros.[8, 9]

[B30] Jazwinski, A. H., *Stochastic Processes and Filtering Theory*. San Diego, CA: Academic Press, 1970.

[B31] Keshner, M., " I/f Noise," *Proceedings of the IEEE*, vol. 70, pp. 212–218, 1982.

[B32] Kitchin, C., with Analog Devices, Inc., "Micromachined complete-on-a-chip sensor measures 5-g accelerations," *Analog Dialogue,* vol. 29-1, 1995.

[B33] Link, B., with Endevco, "Field qualified silicon accelerometers from 1 milli-g to 200,000 g," *Sensors*, Mar. 1993.

[B34] Longman, I. M., "Formulas for computing the tidal accelerations due to the moon and the sun," *Journal of Geophysical Research*, vol. 64, no. 12, pp. 2351–2355, 1959.

[B35] Mandlebrot, B, and J. Van Ness, "Fractional Brownian motions, fractional noises and applications," *SIAM Review*, vol. 10, pp. 422–437, 1969.

[B36] Maybeck, P. S., *Stochastic Models, Estimation, and Control, Vol 2*. San Diego, CA: Academic Press, 1982.

[B37] Melchoir, P., *The Earth Tides*. New York: Pergamon Press, 1986.

[B38] Norling, B. L., "An overview of the evolution of vibrating beam accelerometer technology," *Gyro Technology Symposium*, Stuttgart, Germany, 1991.

[B39] Norling, B. L., "Superflex: A synergistic combination of vibrating beam and quartz flexure technology," *Navigation: Journal of the Institute of Navigation*, vol. 34, no. 4, Winter 1987–1988.

[B40] Nye, J. F., *Physical Properties of Crystals*. Oxford, England: Clarendon Press, 1957, pp. 143–148.

[B41] Papoulis, A., *Probability, Random Variables, and Stochastic Processes*, 3rd ed. New York: McGraw-Hill, 1991.

[B42] Papoulis, A., *Signal Analysis*. New York: McGraw-Hill, 1977.

[8] IEEE publications are available from the Institute of Electrical and Electronics Engineers (http://standards.ieee.org/).
[9] The IEEE standards or products referred to in Annex N are trademarks owned by the Institute of Electrical and Electronics Engineers, Incorporated.

[B43] Parzen, E., *Stochastic Processes*. San Francisco, CA: Holden-Day, 1962.

[B44] Peters, R., and S. Foote, "Determination of nonlinear coefficients in a dry accelerometer by vibration testing," *Proceedings of the Fifteenth Biennial Guidance Test Symposium*, Holloman AFB, NM, Sept. 1991.

[B45] Rabiner, L. B., and B. Gold, *Theory and Application of Digital Signal Processing*. Englewood Cliffs, NJ: Prentice-Hall, 1975.

[B46] Roszhart, T. V., et al., with Kearfott Guidance and Navigation, EG&G, "An inertial grade, micromachined vibrating beam accelerometer," *IC Sensors, Transducers '95-Eurosensors IX*, pp. 656–658, June 1995.

[B47] Rudolf, F., et al., with the Centre Suisse d'Electronique et de Microtechnique, "Precision accelerometers with micro-g resolution," *Sensors and Actuators*, 0924-4247, 1990.

[B48] Sandell, Jr., N. R, and K. I. Yared, "Maximum likelihood identification of state space models for linear dynamic systems," M.I.T. Electronic Systems Laboratory Report ESL-R-814, Cambridge, MA, Apr. 1978.

[B49] Seidel, H., et al., with Messerschmitt-Bolkow-Blohm GmbH, "Capacitive silicon accelerometer with highly symmetrical design," *Sensors and Actuators*, vol. A2l-A23, pp. 312–315, 1990.

[B50] Skeen, M. E., "Maximum likelihood estimation of fractional Brownian motion and Markov noise parameters." Master of Science thesis, M.I.T., Dec. 1991.

[B51] Slater, J. M., *Inertial Guidance Sensors*. New York: Reinhold Press, 1964.

[B52] Solo, V., "Intrinsic random functions and the paradox of l/f noise," *SIAM Journal on Applied Mathematics*, vol. 52, pp. 270–291, 1992.

[B53] Spangler, L., and C. J. Kemp, with Ford Microelectronics, Inc., "ISAAC-integrated silicon automotive accelerometer," *Transducers '95-Eurosensors IX*, pp. 585–588, June 1995.

[B54] Strang, G., *Introduction to Applied Mathematics*. Wellesley, MA: Wellesley-Cambridge Press, 1986.

[B55] Suzuki, S., et al., "Semiconductor Capacitance-type Accelerometer with PWM electrostatic servo techniques," *Sensors and Actuators*, vol. A21–A23, p. 319, 1990.

[B56] Tang, W. C., M. G. Lim, and R. T. Howe, "Electrostatic comb drive levitation and control method," *Journal of Microelectromechanical Systems*, vol. 1, no. 4, pp. 170–178, Dec. 1992.

[B57] Thomson, W. T., *Theory of Vibration with Applications*. Englewood Cliffs, NJ: Prentice-Hall, 1993.

[B58] Timoshenko, S., and G. H. MacCollough, *Elements of the Strength of Materials*. New York: D. Van Nostrand, 1958.

[B59] Tomaschek, R., "Tides of the solid earth," *Handbuch der Physik, BandXL VIII (Geophysic II)*, pp. 775–845, 1957.

[B60] Ueda, K., and A. Umeda, "Improvement of novel NRLM method for accelerometer characterization to the range of 10^2 m/s^2," *Sensors and Actuators*, vol. 54, pp. 517–522, 1996.

[B61] Umeda, A., and K. Ueda, "Davies bar as the reference for impact acceleration metrology," *SPIE Proceedings*, vol. 2880, p. 119; also *Proceedings of Micromachining and Microfabrication 1996*, Austin, TX, Oct. 14–15, 1996.

[B62] Umeda, A., and K. Ueda, "Frequency characteristics of accelerometers measured by impact in the low acceleration," *Technical Digest of the 12th Sensor Symposium 1994*, pp. 171–174.

[B63] Umeda, A., and K. Ueda, "Study on the dynamic force/acceleration measurement," *Sensors and Actuators*, vol. 21, pp. 285–288, 1990.

[B64] Umeda, A., K. Ueda, and T. Usuda, "Generation of motion in microstructures using the reflection of pulse elastic waves," *ASME DSC-VoI.40, Micromechanical Systems*, 1992, pp. 69–81.

[B65] Warren, K., with Litton Guidance and Control, “High performance silicon accelerometers with charge controlled rebalance electronics,” *IEEE Conference*, Paper 0-7803-3085-4/96, 1996.

[B66] Wilkinson, R. H., “High-fidelity low-pass finite-impulse-response filters,” *Journal of Guidance, Control, and Dynamics*, vol. 12, pp. 412–420, 1989.

[B67] Wilks, S. S., *Mathematical Statistics*. New York: John Wiley and Sons, 1962.

[B68] Yun, W., R. T. Howe, and P. R. Gray, with the University of California, Berkeley, “Surface micromachined, digitally force-balanced accelerometer with integrated CMOS detection circuitry,” *IEEE Conference*, Paper 0-7803-04560X/92, 1992.

Consensus

WE BUILD IT.

Connect with us on:

Facebook: https://www.facebook.com/ieeesa

Twitter: @ieeesa

LinkedIn: http://www.linkedin.com/groups/IEEESA-Official-IEEE-Standards-Association-1791118

IEEE-SA Standards Insight blog: http://standardsinsight.com

YouTube: IEEE-SA Channel

IEEE
standards.ieee.org
Phone: +1 732 981 0060 Fax: +1 732 562 1571